Design, modelling and development of filtration processes for household water treatment systems

Arsalan Afkhami

School of Engineering
Ulster University

This dissertation is submitted for the degree of
Doctor of Philosophy

May 2022

Declaration

I hereby declare that except where specific reference is made to the work of others, the contents of this dissertation are original and have not been submitted in whole or in part for consideration for any other degree or qualification in this, or any other university. This dissertation is my own work and contains nothing which is the outcome of work done in collaboration with others, except as specified in the text and Acknowledgements. This dissertation contains fewer than 100,000 words including appendices, bibliography, footnotes, tables and equations and has fewer than 150 figures.

Arsalan Afkhami
May 2022

Note on access to contents

"I hereby declare that with the effect from the date on which the thesis is deposited in the Library of the Ulster University, I permit 1. the Librarian of the University to allow the thesis to be copied in the whole or in part without reference to me on the understanding that such authority applies to the provision of single copies made for study purposes or for the inclusion within the stock of another library.
2. the thesis to be made available through the Ulster Institutional Respiratory and/or EThOS under the terms of the Ulster eThesis Deposit Agreement which I have signed. IT IS A CONDITION OF USE OF THIS THESIS THAT ANYONE WHO CONSULTS IT MUST RECOGNISE THAT THE COPYRIGHT RESTS WITH THE AUTHOR AND THAT NO QUOTATION FROM THE THESIS AND NO INFORMATION DERIVED FROM IT MAY BE PUBLISHED UNLESS THE SOURCE IS PROPERLY ACKNOWLEDGED."

Arsalan Afkhami
May 2022

Acknowledgements

First and foremost, I would like to thank Dr Patrick Dunlop for giving me the opportunity to do the PhD research and express my sincere gratitude and appreciation for his mentoring and support during the whole period as my first supervisor. Furthermore, I would like to thank the other members of the supervisory team, Dr Dorian Dixon for his crucial help with our first publication and later manuscripts, and Dr Nigel Ternan for his insightful guidance. This PhD was not possible without the help and support of Dr Pilar Fernandez and the SAFEWATER team.

I would like to acknowledge the Doctoral College for providing the financial support through the Vice Chancellor's Research Scholarship as well as organising research festivals and workshops.

There were many people who helped me during my PhD in various forms: Dr Helen Lubarsky, Dr Natalia Pichel Mira, Dr Jeremy Hamilton, Dr Preetam Sharma, Mr Damien McDonald, Mr Brian McGrath, and Dr Chris Proctor provided technical support and Mrs Ann Blair, Ms Ruth Holman and Ms Charly Mifsud provided administrative support.

I'm grateful for the teaching experience I gained thanks to the School Office and the lecturers who had me as their teaching assistant: Prof Margaret Morgan (MS Excel), Dr Pilar Fernandez (Engineering Mathematics), Prof Omar Escalona (MATLAB), Prof Alistair McIlhagger (Materials I), and Dr Nikhil Bhalla (Python programming).

I was privileged to conduct a research visit at Cranfield University thanks to Prof Peter Jarvis who showed interest in my research and supervised my work and Mr Paul Barton who provided technical support.

Finally, I would like to dedicate this work to my wife, Elham, who not only supported me during this period, but also created the graphics used in this thesis. Also, I am indebted to my parents for their love and support through all stages of my life.

Publications, Webinars and Presentations

Publications

- Snelling, W. j., **Afkhami, A.**, Turkington, H. L., Carlisile, C., Cosby, S. L., Hamilton, J. W. J., Ternan, N. G., Dunlop, P. S. M. (2022). Efficacy of single pass UVC air treatment for the inactivation of coronavirus, MS2 coliphage and Staphylococcus aureus. *Journal of Aerosol Science*, 10600. DOI:10.1016/j.jaerosci.2022.106003

- Pichel, N., Lubarsky, H., **Afkhami, A.**, Baldasso, V., Botero, L., Salazar, J., Hincapie, M., Byrne, J. A., Fernandez-Ibanez, P. (2021). Safe drinking water for rural communities using a low-cost household system. Effects of water matrix and field testing. *Journal of Water Process Engineering*, 44. DOI: 10.1016/j.jwpe.2021.102400

- **Afkhami, A.**, Marotta, M., Dixon, D., Ternan, N. G., Montoya-Jaramillo, L. J., Hincapie, M., Laila Galeano, Pilar Fernandez-Ibanez, Dunlop, P. S. M. (2020). Assessment of low-cost cartridge filters for implementation in household drinking water treatment systems. *Journal of Water Process Engineering*, 101710. DOI: 10.1016/j.jwpe.2020.101710

- Alrousan, D., **Afkhami, A.**, Bani-Melhem, K., & Dunlop, P. (2020). Organic degradation potential of real greywater using $TiO_2$2-based advanced oxidation processes. *Water (Switzerland)*, 12(10). DOI: 10.3390/w12102811

Webinars

- **Afkhami, A.**. (2020, June 17). Low-cost household water treatment systems: A process engineering perspective [Webinar]. *Institution of Chemical Engineers (IChemE)*. https://www.icheme.org/membership/communities/special-interest-groups/water/events/low-cost-household-water-treatment-systems-a-process-engineering-perspective

- **Afkhami, A.**. (2019, April 10). Efficiency of commercial cartridge filters for turbidity removal in household surface water treatment systems [Webinar]. *ALICE project*.

Presentations

- **Afkhami, A.**, Patrick Dunlop, Dorian Dixon, Nigel Ternan, Helen Lubarsky, Pilar Fernandez-Ibanez. (2019, April 10). Efficiency of commercial cartridge filters for turbidity removal in household surface water treatment systems [Poster]. *Festival of PhD Research*. Ulster University, Jordanstown, United Kingdom.

Abstract

In small water treatment systems, cartridge filters are commonly employed due to their ease of use and small footprint. Readily available commercial filter types (spun, wound and pleated) of different micron ratings (10, 5 and 1) were tested for the removal of turbidity either alone or in series in simulated large volume pilot trials. An initial turbidity of 40±10 NTU was prepared using fine test dust (ISO 12103-1, A2) with the turbidity removal efficiency, pressure drop, and lifespan of the filters evaluated. In pilot trials, the volume of turbid water filtered varied from 0.85 m^3 with a 1 micron wound filter to 6 m^3, with 5 and 1 micron pleated filters in series, which could be used for three filtration cycles. With the pleated filters, turbidity removal efficiency improved over time as a cake built up with the effluent turbidity reaching acceptable quality (<5 NTU). This criterion continued to be achieved with repeated cycles of washed pleated filters, significantly reducing the cost and improving sustainability of the HWT system.

A comprehensive approach to simulation of particle removal in cartridge filtration using CFD was developed to simulate the fundamental mechanisms underpinning the removal of particles within the widely used 10 inch cartridge filter. Laboratory based validation studies confirmed the novel CFD model to accurately model removal of turbidity and predict the pressure drop across the filter with Root Mean Square Percentage Error (RMSPE) value being 2.46%, 1.49% and 1.95% for 1.2m, 3.6m and 4.8m mesh cells. The simulated location of particle deposition on the filter elements closely matched images taken at several stages during filtration experiments with the model aiding understanding of pattern of particle removal along and within the porous filter structure.

A low-cost and multifunctional precoat layer and a simple precoating method were developed, achieving turbidity-free effluent with additional capability to effectively reduce the concentration of both organic matter and pathogenic microorganisms as well as protecting the surface of the filter, facilitating cleaning and re-use. Different test waters were prepared with A2 fine test dust (TD) and/or humic acid sodium salt (HA) to evaluate the performance of the system under different conditions. When tested with 60 mg/L of TD (40±10 NTU), the system effectively removed >95% of influent turbidity in large volume trials (>1000 L) when 1 micron pleated filters were precoated with either

natural or calcined diatomaceous earth (DE); in comparison, with the un-precoated filter, filtrate turbidity never reached the 5 NTU target set by the WHO.

A novel HWT system was implemented by fitting a T-Valve on the suction side of the feed pump to dose the coagulants, eliminating the need for an additional pump. Contact filtration using fibrous cartridge filters did not require frequent coagulant dose optimization due to the large surface area provided by the fibres on which the coagulant could be adsorbed. Both inorganic (alum) and polymeric (PDADMAC) coagulants provided filtrate turbidity of <5 NTU with concentrations as low as 8 and 0.45 mg/L, respectively.

Table of contents

List of figures

List of tables

Nomenclature

Acronyms

CFU	colony-forming unit
CTW	challenge test water
DE	diatomaceous earth
DOC	dissolved organic carbon
HA	humic acid
HWT	household water treatment
NOM	natural organic matter
NTU	nephelometric turbidity units
PDADMAC	polydiallyldimethyl ammonium chloride
PFD	process flow diagram
PSD	particle size distribution
SEM	scanning electron microscope
SGD	Sustainable Development Goal
TD	test dust
TOC	total organic Carbon
WHO	World Health Organization
ZP	Zeta potential

Greek Symbols

α	permeability, m^2
μ	viscosity, kg/(m s)
Ψ	Wadell's sphericity, –
ρ	density, kg/m^3
σ	specific deposition, kg/m
ε	bed porosity, –

Other Symbols

H	Hamaker constant, J
C_D	drag coefficient, –
k_B	Boltzmann constant, 1.381×10^{-23}J/K
Pe	Peclet number
Re	Reynolds number, –
T	absolute temperature, K
UV_{254}	UV absorbance at 254 nm

Subscripts

0	initial
f	fibre
p	particle

Chapter 1

Introduction

Providing safe drinking water for people who do not have access to municipal piped water is a challenging task that requires international effort. Although substantial progress has been made in the past decades, there is a long way to go until universal access to affordable drinking water is achieved.

1.1 Sustainable Development Goals and safe water

In 2015, the UN General Assembly adopted a new resolution, 'Transforming our World: The 2030 Agenda for Sustainable Development' [16], outlining a framework to establish the foundation of the sustainable development agenda for the 2015–2030 period, referred to as the Sustainable Development Goals (SDGs) [17] or Agenda 2030 [18]. SDGs, comprised of 17 goals and 169 targets, aiming to improve the conditions of humans as well as other species and the planet [19].

SDGs are ambitious and globally comprehensive, fostering collaboration across countries and inviting us to embrace interconnectedness. Although these goals required substantial investments, estimated to be around 5–7 trillion USD per year [20, 21], the idea of SDGs got adopted quickly due to the growing need for sustainable development.

For sustainable development, we need to embrace 'the triple bottom line' approach to human wellbeing: social inclusion, economic development and environmental sustainability, even though the two paradigms of economic growth and protection of natural resources seem contrasting. The urgency of this approach arises from the fact that human activity plays a central and threatening role in earth dynamics [19, 22].

SDGs were preceded by the Millennium Development Goals (MDGs), launched in 2002 and ran until 2015 [23]. The MDGs consisted of eight simple goals that were reasonably easy to state, which stuck in the public's mind, leading to public awareness, advocacy and mobilisation [22]. Target 7c of MDG (MDG 7c) aimed to halve the number of people without access to safe water, sanitation and hygiene. The target set for access to safe water was achieved five years ahead of the 2015 deadline [23], with 2.6 billion people gaining access to improved water [18]. However, the level of progress was varied across countries, and the startling economic growth in China had a significant impact on the averaged data [22].

SDGs 1–6 build upon the core agenda of the MDGs, while SDGs 7–17 incorporate new ideas [19]. A self-standing goal (SDG 6) addresses the shortcomings in the indicators of MDG 7c, and aims to ensure availability and sustainability of water and sanitation management for all by 2030, with Target 6.1 set to achieve equitable and universal access to affordable and safe drinking water [23, 24]. Target 6.1 is more ambitious than MDG target 7c as it aims to achieve universal and equitable access, rather than just halving the proportion of people without access to water [1], with the indicator selected for monitoring Target 6.1 being the 'proportion of population using safely managed drinking water services' (Indicator 6.1.1).

The latest data, in 2020, showed that 74% of the global population have access to safely managed drinking water services, a small increase from the baseline status of 70% in 2015, and it has been predicted that with the current rate of progress, global coverage of

81% will be achieved by 2030 [25], while any achievement below 100% is not acceptable as access to safe drinking water is a human right [26].

Moreover, there are interlinkages among the SDGs, leading to important synergies and trade-offs among the goals and their underlying targets [20]. As shown in Fig. 1.1, achieving SDGs such as SDG 2 on food security, SDG 3 on human health, SDG 13 on climate change and SDG 15 on protecting ecosystems and conserving biodiversity relies on the progress on SDG 6 [26, 27]. Therefore, the set of actions need to be pre-designed to take these interlinkages into account; otherwise, they will lead to adverse or sub-optimal outcomes [26].

Fig. 1.1 SDGs are interlinked and progress on SDGs 2, 3, 13 and 15 depend on SDG 6.

Water management is a key to the success of all the interlinked SDGs and failure in this regard propagates the risk of failure in achieving the other goals. Actions taken regarding supplying water at the local scale may trigger environmental stress at regional or even global scales, creating a trade-off between meeting human demands and environmental sustainability [21, 26].

1.2 Water service levels

The WHO/UNICEF Joint Monitoring Programme for Water Supply, Sanitation and Hygiene (JMP), established in 1990, has been responsible for tracking the progress towards the 2015 MDG target 7c as well as 2030 SDG targets 6.1 and 6.2 [1, 28]. JMP has facilitated the comparison of water services by creating a service ladder to classify them. The levels are: Surface water, Unimproved, Limited, Basic and Safely managed (there are separate service ladders for schools [29] and health care facilities [30]).
The 'Basic' level refers to a source, which is 'improved' (rainwater, protected dug wells, etc.) and not 'limited' (collection time exceeding 30 minutes), while 'Safely managed' refers to a service that is additionally accessible on premises, available when needed and free from contamination [24]. However, the definition of 'improved' source fails to take water quality into account; as a result, water sources categorized as 'improved' may be contaminated and *vice versa* [23]. As shown in Fig. 1.2, while coverage of 'improved' drinking water sources for four countries with drinking water quality testing reports ranged from 87 to 96%, the proportion of population with access to water free from faecal contamination was significantly lower [1]. Additionally, although protecting water sources such as springs does reduce faecal contamination and 'improve' the source, the water stored at home will be recontaminated, requiring treatment at the point of use [31].

In 2020, 2 billion people (27% of world population) lacked safely managed drinking water services (safe water at home), of which 771 million (11%) did not have access to a basic drinking water service, 263 million used limited services, spending more than 30 minutes collecting water and 122 million used water directly from surface water sources (Fig. 1.3) [2]. Moreover, there was a disparity in access between the urban and rural populations as shown in Fig. 1.4. It should be noted that the estimates for water quality (i.e. 'free from contamination') are only available for 45% of the global population, suggesting that

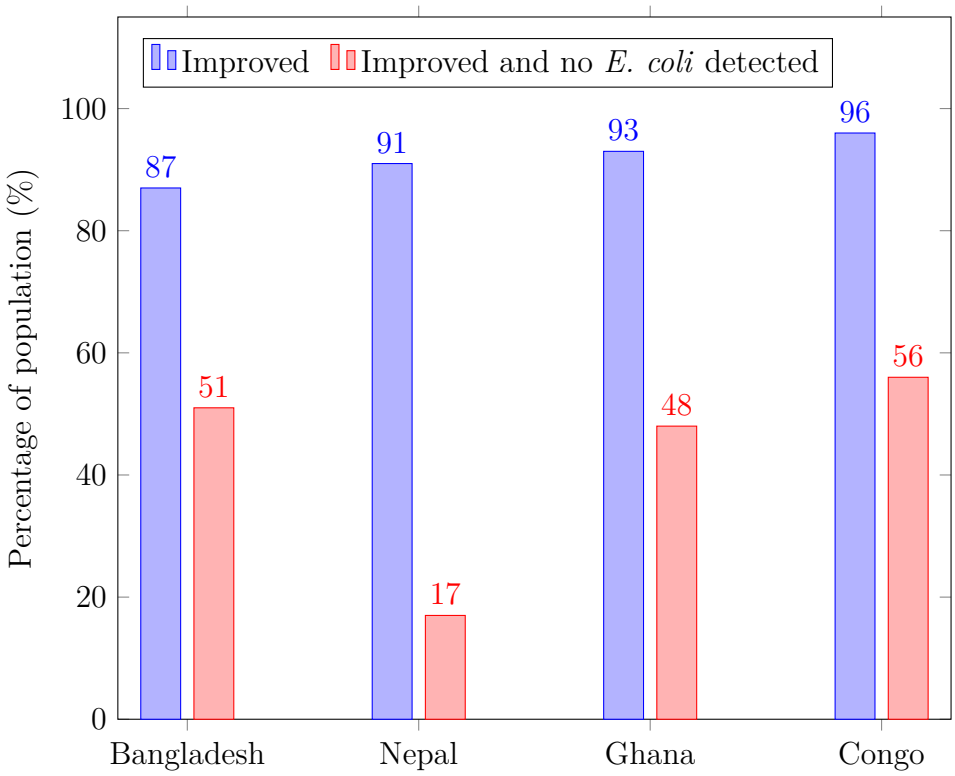

Fig. 1.2 Proportion of improved sources free from feacal contamination [1].

the levels of compliance are low in many developing countries [24]. In 2016, sufficient data were still not available for basic services in schools in Eastern and South-Eastern Asia, Latin America and the Caribbean, and sub-Saharan Africa [32].

The highest priority for global monitoring are faecal contamination, fluoride and arsenic, with microbial contamination being a universal concern whereas the presence of arsenic and fluoride is concerning only in some parts of the world. Faecal contamination can be measured via an indicator bacteria such as *E. coli* [24], which is associated with moderate to severe diarrhoea in developing countries [33]. Water can be considered non-contaminated when containing zero *E. coli* or thermotolerant coliforms in a 100 mL sample [4]; however, the concentration of *E. coli* in natural waters can be highly variable with time, resulting in false classification of a source with serious public health outcomes. Furthermore, *E. coli* is more easily inactivated than other pathogens such as *Cryp-*

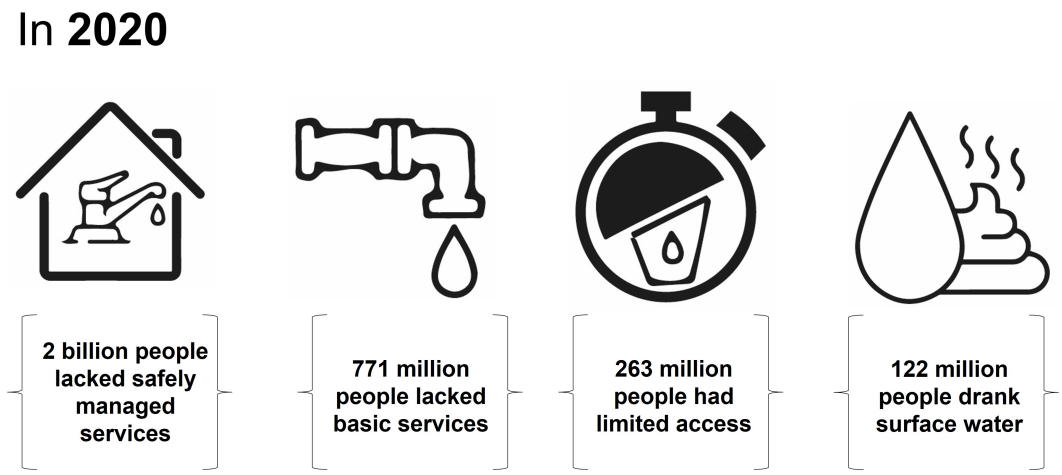

Fig. 1.3 Status of global water access in 2020.

tosporidium parvum [1]. Microscopic parasites of the genus *Cryptosporidium* that live in the intestines of an infected person and animal pass in the stool. Due to its outer shell, *Cryptosporidium* can survive for a long time outside the body and be resistant to chlorine-based disinfectants [8].

1.3 The economics of safe water provision

The only path for humanity is sustainable development, which can be achieved only if a fraction of consumption spending is turned into investments for long-term survival [22]. In order to turn the present SDGs to future reality, the need for finance in developing countries is 2–4 times the current practice. Over the next three decades towards 2050, financing requirements for water will be driven by two uppermost policies—the SDGs agenda and the climate change adaptation agenda related to water resources [18]. Infrastructure costs the developing countries about 20% of all investments, of which 10% is related to water and sanitation. Even with the current investments, services lack coverage, maintained sporadically and are unresponsive to demand, due to poor management, budget constraints and the absence of commercial practices. Consequently,

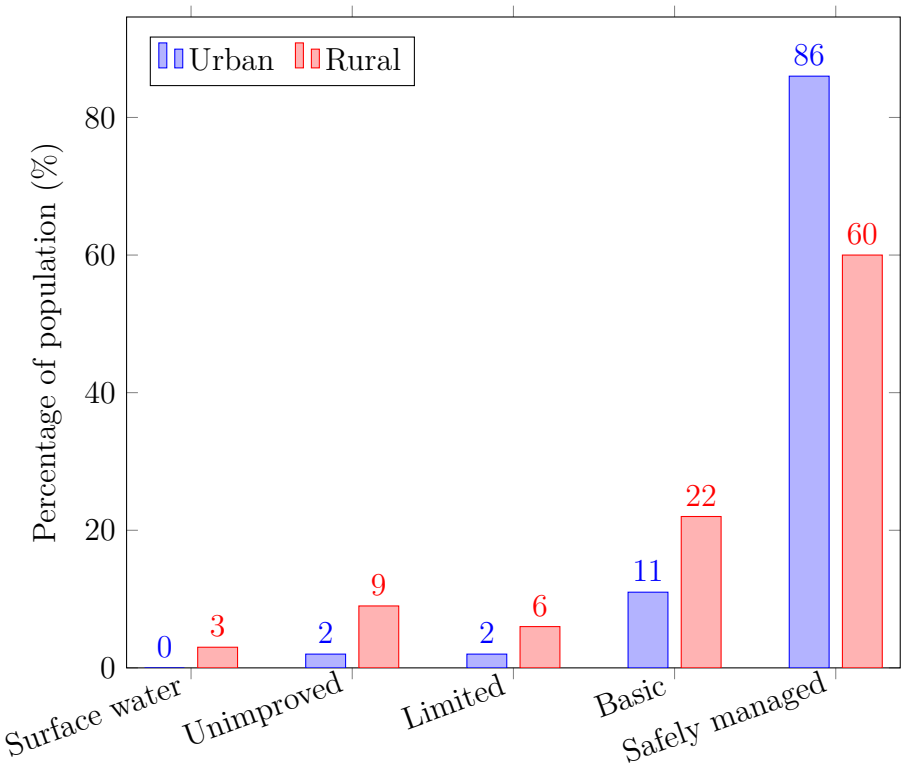

Fig. 1.4 Comparison of water access level for people living in urban and rural areas [2].

the desire for more efficient and better services as well as the need for supplementary sources of finance have led many developing countries to engage the private sector [34]. Even though private provision and financing of some sectors such as power and telecom has blossomed in developing countries, financing in water and sewerage sector is limited and dominated by public budgets, due to the high-risk profiles of many water investments. However, the recently growing Environmental, Social and Governance (ESG) investing that promotes longer-term sustainability, social impact and goodwill in exchange for possibly lower returns can be helpful in alleviating the problem [18, 34].

Financing water projects through philanthropy has led to unsustainable outcomes, and user paid instruments (taxes, tariffs, etc.) can be a more viable alternative since it has been demonstrated that users are prepared to pay more for water services if the benefits can be perceived [26]. However, it has been pointed out by Ahuja et al. [31]

that the studies have not differentiated ease of access (convenient access to water) from water quality since the interventions studied improved both. Nevertheless, their study suggested that increasing access to water without improving its quality does not reduce diarrhoea incidence.

Innovative approaches to financing water projects and programs are required, especially due to the current system of accounting that ignores the costs of environmental impacts, distorting the evaluation of projects [26]. An innovative blended financing model implemented by non-profit organizations is to use funds from a donor fund (philanthropic sources) as seed capital, lowering the risks in deals, which is then complemented by funds from commercial investors to support the service, who will in turn receive competitive returns [18, 26].

There are symbiotic links between economic development and water, as water is essential for sustainable development and development provides the required investments for water security and infrastructure [21]. Therefore, the long-term interests of the water and financial sectors converge [18], and governments should consider water resource management as an integral and central part of macro-economic planning, especially with the global water crisis over the next 2–3 decades [18, 21].

With an economic evaluation, the total quantifiable benefit of an intervention and the annual rate of return on an investment can be estimated. Regarding the economic aspect of investment in WASH, it should be considered that the investment will enhance security and reduce poverty and inequality, with a financial return of at least four times, depending on the region and the intervention [27, 35].

1.4 Household water treatment as a solution

In many settings, the issue is not having access to sufficient quantities of water, but the quality of water available being unsafe for consumption [36]. Centralized treatment

plants are not economically feasible for some rural and peri-urban communities, who are left with the responsibility to treat and store their own water [10, 31]. Currently, at least 2 billion people use drinking-water sources contaminated with faeces [7], and an estimated 1.5 billion people use household water treatment (HWT) for their daily water supply, expected to grow due to the population growth occurring in developing countries [37].

HWT technologies are commonly promoted as a solution to improve water safety at the point of consumption in places where safe piped water supply is either not reliable or feasible and/or water-borne transmission is a dominant transmission pathway [10, 11, 38, 39].

There are four categories of pathogens/ diseases with transmission mode related to water [40]:

- water-borne: caused through consumption of contaminated water (e.g. diarrhoeal diseases, typhoid, infectious hepatitis, etc.);
- water-based: transmitted via an intermediate aquatic host (e.g. guinea worm);
- water-washed: caused due to inadequate amount of water used for personal hygiene (e.g. diarrhoeal diseases, infectious hepatitis, etc.);
- water-related vector: spread through insect vectors (e.g. malaria);

where the first three can be addressed through implementation of HWT solutions.

Using effective HWT methods correctly and consistently can reduce the risk of diarrhoeal disease in populations at risk as much as 45–61% depending on the type of water source [3, 7, 38], while services granting safe and continued piped water supply can reduce waterborne disease by up to 73% [4]. The continuity of supply is important as piped systems that are not continually pressurized are vulnerable to microbial contamination [1].

Although HWT interventions are generally believed to reduce diarrhoeal disease and improve health, it is worth mentioning that there are studies (e.g. by Hunter [41]) disputing the health benefits of HWT, in particular disinfection, based on the available blinded studies. Also, various field tests have shown that it is possible that some HWT systems deteriorate the water microbial quality rather than improving it [10]. Hence, a proper analysis of each situation prior to implementation of HWT is necessary.

There are three key requirements for appreciable health gains from HWT and safe storage: (i) the treatment methods must sufficiently remove pathogens; (ii) technologies should be used correctly and consistently with rates of use over 90%; and (iii) HWT and safe storage is actually needed, i.e water has high levels of faecal contamination and/or individuals are at risk of waterborne disease, particularly pregnant women, young children, etc. [3, 7]. Some key features of an HWT system that are desirable to achieve the above requirements are [9]:

- consistently producing sufficient quantities of microbiologically safe water, meeting the daily household needs;
- effective in treating different water sources including high turbidity and organic matter waters;
- simple to use and not time consuming;
- low cost both in terms of capital investment and cost per litre of treated water produced;
- having reliable supply chain.

There are few peer-reviewed articles on the cost of HWT systems since various factors affect the cost, such as production costs (materials, labour and tools needed), distribution costs (depends on the project area and the weight of the system), taxes (for imported products) and distributors' fees [10].

1.5 WHO's Scheme for evaluation of HWT technologies

The International Scheme to Evaluate Household Water Treatment Technologies [33], referred here as the Scheme, was established by the WHO as a response to the lack of international and national regulations and uncertainty over the effectiveness of commercial products [39]. The Scheme aims to support the implementation of health-based performance criteria for HWT and enable the independent evaluation of commercial HWT products based on harmonized testing protocols, detailing the approach and testing conditions [7]. According to the Scheme, products are tested with two types of test water: General Test Water (GTW) and Challenge Test Water (CTW), representing 'clean' (e.g. groundwater) and 'dirty' (e.g. surface water) water, respectively [7].

WHO has been evaluating the performance of HWT technologies in removing pathogens from drinking water since the publication of the Scheme in 2014. The results of the first global assessment of the performance of HWT technologies—following the voluntary submission of an expression of interest by manufacturers—were published in 'Round I Report' in 2016 [3].

There are three categories of performance for HWT technologies: 3-star (★★★), 2-star (★★) and 1-star (★), indicating the descending order of performance. The performance targets are related to the three main classes of enteric infections and disease pathogens widely occuring in drinking-water supplies due to human and/or animal excreta, namely protozoa, bacteria and viruses, with the reference microorganisms selected representing the three pathogens classes: *Cryptosporidium parvum* (protozoa), *E. coli* (bacteria) and coliphages MS2 and phiX174 (viruses) [3]. Table 1.1 provides the log reduction required for each performance class.

The modelling work done by Bivins et al. [39] showed that the potential gains due to

improved drinking water are realized with 2-star protection, and the highest tier (3-star) yields additional marginal health gains in the case that adherence is 100% and the raw water is very contaminated, requiring high log reductions. In other words, compliance or adherence is more important than removal efficacy when selecting products with comprehensive protection (two- or three-star). Even products with one-star performance can yield health gains similar to the two-star class when microbial contamination of the source water are known to be of the same pathogen classes that the products protect against [3, 7, 39].

Table 1.1 WHO performance criteria for HWT technologies [7].

Performance classification	**Minimum required reduction (log_{10})**			**Protectiveness**
	Bacteria	**Viruses**	**Protozoa**	
★★★	≥ 4	≥ 5	≥ 4	Comprehensive protection
★★	≥ 2	≥ 3	≥ 2	
★	At least 2-star for two classes of pathogens			Targeted protection
–	Fails to meet WHO performance criteria			Little or no protection

1.6 Common HWT technologies

Six most common commercial HWT options are: chemical disinfection (chlorination), filtration (membrane, biosand and ceramic filtration), solar disinfection (SODIS), filtration-chlorination, coagulation-chlorination and coagulation-filtration (Fig. 1.5) [3, 8]; however, there are other methods being used as well. For the sake of brevity, the advantages and limitations of each HWT technology discussed below are summarized in Table 1.2.

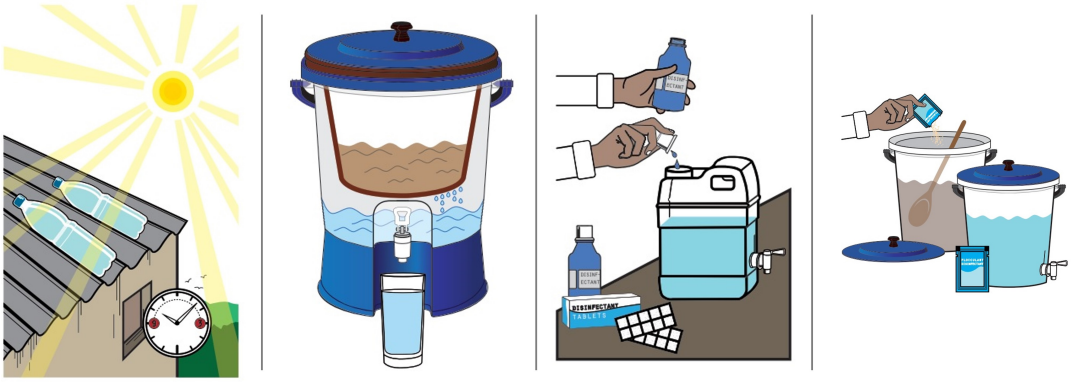

Fig. 1.5 Common HWT options (from left to right): SODIS, ceramic filtration, chlorination, and coagulation/flocculation [3].

1.6.1 Boiling

Boiling is the most commonly used HWT method (Fig. 1.6), with approximately 600 million people using it worldwide. However, it is an inconvenient and energy inefficient method causing indoor air pollution as it is commonly done in a pot using a small wood or charcoal cook stove [37]. Even though boiling is very efficient in reducing pathogens, unsafe storage and handling leads to recontamination after boiling [4].

1.6.2 Filtration

At the time of the report by Lantagne et al. [8] in 2011, filtration was the least studied HWT intervention and the need for regular maintenance was thought to pose a challenge to implementation; however, more recent data show that in some parts of Asia, there is a strong growth in filter markets (Fig. 1.6) [3], and filters have a higher initial and over time use compared to other HWT technologies [7].

There is a wide variety of filters ranging from advanced ultrafiltration modules with pore sizes of $\leq$0.02 μm to ordinary cloths, providing different levels of protection. It has been reported that even simple straining with a folded sari cloth that had an effective pore size of 20 μm reduced cholera cases by half [37]. Furthermore, there are studies (e.g.

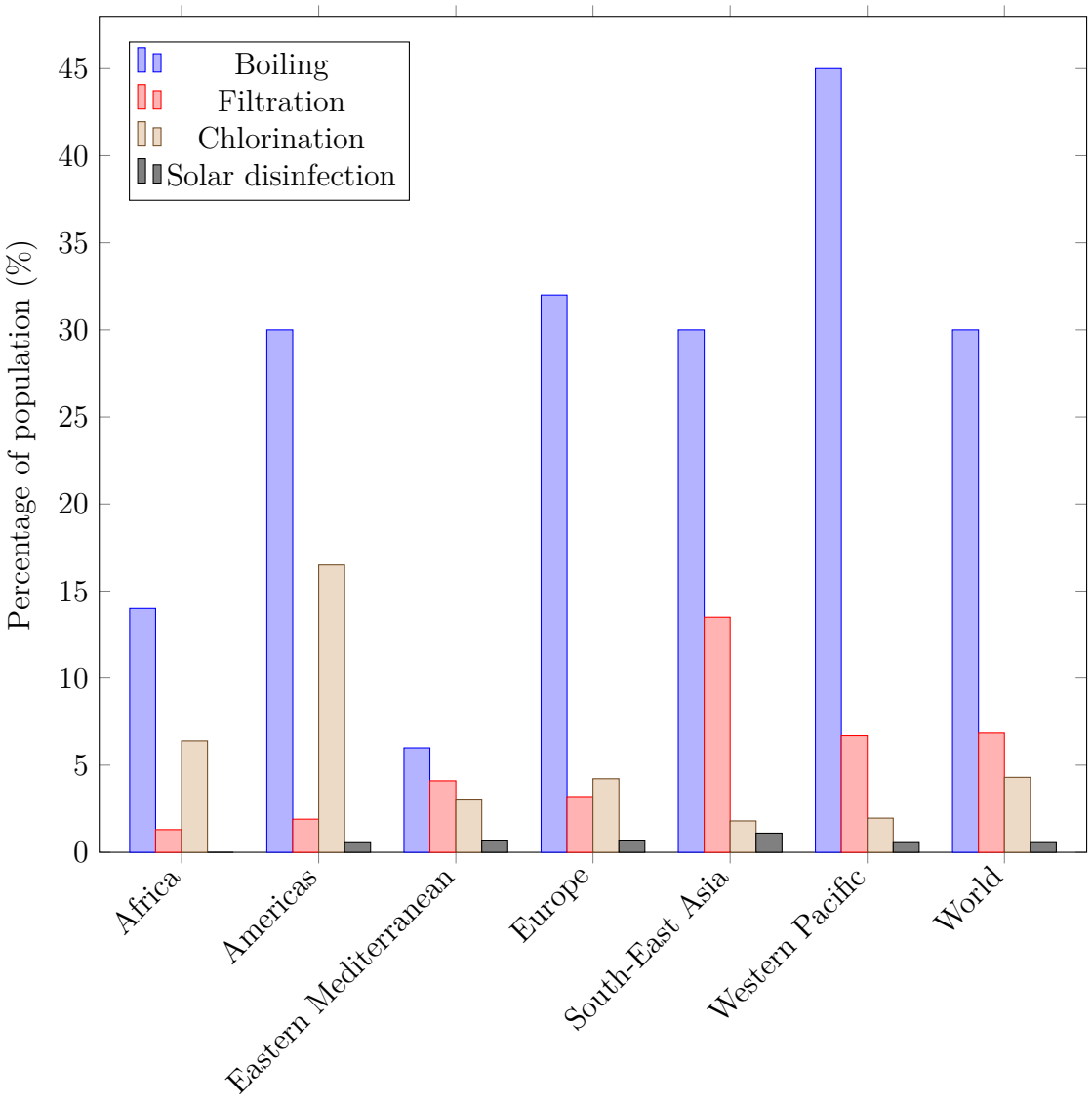

Fig. 1.6 Percentage of population reported treating water in the household, by WHO region, 2012 [4]

Igboro and Daouda [42]) on the application of the luffa plant as a filter media, due to its porous structure, degradability and availability [43].

Since the removal mechanisms of filters are based mainly on size exclusion, testing filtration products can be scaled down to bacteria and viruses that are much smaller than protozoa such as *Cryptosporidium* [7].

Membrane filtration

Membrane filters are typically comprised of hollow fibre membranes in a cartridge. The determinant of a membrane filter's performance is the pore size of the membrane and seal integrity [3, 7]. In membrane filtration, maintenance is required because after a period of use, membrane will be fouled, requiring backwash to remove the reversible fouling [44].

Ceramic filtration

Ceramic filters are made by mixing clay and combustible material such as sawdust, which creates porous structure when burned, through which water is filtered. A typical form of ceramic filters is the clay-pot filter which can be made locally at a low cost. Mechanisms of removal of microorganisms by ceramic filtration are physical, a combination of size exclusion and adsorption, and the determinants of efficacy are pore size and manufacturing quality. Often ceramic filters are coated/impregnated with bacteriostatic agents such as silver nitrate or colloidal silver [3, 7, 10, 11, 37].

In a comparative study by Hunter [41], ceramic filters were estimated to be more effective at reducing disease over 12 months than all other interventions considered (biosand filter, chlorine, coagulant-chlorine and SODIS). However, a drawback of ceramic filters is their very low flow rates (1.5–2.5 L/h for a typical 12- to 14-L ceramic filter pot [37]), necessitating the installation of multiple filters to meet the demand.

Biosand filtration

There are different versions of the biosand filter, but most widely used is a concrete container 0.9 m tall and 0.3 m square, filled with sand (grain size of 0.15–0.35 mm). As the water level is kept few centimetres above the sand by adjusting the outlet height, a biofilm layer grows on the top layer of the sand, called Shmutzdeke, which is responsible for removal of pathogens and colloids [8, 11, 12]. A perforated plate is placed above the sand for better water distribution as well as preventing the disruption of the bioactive layer. The cleaning procedure is simply removing the top few centimetres of sand and disposing the overlaying water [10].

Biosand filtration has shown good *Giardia* and *Cryptosporidium* removal; however, the performance relies on the state of the biofilm layer, which requires time to mature. Similar to ceramic filters, biosand filters have also a limited flow rate, with a reliable production of 15–20 L/d for a typical filter [37].

1.6.3 Disinfection

Disinfection is the inactivation of pathogenic microorganisms including bacteria, viruses and protozoa by exposure to chemical and physical agents [45]. The most common chemical and physical disinfection methods are chlorination and UV disinfection, respectively.

UV disinfection

UV irradiation damages the microorganisms' intracellular proteins and nucleic acids, impairing their cell binding and/or ability to replicate. The efficacy of UV disinfection relies on the delivered dose (a function of light intensity and exposure time). Most commercial UV lamps for small-scale water treatment systems are low-pressure with a wavelength of 254 nm (UVC), which is in the effective range of 200–280 nm [3, 7].

Solar disinfection (SODIS)

Solar disinfection is an effective method in sunny locations such as subtropical regions. It inactivates microorganisms though a combination of mechanisms. The UV irradiation alters nucleic acids, the dissolved oxygen absorbs light causing the generation of photo-sensitive molecules in water (iron oxides), which result in oxidative activities that damage cell structures; moreover, exposure to the sun increases the temperature, denaturing the proteins within the microorganisms. The method is simply done by filling transparent bottles (e.g. 0.3–2.0 litre uncoloured PET water bottles) and exposing them to the sun, usually on rooftops [3, 7, 10].

Despite the method's low cost, there are several drawbacks (not addressed in Table 1.2):

- treatment volume limited by the number of bottles available;
- long treatment time (6 hours–2 days depending on the weather);
- no visual indicator for completion of treatment.

Chemical disinfection (chlorination)

Chemical disinfectant such as chlorine primarily act by damaging (oxidizing) microorganisms' biochemical building blocks and disrupting vital cell functions. The efficacy of chemical disinfectants depends on the chlorine concentration, contact time and water characteristics including temperature, pH and the concentration of natural organic matter (NOM), which vary in natural waters. Therefore, in order to provide residual protection, it is necessary that the treated water is monitored regularly to ensure that the free residual chlorine concentrations of 0.2–0.5 mg/L are maintained, requiring competent technical support [3, 7, 8].

Chlorination is more common as a secondary treatment after coagulation and/or filtration, but also used as the primary treatment in low- and middle-income settings and

emergencies where there is a risk of waterborne disease [3, 7]. The use of chlorine in HWT appears to be limited due to the unfavourable taste that it imparts as well as the psychological aspect of adding a cleaning product (i.e. bleach) to treat water [37]. Moreover, the efficacy of chlorination is diminished at high levels of turbidity as particles shield microorganism from coming into contact with chlorine [7].

1.6.4 Combined methods

A multi-barrier approach to water safety, i.e. combination of technologies to treat water, is recommended by WHO. For instance, chlorine disinfectants that provide only targeted protection against bacteria and viruses can be combined with a method effective against protozoa (e.g. filtration) to achieve comprehensive protection [3].

Coagulation-disinfection

This method provides a multi-barrier approach, in which a coagulant/flocculant (e.g. iron or aluminium salts) causes suspended particles and larger microorganisms such as protozoa to aggregate and settle, while a disinfectant (e.g. calcium hypochlorite) inactivates bacteria and viruses through oxidative reactions [3, 7].

Coagulation-biofiltration

A multi-barrier approach, in which a coagulant aggregates suspended particles and large microorganisms such as protozoa and then the aggregates are removed though filtration. The biologically active layer (biofilm) at the top can inactivate pathogens and the remaining section of the filter medium acts by physical separation of pathogens [7].

Table 1.2 Summary of common HWT options' performance criteria, advantages and limitations [3, 7–13].

HWTS option	Removal effectiveness (log_{10} reduction)			Visual improvement?	Taste alteration?	Limited by turbidity/NOM	Residual protection?	Easy to use?	Frequent maintenance?	Possible to produce locally?	Requires power source?
	Bacteria	Viruses	Protozoa								
Boiling	High	High	High	No	–	No	No	Requires preparation	No	Yes	Yes
Membrane filtration	High	Depends*	High	Yes	No	No	No	Usually	Yes	No	No (most)
Ceramic filtration	Medium** (1.3 or 2.5***7)	Low** (0.4–2.5)	High** (4–6)	Yes	No	No	No	Yes	Yes	Yes	No
Biosand filtration	Low† (0.4–3)	Low† (0–4)	Medium† (2–4)	Yes	No	No	No	Yes	No	Yes	No
UV disinfection	High††	Depends††	Depends††	No	No	Yes	No	Yes	No	No	Yes
Solar disinfection	High‡ (2.5–5.5+)	High‡ (1–4+)	High‡ (1–3+)	No	No	Yes‡‡	No	Requires planning	No	Yes	No
Chlorination	High‖ (3–6+)	High‖ (3–6+)	Low	No	Yes	Yes	Yes	Yes	No	Yes	No
Coagulation-chlorination	High (7–9)	High (2–6)	High (3–5)	Yes	Yes	No	Yes	Multiple steps	No	Yes	No
Coagulation-biofiltration	Medium	Low	High	Yes	Yes	No	No	Multiple steps	No	Yes	No

* Depends on the pore size and seal integrity.
** Depends on the pore size/structure, tortuosity, filter medium composition, etc.
*** Higher removal if coated/impregnated with silver nitrate or colloidal silver.
† Depends on filter maturity, flow rate, grain size, etc.
†† Depends on the UV dose.
‡ Depends on sunlight intensity, exposure time, temperature, container material, etc.
‡‡ Requires pretreatment if water turbidity is above 30 NTU.
‖ Depends on turbidity, contact time, chlorine concentration, water matrix, etc.

1.7 The SAFEWATER project

SAFEWATER was a collaborative project between Ulster University and several universities/NGOs in Brazil, Colombia and Mexico to develop low cost technologies for safe drinking water in developing regions, addressing the socioeconomic impact of waterborne diseases. The HWT system (Fig. 1.7) consisted of two treatment steps, filtration and UV disinfection. This PhD aimed to address the primary limitations and challenges relating to the performance and sustainability of cartridge filters, with outputs feeding into the project.

Fig. 1.7 Images of the SAFEWATER HWT system in the field, consisting of two treatment steps, filtration and UV disinfection.

Chapter 2

Literature review

2.1 Introduction

Universal and equitable access to safe and affordable drinking water for all is Target 6.1 of UN Sustainable Development Goals (SGDs) [24]. Safe drinking water is not only a prerequisite to human health and well-being, but contributes to livelihoods and dignity. Consumption of unsafe water impairs health through diarrhoeal disease, impeding productivity. Investment in safe water is not only investment in equity, security and reducing poverty, but also has an economic return of at least four times [27, 35]. Household water treatment (HWT) technologies have enabled billions of people across the world to treat contaminated surface waters for household use, protecting their children and other vulnerable family members.

2.1.1 Water quality monitoring

Due to the challenges associated with monitoring affordability, data on safely managed services is only available for 45 percent of the global population [2]. Turbidity, which describes the lack of transparency or scattering of light as a result of presence of chemical

precipitates, inorganic and organic particles, can be measured simply and reliably by a variety of devices including online, benchtop and portable meters as well as low-cost turbidity tubes. Turbidity meters measure scattering of light from a range of sources (e.g. LEDs and laser), with results expressed in units indicating the method of measurement. The most common method for turbidity measurement is the nephelometric method, expressed in Nephelometric Turbidity Units (NTU). Turbidity below 4 NTU can be only detected by turbidity measurement devices; however, at 4 NTU and above, a muddy, red brown or black suspension can be visible, affecting the aesthetics of water (see Fig. 2.1) and reducing its acceptability [46, 47].

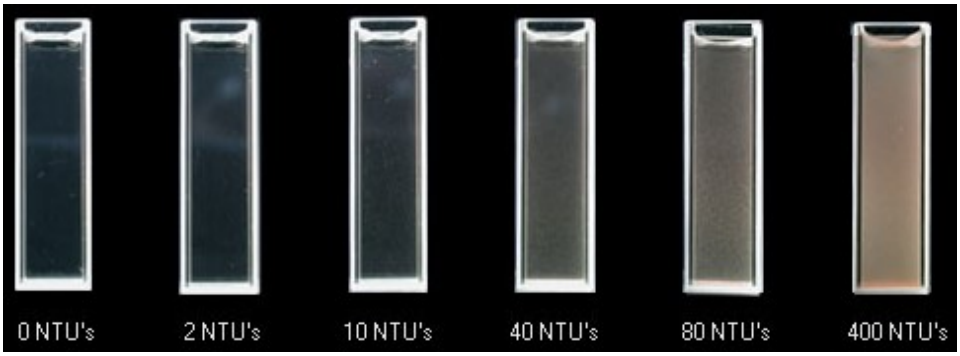

Fig. 2.1 Turbidity and water clarity have a negative relationship [5].

Although turbidity itself does not necessarily represent a direct risk to public health, it can be an indicator of the presence of pathogens (microorganisms attached to particles) and hazardous events throughout the water supply such as sloughing of oxid scales and biofilms or leakage of contaminants through faults [46]. Furthermore, turbidity is a recommended measurement for water quality in the WHO Guidelines for Drinking-water Quality [48]. Turbidity can be a basis for choosing among available source waters and assessing the performance of treatment technologies including coagulation/flocculation, clarification, and filtration [46].

Turbidity reduces the effectiveness of household water treatment (HWT) systems by

clogging filters, lowering UV transmission and shielding microorganisms from chemical disinfectants or UV irradiation [49–51]. A study by Christensen and Linden [52] showed that by increasing water turbidity from 1 to 10 NTU, the average dose in the collimated beam reactor decreased by 5–33%, due to absorption, scattering and blocking of UV light by particles, and in a study by Templeton et al. [51], it was found that even at turbidity below 10 NTU, particles could measurably shield bacteriophage T4.

Despite the lack of a direct proportional relationship between water turbidity and concentration of pathogenic microorganisms in natural waters, turbidity removal is proven to indicate pathogen removal and drinking water safety. In low-resource settings keeping turbidity below 1 NTU, recommended by regulatory agencies (e.g. US EPA [53]), is not always possible and WHO has set the maximum 5 NTU limit for such cases [46, 48].

2.1.2 Testing of household water treatment systems

Household water treatment (HWT) systems should be evaluated according to the testing principles set forth in 'WHO International Scheme to Evaluate Household Water Treatment Technologies' [33]. The testing is devised to model actual field and use conditions. Two types of test water has been proposed: general test water (GTW) representing high quality raw water (groundwater and rainwater), and challenge test water (CTW) representing surface water. The GTW is not technology specific, whereas CTW (Table 2.1) is.

2.1.3 Filtration technologies

Filtration is considered the most practical process for removing turbidity and suspended particles in drinking water application. With proper design and operation, filtration can be an effective and consistent barrier for suspended particles and pathogens, in particular *Cryptosporidium* oocysts which are not inactivated by chlorine disinfection.

Table 2.1 Challenge test water characteristics [14].

Constituent/ organism	**Unit**	**Specification/ concentration**	**Adjustment material/ microorganism**
Chlorine	mg/L	< 0.05	None
TOC*	mg/L	15 ± 5	Humic acid
Turbidity	NTU	40 ± 10	ISO 12103-A2 fine test dust [54]
TDS†	mg/L	1500 ± 150	Sea salts
Alkalinity (as $CaCO_3$)	mg/L	100 ± 20	Sodium bicarbonate
Bacteria	CFU/mL	$\geq 10 \times 10^6$	*E. coli*
Virus	CFU/mL	$\geq 10 \times 10^8$	MS-2 coliphage with host organism *E. coli*
Protozoa	oocysts/mL	$\geq 5 \times 10^4$	*Cryptosporidium parvum*

* Total organic carbon
† Total dissolved solid

There are different filtration technologies such as granular filtration, ceramic filtration, diatomaceous earth filtration, bag and cartridge filtration, microfiltration (MF) and ultrafiltration (UF), with each being suitable for a range of flow rates and raw water characteristics [48, 55–58].

With respect to low-volume filtration, cartridge filtration, which consists of single (or multiple) filter element(s) inside a housing (Fig. 2.3), is suitable for small scale systems. Cartridge filters do not require specialist knowledge to operate and provide a one-step separation without prior coagulation and flocculation. However, cartridge filters require high quality inlet water, and they should be replaced when the pressure drop in the system is above the operating range or a sudden change in pressure is recorded, meaning that the cartridge filter has ruptured [6, 56, 59, 60].

The cartridge filter elements are commonly fibrous, constructed of polypropylene or polyester and manufactured via different technologies (Fig. 2.4). The performance of these filters is attributed to their large surface area formed by fibres and the complex

(a) 10 inch cartridge filter

(b) 10 inch cartridge filter housing

Fig. 2.3 The cartridge filter element is placed inside the housing and sealed.

structure of the pore space. The common cartridge filters on the market are wound, spun (meltblown) and pleated filters, with a variety of nominal ratings, typically 100, 50, 25, 10, 5 and 1 micron. Some vendors might report their filters' absolute rating (98.7% removal of solids above the size rating on a single pass) and Beta ratio (the ratio between the number of particles with a size above the size rating per unit volume of suspension upstream of the filter to the same parameter in the downstream); however, the rating on vast majority of the retail filters is the nominal rating (50% removal of particles above the size rating). Nevertheless, filter media do not not have an immovable structure and pores might be affected by the flow pressure [61–65].

There are only very few publications on the use of fibrous cartridge filters for water treatment. Pawlowicz et al. [66] used cartridge pleated and wound filters to remove a cyanotoxin, microcystin-LR, in deionised water, reporting a removal of 5–6%. Viccione et al. [67] investigated the head loss caused as a function of the amount of fine sand (size: 0.1 mm) trapped in a wound cartridge filter placed in a hydraulic system consisting of a tank, pump, and cartridge filter. The work was continued by Evangelista et al. [68] to enhance the hydraulic performance of the cartridge filters by placing different materials such as marble pebbles or ceramic cylinders between the filter element and housing wall

Fig. 2.4 There are three main types of commercial cartridge filter elements for water treatment: spun (left), wound (middle) and pleated (right).

to create a pre-filtration step to remove the fine sand (size: 0.1 mm) added to water, reporting increased lifetime of the wound filters. However, the results were only presented as pressure drop against the amount of find sand added to water and the fine sand used with a size of 0.1 mm does not represent suspended particles in natural waters—particles with a size of 0.1 mm settle down quickly (settling velocity of 23 mm/s [69]).

Sikorska et al. [63] highlighted that the existing models for granular filtration do not apply to fibrous filtration due to the differences in shape and size of collectors (fibres compared to grains) and flow conditions. They proposed a macroscopic model predicting the pressure drop and the suspension concentration in the filtered water for multi-layered spun filters (non-commercial) by estimating the change in filter's porosity, based on scanning electron microscopy images, against the deposited particle mass in the filter.

2.2 Cake and depth filtration

The two categories of physical filtration (irrespective of the surface chemistry of filters) are cake filtration and depth filtration (Fig. 4.1). In depth filtration, separation happens

through the depth of the medium where particles are deposited. In this type of filtration, particles with smaller size than the pore size of the filter can be removed in a two-step process:

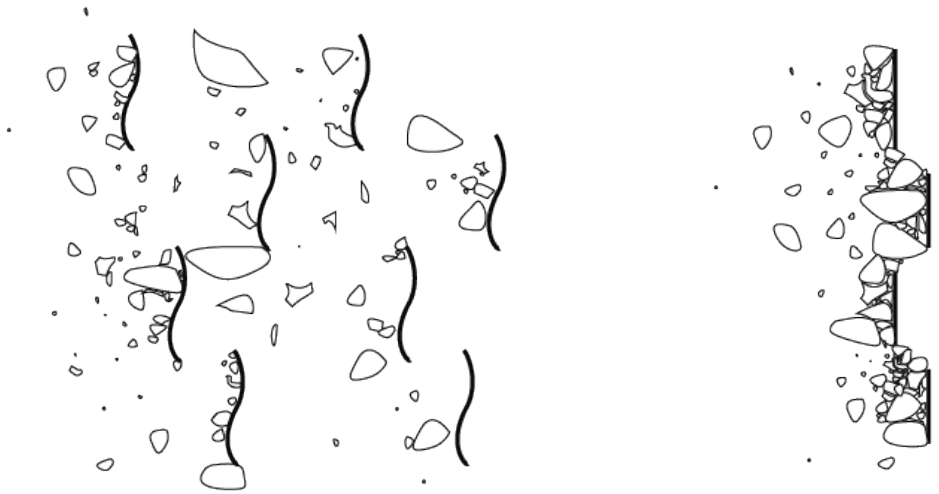

(a) (b)

Fig. 2.5 The two main categories of filtration: (a) depth filtration and (b) cake filtration.

(i) transport (advection), a physical-hydraulic process affected by mass transfer, via different deposition mechanisms, namely, inertial impaction, gravity (only in gravitational flows), interception and Brownian diffusion, depending on the particle size (Fig. 2.6). The dominant transport mechanisms for sub-micron (<1 μm) particles is Brownian diffusion (the random movement of particles in a liquid as a result of bombardment by the surrounding molecules), for particles with the size of 1–5 μm, interception (when a particle following streamline collides with a collector/grain because of its proximity), and for particles larger than 5 μm, inertial impaction and gravitational (both caused by deviation of a particle from the streamline);

(ii) attachment, a chemical process, as a result of attractive close-range molecular forces such as surface chemical interactions, electrostatic forces, hydrophobic interactions, hydration and Van der Waals forces, which can be explained by the Derjaguin, Landau, Vervey, and Overbeek (DLVO) theory [6, 70–75].

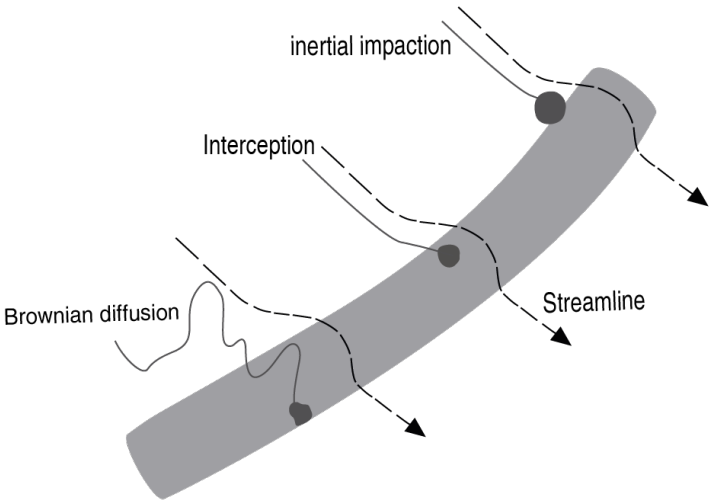

Fig. 2.6 Three main filtration mechanisms: inertial impaction, interception and Brownian diffusion.

In cake filtration, the medium acts as a screen, retaining particles, resulting in the formation of a cake layer. Empirically, cake formation happens when particles are larger than one third of the medium pore size. The filter cake can act as a depth filter itself if it is not too densely packed, retaining finer particles in the cake [6, 57, 76]. A filter cake is classified as either incompressible or compressible, depending on whether the cake shape may be rearranged due to the drag force caused by water flow [77]; thus, the resistance of a compressible cake to flow is variable depending on the pressure it is subjected to [72]. Cake filtration is commonly applied to clarify suspensions of high solid content while depth filtration is used to treat low solid content suspensions [76]. Usage of precoating in cake filtration is desired when clear filtrate is required at the beginning of the filtration cycle [78]. Precoat filtration is used for treatment of swimming pool water, protein

recovery and in food industry for filtration of highly fouling products such as wine and beer [79–81].

2.3 Particle characterisation

Although turbidity is widely used as the main parameter for evaluating water quality, it does not give any information about the characteristics of suspended particles. Knowing the size distribution and surface charge of particles can help understand the underpinning mechanisms in filtration and analyse the results.

2.3.1 Equivalent spherical diameter

Presenting particle size with a single number, i.e. diameter, is preferred for engineering calculations. The concept of the equivalent spherical diameter considers a sphere with the same volume of the particle. A depiction of this concept is shown in Fig. 2.7 [82].

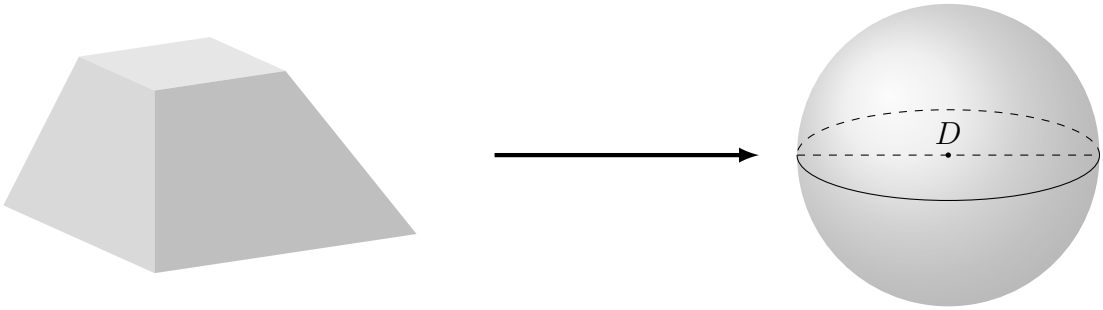

Fig. 2.7 Equivalent volume sphere of a particle with an arbitrary shape.

Dynamic light scattering (DLS) particle size analysers estimate a particle's size by measuring the particle's speed and calculating the diameter of the sphere that diffuses at the same speed. Large particles have minimum movement with small change in their position, whereas small particles exhibit large movements [83]. In some processes, particle shape is important; for example, in sedimentation, a flat particle will oscillate like a feather, taking a longer time to reach the bottom. In such cases that particle shape needs

to be considered, it can be quantified using the Wadell's sphericity (Ψ), defined as:

$$\Psi = \frac{\text{surface area of a sphere with equal volume as the particle}}{\text{surface area of the particle}} \tag{2.1}$$

Sphericity is unitless and its value is fractional, e.g. 0.22 for clays and kaolin, or unity in the case of a sphere [82].

As we deal with more than one particle, the mean diameter is reported. There are three types of mean diameter: arithmetic, geometric and harmonic, each being calculated differently. The mean particle size given by DLS particle size analysers, called Z-average, is the the intensity weighted harmonic mean, derived from a cumulants analysis of the measured correction curve [83, 84]. Another size classification is based on a subscript for diameter, d, defining the percentage of particles below a specific particle size. Two frequently reported diameters are d_{10} and d_{50}, called efficient and median diameter, respectively [77, 83]. Therefore, particle size data will be represented differently depending on the statistical diameter utilized [82].

2.3.2 Particle size distribution

Particle size distribution (PSD) is the representation of size of particles based on the fraction of different size ranges in terms of volume, number or surface area. PSD is commonly presented in volume/mass distribution rather than number. Volume fraction of a size range can be calculated by Eq. 2.2.

$$m_\mathrm{i} = \frac{k_\mathrm{v} x_\mathrm{i}^3 \rho_\mathrm{s} f_\mathrm{i}}{\sum k_\mathrm{v} x_\mathrm{i}^3 \rho_\mathrm{s} f_\mathrm{i}} = \frac{x_\mathrm{i}^3 f_\mathrm{i}}{\sum x_\mathrm{i}^3 f_\mathrm{i}} \tag{2.2}$$

where k_v is the volume shape coefficient ($\pi/6$ for spheres), and x_i and f_i are the size and number of particles in the range i, respectively.

In case volume shape coefficient is constant through all size grades, it will be cancelled

out [82]. It is evident from Eq. 2.2 that in a volume/mass-based PSD, larger particles constitute a larger fraction compared to a number based PSD. Particles are classified as monodisperse if all have the same diameter, otherwise they are classified as polydisperse [77].

Another way to present PSD is by a cumulative distribution, a curve starting at 0 that goes up to 100 (or 1). A cumulative curve has an 'S' shape and a distribution curve has a bell shape. In essence, a cumulative curve can be obtained by integration of a distribution curve and a distribution curve can be obtained by differentiation of a cumulative curve [82].

2.3.3 Particle surface charge

The surface charge of particles can be measured indirectly by estimating the electrophoretic mobility/ zeta potential. As a colloidal particle moves in an electric field, some of the counterions in the ion cloud surrounding the charged particle move with it, causing a shear plane that marks the separation between the fixed ions and the ion cloud. The electric potential from the shear plane to the bulk of the solution is zeta potential (Fig. 2.8), ξ, considered as the particle charge, reported in millivolt (mV). However, zeta potential cannot be measured directly, but can be calculated using experimentally-determined electrophoretic mobility.

Negatively charged particles in an electrical field move toward the positive, with their velocity depending on the particle charge, the voltage gradient and water viscosity. The ratio of the particle velocity to the voltage gradient is termed electrophoretic mobility with the units μm/s/V/cm, which can be used for calculating zeta potential. Measuring charges on particles can facilitate determining the coagulant dose for neutralizing particles (reaching the isoelectric point) by plotting zeta potential versus coagulant dose (further discussion in Section 2.5) [6, 69, 85].

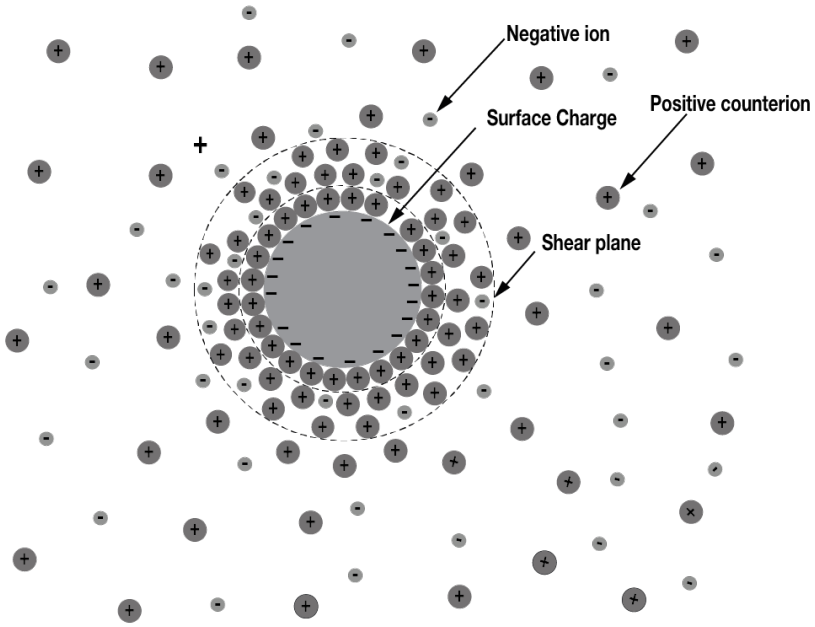

Fig. 2.8 Counterions surround the negatively charged particle. Zeta potential is the potential measured at the shear plane.

2.4 Precoat filtration

2.4.1 Precoat filtration in water treatment application

Cake/precoat filtration has evolved from the application of fossil diatoms to drinking-water treatment after it was discovered in Germany. A precoat filter consists of a medium, e.g. diatomaceous earth, deposited on a septum with a sufficiently small mesh size (commonly 60 μm) to retain the media. The septum is a fabric made from materials such as stainless steel, titanium, polypropylene, polyester, and so on [69, 86, 87].

In practice, a slurry of media is circulated through the septum until the outlet is clear (turbidity is <0.5 NTU), resulting in a deposit of media (precoat). The precoat would be distributed uniformly as areas with less deposits carry a higher velocity and thus a higher mass flux. During circulation, smaller particles are captured as bridging happens between larger particles. After that a cake layer is formed, the filtration process is commenced and resumed until the headloss reaches the design limit; then, the cake layer is removed, and

the whole procedure is repeated for another cycle. During filtration, body feed, usually the same material as the precoat, can be injected into the raw water to inhibit suspended matter from creating a cake layer of its own, blinding-off the filter and increasing the pressure drop rapidly (Fig. 2.9) [69, 88, 89].

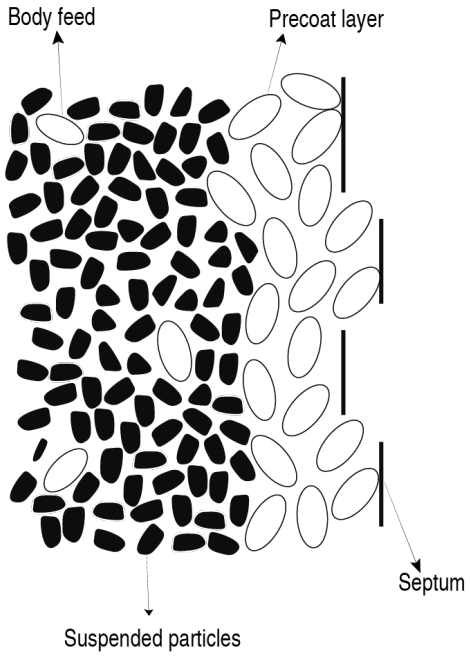

Fig. 2.9 A schematic showing the role of the precoat layer and the body feed. The precoat layer strains finer particles and protects the septum; the body feed prevents the development of a dense cake layer, improving permeability.

2.4.2 Filter aids for precoating

In industry, the filter media in precoat filtration such as diatomaceous earth, perlite and cellulose are known as 'filter aid'. Filter aid materials are used for two operations, precoating and body feeding [78, 90]. The precoat layer has three primary functions: (i) to remove particles from raw water; (ii) to protect the septum from fouling; (iii) to facilitate cake removal at the end of a cycle. Common filter aids are diatomaceous earth (DE or diatomite), perlite (a volcanic ash) and cellulose [69, 91].

Diatomite/diatomaceous earth (DE) is the most common filter aid, composed of fossilized

skeletons of microscopic single-celled algae called diatoms. The are two categories of diatoms: seawater and freshwater, with small differences in their composition [90, 92]. For turbidity removal, diatomites of marine origin are more effective, removing particles sizes below 0.5 μm [78]. DE is almost pure hydrous silica ($SiO_2 \cdot nH_2O$), an inert material (i.e. no taste or color is caused by it when in contact with water). Due to its features such as highly porous, permeable and chemical resistant structure as well as high specific surface area, it is used for filtration in different industries including pharmaceuticals, sugar syrup, wine, beer and water treatment [69, 90, 93, 94].

Shapes and sizes of diatoms are varied, most in the range of few microns to over 100 µm. The DE used for water filtration has a wet specific gravity of about 2.3 and median particle size of 23–36 μm, resulting in a precoat mean pore diameter of 7–17 μm [69, 89, 94].

Perlite is a glassy volcanic rock that is made into filter aid by heating its ore to its melting temperature, causing it to expand 4–20 times of its original volume and fracture; then, it is milled and classified. The product is a highly porous material with plenty of interstices. Compared to DE, perlite has the advantage of being pure and have a lower density (32–70% of DE) [78, 94, 95].

Cellulose is the main constituent of wood, obtained by treating wood with heat and chemicals which dissolve the lignin and separate fibres. Cellulose that is processed for filtration application is an environmental friendly alternative to other conventional filter aids. As a rough approximation, cellulose filter aids are up to 50% more expensive, but the amount required for precoating is 50% less [78, 96]. Selection of filter aids practically comes down to their availability as transportation costs determine an option's viability [78].

2.4.3 Precoat filtration guidelines

The precoat layer has small and numerous water passageways, making the removal of very fine particles possible, with DE filtration removing all *Giardia* cysts. However, precoat filtration is most effective and economical at moderate to low turbidity (<10 NTU). Moreover, precoat filtration offers several advantages over granular filtration, most importantly the physical nature of the process, which does not require the addition of coagulants and operator expertise in water chemistry. In the case of turbidity levels above 10 NTU, pretreatment should be evaluated in terms of economics and efficiency. The nature of suspended particles affects the efficiency and filter fouling. Therefore, knowledge of the types and quantity of algae present, fine clays or organic colloids in a water source is important [89, 94, 97].

The primary removal mechanism in DE filtration is straining and embedding, i.e. particles are removed when they are larger than the pore openings. For example, the finest commercial grade of DE, Filter-Cel™, has an average pore size of 1.5 μm; therefore, viruses (10–400 nm) are small enough to move within the cake while *Giardia* cysts (10 μm, oblong form) cannot. However, bacteria (1 μm) would be also captured despite a smaller size than pore openings. Another factor that would also influence the removal is hydraulic loading rate (HLR) or filtration velocity. It does not affect cyst removal as they are large relative to the commonly used DE grades in water treatment ($18 \leq d_{50} \leq 24$ μm), but bacteria can be mobile in coarser grades of DE [69, 94, 97, 98].

Filter aid surface modification

The finest grade of DE has a particle removal size range of down to 0.1–1 μm; however, DE can be coated to remove even finer particles. Coated DE is a term used when DE is conditioned with coating of chemicals. Conditioning with aluminium hydroxide or specific polymers enhances the removal efficiency of bacteria, viruses and mineral colloids,

at the expense of increasing the rate of pressure drop [69, 94, 98].

Beauman et al. [99] have patented a blend precoat to overcome the problem of bacteria growth on filtration media. The composition used for precoating is silver-treated powdered cellulose mixed with a major proportion of 'precoatable' activated carbon. Fine filtration was achieved with the novel precoat and the bacteria on the media were inactivated—within 68 hours of water stagnation after treating 9 m^3 of contaminated water, an initial bacteria concentration of 3.2×10^5 CFU/ml was reduced to 2 and 7 for the two filter elements tested, proving the bacteriostatic effect of the coating.

2.4.4 Precoat filtration in practice

Research on DE filtration started during World War II when the U.S. military was looking into a more suitable technology for particle removal than sand filtration, in which straining is limited to particle size of about 80 μm and larger. The consequent research established that *G. lamblia* cysts are removed by all grades of commercial DE while turbidity and bacteria removals depend on the DE grade and whether a coagulant is added [6, 69, 89].

In a study by Boittelle et al. [80], wine was filtered with DE (Diatomyl® P00, permeability of 4500±1 mD), with a 2 kg/m^2 precoat layer (50 g deposited on 0.024 m^2). In the experiments, the inlet turbidity of 20±2 NTU was reduced to 9.8±0.6 NTU, the yeast concentration from 2.7×10^4 CFU/100 ml to 3.4×10^2 CFU/100 ml and total bacteria from 2.5×10^5 CFU/100 ml to 1.3×10^5 CFU/100 ml, while chemical properties were unchanged.

Christensen et al. [79] compared the performance of precoat filtration, using three different filter aids—Harbolite®, Aquatec perlite and Arbocel®—with a conventional sand filter for treatment of swimming pool water. The septum used for precoat filtration was a polyester twill woven mesh with a thickness of 1 mm and thread thickness of 0.5 mm,

taken from a tube in a full-scale precoat filtration tank. They concluded that removal efficiency of the precoat filters were generally higher than the sand filter, especially in the case when particles were smaller than 10 μm. In addition, the filtration cycles in precoat filtration were longer (two weeks) than sand filtration (one week), reducing the consumption of wash water by 88%. However, the addition of a flocculant to the raw water upstream of the sand filter resulted in a similar efficiency as the precoat filter. In addition, TOC and conductivity were measured, showing that neither precoat filtration nor sand filtration were capable of removing organic carbon or dissolved solids.

In summary, studies have showed that precoat filtration is a better option than sand filtration when prior flocculation is not implemented, which is usually the case in HWT systems. Hence, a dual media filtration unit made up of a disposable layer of precoat on a cartridge filter will benefit from both technologies and provide a higher level of safety.

2.4.5 Commercial pleated filter elements as septa

One way to improve the dirt-holding capacity is to change the 'density' of the filter media from inlet to outlet, so that particles are removed gradually throughout the media. For example, dual layer structures with a high porosity layer on the upstream side and a layer with smaller pores on the downstream side behave like multi-stage filters [65].

Typically in precoat filtration, particles are removed by the precoat (cake) layer and the septum is just a barrier to avoid cake particles entering the effluent. However, using a pleated filter as the septum would result in a 'gradient density' filter media, which is essentially a two-step filtration process.

2.5 Coagulation

In natural waters, particles are either organic (e.g. microoganisms and plant litter) or inorganic (e.g. clay), but both categories typically have a negative surface charge, preventing aggregation for long periods of time. In addition, as a result of decay of organic debris, water can contain dissolved organic matter (DOM), which also has a negative charge. As a result, these particles are naturally repelled by the negatively charged surfaces of filter media.

The addition of hydrolyzed or prehydrolyzed metal salts or cationic organic polymers, known as the coagulation process, can neutralize the negative surface charge of most particles in natural waters with neutral pH (6–8). Coagulation conditions the suspended, colloidal and dissolved matter, allowing for subsequent removal [6, 69, 85].

There are various factors affecting the required type and dose of a coagulant, namely, water temperature and quality, concentration and characteristics of NOM, and concentration and type of particulates. Hence, the performance of a coagulation process cannot be predicted theoretically, and jar testing is typically used for coagulant screening, with results being evaluated in full-scale operation [6]. However, the jar test does not work well for low turbidity (e.g. <0.5 NTU) or low alkalinity (e.g <50 mg/L as $CaCo_3$) water, as settleable flocs do not develop. For such situations, in-line filtration (rapid mix and filtration) is appropriate [69].

For coagulation to achieve the desired outcome, there are two steps that need to be considered: (1) choosing the proper pH, the proper coagulant and the proper dosage, and (2) causing contacts between the colloidal particles and the coagulant [6, 69].

2.5.1 Natural organic matter (NOM)

Particulate organic matter (POM) and dissolved organic matter (DOM) are referred to as natural organic matter (NOM). NOM have negative charge (in pH> 5) as they contain

carboxylic acid groups, and in surface waters, their molecular weight, charge density, molecular structure and acidity varies temporally and spatially [85]. The particulate fraction of NOM, similar to inorganic particles, is easily removed from water following coagulation [6, 69]. However, the dissolved fraction carries a much greater charge and reacts or binds with metal ion coagulants; hence, the coagulant dosage is determined by NOM-metal ion interactions and not metal-ion interactions [6, 69, 85]. Mechanisms involved in NOM removal by hydrolysing coagulants are charge neutralization, adsorption, complexation and entrapment [100].

DOM is categorised into two components: hydrophobic/High Molecular Weight and hydrophilic/Low Molecular Weight. The hydrophobic fraction of DOM is mainly composed of humic substances—humic acid (HA) and fulvic acid (FA) [101]—as a result of aquatic and terrestrial biomass decomposition. Humic substances are regarded as natural anionic polyelectrolytes (in pH>4), representing approximately more than 50% of DOM in surface waters. The hydrophobic fraction has a higher specific colloidal charge, making it easier to be removed. Therefore, the coagulant is significantly affected by NOM hydrophobicity [85].

The concentration of NOM can be measured as total organic carbon (TOC), which has two components: particulate organic carbon (POC) and dissolved organic carbon (DOC), which is the fraction of TOC that passes through a 0.45-μm filter. Additionally, the NOM concentration can be estimated via UV absorbance measurement at 254 nm, which is a quicker and more economical method [6, 69].

In surface waters, NOM concentration is in the range of 1–50 mg/L as dissolved organic carbon (DOC), with a median of about 4 mg/L [69]. NOM imparts colour to water, causes odour and taste, provides substrate for bacteria, increases corrosion and most importantly is a precursor to the formation of cancerogenic disinfection by-products (DBPs) such as trihalomethanes (THMs) and halo-acetic acids (HAAs) when water is

disinfected with chlorine [85].

While mineral turbidity is effectively removed at the neutral pH range, NOM optimum removal occurs at slightly acidic pH values (4.5–6). At a higher pH than the minimum solubility of inorganic coagulants, NOM removal occurs primarily by sweep flocculation and bridging [100].

2.5.2 Coagulants

Inorganic coagulants

Inorganic coagulants such as aluminium sulphate or ferric chloride rapidly hydrolyze in water and form insoluble precipitates that adsorb to the surface of particles, which reduces the repulsive charge of particles and/or forms bridges between them [6, 69].

In water industry, alum (aluminum sulfate) is the first coagulant of choice due to its availability and lower cost [102], sold in a hydrated form as $Al_2(SO_4)_3 \cdot xH_2O$ (x is usually 14). The optimal pH for coagulation with alum is 6.9–7.2 and the typical dose range is 10–150 mg/L, depending on the raw-water quality and turbidity. The optimum removal due to the sweep floc mechanism, however, occurs in the pH range of 7–8 with an alum dose of 20–60 mg/L. If too much coagulant is added, the particles will attain a positive charge and become stable again [6, 100, 102].

Depending on water pH, the reaction of metal ions (Al^{3+} or Fe^{3+}) with water results in different products. When 4 <pH< 6, complexes are formed (Eq. 2.3), while at higher pH (6 <pH< 10), metal hydroxide is the major product (Eq. 2.4):

$$Al_2(SO_4)_3 + nH_2O \rightarrow 2Al \cdot (OH)_n (H_2O)_n^{n+} + H^+ + 3SO_4^{2-} \tag{2.3}$$

$$Al_2(SO_4)_3 + 6H_2O \rightarrow 2Al(OH)_3 + 6H^+ + 3SO_4^{2-} \tag{2.4}$$

where $Al_2(SO_4)_3$ is aluminium sulphate, $Al{\cdot}(OH)_n(H_2O)_n^{n+}$ hydrated aluminium complex with water (variable charge and waters of hydration), and $Al(OH)_3$ aluminium hydroxide precipitate.

Consequently, due to the different reaction products, there are two coagulation zones for Al^{3+} or Fe^{3+}: (1) charge neutralization at low pH (pH$<$ 6), in which the positively charged complexes become incorporated within a negatively charged particle's diffuse double-layer, forming a colloid-metal ion complex (Eq. 2.5) and (2) sweep-floc at high pH (pH$>$ 6), in which the positively charged metal precipitate contacts the negatively charged colloids, resulting in particle attachment and enmeshment (Eq. 2.6):

$$\text{colloid}^{\,n-} + Al \cdot (OH)_n (H_2O)_n^{\,m+} \rightarrow \text{ colloid } \cdot [Al \cdot (OH)_n (H_2O)_n]^{(m-n)+} \tag{2.5}$$

$$\text{colloid}^{\,-} + Al(OH)_3 \rightarrow \text{ colloid } \cdot [Al(OH)_3] \tag{2.6}$$

In the presence of natural organic matter (NOM), the sweep floc mechanism is not affected by the type of particles and same dosage is required, instead the dose depends on the type and concentration of NOM as well as pH [6].

Due to the short life time of the complexes (milliseconds), a rapid mixing is required so that collisions between reactants occur [6, 69]. For waters that contain low concentrations of particles, coagulant aids such as clay and diatomite can be added to enhance the coagulation process by forming nucleating sites for the formation of larger flocs [6].

In the selection process of the coagulant for a water treatment system, the drawbacks of metal salt coagulants should be considered as well: (i) alum and ferric increase the total dissolved solids (TDS) concentration in the finished water; (ii) alum and ferric cause a drop in pH as they consume alkalinity, requiring the addition of lime in case the raw water's alkalinity is low; (iii) ferric-based coagulants are corrosive and cause rust-coloured stains if spilled [85, 102]. However, recently developed pre-hydrolized coagulants such as

polyaluminium chloride (PACl) have overcome some of the limitations of the conventional coagulants, e.g. less impact on water pH [102].

Organic coagulants

Since 1960, synthetic ionic polymers, called polyelectrolytes (PEs), have been increasingly used in drinking water treatment, and now they are used in almost every water utility. PEs have several advantages compared to inorganic coagulants including lower dose requirement, lesser sludge production, no effect on pH/alkalinity and working well at a wider range of pH [69, 102, 103].

Cationic polyelectrolytes adsorb strongly to negative particle surfaces, with unattached segments attaching to other particles. Removal of natural organic matter (NOM), essentially natural anionic polyelectrolytes, can be achieved with cationic polyelectrolyte as well [103]. However, PEs such as PDADMAC (polydiallyldimethyl ammonium chloride) do not have the same performance as the inorganic coagulants when it comes to removing NOM [102].

Selection of the polymer and its dosage, point of injection and mixing intensity are variables that need to be optimized prior to full-scale implementation; also, the effect of these variables on the consequent filtration unit in terms of treated water turbidity, headloss increase and clogging should be considered [69].

Performance of cationic polyelectrolytes depend on their molecular weight (MW), charge density (CD), and the chemical structure of the monomer [104]. MW is categorized as low, medium and high when it is $<10_5$, 10_5–10_6, $>10_6$, respectively, and CD, expressed as mol% of ionic groups, is categorized into low, medium and high when it is 10%, 25%, 50–100%, respectively. For example, PDADMAC is a 100% cationic polymer of low-to-medium MW [103].

2.5.3 Enhanced coagulation

Enhanced coagulation is the process of removing dissolved constituents that form disinfection by-products, which requires a higher dose than coagulation for turbidity removal [6], and is additionally affected by conditions such as type, dose and basicity of coagulants, composition and fractionation of NOM, presence of ions and so on [85].

Saxena et al. [100] studied the coagulation of different concentrations of HA as organic matter (0–10 mg/L TOC) and kaolin clay as turbidity (0–20 NTU) in a high alkalinity test water (18–205 mg/L), using high basicity PACl. It was observed that the percentage removal was directly related to TOC concentration as it affected the collision frequency. Similarly, increasing the turbidity above 5 NTU increased particle collisions and TOC removal. They reported that at the optimum doses (4–9 mg Al/L), zeta potential was negative (-15.53– -1.3 mV) and DOC removal of 30–90% was achieved, with residual TOC (0.5–2 mg/L) and DOC (0.4–1.4 mg/L) in the treated water.

2.6 Direct filtration

Many water sources contain low concentrations of suspended particles; consequently, the conventional flocculation process is kinetically suboptimal, while the flocculation and sedimentation basins account for a significant part of the water treatment plants' capital cost [105]. Direct filtration, defined as filtration not preceded by sedimentation after coagulation/ flocculation, is an economical alternative to the conventional filtration for low turbidity (max. 16 NTU) raw waters [106, 107].

Direct filtration can achieve a high rate at reduced costs by injecting a coagulant at the filter inlet, bringing about a strong attachment of the particles to the filtration medium. The attachment is a result of physico-chemical mechanisms, classified according to two models, the 'double-layer model' (interactions between the electrostatic repulsive forces

and van der Waals's forces) and the 'bridging model' (chemical bonding and bridging due to the reaction of the coagulant and the suspension particles) [71, 105].

In the fixed rate direct filtration process, the breakthrough and head loss depend on the attachment forces. As more particles are accumulated, the shear forces increase and when they become greater than the attachment forces, breakthrough occurs. Although alum is the coagulant of choice in many settings, the flocs formed are too weak to withstand the shear forces, whereas PEs form strong flocs [105]. Therefore, PDADMAC is used in combination with metal salts, or in direct filtration plants when low doses are required [102].

In designs that there is no coagulation/flocculation basin, the dose and the injection point of the coagulant directly affect the effluent quality [107]; however, the range of effective dose is wider due to the contact surface area provided by the filtration medium [105]. Yuksel et al. [107] compared different coagulant injection points—the filter inlet and three different depths of the filter—in a sand filter bed. A cationic PE coagulant and an approach velocity of 10 m/h were chosen, with the effluent turbidity, particle count and head loss at different locations of the filter measured. They reported that the same amount of coagulant (0.3 mg/L) injected into the top, centre and bottom of the media at the same time (each 0.1 mg/L) extended the filtration run more than 2.5 times compared to injecting the total amount (0.3 mg/L) at the filter inlet, while achieving a turbidity below the set limit. The increased filtration time was attributed to the deeper penetration of particles and a better use of the filter depth, preventing clogging in the upper region of the bed.

Adin and Rebhun [105] investigated direct filtration of a low turbidity (20 mg/L of kaolinite) synthetic water with different doses of an organic coagulant, PDADMAC (0.005–0.5 mg/L), and an inorganic coagulant, alum (10 mg/L, the optimum concentration). There were no mixing basin and the flocculant and the suspension were mixed only at

the injection point and in the pipes, with a contact time of a few minutes. The optimum polymer dose obtained in the jar test and the filtration test was the same (0.05–0.06 mg/L). They reported that despite the short depth used in the preliminary tests, the removal was in the same range as other studies with a prior flocculation basin. When alum was used, the removal improved at a faster rate because of the quicker coating of the bed grains with alum; however, the working stage was shorter, demonstrating the advantage of PEs under stringent hydraulic conditions. They observed that head loss had a direct relationship with the grain size and the flow velocity; however, increasing the flow velocity did not increase the head loss rate based on volumetric output.

In a later work, the same researchers, Rebhun et al. [108], compared the removal of humic acid (10 mg/L) in direct filtration with two sand filters (grain sizes 0.62 and 1.2 mm) dosed with alum (10% solution of $Al_2(SO_4)_3 \cdot 18H_2O$) and/or commercial PEs such as PDADMAC (mol. wt 5×10^4). The jar tests showed that a dose of 25 mg/L of alum was sufficient for complete precipitation of humic acid. Although the raw water had no turbidity, after the addition of alum, the measured turbidity was 8.0 FTU (Formazin Turbidity Units), caused by aggregation of humic acid particles. It was reported that the accumulation of deposited alumo-humate in the filter bed caused a sharp decrease in removal efficiency, and the breakthrough occurred earlier than when turbidity removal (20 mg/L kaolinite) was tested with the same bed (3–4 h vs. 8–10 h). Similarly, the deposited mass per unit bed volume was lower in the tests with humic acid than turbidity (8.1 vs. 25.5 mg solids/cm^3). Direct filtration with cationic PEs reported to be ineffective for HA removal, with very high and impractical dose requirements. However, using the PEs in addition to alum increased the deposited mass per unit bed volume (compared to alum alone).

In summary, the direct filtration process has showed to be very effective when the turbidity is low (e.g., 10 NTU). However, the process should be adapted for household

water treatment systems to address the practical limitations such as coagulant dosing and users' lack of water chemistry knowledge.

2.7 Filtration models

Modelling the filtration processes can help optimise and design filtration units for a specific task, as the models will provide estimates for different scenarios without the need for experimental set-ups. Filtration processes can be categorised as depth or cake filtration, discussed separately below.

2.7.1 Depth filtration

Physical mechanisms involved in filtration can be addressed at microscale level by fundamental models or at macroscale level by phenomenological models. The former considers the complex structure of the filter medium and particles in their actual form while in the latter, medium is defined by its permeability, porosity and possibly pore size distribution [6, 77].

Phenomenological models can be used to find the optimized design by varying the design parameters so that the breakthrough happens at the maximum allowed headloss. Fundamental models, however, are not suitable for the purpose of design as they are not capable of predicting changes in the headloss or particle removal when the design or operating conditions are adjusted.

In the macroscopic view, filtration is described by the change in concentration (C) of the suspended particles with time (t). This can be modelled by considering the mass conservation including accumulation in the continuity differential equation. Concentration change is then expressed as $\partial\sigma/\partial t = f(C, \sigma)$, where σ is the specific deposition (deposition per unit volume of the medium) [6, 64, 109]. This equation be solved explicitly with the

first order upwind scheme [110].

Adin and Rebhun [111] developed a model for deep-bed filtration based on the material balance for an infinitesimal element of a filter bed and a constant diffusion coefficient (D). When particle attachment is added to the equation, it becomes

$$-v\frac{\partial C}{\partial x} = \frac{\partial(\epsilon C)}{\partial t} - D\frac{\partial^2 C}{\partial x^2} + \frac{\partial \sigma}{\partial t} \tag{2.7}$$

where v is the filtration rate, C the concentration of the suspension and σ deposition. By assuming negligible diffusion and porosity change, the equation can be simplified as

$$\frac{\partial C}{\partial x} + \frac{\partial \sigma}{\partial V} = 0 \tag{2.8}$$

where V is the filtrate volume in time t (vt), which is more useful than t when the filtration rate is not constant.

In order to obtain the numerical solution, a kinetic equation was derived based on the idea that the accumulation rate is a result of accumulation and detachment of particles or

$$\frac{\partial \sigma}{\partial V} = k_1 C(F - \sigma) - k_2\frac{\sigma}{K} \tag{2.9}$$

where k_1 and k_2 are the accumulation and detachment coefficients, F the filter capacity and K the hydraulic permeability coefficient, which can be expressed as a function of the specific deposit as

$$K = K_0(1 - \sqrt{\sigma/F})^3 \tag{2.10}$$

Eq. 2.8 can be solved analytically by assuming proper boundary conditions

$$\begin{aligned} x = 0, V \geq 0 \quad C = C_0 \\ x \geq 0, V = 0 \quad \sigma = 0 \end{aligned} \tag{2.11}$$

where C_0 is the concentration at the inlet, resulting in

$$C = C_0 e^{-(k_1 F)x} \tag{2.12}$$

Another model for deep-bed filtration was proposed by Wojciechowska [112] based on the same principles; however, instead of considering the accumulation and detachment coefficients, the filter coefficient, λ, based on the famous work of Iwasaki et al. [113] determined the change in the concentration of the suspension, obtained by

$$\frac{\partial C(t,x)}{\partial x} = -\lambda C(t,x) \tag{2.13}$$

where λ itself is a function of the initial filter coefficient, λ_0, local deposition, σ, and filtration rate, v.

Mays and Hunt [114] provided a single parameter model for head loss, based on the famous work by O'Melia and Ali [115], given in Eq. 2.14.

$$\Delta H/\Delta H_0 = [1 + \gamma\sigma]^2 \tag{2.14}$$

where

$$\gamma = \frac{\beta' d_c}{6(1-\epsilon)} \frac{A_p}{V_p} \tag{2.15}$$

γ is the only parameter that includes the particle surface area to volume, A_p/V_p, and β' is an empirical coefficient representing the fraction of the particles that are responsible for the increased specific area.

Particle penetration is important because permeability would be different if most particles were accumulated near the inlet rather than evenly distributed throughout the medium—it would be higher in the former case. However, it was argued that deposit morphology was the controlling factor for headloss rather than the particle penetration depth.

Alternatively, pressure drop can be obtained by the Ergun equation, which was originally proposed for pressure drop estimation in packed bed columns. It models both laminar and turbulent flows by including an empirical coefficient, written as

$$\frac{\Delta P}{L} = \frac{150\mu(1-\varepsilon)^2}{\varepsilon^3 d_P^2} v + \frac{1.75(1-\varepsilon)\rho}{\varepsilon^3 d_P} v^2 \tag{2.16}$$

where d_p is the diameter of filter media grains and ε the porosity.

2.7.2 Cake filtration

The body of knowledge created by the analysis of cake filtration as a result of the works of B. F. Ruth [116, 117] and subsequent studies by other researchers from 1930s to 1980s are referred to as the conventional theory of cake filtration. The theory can be used to perform a simple analysis and predict filtration performance, which is still widely used for design and scale up [76]. The basic equations for cake filtration are based on the assumption that all particles are retained by the media. The 1D continuity equation is written as

$$\frac{\partial q_\ell}{\partial x} = -\frac{\partial \epsilon_s}{\partial t} \tag{2.17}$$

where q_ℓ is the superficial liquid velocity (in the opposite direction of x), x the distance from the medium, and ϵ_s the cake solidosity.

When $0 < x < L(t)$, we can write the equation for solids as

$$\frac{\partial q_s}{\partial x} = \frac{\partial \epsilon_s}{\partial t} \tag{2.18}$$

where q_s is the particle velocity and L the cake thickness.

Adding Eq. 2.17 to 2.18, we have

$$\frac{\partial}{\partial x}(q_\ell + q_s) = 0 \tag{2.19}$$

demonstrating that the sum of the liquid and particles velocities is constant across the cake.

The conventional theory assumes that particles do not move in the cake layer, and consequently, liquid velocity has a constant value across the cake at any instant, and solidosity does not change in time ($\partial\epsilon_s/\partial t = 0$). Another assumption is that the liquid flow obeys the Darcy's law, written as

$$q_\ell = \frac{K}{\mu}\frac{\partial p_\ell}{\partial x} \tag{2.20}$$

where K is the permeability, μ the liquid viscosity and p_ℓ the pore liquid pressure. Assuming that p_ℓ is equal to p_o at $x = 0$ (zero at the downstream side of the medium) and the pressure drop across the cake and the medium are Δp_c and Δp_m, respectively, we have

$$p_o = \Delta p_c + \Delta p_m \tag{2.21}$$

Eq. 2.20 can be integrated across the cake ($x = 0$ to $x = L(t)$) by reordering and multiplying both sides by $\rho_s\epsilon_s$ and letting $\alpha = (K\rho_s\epsilon_s)^{-1}$, giving

$$\mu q_\ell \int_0^L \rho_s\epsilon_s dx = \int_{p_o-\Delta p_c}^{P_o} (\frac{1}{\alpha}) dp_\ell \tag{2.22}$$

where ρ_s is the density of solids [76].

2.7.3 Conclusion on filtration models in the literature

All the filtration models reviewed had several empirical parameters that needed to be fine-tuned either manually or by using parameter estimation methods such as the Monte-Carlo methods. This is a flaw as the models may be overfitted, but seems inevitable.

All these models have been developed to explain the filtration performance in one dimension (1D), ignoring the effects of hydrodynamics that can only be modelled in two or three dimensions. However, it might be acceptable to simulate filtration in a simple vertical flow sand filter in 2D or even 1D by ignoring the effect of the wall region—in a homogenous sand filter bed, the wall region has a higher porosity than the core porous region, exacerbated at higher velocity as the increased porosity at the wall provides less resistance to the flow [118, 119].

In the case of radial flow cartridge filters, flow fields are more complicated and their effect on particle deposition and filter performance needs to be considered. For this reason, computational fluid dynamics (CFD), in which the flow fields as well as other transport mechanisms are resolved, can be utilized to provide a better simulation of the process. There has been no study dedicated to the simulation of cartridge filtration even though the best approaches have been determined by other researchers.

2.8 Computational fluid dynamics (CFD)

With computational fluid dynamics (CFD), it is possible to get the flow properties at locations that are not possible with measuring instruments. When CFD is utilized, the enormous data generated as a result of numerical solution can be effectively presented by visualization using vectors, contours, or animated movies [120–122]. This leads to CFD being used as a design tool to test different designs before conducting an experiment, which would be more costly; nevertheless, the final design needs to be validated with

experiments [65].

In general, CFD deals with analysis of systems in terms of fluid flow, heat transfer, chemical reactions and so on by means of computer-based simulation [123]. In water and wastewater treatment, CFD is frequently applied to processes such as disinfection, final sedimentation and activated sludge, while other areas require further work [124].

The limitations of using CFD for water treatment processes such as requiring powerful computers, highly specialised engineers and long simulation times should be considered. In most cases, the geometry of the treatment unit needs to be simplified (e.g., sharp corners should be avoided), various unrealistic assumptions be made (e.g., all particles are removed within the filter), or empirical models be employed to be able to successfully simulate the process.

2.8.1 Governing equations for CFD

Solving practical problems in fluid mechanics requires investigation of the behaviour of a finite control volume on the basis of fundamental laws of physics (conservation of mass, first and second laws of thermodynamics and Newton's second law of motion) [121, 122].

The continuity equation

The law of conservation of mass basically means that the rate of change in the mass in a system is equal to the rate of change inside the control volume and the net rate of mass flow through the control surface. The continuity equation is the control volume expression for conservation of mass, and expressed as Eq. 2.23 for a fixed, non-deforming control volume.

$$\frac{\partial}{\partial t}\int_{cv}\rho dV + \int_{cs}\rho \mathbf{V}\cdot\hat{\mathbf{n}}dA = 0 \tag{2.23}$$

where $\mathbf{V}\cdot\hat{\mathbf{n}}dA$ is the volume flow rate through dA, and A the surface area.

The momentum equation

Newton's second law of motion states that the linear momentum of a system changes with a rate equal to the sum of external forces acting on the system ($\sum \mathbf{F}$). For a fixed and non-deforming control volume, the linear momentum equation can be derived as Eq. 2.24 [125].

$$\frac{\partial}{\partial t}\int_{\text{cv}} \mathbf{V}\rho dV + \int_{\text{cs}} \mathbf{V}\rho\mathbf{V}\cdot\hat{\mathbf{n}}dA = \sum \mathbf{F}_{\text{contents of the control volume}} \tag{2.24}$$

Newton's second law describing the conservation of momentum in fluid flow is known as the Navier-Stokes equations.

2.8.2 Flow regimes and turbulence modelling

In water treatment systems, flow regimes are turbulent due to the large dimensions of installations and high velocities (0.1–2 m/s) [123]. The velocity that is referred to in the porous media literature is superficial velocity, which ignores the influence of the porous structure. In packed bed applications, Reynolds number is calculated as

$$Re_p = \frac{\rho v d_p}{\mu} \tag{2.25}$$

where Re_p is the particle Reynolds number, v superficial velocity and d_p particle equivalent diameter as the scaling length.

It is not possible to determine the exact value of the Reynolds number for transition from laminar to turbulent flow due to the properties that are not accommodated by the Reynolds number, e.g. surface roughness. However, based on empirical data a flow regime can be determined as: laminar ($Re_p < 10$), transitional ($10 < Re_p < 300$) or turbulent ($Re_p > 300$) [118].

2.8.3 Descriptions of fluid flows

Fluid mechanics problems can be analysed based on two general approaches. One is the Eulerian approach which considers a field concept, and fluid motion is given by prescribing properties such as velocity, pressure, density, etc. as functions of space and time. The other is the Lagrangian approach, which determines the fluid properties associated with individual fluid particles as they move about as a function of time [125]. The advantage of the Lagrangian approach is that it provides a higher-order statistics for different desired quantities (e.g. residence time) [123]. The Lagrangian viewpoint (following a particle) can be transferred to the Eulerian viewpoint (observation at a given location in space) by material derivative or Reynolds transport theorem [125].

2.8.4 Mesh generation

In order to solve the Navier-Stokes equations, the equations need to be discretized. For CFD problems, the finite volume method (FVM) is the preferred discretization method. The use of FVM in CFD codes stems from the concept of the control volume approach that the governing equations are based on. Grid/mesh generation is, therefore, part of the solution procedure.

There are two main types of mesh: structured mesh (Fig. 2.10a) and unstructured mesh (Fig. 2.10b). The latter is allowed to assemble freely within the computational domain; however, the points of a cell element cannot be simply addressed by a double (i,j) or triple (i,j,k) indices in 2D or 3D, respectively, because each cell may have an arbitrary number of neighbouring cells, making data treatment complicated.

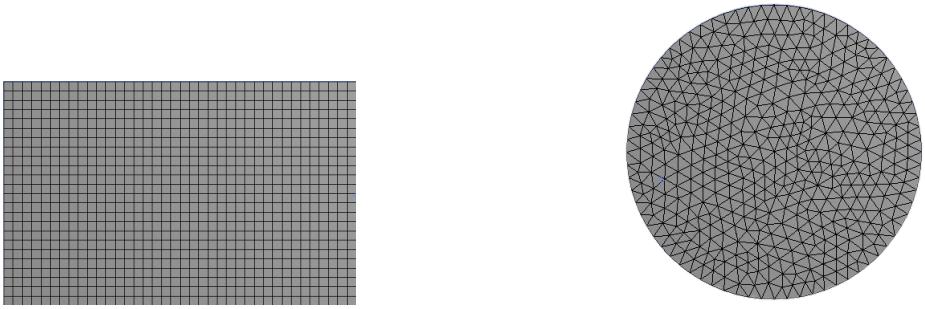

(a) (b)

Fig. 2.10 Two main types of mesh: (a) structured mesh, and (b) unstructured mesh.

There should be no jumps in the mesh (the spacing needs to be continuous). Discontinuity in the mesh size would cause the solution to diverge due to accumulation of truncation errors in high gradient regions [120, 126]. If a suitable mesh is not generated, the geometry will not be represented correctly and instabilities occur during the computation [118].

2.8.5 Application of CFD in filtration

Despite the importance of predicting filter performance in industry, accurate models have not yet been developed [127]. While theories and models help us to understand the filtration mechanisms, they are based on simplifying assumptions to make the equations tractable. Also, these models rely on parameters that are fitted empirically; therefore, they are useful as long as the filter structure and the operating conditions under investigation do not deviate from the ones used for derivation of these models.

To have flexibility in the approach to filtration problems, a more general solution is needed. CFD is a powerful tool in this regard, with the advantage of tracking particle movement and deposition, which is not practically possible in experimentation. The downside to using CFD, however, is that it is computationally intensive, requiring fast CPUs, large memories (RAM) and highly specialized users to define the process [65].

Two main approaches can be considered to simulate filtration:

1. *Microscopic scale:* simulation of flow at this scale requires precise presentation of the structure's geometry. This would be possible when done for a small domain of the filter, resulting in an accurate prediction of pressure drop and particle capture efficiency.

2. *Macroscopic scale:* in this approach, the filter element is treated as a porous media domain (i.e. the internal structure is not considered) and is modelled via a resistance tensor. The Eulerian method is used for the fluid flow and either the Eulerian or Lagrangian approach can be applied for particles. In the Eulerian method particles are described in terms of their concentration and included in a mass balance. Alternatively, the Lagrangian method may be utilized, tracking each particle as it moves in the domain [65].

Subrenat et al. [128] investigated the rate of pressure drop of an activated carbon pleated filter for removal of VOCs, by utilizing 3D numerical simulation as well as experimentation. The medium comprised of two layers of activated carbon cloth that were pleated together with a thickness of 1.2 mm. The flow regime was considered to be turbulent as the Reynolds number at the device inlet was 2400–9100. To include the porous medium and account for the additional pressure gradient, a source term was added to the momentum conservation equations, with the porous material properties considered isotropic.
The results showed that when a 45-pleat filter was used, only 60% of the medium surface was involved in adsorption, due to the overlapping of the edges. By altering the number of pleats, which affected the surface area (direct relationship) and distance between each pleat (inverse relationship), it was concluded that an optimum pleat number existed to achieve the lowest pressure drop—30 pleats for the geometry used in this study.
Roegiers and Denys [129] used CFD to investigate pressure drop and adsorption capacity of activated carbon fibers installed in an indoor air purifier. Laboratory experiments were conducted for estimation of Darcy-Forchheimer parameters: permeability K (m^2)

and Forchheimer term β (1/m) in Eq. 2.26, obtained by measuring pressure as a function of velocity.

$$\frac{\Delta P}{\Delta x} = -\frac{\mu}{K}v - \beta\rho v^2 \tag{2.26}$$

In Eq. 2.26, ΔP is pressure drop (Pa) across the filter thickness (m), μ dynamic viscosity (Pa·s), ρ density (kg/m$_3$) and v flow velocity (m/s). Permeability represents filter resistance to fluid flow and the Forchheimer term accounts for non-linear inertial effects as a result of high flow rates.

The goal was to predict the breakthrough concentration for the model pollutant, acetaldehyde. Their simulation showed that the air flow of 0.2 L/min at the inlet of the filter module moved straight towards the filter sheet, with acetaldehyde concentration increasing from the centre and moving towards the edges as it diffused in the porous medium.

Liu et al. [130] simulated dust removal and deposition by ceramic candle filters. The deposition process was included in the simulation by creating 2 mm thick grid cell zones each attached to one of the four ceramic filters, which were then populated by incoming particles according to a 'less computation cost' method. The number of deposited particles in each cell was summed and the mass in each cell calculated so that the pressure drop could be estimated by an empirical formula, and the flow fields could be updated. In order to reduce the computational cost, a method called 'multiphase particle-in-cell (MP-PIC)' was adopted, which assumes a certain number of particles as one imaginary sphere cluster with the same velocity. The filters were modelled at macroscale as porous media, and particle motion was simulated by considering the drag force on particles.

The numerical and experimental results were compared, and with the help of CFD, more details could be extracted. For instance, they found out that deposition started at the bottom and middle of the filters before moving upwards, and after 120 seconds the upper area with less deposition was reduced from 160 mm to 80 mm. Also, they visualized the

pattern of particle deposition on windward and leeward of the filter candles, showing that the patterns were the same as on the actual filters.

Feng and Long [131] provided a comparison of the Eulerian and the Lagrangian methods in a 2D CFD simulation of transient air filtration by pleated filters. Simulation was set-up at macroscale with the filter and cake layer modelled as porous zones. The permeability constant for the cake layer was calculated by the Kozeny-Carman equation. Both methods proved to be similar in terms of accuracy and uniformity of the cake layer; however, the Eulerian method was computationally faster. This was significant because the Lagrangian method is widely used due to its ability to capture unsteady clogging, while in the Eulerian method, particles are considered as a continuous phase, with their concentration used in the transport equation.

Since in industrial vacuum pumps lubricated with oil air stream may carry oil droplets causing problems in downstream processes, Basha [132] used CFD simulation to investigate air/oil separation in cartridge filters installed at the outlet of a vacuum pump. In the study, the flow characteristics and the droplet trajectory which were not feasible to obtain by experimentation, were simulated. As oil droplets deposited over time, the decline in permeability was addressed by updating the inertial and viscous resistances in every cell of the porous zone. Particle tracking was feasible in this work because the aerosol volume fraction was small (0.0001%). The computational results showed a non-uniform deposition, confirmed by experimental observation. The work proved that CFD can be an effective tool in the study of aerosol loading over time.

Osterroth [77] studied the mathematical models for the simulation of combined depth and cake filtration processes. The conditions and assumptions were: a dilute suspension, a constant flow rate, spherical particles with the same density, absence of sedimentation, an incompressible cake, and isotropic permeability.

It was reported that the removal efficiency at the beginning of the experiments when

the flow was not yet established could not be captured by the model. Also, similar to other modelling studies in the literature, the importance of accumulation and detachment coefficients was highlighted. In these simulations, it became evident that the deposition in the cake predominately happened at the surface and therefore, the capture efficiency was mainly improved due to surface deposition.

All of the CFD studies reported here have helped to understand and visualise the physical interactions during different filtration processes; however, there is no work on water cartridge filtration.

2.9 Summary

In the context of household water treatment, water quality monitoring is challenging, choosing an easy to measure parameter such as turbidity can help evaluate the effectiveness of filtration processes. However, the characteristics of suspended particles in water and the internal structure of filters should be studied as it can help in fine-tuning filter design. For example, particle size distribution would determine the dominant filtration mechanisms and particle zeta potential the effectiveness of preconditioning processes (i.e. coagulation).

Filtration processes can be categorised into depth and cake filtration, each having different removal mechanisms. Cake or precoat filtration was used in the water industry as a substitute for sand filtration as the pore sizes are finer, providing a higher quality treated water without requiring prior coagulation. In this process, a precoat layer is formed on a septum and once clogged, it can be replaced at a low cost.

Suspended particles in water can be too fine to be removed via cartridge filters. Dosing a coagulant immediately before the filter would neutralise the surface charge of particles and improve removal without requiring clarification basins, a process called direct filtration.

The modelling studies on filtration are limited to sand filters and mainly to 1D models

limited to very narrow operational conditions. Computational fluid dynamics (CFD) is a tool that allows 3D study of different processes, with the possibility of including user defined models to investigate different process designs more accurately.

2.10 Aim, Objectives and Novelties

2.10.1 Aim

The aim of this study was to evaluate the performance (i.e., turbidity removal efficiency and pressure drop) of low-cost commercial cartridge filters based on the turbidity level specified for the Challenge Test Water within the WHO HWT testing scheme which represents low-quality surface waters, and subsequently, to enhance the performance and re-usability of the filters by either improving the structure of the filtering medium (e.g., by precoating the filters) or incorporating another process (e.g., coagulation) prior to filtration. The study is mainly focused on treating surface waters with variable quality in developing countries where the cost would be the major issue; hence, only low-cost methods/processes were investigated.

2.10.2 Objectives

- To provide assessment information for cartridge filters based on WHO guidelines.
- To propose a modelling approach for cartridge filters using computational fluid dynamics (CFD) and validating the results with experiments.
- To investigate methods to enhance the removal efficiency, reaching a treated turbidity of <5 NTU, the limit defined by the WHO for HWT systems.

- To investigate organic matter and pathogen removal and methods to achieve a removal of >25-50% of organic matter depending on water hardness, according to US EPA requirements.
- To investigate methods to clean and reuse cartridge filters safely.

2.10.3 Novelties

- For the first time, different micron ratings of common cartridge filter types (i.e., pleated, spun and wound) were assessed based on the WHO HWT testing scheme, providing comprehensive information on turbidity removal efficiency, pressure drop and re-usability of these filters.
- A novel computational fluid dynamic (CFD) model was developed to simulate the fundamental mechanisms underpinning the removal of particles within the widely used 10-inch cartridge filter, informed by, and complemented with laboratory validation.
- Due to the absence of any publications on precoat filtration for HWT, a unique precoating process and precoat materials using commercial pleated cartridge filters were developed.
- An innovative method for in-line dosing of coagulants in HWT systems were introduced showing the effectiveness of contact filtration using cartridge spun filters in contrast to the findings with sand filters used in large-scale municipal water treatment plants.

Chapter 3

Materials and Methods

This chapter presents the materials, methods and equipment used throughout this research. The process flow diagrams (PFDs) of experimental set-ups, the components and procedures followed such as test water preparation have been provided. Water quality and process measurements performed and the required instruments have been explained. Characterisation of powders, suspended particles in water and filter cakes have been explored. In addition to experimental methods, numerical models and equations for simulation of the filtration process have been discussed.

3.1 Experimental set-ups and procedures

3.1.1 Cartridge filter elements and housing

The commercial, fibrous cartridge filter elements used were obtained from three UK distributors (Finerfilters Ltd., Aqua Cure Ltd. and The Water Filter Men). The spun and wound filters were made of polypropylene and pleated filters from polyester. Filter elements trialled were of the double open-ended type with the standard 10 inch dimensions ($\varnothing 63 \times 250$ mm) and different micron ratings. Each filter element was placed inside a 10

inch housing (Finerfilters, Ltd) with the dimensions of ⌀119 mm × 320 mm. Water was transferred with a pipe, entered the filter element from its outer surface and exited from the inner hole (outside-in flow). Images of the spun, wound and pleated filters (5 micron) prior to use and the housing are shown in Fig. 3.1.

(a) (b)

Fig. 3.1 (a) The three types of cartridge filter elements used in this study: spun (left), wound (middle) and pleated (right); (b) The (10 inch) housing used for the trials.

3.1.2 Preparation of the test water

The test waters were prepared based on the concentration/level of constituents in 'Challenge Test Water' of 'WHO International Scheme to Evaluate Household Water Treatment Technologies' [33]. Tap water (Belfast, UK) with a pH of 6.9–7.4, turbidity of 0.05–0.3 NTU and no detectable residual chlorine was fed into the inlet tank by a hose. A turbidity agent (TD or kaolinite) was added to the feed tank and turbidity was usually controlled to be 40±10 NTU either manually in the case of batch experiments or in the case of continuous experiments, by dosing using a peristaltic pump (101U, Watson Marlow) from a concentrated stock of either TD or kaolinite. An aquarium pump (Intercept, PF Mini) was utilized to internally recirculate the inlet tank suspension preventing settlement of large particles inside the tank.

3.1.3 Assessment of different types of cartridge filters

The process flow diagram (PFD) of the HWT system to permit study of filter performance (turbidity removal and pressure drop) is shown in Fig. 3.2, comprising two 10 inch standard filter housings, suitable for double open-end (DOE) filter elements. A 12V DC on-demand pump (Model 2095-204-412, Shurflo) was used as the main feed pump for the filtration system. The pump had a maximum operating pressure of 1.6–1.8 bar, and during the filtration trials, the initial flow rate of 5.2 L/min decreased to 4.4 L/min as the pressure increased to 1 bar (both flow rate and pressure were variable). Each filter assessment trial consisted of several runs spanning days or weeks in duration with a test volume for each run being 0.5 m^3. Following processing of 50 or 100 L, samples (50 mL) were taken from the feed tank and the sampling valves after each filter, and their turbidity was measured. In addition, the pressure drop of each filter and the cumulative treated water volume and flow rate were recorded.

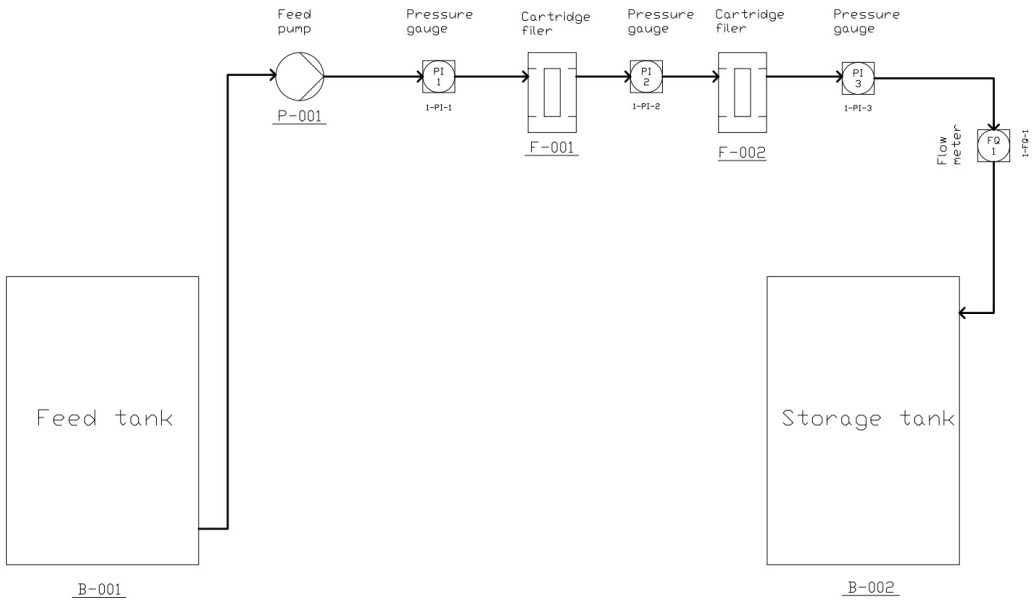

Fig. 3.2 The process flow diagram (PFD) of the filtration system used for testing the commercial cartridge filters.

3.1.4 Filter cleaning and reuse

Pleated filters were cleaned simply by running under a tap, shaking in a housing full of water for 3–5 minutes and if any cake was still attached, it was gently removed by hand. After cleaning, some cake remained on the folds, and particles were observed to be entrapped in the filter medium, these were not removed. Sodium hypochlorite with 6–14% active chlorine (Millipore) was used for cleaning and disinfecting filters after the trials in which *E. coli* was present, in order to investigate the feasibility of safe filter reuse.

Cleaning and reuse of spun and wound filters was not possible as particles were entrapped in the filter medium, as such they were discarded after single use.

3.1.5 Precoat filtration experimental procedure

In precoat filtration, several components are essential, including a filter housing, a septum, a tank for filter aid-water slurry, a pump, pressure gauges, pipes, valves, and so on. The process flow diagram (PFD) of the system is shown in Fig. 3.3.

To precoat filters, 25 g of a filter aid (DE or calcined DE) was added to 3 L of tap water and stirred on a magnetic stirrer. After 10 min of stirring, the pump was turned on and the slurry recirculated until most DE particles were captured by the precoat layer, achieving a turbidity of <1 NTU. Then, the trials began, and samples (50 mL) were taken from the inlet and the outlet of the system, after 5 L and 50 L for trials spiked with *E. coli* and 50 L or 100 L (depending on the gradient of pressure drop increase) for trials without *E. coli*, with pressure drop, volume of water treated and turbidity of samples recorded (process measurements are discussed in Section 3.6).

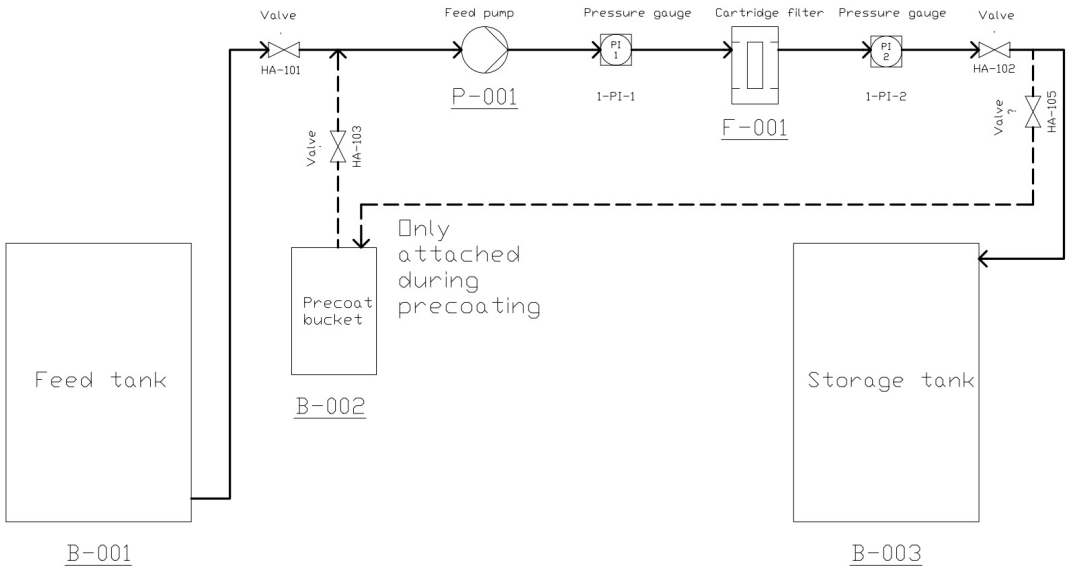

Fig. 3.3 The process flow diagram (PFD) of the precoat filtration system, showing the piping and fittings needed.

3.1.6 Direct contact filtration experimental procedure

The process flow diagram (PFD) of the system is shown in Fig. 3.4. A coagulant solution with high concentrations of either alum or PDADMAC was prepared and directly injected to the feed stream using a T-valve. There was no need for an additional dosing pump because the T-valve was located on the suction side of the feed pump (described in Section 3.1.3), with the concentration of the coagulant in the stream controlled by adjusting the stock concentration and the diameter of the intake. The mixing of the coagulant with suspended and colloidal particles only occurred in few seconds in the pipes, fittings and the filter housing, before coming into contact with the fibres of the filters.

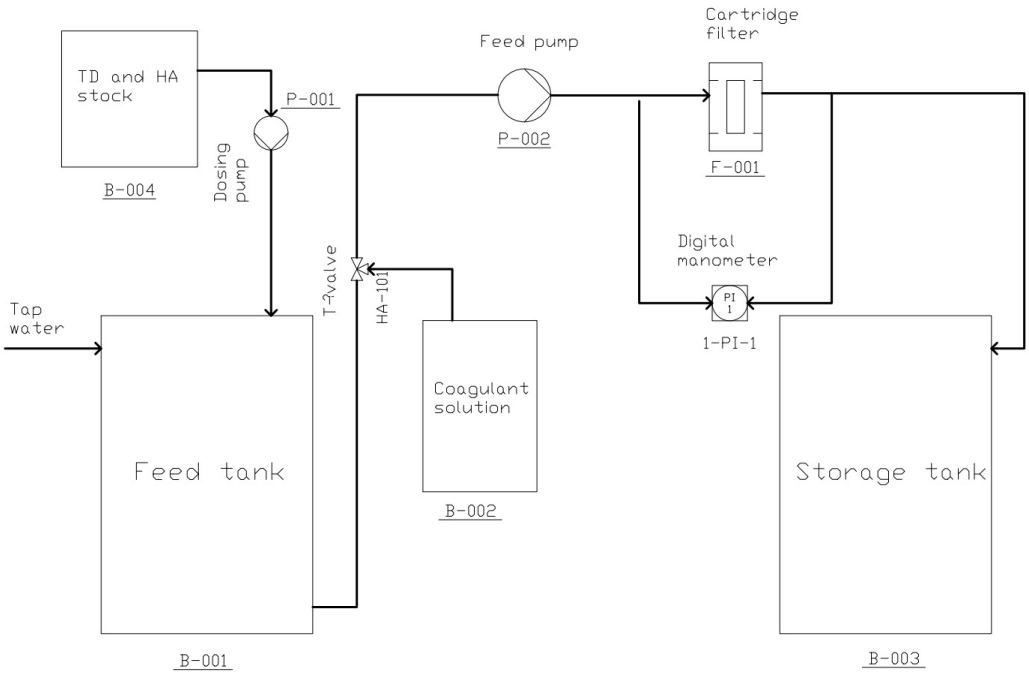

Fig. 3.4 The process flow diagram (PFD) of the direct filtration system.

3.2 Numerical simulation

In order to simulate the filtration process, several models were needed in addition to the equations that are solved in a CFD study (see Section 2.8).

3.2.1 Particle size distribution function

For modelling purposes, it was necessary to use a distribution function such as Rosin-Rammler [133], expressed as:

$$Y = 1 - e^{[-(\frac{X}{X_0})^n]} \tag{3.1}$$

where Y is the cumulative fraction by weight less than size X, n the 'uniformity constant' or 'spread parameter' describing the particles' uniformity, and X_0 the 'characteristic particle size', the size that 63.2% of particles were smaller than.

3.2.2 Porous media model

In the simulations, the filter was considered as a homogeneous porous medium and included as a computational zone with an additional momentum source term including the viscous and inertial resistances as

$$S_i = -\left(\frac{\mu}{\alpha}v_i + C_2\frac{1}{2}\rho|v|v_i\right) \tag{3.2}$$

where α is permeability, C_2 inertial resistance factor and v_i velocity in i direction—α and C_2 should be determined empirically [134].

3.2.3 Particle deposition model

In order to include particle deposition, numerical models for removal efficiency were needed. In this work, the fundamental model proposed by Tufenkji and Elimelech [135] has been used, which provided equations for predicting single-collector (e.g. fibre) removal efficiency. In this model, the overall removal efficiency was the sum of the removal of different transport mechanisms—interception, gravitational sedimentation and Brownian diffusion. Equations 5.7–5.17 [6] have been used to estimate the overall efficiency for each particle.

$$N_R = \frac{d_p}{d_c} \tag{3.3}$$

$$N_G = \frac{v_S}{v_F} = \frac{g\left(\rho_p - \rho_w\right) d_p^2}{18 \mu v_F} \tag{3.4}$$

$$\mathrm{Pe} = \frac{v_F d_c}{D_L} = \frac{3\pi\mu d_p d_C v_F}{k_B T} \tag{3.5}$$

$$N_A = \frac{N_{vdW}}{N_R Pe} = \frac{Ha}{3\pi\mu d_p^2 v_F} \tag{3.6}$$

$$N_{vdW} = \frac{Ha}{k_B T} \tag{3.7}$$

$$\gamma = (1-\varepsilon)^{1/3} \tag{3.8}$$

$$A_S = \frac{2\left(1-\gamma^5\right)}{2-3\gamma+3\gamma^5-2\gamma^6} \tag{3.9}$$

$$\eta_I = 0.55 \mathrm{A}_S N_A^{1/8} N_R 1.675 \tag{3.10}$$

$$\eta_G = 0.22 N_R^{-0.24} N_{\mathrm{vdW}}^{0.053} N_G^{1.11} \tag{3.11}$$

$$\eta_D = 2.4 A_S^{1/3} N_R^{-0.081} N_{vdW}^{0.052} \mathrm{Pe}^{-0.715} \tag{3.12}$$

$$\eta = \eta_l + \eta_G + \eta_D \tag{3.13}$$

A_S = porosity function, –

d_p = particle diameter, m

d_c = collector diameter, m

k_B = Boltzmann constant, 1.381×10^{-23}J/K

T = absolute temperature, K

v_F = filtration rate, m/s

v_S = Stokes settling velocity, m/s

ε = bed porosity, –

γ = porosity coefficient, –

ρ_p = particle density, kg/m^3

ρ_w = liquid density, kg/m^3

μ = liquid viscosity, kg/(m s)

N_R = relative size group, –

N_G = gravity number, –

N_A = attraction number, –

N_{vow} = van der Walls number, –

Pe = Peclet number, –

D_L = diffusion coefficient, m^2/s

Ha = Hamaker constant, J

η_I = transport efficiency due to interception, –

η_G = transport efficiency due to gravity, –

η_D = transport efficiency due to diffusion, –

η = total transport efficiency, –

$1/\eta$ is the number of possible collisions with a fibre required so that one real collision can be registered. Therefore, in order to determine whether a particle was deposited or

not, $1/\eta$ was compared to the number of fibres that a particle has passed based on its location (Fig. 5.2), calculated by multiplying the distance of the particle from the outer surface of the filter (R_p) by the number of fibres per mm, obtained by SEM imaging. This calculation was performed for every particle that reached the filter zone.

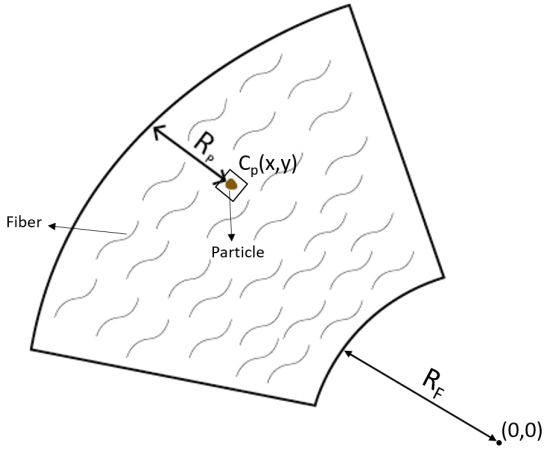

Fig. 3.5 Location of a particle in the porous zone

Possible collisions $= n_{fibre} \times 1000 \times R_p$

where, $R_p = \sqrt{x_{C_p}^2 + y_{C_p}^2} - R_F$

R_p = Particle distance from the outer surface of the filter, m

n_{fibre} = approximate number of fibres in 1 mm

Once a particle was deposited, its mass was registered in a User Defined Memory (UDM) for the mesh cell in which it was located ($C_p(x, y)$), and the local resistance was updated.

3.2.4 Particle motion

The Lagrangian framework was adopted for the motion of small particles. The particle trajectories were predicted by integrating the force balance acting on the particles, written as

$$m_p \frac{d\vec{u}_p}{dt} = m_p \frac{\vec{u} - \vec{u}_p}{\tau_r} + m_p \frac{\vec{g}\,(\rho_p - \rho)}{\rho_p} + \vec{F} \tag{3.14}$$

where m_p, u_p, ρ_p and τ_r are the particle mass, velocity, density and relaxation time, respectively [136]. The first term on the right side is the drag force, which is a function of the particle relaxation time (τ_r), the time required for a particle to adjust its velocity,

expressed as,

$$\tau_r = \frac{\rho_p d_p^2}{18\mu} \frac{24}{C_D \,\mathrm{Re}} \tag{3.15}$$

where Re is the relative Reynolds number [137]. The drag coefficient (C_D) for non-spherical particles can be expressed as

$$\begin{aligned} C_\mathrm{D} = & \frac{24}{Re}\left[1 + e^{(2.3288-6.4581\psi+2.4486\psi^2)} Re^{(0.0964+0.5665\psi)}\right] \\ & + \frac{Re \times e^{(4.905-13.8944\psi+18.4222\psi^2-10.2599\psi^3)}}{Re + e^{(1.4681+12.2584\psi-20.7322\psi^2+15.8855\psi^3)}} \end{aligned} \tag{3.16}$$

where ψ is the Wadell's sphericity [138].

3.2.5 Particle-wall collision

Particle rebound following collision with a wall was calculated by the default model within Ansys Fluent [136], based on the work of Wakeman and Tabakoff [139], which calculates the rebound velocity by considering the coefficient of restitution (e):

$$e_n = \frac{V_{2,n}}{V_{1,n}} \tag{3.17}$$

$$e_t = \frac{V_{2,t}}{V_{1,t}} \tag{3.18}$$

where V_n and V_t are the particle velocity normal and tangent to the wall, respectively, and the subscripts 1 and 2 refer to before and after collision, respectively.

3.2.6 Computational mesh

Mesh generation is a part of the solution procedure, and if a suitable mesh is not generated, the geometry will not be represented correctly and instabilities occur during the computation [118]. The computational mesh for this study was created by Ansys ICEM CFD.

3.3 Materials

3.3.1 Turbidity agent

In this research, two turbidity agents were used: fine test dust and kaolinite. Fine test dust (ISO 12103-1, A2, Powder Technology Inc.) is a red brown insoluble mineral composed mainly of silica with a density of 2500–2700 kg/m^3, recommended agent by the WHO scheme for evaluating HWT technologies [33].

In addition, kaolin clay (Sigma-Aldrich) which has a different particle size distribution (PSD) from the test dust and is a common turbidity agent in academic research (e.g. [140, 141]), was used in few experiments. The difference in the PSD of the kaolin and the TD can be observed in Fig. 3.6. The TD had a d_{10}, d_{50} and d_{90} of 1.49 μm, 7.55 μm and 43.9 μm, respectively, while the kaolin had a finer PSD with d_{10}, d_{50} and d_{90} of 0.54 μm, 3.95 μm and 9.85 μm, respectively. Moreover, the relationship between concentration and turbidity was different for these two agents (Fig. 3.7)—both have a linear correlation, which can be used to produce water-kaolin/test dust suspensions achieving a specific turbidity.

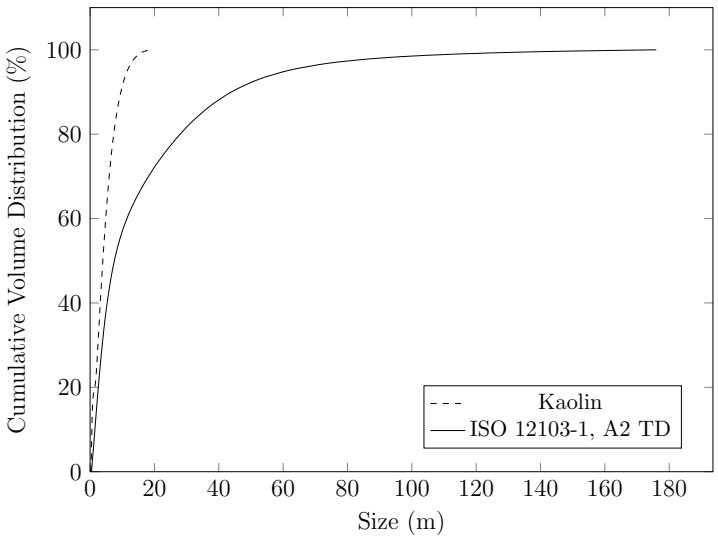

Fig. 3.6 Cumulative volume PSD of A2 test dust and kaolin measured by a particle size analyser.

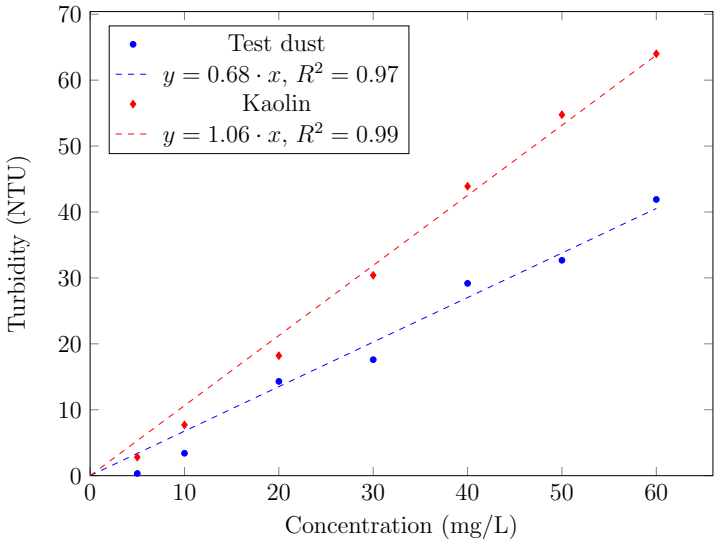

Fig. 3.7 Correlation of A2 test dust and kaolin concentrations with turbidity in tap water.

3.3.2 Organic matter agent

Among the various naturally occurring organic compounds, humic substances are the most widespread in water. Humic substances represent a class of complex molecular structures bound by or associated with mineral fractions, requiring physical and/or chemical separation. Therefore, research using these substances is complex, and in water research, synthetic test waters are typically prepared with a fraction of humic substances, humic acid (HA), as a surrogate compound (e.g. [142, 143]), in particular because HA is considered to react with disinfectants, generating toxic by-products [144]. Similarly, in this research, humic acid (HA) sodium salt (Sigma-Aldrich) was used.

3.3.3 Dechlorinating agent

For trials involving the addition of *E. coli*, the water in the feed tank was dechlorinated by 30 mg/L of sodium thiosulfate (Minerals Water Ltd., UK). The reaction between sodium thiosulfate (the reducing agent) and any chlorine forms is relatively rapid, requiring only good mixing. Depending on water pH, sodium thiosulfate undergoes various reactions

with free chlorine (e.g. Eq. 3.19) but with no appreciable effect on water pH. The required dose also depends on the pH, with 1.9 mg/mg Cl being the estimated dose at pH 7.0 [145, 146].

$$\underset{\text{sodium thiosulfate}}{Na_2\,S_2O_3 +} \quad \underset{\text{hypochlorous acid}}{4HOCl + H_2O} \quad \rightarrow \quad \underset{\text{sodium bisulfate}}{2NaHSO_4 +} \quad \underset{\text{hydrochloric acid}}{4HCl} \tag{3.19}$$

3.3.4 Filter aids

Food grade, fine diatomaceous earth (FoodPURA®, UK) either as purchased or calcined was used to precoat the septum. Calcination was performed by heating the DE in a laboratory chamber furnace (AWF 12/12, Lenton) at 1000 ℃ for 45 min, which resulted in a pink powder with a coarser PSD. During the calcination process, lumps had formed, which were broken manually using a mortar and pestle.

Additionally, the finest commercial grade of diatomaceous earth (DE) that was readily available, Celite® Standard Super-Cel, was purchased for comparison.

3.3.5 Coagulants

Poly(diallyldimethylammonium chloride) or PDADMAC (Mw 200,000–350,000, 20 wt. % in water, Sigma-Aldrich), and ferric chloride (FC) anhydrous (BDH Chemicals Ltd.) were used to coat diatomaceous earth (DE). PDADMAC and aluminium sulphate 17% Al_2O_3 (Pure Chem, UK) were used as coagulants in direct filtration experiments.

3.4 Water quality measurements

3.4.1 Turbidity

A portable turbidity meter (HI-93703, Hanna Instruments) with a detection limit of 0.00 NTU was used to measure turbidity of water samples. The device functions by passing an infrared light beam, emitted from a High Emission Infrared LED (wavelength peak at 890 nm), through a vial containing the sample, with the sensor photocell positioned at 90° angle to the light path, measuring the amount of scattered light. The reading is then converted into Formazin Turbidity Unit (FTU), equivalent to NTU [147, 148].

Before every measurement, samples were shaken in order to avoid underestimation of turbidity due to settled particles. Each sample was measured three times and the average reported.

3.4.2 Total and dissolved organic carbon

Total organic carbon (TOC) was measured by a TOC analyser (TOC-5000A, Shimadzu) with a detection limit of 4 μg/L, based on the combustion/non-dispersive infrared gas analysis method [149]. In this method, a micro-sample is injected into the total carbon (TC) combustion furnace, which is then vaporized and oxidized in a stream of oxygen on a contact catalyst bed. The generated CO_2 is passed through a non-dispersive infrared analyser which in turn sends a signal to a recorder. To measure inorganic carbon (IC), a second micro-sample is injected into the inorganic carbon combustion chamber operating at a low temperature (150 ℃) to avoid oxidation of organic matter.

The chamber contains quartz chips wetted with phosphoric acid, which causes the release of CO_2. The water vapour and CO_2 are swept by oxygen through a condenser before entering the infrared analyser. An already developed standard curve is then used to determine the concentration of TC and IC in the sample. TOC is determined by

subtracting the IC from the TC. Dissolved organic carbon (DOC) can be determined by first filtering the samples (prior to measurement) with a membrane filter with pore size of less than 0.45 μm to remove particulate organic carbon (POC) [150, 151].

3.4.3 UV_{254} transmission

UV absorbance at 254 nm is a surrogate measurement for estimating the concentration of organic matter in water and a better indicator than TOC concentration for chlorination by-products. In addition, UV_{254} measurement can be performed more easily, rapidly and inexpensively than TOC. However, although UV absorbance is a good technique for measuring the concentration of naturally occurring humic substances, some organic compounds such as sugars, alcohols and aliphatic acids do not absorb UV light, and the plot of UV_{254} versus TOC will not pass through zero [152, 153]. In this research, the test water was synthetic (the only organic matter was humic acid); thus, there was no concern regarding non-absorbing organic compounds.

The concentration of humic acid in the samples was estimated based on the UV absorbance measurement at 254 nm using a spectrophotometer (6305, Jenway). The instrument has four main components: (i) a xenon lamp emitting light with a high and constant amount of energy over the wavelength spectrum; (ii) a grating separating the light into discrete wavelength; (iii) a sample holder; (iv) a light detector calculating the percent transmittance (T), which is the proportion of the light passed through the sample:

$$T = \frac{I}{I_0} \tag{3.20}$$

where I_0 and I are the incident and transmitted light, respectively. Consequently, absorbance (A) can be obtained by Eq. 3.21:

$$A = \log_{10} \frac{I_0}{I} \tag{3.21}$$

The concentration of molecular entities can be determined by using either the calibration method—measurement of absorbance for several concentrations of the compound being measured and plotting the absorbance versus concentration—or the Beer-Lambert law:

$$A = \varepsilon l C \tag{3.22}$$

where ε is the molar absorption coefficient (L/mol/cm), l the path length (cm) and C the compound's concentration (mol/L). However, this law is only valid for limited absorbance ranges [147, 154]. Another limitation of UV_{254} absorbance is the presence of particles in the sample, scattering the radiation; in this case, the positive bias should be compensated either manually or by an internal algorithm of the instrument [155].

3.4.4 pH and temperature

A pH/temperature bench meter (pH510, Eutech Instruments) with a pH electrode and a temperature probe was used to periodically determine the pH and temperature of water samples.

In this method of pH measurement, the pH electrode, consisting of a glass membrane electrode and a reference electrode, determines the potential between the two electrodes as a result of the level of hydrogen ion activity in a sample and converts it to a signal, which is then displayed by the device [156].

3.4.5 Free chlorine

A portable, strip based chlorine measurement photometer (eXact® Chlorine Plus Photometer, Industrial Test Systems, Inc) with DPD strips (anhydrous N,N-Diethyl-p-phenylenediamine sulfate salt) with a detection limit of 0.05 ppm were used to measure free chlorine. The device works based on a photometric analysis method, in which an

aqueous sample is added to the cell chamber of the device and an effective amount of a water soluble analytical agent is delivered and mixed before photometric analysis [157]. The use of strips facilitates reagent delivery and mixing as their tips contain the required amount of the reagent, minimizing the variability of measurements [158].

3.5 Particle characterisation

3.5.1 Bulk density and specific gravity

The bulk densities of particles were obtained by measuring the volume of 10 g of their powders in a graduated cylinder, which was tapped and sonicated before reading the volume, and specific gravity was measured using a pycnometer.

3.5.2 Particle size distribution

Particle size distribution (PSD) was measured by a particle size analyser (Mastersizer 2000, Malvern Panalytical), which works by capturing the actual scattering pattern from a field of particles and calculating the size of particles based on the Mie theory. However, the Mie theory requires some information about the particle, such as its adsorption and refractive index to predict the way the light is scattered or adsorbed by the particles [159].

3.5.3 Zeta potential

Zeta potential (ZP) was measured via electrophoretic light scattering (Zetasizer Nano ZS, Malvern Panalytical), which works by using Laser Doppler Velocimetry (LDV) to measure the velocity of particles in an electrophoresis experiment on the sample, calculating the electrophoretic mobility and then applying the Henry's equation.

The micro-electrophoresis system is essentially a cell with electrodes at either ends where

an electrical potential is applied [83]. In this study, folded capillary cells (DTS 1060, Malvern Panalytical) were used.

3.5.4 Imaging

A scanning electron microscope (JEOL, JSM-6010) was used to take high magnification and resolution images of the test dust and the filter aid particles as well as fibres of the filters. The instrument works by generating high-energy electron beam and analysing its interaction with the atoms in the specimen [160].

Prior to imaging, samples were gold coated using a sputter coater (K500X, Emitech) to create conductivity on the particles/fibres surfaces.

3.6 Process measurements

3.6.1 Pressure drop

Analogue pressure gauges (M6306R, Ferro Group) with operational ranges of 0–4 bar were installed to measure the gauge pressure before and after of each cartridge filter. The pressure gauges were Bourdon (C-shaped) tube type, in which the tube is actuated by pressure, positioning a pointer to indicate the measurement [156].

For experiments that the change in pressure drop was small, a portable digital manometer (Digitron, 2028P7) was used. The main advantages of manometers are their high accuracy and simplicity, with digital manometers not being subject to limitations of visual manometers [161].

3.6.2 Water volume and flow rate

A water meter (CDSD15AFPLUS, Ferro Group) was installed to measure the cumulative treated water volume and estimate the water flow rate (by timing). The water meter

was a single-jet dry dial water meter, under the category of velocity meters, in which the water enters the meter perpendicular to the rotational axis of the impeller placed inside the body of the meter. The impeller is made of a plastic with a lower specific gravity than water to avoid friction, with its rotational velocity proportional to the impact velocity of the water [162, 163].

3.7 Preparation and enumeration of *E. coli*

Non-pathogenic *E. coli*-K12 (NCTC 10538) was used as a model of faecal contamination when pathogen removal of a system was investigated.

3.7.1 Preparation of *E. coli* stock

A single colony of *E. coli* (extracted with a sterilized loop from a stock agar plate) was spiked in autoclaved tryptic soy broth (Oxoid, UK), which was then placed in a shaking incubator (SI 50, Stuart Scientific) for 24 h for incubation at 37°C.

3.7.2 Enumeration of *E. coli* colonies

The spread plate method was used to isolate and enumerate *E. coli* bacteria. A dilution series from a water sample was made and 0.1 mL was pipetted out from each dilution onto the centre of the surface of a Chromocult® agar (Millipore) plate, spread evenly on the surface using an L-shaped spreader and incubated at 37°C for 24 h (INC Genlab incubator). Then, the plates were taken out to count the number of colonies, which are clusters of microorganisms cultured from a single cell and unlike in direct microscopic counts where all cells, dead and living, are counted, colonies represent only the viable cells; hence, the results are given in colony-forming units per millilitre (CFU/mL). Once

the colonies were counted, the number was multiplied by the dilution factor to determine the number of CFU/mL in the original sample.

Chapter 4

Assessment of low-cost cartridge filters

This chapter has already been published in the Journal of Water Process Engineering.

4.1 Introduction

Cartridge filters are widely available in most countries due to the low cost and easy installation. It was necessary to assess the filters based on the WHO guidelines and provide the performance data as a reference for later developments.

Turbidity, described as the scattering of light at 90 degrees from a reference beam, due to the presence of inorganic particles (clay and silt), chemical precipitates (manganese and iron), and organic particles (organisms and plant debris) is often used as a simple indicator of water quality with presence assumed to equate to contamination. It can be measured easily, quickly and reliably by a variety of devices including the low-cost, portable turbidity tubes. Turbidity is also a recommended measurement for water quality in the WHO's 'Guidelines for Drinking-water Quality' [46].

Turbidity can reduce the effectiveness of disinfection treatments, such as UVC radiation,

causing shielding of microorganisms from the radiation. Turbidity is commonly expressed in Nephelometric Turbidity Units (NTU); values above 4 NTU would visibly affect the aesthetics of water and from a treatment perspective, increase the UV dose requirement and the residence time required to guarantee the absence of pathogens in the treated water. Consumers often associate low turbidity with safe drinking water despite the fact that turbidity in itself does not always represent a risk [12, 46, 49–52]. However, with respect to water treatment, removal of turbidity is an important efficiency measurement for physical filtration based systems [48].

Filtration is considered the most practical and affordable process to remove turbidity and suspended particles for drinking water applications. Cartridge filtration is suitable for small volume applications, which consists of a single (or multiple) filter element(s) inside a low cost housing. These filters do not require specialist knowledge in relation to operation and maintenance [6, 56, 59], while providing a one-step separation process without the need for prior coagulation and flocculation, considered as an essential step in conventional water treatment [100]. However, cartridge filters need to be discarded when the pressure drop exceeds the operating range. These filters are commonly made of polypropylene or polyester with commercial cartridge filter types being wound, spun (meltblown) and pleated [61, 63].

With respect to removal of particles, filtration can be categorized into two types (a) depth filtration and (b) surface/cake filtration, depending on where the filtered solid is located. In depth filters (Fig. 4.1a), particles are removed throughout the depth of the medium. In this type of filtration, particles of diameters smaller than the filter's pore size can be removed in a two-step process of transport (advection) and attachment via different deposition mechanisms, namely, inertial impaction, gravity (only in gravitational flows), interception, and Brownian diffusion. In surface filtration (Fig. 4.1b), particles of larger diameter than the filter's pore size are strained and form

an external filter cake, which improves the filtration efficiency as the cake itself acts as a depth filter [6, 57, 71, 72]. By this definition, spun and wound filter elements are classified as depth filters and pleated filter elements are surface filters.

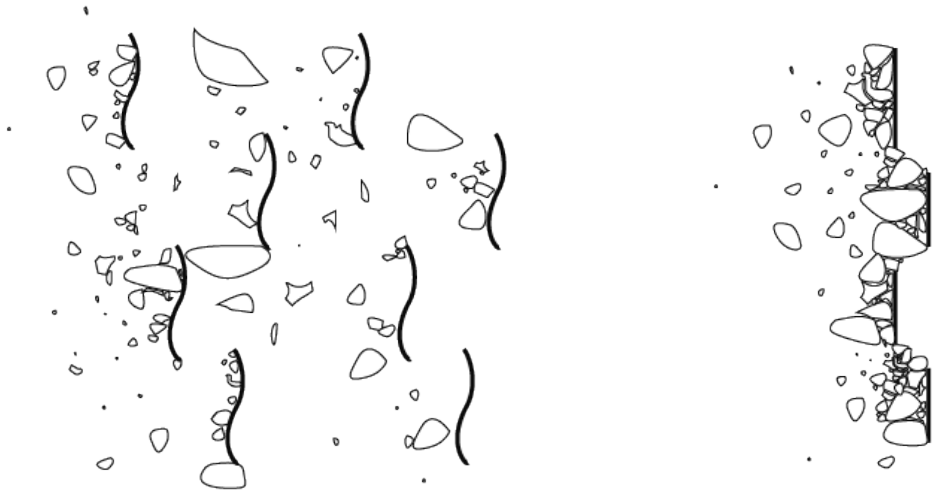

(a) (b)

Fig. 4.1 Two main categories of filtration: (a) depth filtration and (b) cake filtration.

Given the need for provision of safe water for a range of household level applications, in addition solely to consumption, the UN and WHO recommend the amount of safe drinking water required for one person per day may vary from 20 to 50 litres [40], depending on the climate and geographic area. Therefore, with system output of 250 L per day for a family of 5 members; the implementation of conventional treatment methods such as slow sand filtration [12, 143], rapid sand filtration [51], or ceramic filtration [13, 164] which require high installation costs and long treatment times would not be appropriate.

Although cartridge filters are commonly used in domestic water treatment systems, very

few studies focus on measuring the efficiency of such system specifically for drinking water treatment [67], with research mostly focused on air pollution [57]. Moreover, filter manufacturing companies report only the micron rating, pressure drop in clean filters and the Beta ratio in product literature, they do not test their filters under conditions of turbid water suspensions in accordance with the protocol of the WHO 'International Scheme to Evaluate Household Water Treatment Technologies' [33] nor investigate the long-term performance of their products.

The nominal micron rating reported by manufacturers is only a rough indicator of the particle size that might be removed by the filter medium as this corresponds to the particle size which the filters may retain – therefore, in practice two filters with the same micron rating can have differing performances. Instead, the Beta ratio is recommended by the Filter Manufacturers Council as a suitable filtration comparison parameter [65]. However, the Beta ratio ignores particles smaller than a filter's micron rating. Therefore, when using A2 fine test dust as the turbidity agent, even if a high Beta ratio is achieved by a 1 micron filter, low turbidity reduction might be observed given turbidity is number dependent [165] and 82% of A2 fine test dust particles are smaller than 1 µm. This loose characterization also relies on close quality control during manufacture; however, the only performance related information available for low-cost commercial cartridge filters is the nominal micron rating.

Published academic works on cartridge filtration for water treatment do not provide the comprehensive information required to develop a HWT system, with only either hydraulic performance [67, 68] or removal of a specific contaminant [66] investigated. Recently, Sikorska et al. [63] investigated both pressure drop and turbidity removal, using a tailor-made filter with six layers, which is a new approach.

4.2 Aim and Objectives

4.2.1 Aim

This chapter intends to provide an assessment of the turbidity removal efficiency and pressure drop of commercially available low-cost cartridge filters for household water treatment (HWT) application. The information provided by the manufacturers was limited, only including the nominal micron rating, which does not relate to turbidity removal efficiency and lifetime of these filters. Even though the filters are low-cost, prolonging their lifetime can significantly help their adaptation in impoverished areas. Thus, reuse of the filters was investigated.

4.2.2 Objectives

i. To assess the effect of filter micron rating of commercial filters (10, 5, 1 micron) on removal of turbidity in accordance with WHO HWT testing scheme and report the turbidity removal and pressure drop in simulated long-term trials.

ii. To investigate the structure of the fibrous filters in terms of void area, fibre size and fibre orientation.

iii. To provide information regarding the turbidity agent (ISO 12103-1 A2 test dust) chosen by the WHO HWT testing scheme in regards to particle size distribution and morphology as well as the correlation of its concentration and turbidity caused by it in order to provide a reference for future studies.

iv. To investigate whether the maximum allowable turbidity (5 NTU) recommended by WHO's 'Guidelines for Drinking-water Quality' can be achieved with cartridge filters.

v. To investigate the re-usability of the filters for several filtration cycles.

vi. To evaluate the effect of a high turbidity influent (120 ± 10) on turbidity removal efficiency, pressure drop and lifetime.

4.3 Materials and Methods

4.3.1 Instrumentation

A portable meter (Hanna Instruments, HI-93703) was used to measure the turbidity of water samples. A Scanning Electron Microscope (JEOL, JSM-6010) was used to take detailed images of test dust particles and fibers of the filters.

4.3.2 Preparation of turbid challenge water

Fine test dust (ISO 12103-1, A2, Powder Technology Inc.), a red brown insoluble mineral composed mainly of silica with a density of 2500–2700 kg/m^3, was used to prepare turbid water, based on the recommendations of the WHO scheme for evaluating HWT technologies [33]. The same grade of test dust is used in ISO 4572:1981, 'Hydraulic fluid power – Filters – Multi-pass method for evaluating filtration performance' [166], while the updated version, ISO 16889:2008, requires the use of ISO 12103-1, A3 medium test dust [167]. The subtle change in test dust parameters have been reported to not affect the actual performance of a wide range of filters [168].

Particle size distribution (PSD) by volume was provided by the manufacturer, and equivalent PSD by number presented in Fig. 4.2. A2 test dust particles were mostly smaller than 1 µm by number distribution, with the mean diameter of 0.779 µm, while the mean diameter by volume was much larger at 16.99 µm. Moreover, an SEM image of sample particles (Fig. 4.3) confirms the polydisperse nature of the test dust particles. Experimental measurements showed a linear correlation (R^2=0.97) between test dust concentration and turbidity with a slope coefficient of 0.68 and intercept set at 0

(Fig. 3.7). This correlation was used to produce water-test dust suspensions achieving a specific turbidity.

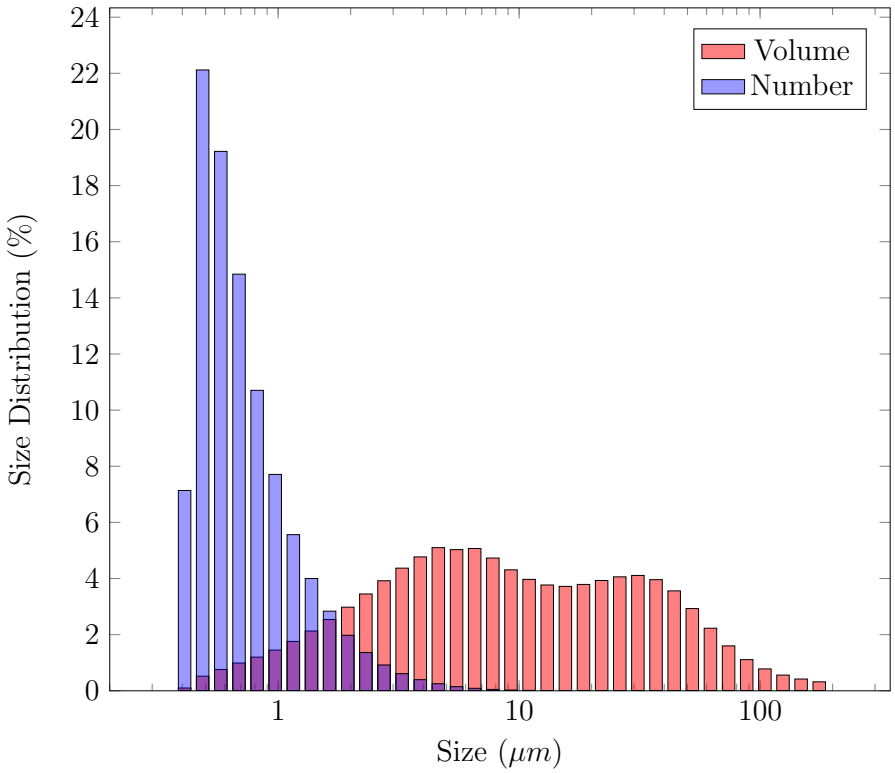

Fig. 4.2 Volume and number particle size distribution (PSD) of A2 fine test dust used in the trials (calculated using the data provided by Powder Technology Inc.).

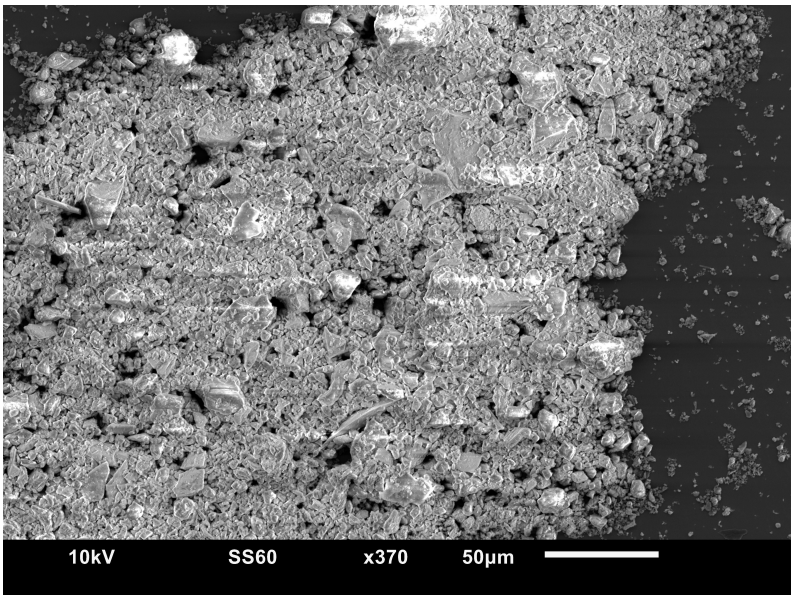

Fig. 4.3 An SEM image of A2 fine test dust particles used in the trials showing the shape of particles.

The initial turbidity of the feed tank was controlled to be 40 ± 10 NTU, in keeping with the WHO HWT systems challenge water criteria [33], using the correlation described above with confirmation by manual assessment. An additional trial with an initial turbidity of 120 ± 10 NTU was performed to investigate a potential worst case scenario as well as the effect of very high inlet turbidity on filtration cycle duration when pleated filters were used.

In addition, two trials were performed with kaolin clay (Sigma-Aldrich) which has a different PSD to test dust (Fig. 3.6). The concentration of the kaolin added was the same as the test dust, 60 mg/L, with the correlation of the kaolin concentration and turbidity given in Fig. 3.7.

4.3.3 Experimental Set-up

A drawing of the test system used is shown in Fig. 4.4, comprising two 10 inch standard filter housings, suitable for Double Open End (DOE) filter elements. Belfast tap water

(Antrim, UK) was fed into the inlet tank by a hose, and the water level kept constant by a float valve. A concentrated test dust stock was prepared by adding 34 g of A2 fine test dust to 3 L of tap water, which was dosed at 28.8 mL/min to the feed tank by a peristaltic pump (101U, Watson Marlow) ensuring a concentration of 60 mg/L and a turbidity of 40 ± 10 NTU.

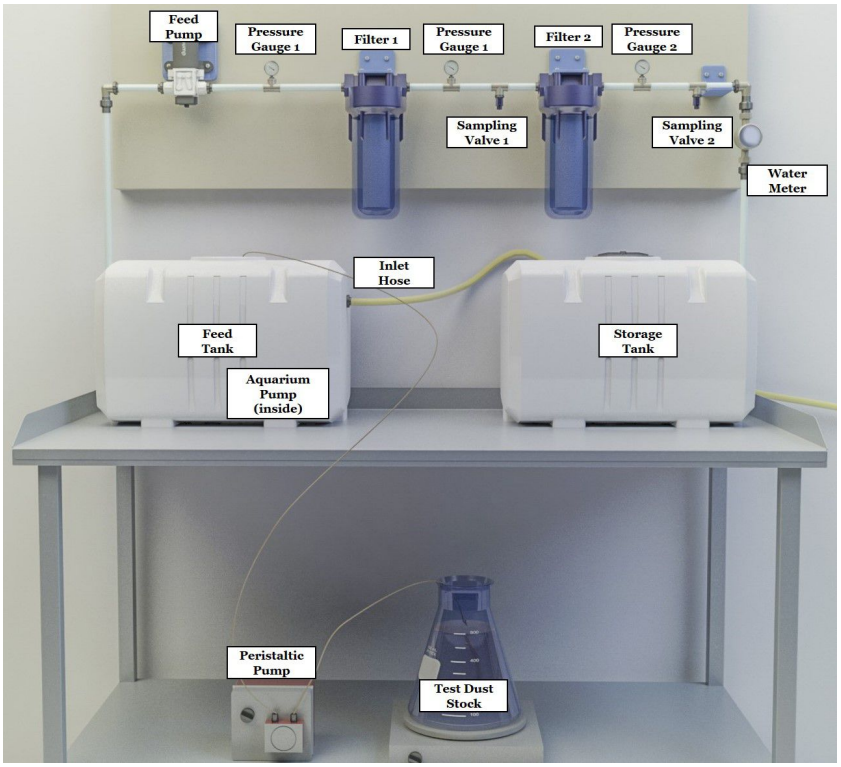

Fig. 4.4 A drawing of the test system used for testing the commercial cartridge filters.

To achieve 120 NTU for one of the trials, 102 g of test dust was used in 3 L. Particles in the stock were kept fully suspended during the trials using a magnetic stirrer at 100 rpm. An aquarium pump (Intercept, PF Mini) was utilized to internally recirculate the inlet tank suspension preventing settlement of larger particles inside the tank. A small 12V DC on-demand pump (Shurflo, Model 2095-204-412) was used as the main feed pump for the filtration system. This pump was chosen because it is suitable for household use, being wall mountable with a low noise level (50 dB measured by a mobile application

at a distance of 10 cm). The pump had a maximum operating pressure of 1.6 bar, and during the filtration trials, the initial flow rate of 5.2 L/min decreased to 4.4 L/min as the pressure increased to 1 bar (both flow rate and pressure were variable). Each filter assessment trial consisted of several runs spanning days or weeks in duration with a test volume for each run being 0.5 m^3.

Following processing of 50 or 100 L, samples (50 mL) were taken from the feed tank and the sampling valves after each filter. Samples were shaken before measurement of turbidity in order to avoid underestimation of turbidity due to settled particles. Each sample was measured three times and the average calculated.

The commercial filters used in this study were obtained from three UK distributors (Finerfilters Ltd., Aqua Cure Ltd. and The Water Filter Men), details are presented in Table 4.1. Filters with a similar technical parameters can be readily found in other countries from a range of suppliers. The spun and wound filters were made of polypropylene and pleated filters from polyester. As different filter elements were used in the trials, the following notation was used to describe the filter type ('S' for spun, 'P' for pleated and 'W' for wound) with the subsequent number referring to the micron rating. If two in-line filters were used (i.e two filters in series), a '+' sign is shown, e.g. S10 + S1 represents a 10 micron spun filter (Filter 1 in Fig. 4.4) followed by a 1 micron spun filter (Filter 2 in Fig. 4.4). In addition, a 10 inch ceramic cartridge filter and a 10 inch cartridge sand filter were also prepared; however, due to a high initial pressure drop (ΔP) >1 bar, turbidity removal trials were not performed. Filter elements with micron ratings of 10, 5 and 1 micron were trialled.

Three analogue pressure gauges were used to measure pressure drop after each filter, and a water meter (Ferro) was included to measure cumulative treated water volume and flow rate (by measuring time). Most trials were stopped when the initial pressure gauge reached 1 bar, due to leakage of influent into the outlet at high pressures in DOE filter

Table 4.1 Cartridge filter elements used in this study.

Abbreviation	Filter Type	Micron Rating	Manufacturer/Supplier
S10	Spun	10	SPECTRUM
S5	Spun	5	Finerfilters Ltd.
S1	Spun	1	Finerfilters Ltd.
W5	Wound	5	Aquafilter
W1	Wound	1	Aquafilter, The Water Filter Men
P5	Pleated	5	The Water Filter Men
P1	Pleated	1	The Water Filter Men
-	Ceramic*	-	The Water Filter Men
-	Sand*	-	The Water Filter Men

* not trailed due to high pressure drop.

housings. Moreover, the pump used in this HWT system provided a maximum pressure of 1.6–1.8 bar, and considering an extra static head required for piping in the field and the required elevation of a storage tank, 1 bar was considered the maximum available head for the filtration system.

4.3.4 Filter cleaning procedure

Potential to wash and reuse filter elements was assessed following achievement of the 1 bar pressure limit. Pleated filters were cleaned simply by running under a tap, shaking in a housing full of water for 3–5 minutes and if any cake was still attached, it was gently removed by hand. After cleaning, some cake remained on the folds, and particles were observed to be entrapped in the filter medium, these were not removed. Cleaning and reuse of spun and wound filters was not possible as particles were entrapped in the filter medium, as such they were discarded after single use.

4.4 Results and discussion

4.4.1 Filter characterisation

Images of the spun, wound and pleated filters (5 micron) prior to use (clean) are shown in Fig. 4.5a. A slice was physically removed from each filter and imaged with SEM (Fig. 4.6).

(a) Clean (b) Dirty

Fig. 4.5 The three types of cartridge filter elements used in this study: spun (left), wound (middle) and pleated (right).

It was observed that spun filters are constructed of many layers of fibers each of different diameters (1.1–34.3 µm) arranged in random orientation (Fig. 4.6a). Whilst there was no noticeable difference between the pore size within filters of different micron ratings (SEM images in Fig. 4.7), spun filters with lower micron rating had more compact layers of fibers.

Fibers in pleated filters (Fig. 4.6b) were randomly oriented with a uniform diameter distribution (14.23 ± 2.15 µm). Pleated filters of different micron ratings, show no significant variability in the pore structure (Fig. 4.8), only the thickness of the filter media (mat) was different.

Fig. 4.6c shows the wound filter structure as a single yarn, diameter of approximately 2

mm. The fibers are somewhat aligned with diameter varying from 30.29 ± 10.01 µm. However, the gaps between yarns are larger than the internal gaps between the wound filter fibers shown in Fig. 4.6c. It was observed that wound filters of different micron rating had yarns of different diameters, e.g. 1.4 mm for 1 micron filter (Fig. 4.9), which affects the size of the gap between the yarns, and hence the size of particles that are removed.

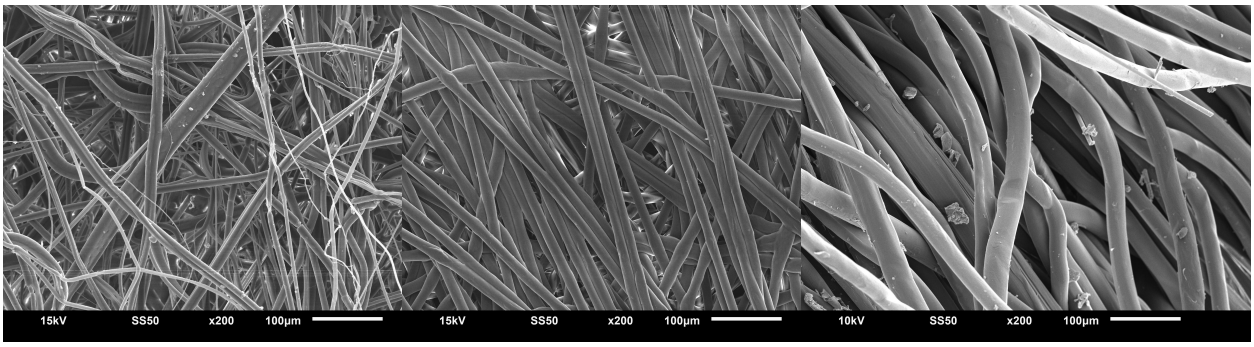

(a) (b) (c)

Fig. 4.6 SEM images of a cross-section of cartridge filters used in this study: (a) 5 micron spun, (b) 5 micron pleated and (c) 5 micron wound filters.

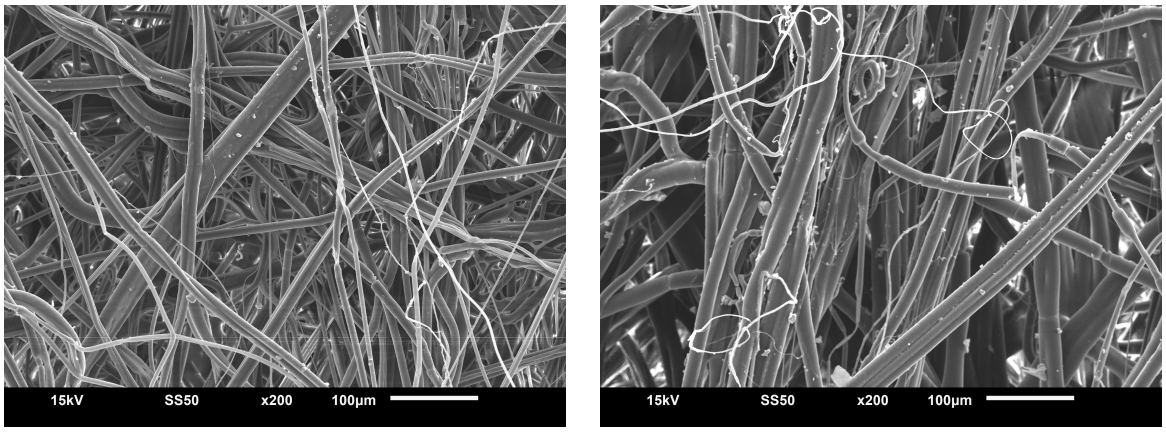

(a) (b)

Fig. 4.7 SEM images of a cross-section of spun filters with different micron ratings: (a) 5 micron and (b) 1 micron.

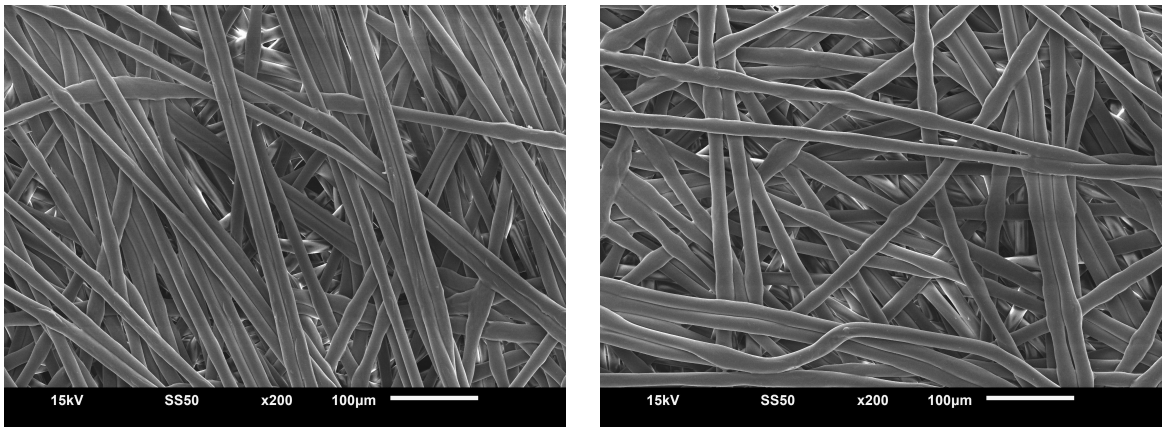

(a) (b)

Fig. 4.8 SEM images of a section of pleated filters with different micron ratings: (a) 5 micron and (b) 1 micron.

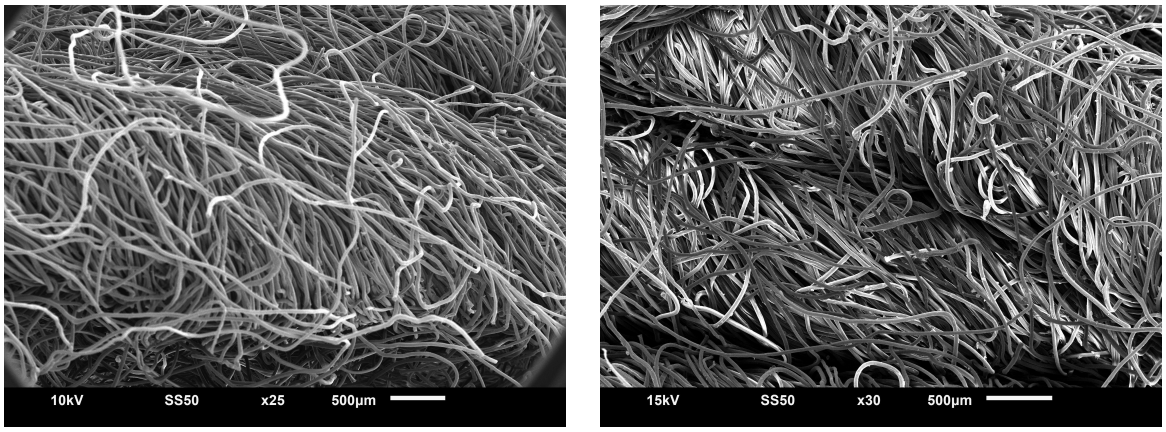

(a) (b)

Fig. 4.9 SEM images of yarns in (a) 5 micron and (b) 1 micron wound filters, showing yarns have different diameters.

4.4.2 Filtration trials with different types of cartridge filters

During the initial stages of filtration, it was observed that particles deposit randomly on the middle and lower regions of the filter elements, due to the flow path inside the housing. As the permeability of these regions decreased, particles then deposited onto regions above with less resistance to flow – until the entire filter became 'dirty' (Fig. 4.5b).

In the first trials, S10 + S5 and S5 + S1 filters were used, respectively (Fig. 4.10). To ensure clarity, trend lines obtained via fitting the experimental results to a linear model have been included. It was observed that despite the smaller micron ratings of S5 + S1, turbidity reduction after the 2nd filter does not show any improvement and does not reach the target <5 NTU.

In S10 + S5, an improved reduction was observed only after a flow volume of between 0.9 and 1.2 m^3, which corresponds to the sudden pressure increase due to clogging (Fig. 4.11). The next day, when a new run was started with the same filter, it was observed that particles were detached as the outlet water became cloudy, hence, increasing the turbidity and delaying the increase in ΔP (pressure drop). In the S10 + S5 trial, the observed lagging change in ΔP after the total gauge pressure reached 1 bar was thought to be due to leakage which also corresponds with the lack of improvement in turbidity reduction.

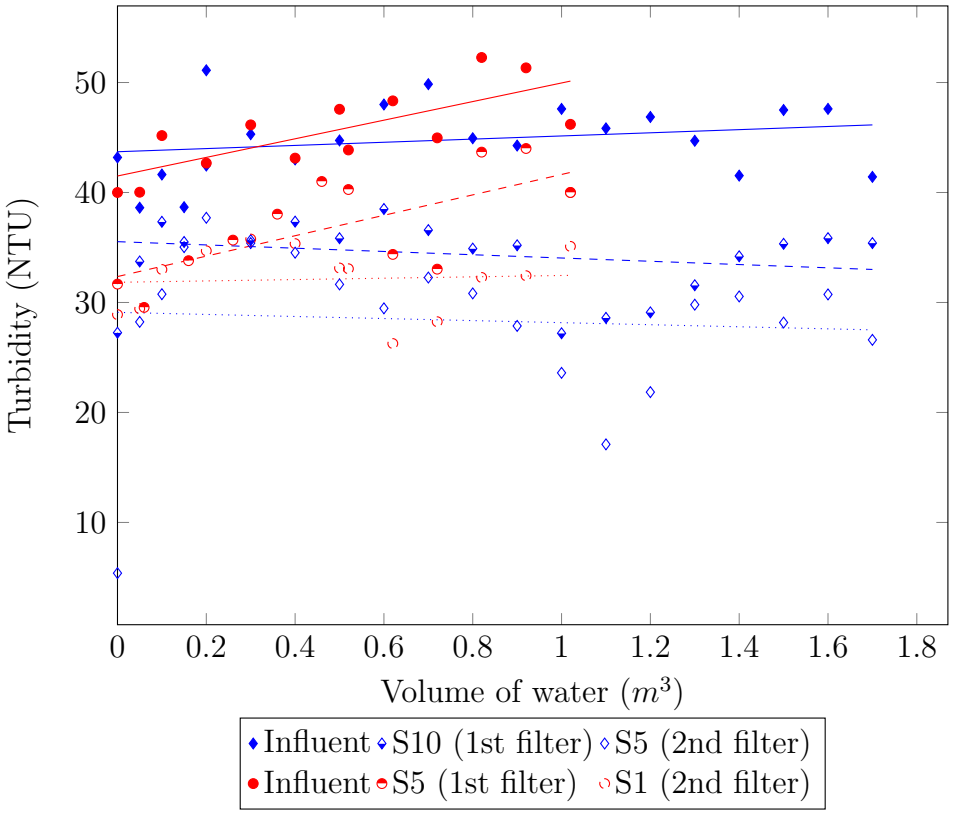

Fig. 4.10 Turbidity measurements of influent and effluent of spun filters. S10 + S5 two spun filter elements (10 and 5 micron) in series, S5 + S1 two spun filter elements (5 and 1 micron) in series.

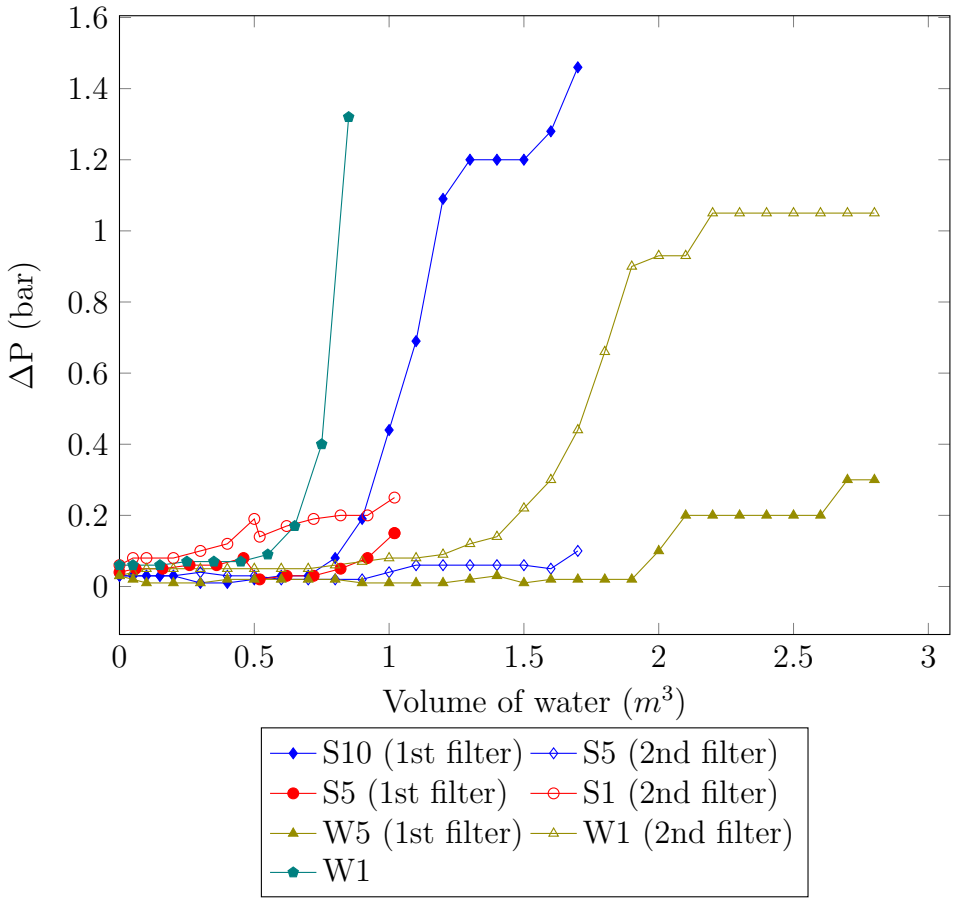

Fig. 4.11 ΔP measurements of each filter element. S10 + S5 two spun filter elements (10 and 5 micron) in series, S5 + S1 two spun filter elements (5 and 1 micron) in series, W5 + W1 two wound filter elements (5 and 1 micron) in series and W1 one wound filter element (1 micron).

In order to investigate whether the difference in filters' micron ratings (5 versus 1 micron) would alter turbidity removal efficiency, additional trials (Fig. 4.12) were performed with kaolinite and two spun filters with the same micron ratings in series (S5 + S5 and S1 + S1). Although kaolinite particles are finer than the test dust (Fig. 3.6) and based on volume distribution ≈60% of particles are smaller than 5 μm and ≈18.5% smaller than 1 μm, the difference in removal efficiency between the two filter set-ups was small (≈10%). In almost a third of measurements, the total removal via S5 + S5 was higher than S1 + S1 and in almost half of the turbidity measurements at the first filter, S5 had a higher removal percentage than S1. When either test dust or kaolin was used, the particles were

much smaller than the pores, and they were not removed by straining, but rather by other deposition mechanisms (i.e. inertial impaction, interception and Brownian diffusion). This demonstrates that relying only on a filter's nominal micron rating as an indicator of removal efficiency was not sufficient and that the pilot testing was essential to inform accurate filter choice.

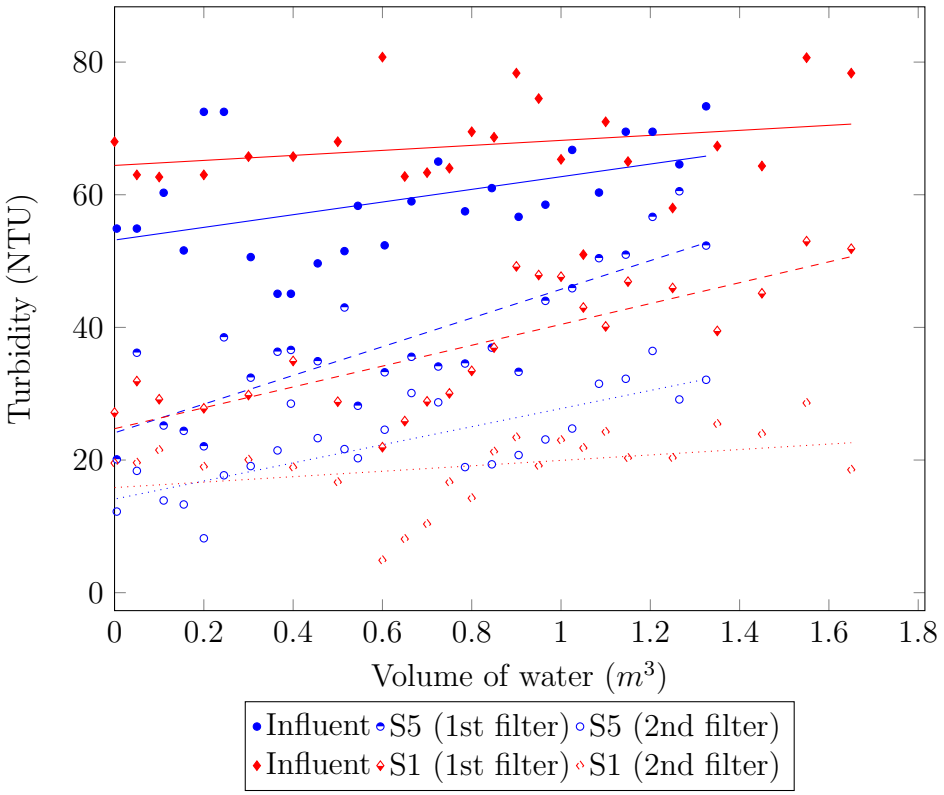

Fig. 4.12 Turbidity measurements of influent and effluent of spun filters against the volume of water treated (tested with 60 mg/L of kaolin). S5 + S5 two spun filter elements (5 and 5 micron) in series, S1 + S1 two spun filter elements (1 and 1 micron) in series.

Trials with wound filter elements used the smallest micron ratings available on the market, W5 + W1 and W1 (single filter trial). Data in Fig. 4.13 shows poor turbidity removal efficiency, with effluent >20 NTU frequently exiting the W5 + W1 system during that trial, the ΔP started to increase in the 1st filter after 1.4 m^3, while ΔP in the 2nd filter remained constant until 1.9 m^3 (Fig. 4.11). In the trial of W1, the outlet turbidity approached zero as more particles were retained by the filter, and the ΔP increased

accordingly.

The benefit of two filters in series against a single filter became clear as the 1 micron filter operating alone clogged quickly requiring replacement after only 0.85 m^3. The second filter is effectively 'protected' by the first filter from the volume of large particles that are primarily responsible for clogging.

Of the depth filters examined, only the trial using W1 reached the acceptable threshold of <5 NTU (according to the WHO [48]), but a rapid increase in pressure was observed with a volume of <1 m^3 treated (Fig. 4.11).

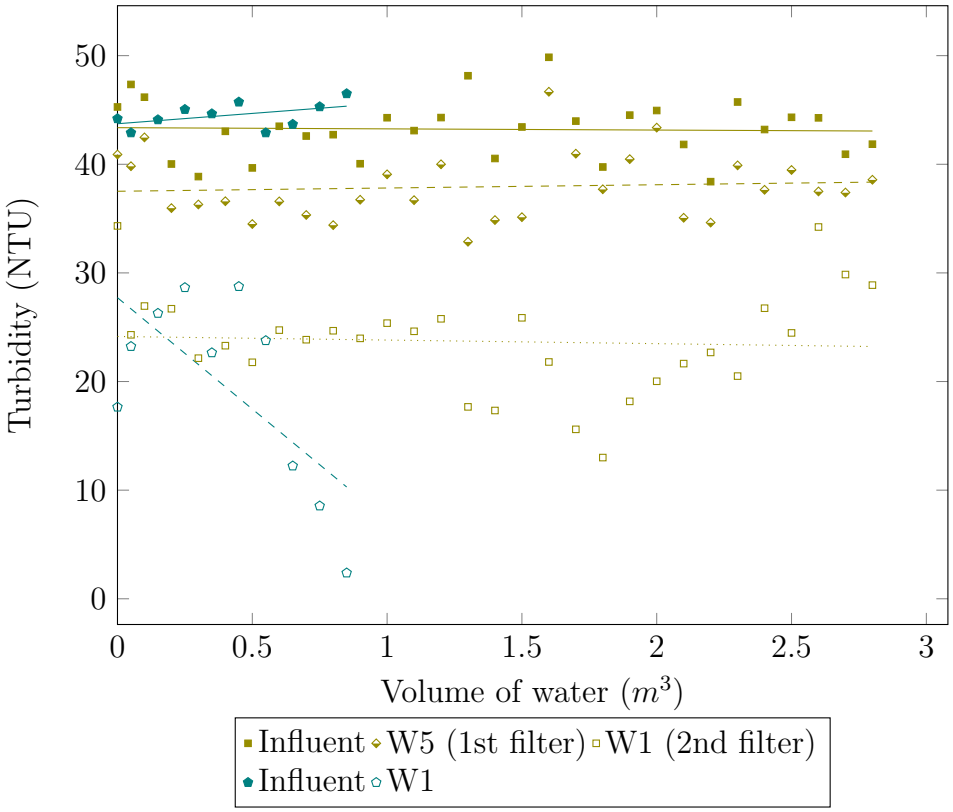

Fig. 4.13 Turbidity measurements of influent and effluent of wound filters. W5 + W1 two wound filter elements (5 and 1 micron) in series and W1 one wound filter element (1 micron).

In trial P5 + P1, 5 and 1 micron pleated filters were tested in series (Fig. 4.14) permitting direct comparison of micron rating with spun and wound filters. The final turbidity reached <5 NTU at a treated volume of 0.35 m^3, which was further reduced to 0.00 NTU

after 0.65 m^3. It can be observed that turbidity removal following the 1st filter improved as the pores were blocked by particles, effectively reducing the filter pore size. As the pressure increased (Fig.4.15), the turbidity removal declined, while the effluent turbidity of the 2nd filter remained constant upon reaching 0.00 NTU.

As with the previous trials, a gauge pressure of 1 bar was considered the operational limit of this experimental set-up. It should be noted that the decline in ΔP observed at intervals of approximately 0.5 m^3, was due to the stop-start nature of the experimental runs. It was observed that when a run was stopped and housings were no longer pressurized; that some particles detached from the surface, dispersed in water, and settled on the bottom of the housing. Particles also settled in the filter housing during the runs, more so when the ΔP increased and the fluid velocity decreased.

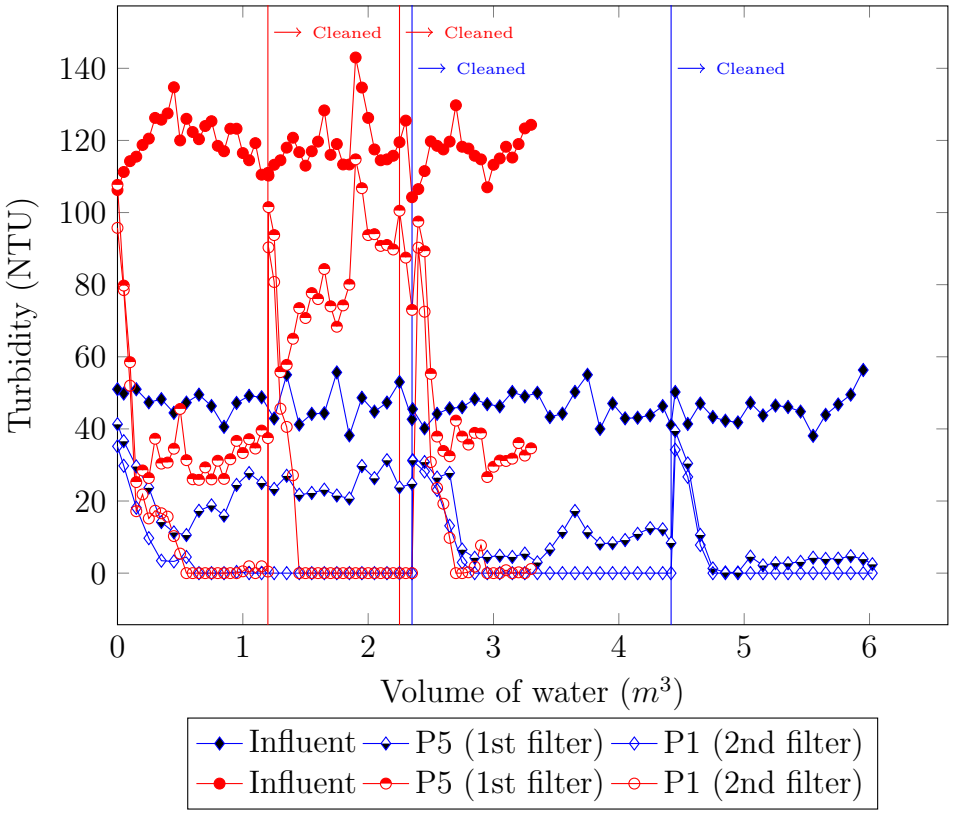

Fig. 4.14 Turbidity measurements of influent and effluent of each pleated filter. P5 + P1 (blue) two pleated filter elements (5 and 1 micron) in series and intial turbidity of 40 ± 10 NTU, P5 + P1 (red) two pleated filter (5 and 1 micron) in series and initial turbidity of 120 ± 10 NTU.

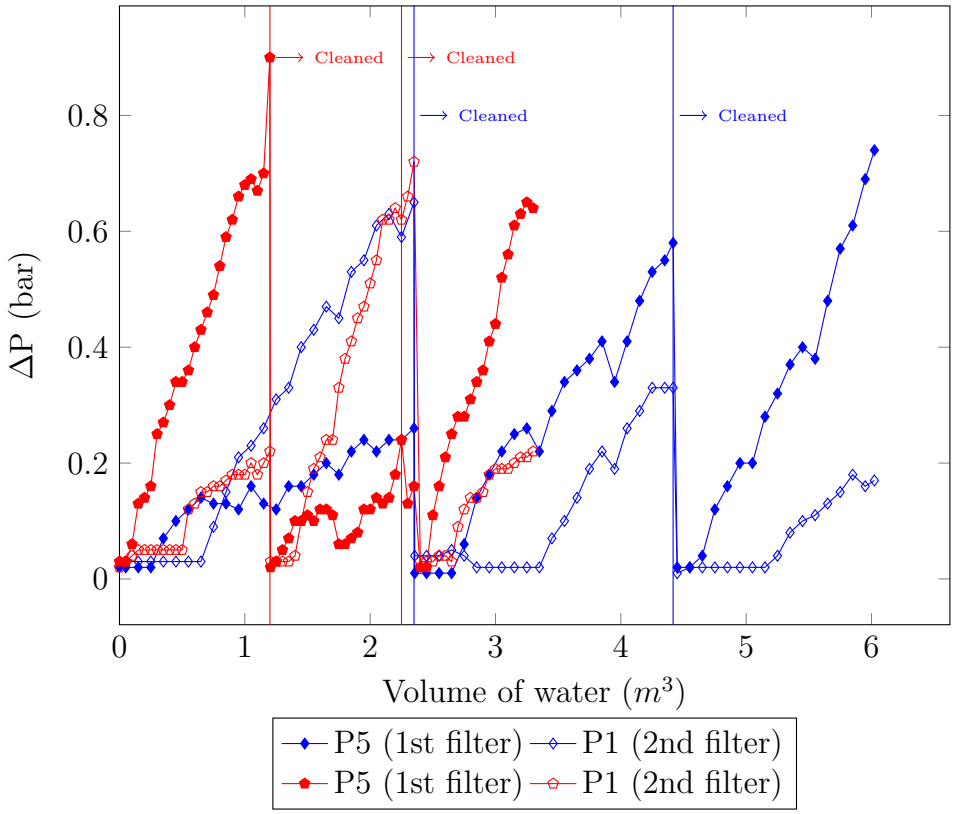

Fig. 4.15 ΔP measurements of each pleated filter element. P5 + P1 (blue) two pleated filter elements (5 and 1 micron) in series and intial turbidity of 40 ± 10 NTU, P5 + P1 (red) two pleated filter (5 and 1 micron) in series and initial turbidity of 120 ± 10 NTU.

4.4.3 Filtration trials with pleated filters after cleaning and re-use

After washing, the cleaned pleated filters were placed back in the housings (procedure described in Section 4.3.4) and used for another filtration cycle (Fig. 4.14). In this 2nd cycle, turbidity reached <5 NTU after 0.3 m^3 and 0.00 NTU after 0.5 m^3; due to more rapid development of cake on the filter resulting from the reduced porosity by entrapped particles from the initial cycle. Similarly, when washed and used in the 3rd cycle, turbidity reached 0.00 NTU at 0.3 m^3.

However, the observed pattern of ΔP during the three cycles was not the same (Fig. 4.15). In the 1st cycle, the ΔP of the 1 micron filter increase sharply after 0.65 m^3, which

corresponded to the same point that turbidity reached 0.00 NTU, while ΔP of the 5 micron filter started to increase steadily but slowly initially (after 0.35 m^3). In contrast, during the 2nd cycle, the ΔP of the 1st filter increased sharply after 0.4 m^3. This effect was amplified during the 3rd cycle, with the ΔP of the 1st filter increased sharply only after 0.2 m^3, while the ΔP of the 2nd filter was constant up to 0.7 m^3 and increased slower than the previous cycle. In the 1st cycle, the open pores of the 1st filter permitted larger particles to pass, causing clogging in the 2nd filter; however, in the 2nd cycle, the size of pores of the 1st filter had been decreased due to the entrapped particles within the filter, resulting in the large particles being captured by the first filter during the 2nd cycle.

The observed ΔP trend correlates well with turbidity removal, reaching 6.60 and 0.00 NTU in the 2nd and 3rd cycles, respectively. As the volume of particles entrapped within the filter increased, the duration of each cycle (i.e. the volume of water processed prior to reaching the 1 bar limit) decreased from 2.35 m^3 in the 1st cycle to 2.07 and 1.53 m^3 in the 2nd and 3rd cycles, respectively.

4.4.4 Filtration trials with pleated filters at elevated turbidity levels

Assessment of P5 + P1 with an initial turbidity of 120 ± 10 was performed, lasting for three cycles processing 1.05, 1.2 and 1.05 m^3 (Fig. 4.14, red data points). It was observed that the turbidity of <5 NTU could be reached and filters could also be cleaned and reused effectively. Analysing the effluent turbidity results showed that despite the much higher concentration of particles in the influent, the formation of a uniform cake layer on the 2nd filter takes approximately the same volume of turbid water. This provides further evidence for the above concept relating to retention of only large particles within pristine filters, with the difference in the total volume of particles arriving to the 2nd

filter irrespective of initial turbidity of either 40 or 120 NTU being small. This is also reflected in ΔP within the P5 + P1 trial at 120 NTU, pressure increased at a much faster rate than the trial with lower turbidity. Interestingly, in the 2nd cycle of the trial with P5 + P1 at high initial turbidity, although the 1st filter performed poorly, the effluent turbidity at the 2nd filter (1 micron) reached 0.00 NTU, which is also reflected in the filter's ΔP. Lower particle removal of the 1st filter during the 2nd cycle could be attributed to the very high volume of particles that reach the surface of the filter causing different cake structures or coverage in each cycle.

Comparing the volume of water processed in the 1st, 2nd and 3rd cycle of the 120 NTU experiment to the same cycle of the 40 NTU trial, we observe a reduction to 45%, 58%, 69%, respectively. Expressed as a function of time rather than volume treated (Fig. 4.16), a reduction to 52%, 56% and 60% was observed. We hypothesize that several factors are responsible for the lack of correlation, such as differences in the structure of the filter media and cleaning efficiency. Other factors might be related to the fluid flow field inside the housing as well as different particle-particle interaction at varying concentrations, which will be the topic of future research.

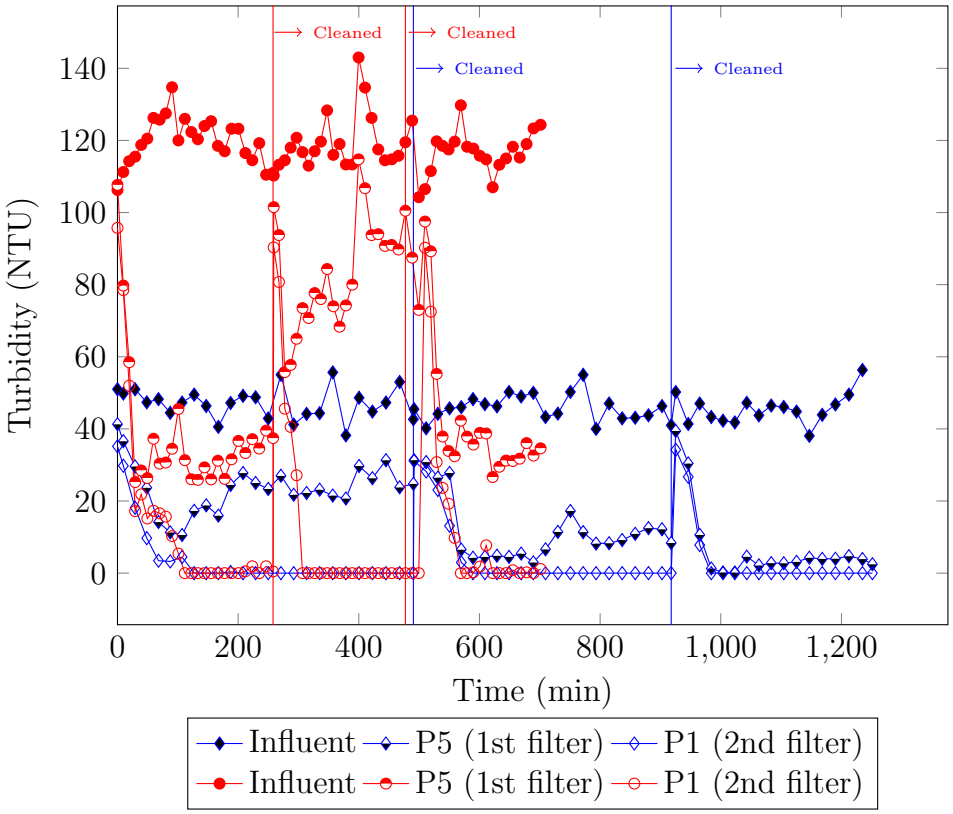

Fig. 4.16 Turbidity measurements of influent and effluent of each pleated filter against experimental time. P5 + P1 (blue) two pleated filter elements (5 and 1 micron) in series and intial turbidity of 40 ± 10 NTU, P5 + P1 (red) two pleated filter (5 and 1 micron) in series and initial turbidity of 120 ± 10 NTU.

4.4.5 Filtration trials with a single 1 micron pleated filter

As with the single depth filter trial (W1), the performance of a single 1 micron pleated filter (P1) was examined to potentially reduce costs (housing, filter element and piping). As can be observed in Fig. 4.17, turbidity decreased to <5 NTU after 0.45 m^3 reaching a minimum of 1.53 NTU at 0.55 m^3. Turbidity removal subsequently decreased as ΔP began to rise (Fig. 4.18). An outlet turbidity of 26.65 NTU was observed with a ΔP of 0.6 bar after 3.1 m^3.

Following cleaning, a similar initial reduction of turbidity was observed in the 2nd cycle, turbidity reached <5 NTU at 0.3 m^3 and 0.00 NTU at 0.4 m^3, with subsequent decrease

in particle removal resulting in a turbidity of 21.78 NTU and pressure of 0.9 bar (at 3.1 m^3). The observed trend for a single 1 micron filter was similar to the 1st filter of the two-filter trials – and we hypothesize that as the pores became smaller, turbidity removal improved; and as a result the pressure increased and the turbidity removal declined.

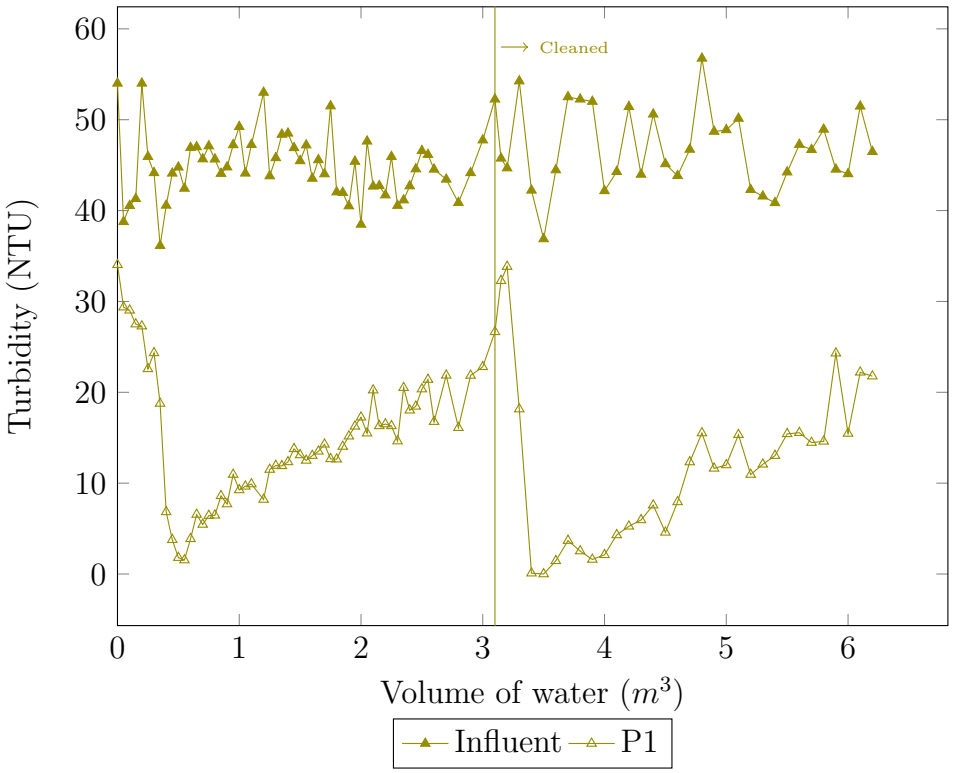

Fig. 4.17 Turbidity measurements of influent and effluent of P1 a single pleated filter (1 micron) and initial turbidity of 40 ± 10 NTU.

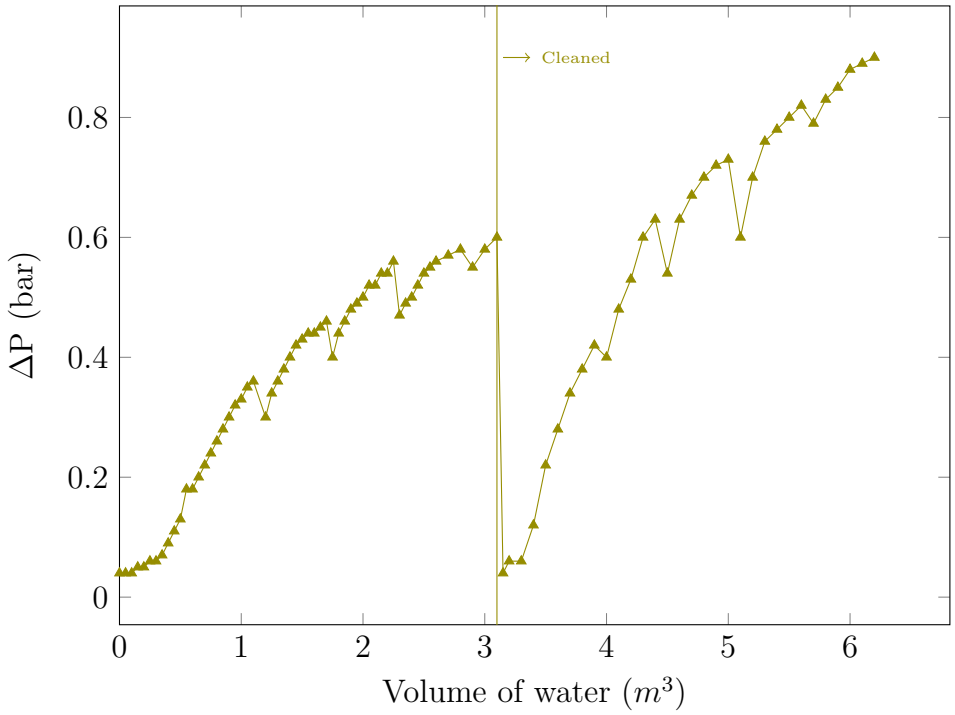

Fig. 4.18 ΔP measurements of P1 a single pleated filter (1 micron) and initial turbidity of 40 ± 10 NTU.

Comparing 5 and 1 micron filters when used as the 1st filter, it can be seen that in the initial cycles, the 5 micron filter reached a minimum effluent turbidity of 10.57 NTU at 0.55 m^3 with turbidity removal gradually decreasing to a value of 24.77 NTU as the pressure reached 1 bar at 2.35 m^3.

With the 1 micron filter, effluent turbidity of 1.53 NTU was observed at 0.55 m^3 again the pressure increased resulting in turbidity removal falling to 20.5 NTU at 2.35 m^3 of processed water. Each cycle of the trial with P1 lasted for a larger volume than with P5 + P1 because the removal efficiency was lower, hence less particles were accumulated in the cake. The pressure change resulting from the single filter is also likely to have an influence on the cake formation and filtration efficiency. As the criterion of an effluent turbidity of <5 NTU was only satisfied during a short period, the data confirms the need for multi-step filtration.

4.5 Conclusion

The internal structure of the filter elements were investigated by SEM imaging, showing the size and arrangement of fibres in spun, wound and pleated filters. It was observed that micron rating does not relate to the pore size but the compactness (number of layers of fibres) of the filters, which affect the probability of particles coming into contact with a fibre.

The A2 fine test dust recommended as the model suspended particles by the WHO HWT scheme was characterised and a linear relationship between its concentration in water and turbidity was established. Due to polydispersity, the volume- and number-based particle size distribution (PSD) of A2 test dust were drastically different as the number-based mean diameter was 0.779 µm, whereas the volume-based mean was 16.99 µm. SEM images taken from the particles also visually confirmed the polydisperse nature of the test dust particles.

The trials demonstrated the general turbidity removal and pressure drop (ΔP) trends of a range of commercial filters in a study designed to simulate long term performance.

When A2 test dust was used, pleated filters outperformed spun and wound filters reaching the goal of effluent turbidity of <5 NTU, both when the initial turbidity was 40 $\pm$ 10 NTU and with higher initial turbidity of 120 $\pm$ 10 NTU. In addition, pleated filters improved sustainability through the opportunity to clean and reuse the cartridge element for at least three cycles while delivering a higher quality effluent output.

Given the range of particle sizes occurring naturally in water and in the model test dust, we demonstrate that a 'multi-barrier approach' to filtration based systems, results in consistent and reliable turbidity removal and effluent quality.

However, effluent turbidity only reached the WHO HWTS criterion of <5 NTU after 0.35 m^3 of water was processed using pleated filter elements of 5 and 1 micron. During the initial lag time, water should be discarded until a cake builds up and particle removal

reach the target; in practice, this is not feasible in regions where water is not abundant. Studying the fluid dynamics in the filter housing was also undertaken (Chapter 5) to provide a better understanding of the role of the fluid flow field. Further research was conducted (Chapters 6 and 7) to reduce the lag time ensuring that all treated water meets a turbidity threshold of <5 NTU.

Chapter 5

Simulating particle removal from water via cartridge filters using CFD

5.1 Introduction

In the previous chapter (Chapter 4) spun filters were tested and the trend of particle deposition on the filters were described: at the beginning of the experiments, particles deposited randomly on the middle and lower regions of the filter elements and later, on the upper region of the filters (See Section 4.4.2). The design of cartridge filters could be improved with a greater understanding of how and where particles build up on the surface, resulting in poor filtration performance. To aid with physical experiments in the lab, a modelling approach that can consider the transport and entrapment of particles and its effect on the fluid dynamics and *vice versa* could be an important approach to understand the filtration process and aid in suggesting improvements.

The physical mechanisms involved in removal of particles from solutions via filtration processes can be considered at microscale using fundamental mathematical and kinetic models and at macroscale by observational (phenomenological) models. The former considers the complex structure of a filter medium and particles in their actual form, while

in the latter, the medium is defined by its physical attributes (permeability, porosity and possibly pore size distribution) [6, 77]. However, accurate models have not been developed for cartridge filters despite the importance of prediction of filtration performance in industry [127].

Adin and Rebhun [111] developed a model based on the material balance for an infinitesimal element of a filter bed. They assumed a constant diffusion coefficient and porosity, and therefore used a simplified mass transfer equation (Eq. 5.1).

$$\frac{\partial C}{\partial x} + \frac{\partial \sigma}{\partial V} = 0 \tag{5.1}$$

where x is the filter depth, C the suspension concentration, σ the specific deposition and V the filtrate volume.

Eq. 5.1 was solved together with a kinetic equation (Eq. 5.2) for the accumulation and detachment of particles,

$$\frac{\partial \sigma}{\partial V} = k_1 C(F - \sigma) - k_2 \frac{\sigma}{K} \tag{5.2}$$

where k_1 and k_2 are the accumulation and detachment coefficients, F the filter capacity and K the hydraulic permeability coefficient.

Many macroscopic models in literature are also based on the same approach, for example Han et al. [169] developed a model where the particle accumulation rate was based on a fundamental approach estimating the removal efficiency of a single collector. Similarly, Gitis et al. [109] provided a model for a full filtration cycle of a sand filter, assuming a uniform velocity and distribution of particles across the filter cross-section. However, in these models the effect of fluid dynamics and particle size distribution was ignored. Mays and Hunt [114] demonstrated that both particle deposition and deposit morphology depend on the fluid flow fields and the characteristics of the particles (e.g. diameter and density) and the porous media (e.g. porosity and collector diameter). Consequently,

the models described above are only useful as long as the filter structure and operating conditions under investigation do not deviate from the model parameters. This would not be true for HWT systems incorporating cartridge filters, and as such there is a gap in knowledge around this important topic.

Therefore, a more general approach is needed to ensure flexibility in modelling of the cartridge filtration process, while considering the geometry of the unit. Computational fluid dynamics (CFD) is a powerful tool in this regard, allowing evaluation of flow properties at locations in a filtration unit that are not possible with lab based measuring instruments [65]. The large volume of data generated as a result of numerical CFD solutions can be visualised by vectors and contours [120], which has aided understanding to processes such as sedimentation [124]. Moreover, the data generated can be used to develop deep learning models to lower the computational time/costs of the simulations [170].

The application of CFD for simulation of filtration technologies has been widely applied, however few reports focus on HWT systems [171]. Subrenat et al. [128] investigated the pressure drop inside a cartridge housing with an activated carbon pleated filter for removal of volatile organic carbon compounds using a combination of 3D numerical simulation and experimentation, to optimise pleat number for the filter element thereby minimising the pressure drop. Similarly, pressure drop and adsorption capacity of an activated carbon filter installed in an indoor air purifier was modelled by Roegiers and Denys [129], showing the spatial variation of adsorbed acetaldehyde at different time intervals.

Saalbach and Hunze [172] applied CFD to simulate the flow fields within membrane bioreactor (MBR) tanks for both hollow fibre and sheet membrane modules. The MBR plant was modelled at macro-scale level by considering membrane modules as porous media. Their work provided an approach to simulate large scale treatment systems that

can be applied to other water and wastewater treatment plants.

Simulation of air/oil separation by cartridge filters was carried out by Basha [132], in which the flow fields and droplet trajectory were obtained. The Lagrangian approach was adopted for oil droplets while the Eulerian approach was used for the fluid flow. As oil droplets deposited over time, a decline in permeability was addressed by updating the inertial and viscous resistances in every cell of the porous zone.

Liu et al. [130] simulated dust removal by four ceramic filters, which were modelled as porous media in a housing. The number of deposited particles was summed to give the deposition mass in each cell and the pressure drop subsequently calculated by an empirical formula. The approach helped to explain experimental observations of non-uniform deposition of particles on the surface of the filter element.

Previous CFD studies have not investigated particle removal by cartridge filters commonly used for HWT; however, as described above, best practice was established through the Eulerian approach for the simulation of fluid flow and the Lagrangian approach for solid particles.

5.2 Aim and objectives

5.2.1 Aim

This chapter aims to simulate the filtration process using computational fluid dynamics to gain an understanding of the process determining the separation of particles on low-cost cartridge filters. Through laboratory validation of the model, the combination will provide an approach to evaluate the design of different filter units.

5.2.2 Objectives

i. To theoretically investigate the physics involved in cartridge filtration and provide the most appropriate mathematical model for each physical interaction.

ii. To study the effect of particle size on penetration in the depth of the filter.

iii. To visualise the fluid flow inside the cartridge housing and its effect on location of particle deposition during the simulation.

iv. To validate the CFD model using experimental approaches—study the build-up of particles in the filter and resultant pressure drop across the system.

5.3 Experimental materials and methods

Physical analysis of the filter materials and particles was required to inform and develop the parameters of the model and for experimental validation.

5.3.1 Instrumentation

A particle size analyser (Mastersizer 2000, Malvern Panalytical) was used to determine the size distribution of particles, with a scanning electron microscope (JSM-6010, JEOL) used to determine the shape of particles and the internal structure of the fibrous filter. Prior to SEM imaging, samples were gold coated using a sputter coater (K500X, Emitech). Post-acquisition image analysis was undertaken using ImageJ software [174].

The pressure drop of the filter was measured using a digital manometer (2028P7, Digitron). A portable turbidity meter (HI-93703, Hanna Instruments) was used to measure the turbidity of water samples before and after filtration as a surrogate measurement for particle removal.

5.3.2 Materials

The filtration unit consisted of a standard 10 inch polypropylene spun filter element (Filter Logic, UK) and a filter housing (Finerfilters, UK) commonly used in small water treatment systems (Figure 5.1). A commercial grade of diatomite, Standard Super-Cel® (Alfa Aesar, UK) with a density of 2300 kg/m^3 was added to water to represent polydisperse particles in turbid waters.

5.3.3 Experimental set-up and procedure

Two separate tanks were used to store the test water (feed tank) and the filtrate (storage tank). To prepare the test water, 3 g of Super-Cel was added to 25 L of tap water (Belfast, UK), making a 0.12 g/L suspension. The filter was placed inside the housing filled with water (the computational domain was also filled with water at the start). The feed pump (Model 2095-204-412, Shurflo), pipes, fittings and digital manometer were connected as shown in the process flow diagram of the system (Figure 5.1). Subsequently, the feed pump (fixed flow rate of 5 L/min) was turned on to pass the suspension through the filter. Trials were performed in triplicate, with pressure drop and turbidity measured every 2.5 L (the last 5 L in the tank was not processed).

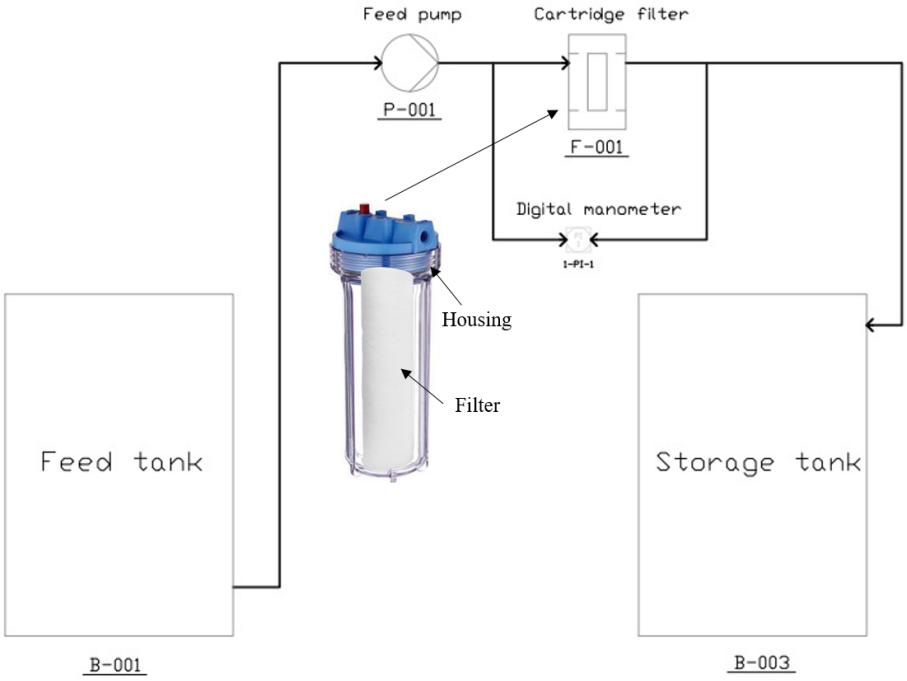

Fig. 5.1 The process flow diagram (PFD) of the filtration system and 10 inch cartridge filter element and housing used for the experiments.

5.4 Numerical methods

5.4.1 Particle size distribution function and shape

In order to represent the size of particles for modelling purposes, the Rosin-Rammler distribution function [133] was used; expressed as

$$Y = 1 - e^{[-(\frac{X}{X_0})^n]} \tag{5.3}$$

where Y is the cumulative fraction by weight less than size X, n the 'uniformity constant' or 'spread parameter' describing the particles' uniformity, and X_0 the 'characteristic particle size', the size that 63.2% of particles were smaller than.

For non-spherical particles, shape can be quantified using the Wadell's sphericity (Ψ) [175], expressed as

$$\Psi = \frac{\text{surface area of a sphere with equal volume as the particle}}{\text{surface area of the particle}} \tag{5.4}$$

where Ψ is unitless and its value fractional.

5.4.2 Flow regime

In packed bed applications, Reynolds number is calculated as particle (fibre) Reynolds number (Re_f) via

$$Re_f = \frac{\rho v d_f}{\mu} \tag{5.5}$$

where v is superficial velocity, ρ density, μ dynamic viscosity, and d_f fibre equivalent diameter.

The flow regime was initially assumed to be laminar within the filter, while turbulent outside of the filter medium given water entered the housing via a 10 mm I.D. pipe. For turbulent flow regimes outside the filter, Reynolds-averaged Navier–Stokes (RANS) equations were used. Whilst based on laminar flow equations, the RANS include an additional turbulent viscosity in the terms for diffusion and non-pressure gradients of the momentum equation. There are several turbulence models, with k-ϵ being the most common in engineering applications [120]. Liu et al. [176] reported that for ceramic filters, pressure drop was predicted more accurately with k-ϵ than k-ω model and RSM (Reynolds stress model) and was therefore used in this study.

For turbulent flows, a wall function is used to approximate the drag at the wall and obtain the transition from zero velocity at the wall with no-slip boundary condition to the free stream turbulent core. Scalable wall functions were used due to the value of Y-plus ($y^+ > 11.225$), obtained from preliminary calculations.

5.4.3 Porous media model

The filter was considered as a homogeneous porous medium and included in the model as a computational zone with an additional momentum source term (S_i), including the viscous and inertial resistances as shown in Eq. 5.6.

$$S_i = -\left(\frac{\mu}{\alpha}v_i + C_2\frac{1}{2}\rho|v|v_i\right) \tag{5.6}$$

where α is permeability, C_2 the inertial resistance factor and v_i velocity in i direction—α and C_2 should be determined empirically [134].

The permeability (α) was determined by running clean water through a clean cartridge filter, measuring the pressure drop and applying Darcy's law. The inertial resistance term was considered negligible as the relationship between flow rate and pressure drop was linear, due to the relatively small flow velocity.

Average fibre diameter was measured via analysis of the SEM images and where required in a model, a random number was generated within the 90th percentile of the measured fibres.

5.4.4 Particle deposition model

In order to include particle deposition, numerical models for removal efficiency were needed. In this work, the fundamental model proposed by Tufenkji and Elimelech [135] was adopted, which provided equations for predicting single-collector (e.g. fiber) removal efficiency. In this model, the overall removal efficiency was the sum of the removal efficiency of different transport mechanisms—interception, gravitational sedimentation and Brownian diffusion. Eqs. 5.7–5.17 [6] were used to estimate the overall efficiency for each particle.

$$N_R = \frac{d_p}{d_f} \tag{5.7}$$

$$N_G = \frac{g\left(\rho_p - \rho_w\right) d_p^2}{18 \mu v_p} \tag{5.8}$$

$$N_{Pe} = \frac{3\pi \mu d_p d_f v_p}{k_B T} \tag{5.9}$$

$$N_{vdW} = \frac{H}{k_B T} \tag{5.10}$$

$$N_A = \frac{N_{vdW}}{N_R N_{Pe}} \tag{5.11}$$

$$\gamma = (1-\varepsilon)^{1/3} \tag{5.12}$$

$$A_S = \frac{2\left(1-\gamma^5\right)}{2-3\gamma+3\gamma^5-2\gamma^6} \tag{5.13}$$

$$\eta_I = 0.55 \mathrm{A}_S N_A^{0.125} N_R^{1.675} \tag{5.14}$$

$$\eta_G = 0.22 N_R^{-0.24} N_{\mathrm{vdW}}^{0.053} N_G^{1.11} \tag{5.15}$$

$$\eta_D = 2.4 A_S^{1/3} N_R^{-0.081} N_{vdW}^{0.052} N_{Pe}^{-0.715} \tag{5.16}$$

$$\eta_t = \eta_l + \eta_G + \eta_D \tag{5.17}$$

A_S = porosity function, –

d_p = particle diameter, m

d_f = fibre diameter, m

k_B = Boltzmann constant, 1.381×10^{-23}J/K

T = absolute temperature, K

v_p = particle velocity, m/s

v_S = Stokes settling velocity, m/s

ε = bed porosity, –

γ = porosity coefficient, –

ρ_p = particle density, kg/m^3

ρ_w = liquid density, kg/m^3

μ = liquid viscosity, kg/(m s)

N_R = relative size group, –

N_G = gravity number, –

N_A = attraction number, –

N_{vow} = van der Walls number, –

N_{Pe} = Peclet number, –

D_L = diffusion coefficient, m^2/s

H = Hamaker constant, 1×10^{-20} J

η_I = transport efficiency due to interception, –

η_G = transport efficiency due to gravity, –

η_D = transport efficiency due to diffusion, –

η_t = total transport efficiency, –

$1/\eta_{\mathrm{t}}$ is the number of possible collisions with fibres required so that one real collision can be registered. Therefore, in order to determine whether a particle was deposited

or not, $1/\eta_t$ was compared to the number of fibres that a particle has passed based on its location (Figure 5.2), obtained by multiplying the distance of the particle from the outer surface of the filter (R_p) by the number of fibres per mm (n_f), estimated from SEM images (filter slices were imaged vertically). Any deposited particle was added to the number of collectors for the respective cell. This calculation was performed for every particle that reached the filter zone.

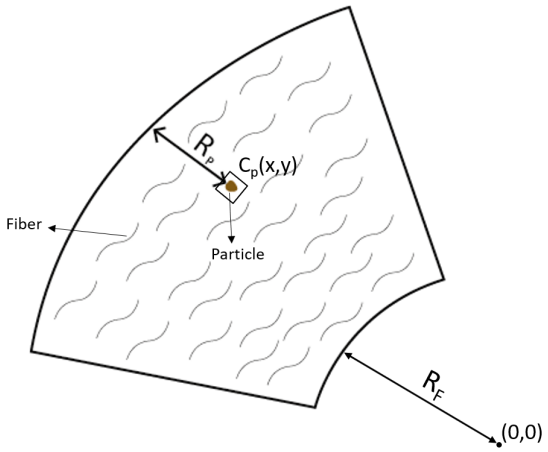

Fig. 5.2 Location of a particle in the porous zone, obtained by determining the coordinates of the cell (C_p) it is currently located in.

Possible collisions $= n_f \times 1000 \times R_p$

$R_p = \sqrt{x_{C_p}^2 + y_{C_p}^2} - R_F$

R_p = particle distance from the outer surface of the filter, m

R_F = the inner radius of the filter, m

n_f = approximate number of fibres in 1 mm

5.4.5 Filter cut-off size

In the deposition model explained above Tufenkji and Elimelech [135], the straining mechanism has not been considered, whereas in this study some particles are larger than the pores of the filter. Therefore, based on several SEM images of the filter, a cut-off size was estimated (90 µm).

5.4.6 Particle detachment model

A depositing particle might slide on the fibre because of the tangential drag force acting on it, resulting on its detachment. Bai and Tien [177] proposed a model to determine whether a particle detaches, in which the magnitude of the net force between the tangential force and the friction force in the opposite direction is calculated, through Eqs. 5.18–5.22.

$$F_f = k_f \times \frac{H d_p}{12\delta^2} \tag{5.18}$$

$$k_f = k'_f S \tag{5.19}$$

$$S = \frac{6\,(1-\epsilon_0)}{d_f} \tag{5.20}$$

$$F_S = 2.551 \times 3\pi\mu \frac{A_S}{d_f} d_p^2 \frac{v_p}{\epsilon_0 - \sigma} \tag{5.21}$$

$$F = F_f - F_S \tag{5.22}$$

F_f = friction force against particle sliding, N

k_f = coefficient of sliding friction, –

δ = the separation distance between the particle and the fibre plane, 3×10^{-10} m

k'_f = proportionality constant, 3.79×10^{-6} m

S = specific surface area, m^{-1}

F_s = hydrodynamic drag force on a particle, N

F = net force acting on an depositing particle along the tangential direction, N

A particle slips when F is a negative value, i.e. the tangential drag force is dominant over the friction force.

5.4.7 Local permeability

As the simulations were transient, an equation that related local permeability to the deposited particles in mesh cells at every time step was needed. Local porosity at time t (ϵ_{c_t}) was given by Eq.5.23.

$$\epsilon_{c_t} = \epsilon_{c_{t-1}} - \frac{V_{p_t}}{V_{c_t}} \tag{5.23}$$

where V_{c_t} and V_{p_t} are the volume of the cell and the deposited particle(s) at time t, respectively.

An equation was written for local resistance based on the Kozeny–Carman equation and Darcy's law,

$$\alpha_{c_t} = \alpha_{c_{t-1}} + \sum_{t=0}^{t} \left(\frac{D \cdot V_{p_t}}{\epsilon_{c_t}^2}\right) \tag{5.24}$$

where D is an empirical constant, obtained by performing preliminary trials with multiple commercial cartridge filters and Super-Cel particles.

Therefore, every time step, the volume of the deposited parcels is multiplied by an empirical constant, divided by the square of the porosity and added to the local resistance in the previous time step stored in a User Defined Memory (UDM) for the respective mesh cell.

Complete filling of a cell volume with particles was not considered as the amount of particles in the experiment was relatively small relative to the filter's volume.

5.4.8 Particle motion

The Lagrangian framework was adopted for the motion of particles. The trajectory of particles was predicted by integrating the force balance acting on the particles, written as

$$m_p \frac{d\vec{u}_p}{dt} = m_p \frac{\vec{u} - \vec{u}_p}{\tau_r} + m_p \frac{\vec{g}\,(\rho_p - \rho)}{\rho_p} + \vec{F} \tag{5.25}$$

where m_p, u_p, ρ_p and τ_r are particle mass, velocity, density and relaxation time, respectively [136].

The first term on the right side is the drag force, which is a function of the particle relaxation time (τ_r), the time required for a particle to adjust its velocity, expressed as

$$\tau_r = \frac{\rho_p d_p^2}{18\mu} \frac{24}{C_D Re} \tag{5.26}$$

where Re is the relative Reynolds number [137]. The drag coefficient, C_D, used for non-spherical particles can be expressed as,

$$\begin{aligned} C_{\mathrm{D}} = & \frac{24}{Re}\left[1 + e^{(2.3288-6.4581\psi+2.4486\psi^2)} Re^{(0.0964+0.5665\psi)}\right] \\ & + \frac{Re \times e^{(4.905-13.8944\psi+18.4222\psi^2-10.2599\psi^3)}}{Re + e^{(1.4681+12.2584\psi-20.7322\psi^2+15.8855\psi^3)}} \end{aligned} \tag{5.27}$$

where ψ is Wadell's sphericity [138].

Turbulent dispersion was also considered in particle motion. When particles are not located near a wall, turbulence dispersion dominates over gravity and Brownian motion [178]. Using the built-in stochastic tracking model in Ansys Fluent software, the dispersion of particles can be predicted by making use of the integral time scale, T_L, which is proportional to the particle dispersion rate. For small particles which move with the fluid, the integral time scale can be approximated as,

$$T_L = C_L \frac{k}{\varepsilon} \tag{5.28}$$

where T_L and C_L are the fluid Lagrangian integral time and time scale constant, respectively.

Other forces such as lift, Brownian and virtual mass have not been considered due to their negligible effect.

In simulations where the volume fraction of particles is small, one way coupling (particles to the fluid flow) is deemed sufficient [179], which has been implemented in this work. As it was prohibitive to track the same number of particles as in the real experiment, in the simulations, a number of 'parcels' were tracked instead—2000 parcels were injected every time step (0.01s). Each parcel represented a fraction of the total mass flow rate released

in a time step with a specified particle diameter and a relaxation time appropriate for a single particle [136].

5.4.9 Particle-wall collisions

Particle rebound following collision with a wall was calculated by the default model within Ansys Fluent [136] based on the work of Wakeman and Tabakoff [139], which calculates the rebound velocity by considering the coefficient of restitution (e):

$$e_n = \frac{v_{2,n}}{v_{1,n}} \tag{5.29}$$

$$e_t = \frac{v_{2,t}}{v_{1,t}} \tag{5.30}$$

where v_n and v_t are the particle velocity normal and tangent to the wall, respectively, and the subscripts 1 and 2 refer to before and after collision, respectively.
The coefficient should be determined based on the material of the wall, which in the case of the filter housing, hard plastic, the restitution coefficient value was 0.75–0.8 [180].
In order to avoid particles re-circulating near the bottom of the housing, without limiting the number of time steps for trajectory calculation, an arbitrary small value was considered for the velocity of particles hitting the bottom wall (v_{crit} = 0.005 m/s) below which the mass of a particle was registered in a UDM and removed from the domain.

5.4.10 Computational mesh

The computational mesh for this study was created by Ansys ICEM CFD, shown in Figure 5.3a, with ≈1.2 million high quality hexahedral mesh cells. As the cartridge filter was symmetrical, only half was considered in the model to reduce the required computational time. Mesh near the housing wall and the filter inner and outer surfaces was refined (Figure 5.3b) by determining a first element thickness and an expansion

factor (1.1) in order to capture the fields' gradients.

To evaluate the effect of mesh size on the pressure drop results, simulations with two smaller meshes—3.6 and 4.8 million mesh cells—were also performed. In Eq. 5.24, α_{c_t} defines the resistance for a cell; therefore, as mesh cells are divided, when a particle deposits, a smaller volume of the filter zone is affected. To counter this effect, the empirical parameter D was multiplied by the size ratio of the new mesh to the original mesh.

$$D' = D \times \frac{\text{No. of mesh cells in the current domain}}{\text{No. of mesh cells for which D (Eq. 5.24) was obtained}} \tag{5.31}$$

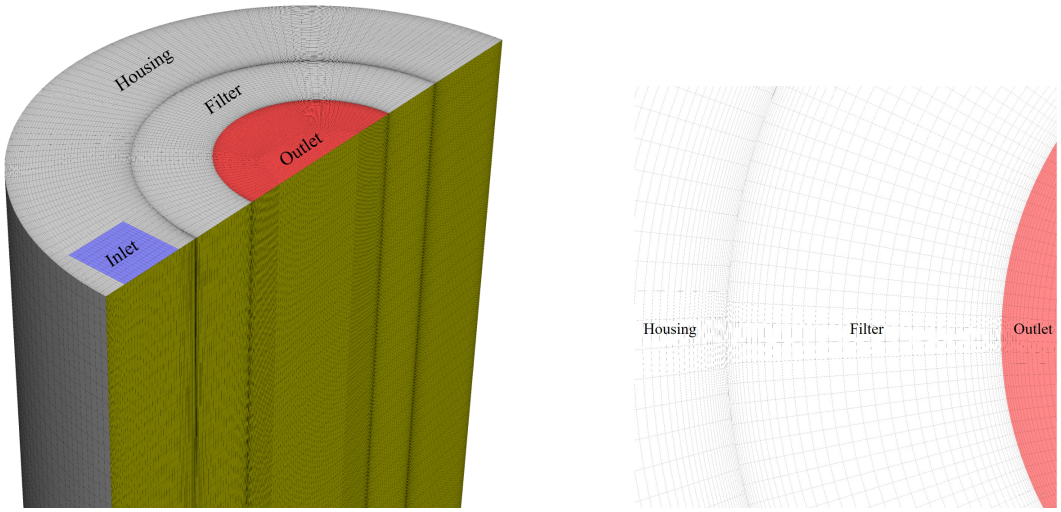

(a) (b)

Fig. 5.3 (a) The computational mesh used in this study, showing the filter inlet (blue), the outlet (red), the axis of symmetry (yellow) and the wall surface (grey); (b) the top surface of the domain, showing the mesh refinement near the filter outer and inner surfaces.

5.4.11 Solution

The calculation sequence for the simulation is summarized in the flow chart shown in Figure 5.4, and the simulation settings in Table 5.1. A commercial software (ANSYS

Fluent) was used to solve the governing equations, and custom User Defined Functions (UDFs), summarised in Table 5.2, were developed in order to include the additional models/functions required. In the simulation, the SIMPLE scheme with double-precision accuracy, the first-order implicit scheme for temporal discretization, the second-order upwind scheme for momentum, and the PRESTO! scheme for pressure coupling were used. The time step in the simulations was 0.01 s for both the fluid and particle phase, and the simulations were stopped when 2.4 g of Super-Cel was processed (i.e. deposited within the filter, on the bottom wall or escaped from the outlet), which made the simulation computational time much shorter than the real experiment.

The computer used was equipped with two Intel® Xeon® Processor E5645 (12 CPU cores) and 48 GB of RAM.

Table 5.1 Simulation settings.

Parameters	**Value**
Computational domain	
Domain size $i \times j \times k$ (m)	$0.045 \times 0.25 \times 0.045$
Mesh cells (millions)	1.2, 3.6, 4.8
Fluid phase	
Fluid density, ρ_w (kg/m^3)	998.2
Viscous model	Realizable k-ε
Fluid viscosity, μ_g (Pa·s)	0.001003
Inlet flow velocity (m/s)	0.3946
Fluid update time-step (s)	0.01
Particle phase	
Particle density, ρ_p (kg/m^3)	2300
Particle-wall restitution coefficient	e_n=0.75 , e_t=0.75
No. of injection parcels (parcels/s)	2000
Drag force coefficient	Levenspiel and Haider [138]
Turbulent dispersion time scale constant, T_L	0.05
Particle update time-step (s)	0.01
New particle injection interval (s)	0.01

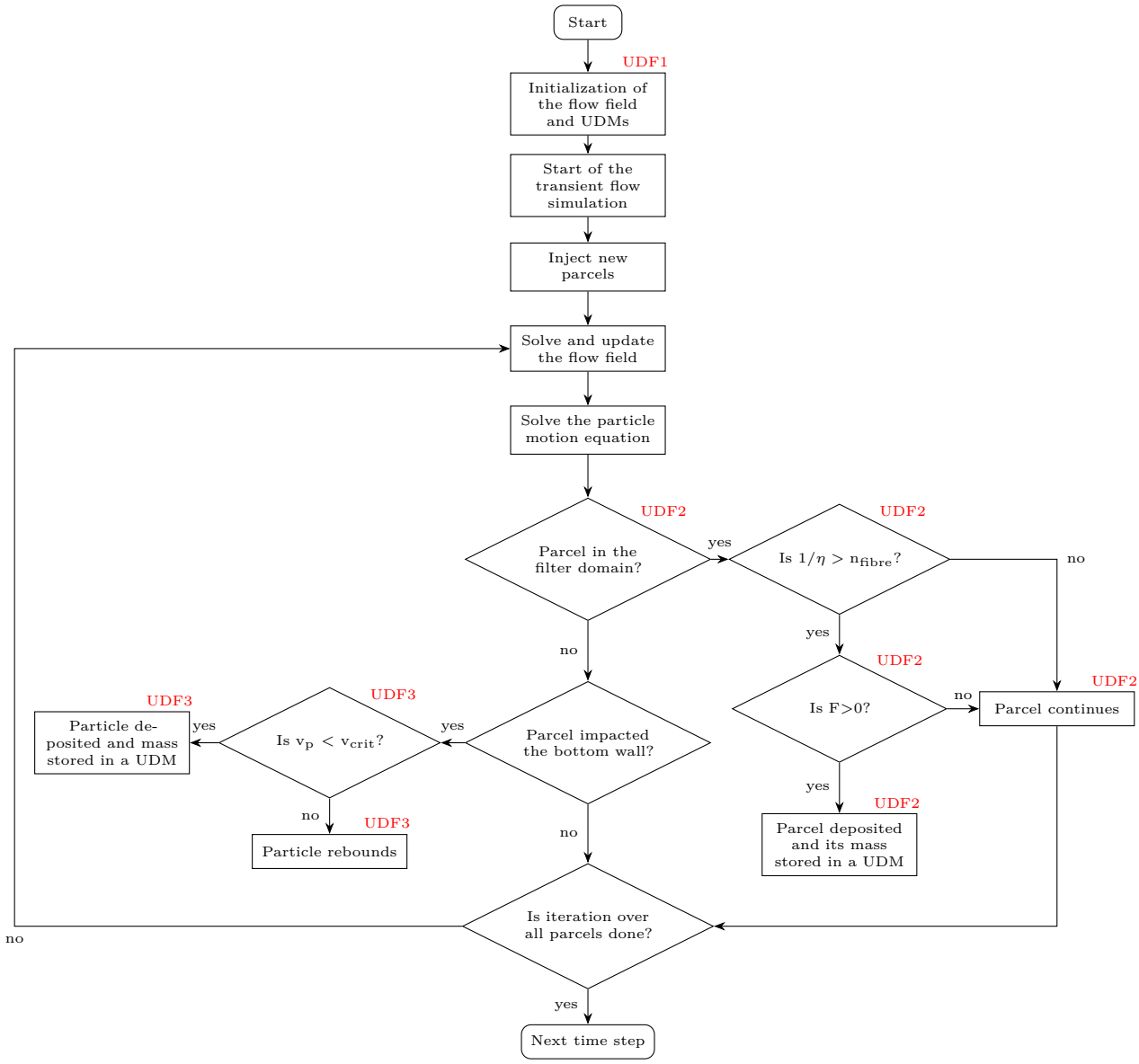

Fig. 5.4 Flow chart of the calculations implemented in this study.

Table 5.2 User Defined Functions (UDFs) included in the simulations.

UDF	Function
UDF1	Initialize the UDMs for local porosity and permeability.
UDF2	Include the deposition and detachment models.
UDF3	Determine whether a particle deposits on the bottom wall or rebounds.

5.4.12 Model validation

In order to validate the results obtained in the CFD simulations and demonstrate the accuracy of the modelling work, physical changes that could be experimentally measured were reported. The deposited particles on a cross section at the middle of the filter (12.5 cm from the top) after processing 2.4 g Super-Cel were visualised and compared with SEM images taken from slices removed from the outer surface at a depth of 1.5 cm (half of the distance between the outer and inner surfaces). The deposited particles within the volume of the filter were visualised and compared with digital photographs taken from the filter's surface using a camera. Lastly, the predicted pressure drop based on Eq. 5.24 and Eq. 5.31 was reported for three mesh sizes (1.2 m, 3.6 m and 4.8 m) and compared with the pressure drop measured during the experimental validation.

5.5 Results and discussion

To inform model development, physical analysis of the filter materials and particles was undertaken.

5.5.1 Filter, particle and flow characterisation

SEM images of the filter element (e.g. Figure 5.5a) showed the filter to comprise of randomly oriented fibres, with diameter sizes varying from 1.1 to 34.3 μm; 90% were between 14.57 and 34.3 μm, with the mean fibre diameter (d_c) being 25 μm. The number

of fibres per mm (n_f), obtained by SEM imaging (e.g. Figure 5.5b), was 44 per mm. The cut-off size of the filter was determined to be 90 μm. The porosity (ϵ) of the filter was estimated to be 0.78 based on the density of polypropylene fibres, 0.9 g/cm^3 [65], and the measured volume and weight of the filter.

The Reynolds number within the filter was calculated to be 0.044 by considering the mean fibre diameter (25 μm) and the superficial velocity (0.00196 m/s)—pump flow rate was 5 L/min and the surface area of the filter 0.0424 m^2. In Eq. 5.5, due to the exclusion of properties such as surface roughness, Reynolds number for transition between laminar and turbulent flow was empirical based give the flow regime: laminar ($Re_f < 10$), transitional ($10 < Re_f < 300$) or turbulent ($Re_f > 300$) [118].

By fitting the PSD data obtained for Standard Super-Cel® to the Rosin-Rammler distribution function (Eq. 5.3), the characteristic particle size and the spread parameter were determined to be 11.48 μm and 1.26, respectively. The measured and calculated PSD values (Figure 5.6) agreed well with an R-squared (R^2) of 0.994. Given Super-Cel® particles were observed to be mostly disk shaped (Figure 5.5c), the sphericity value for a thin disk can be assumed to be 0.66 [181].

The average permeability of the filter, estimated empirically to be 11.5×10^{-12} m^2, which assumed to be isotropic; the empirical constant in Eq. 5.24 was determined to be 1.49×10^{17} 1/m^5. A summary of the experimental results obtained for the simulations is provided in Table 5.3.

5.5.2 Particle deposition and detachment

In order to establish the relationship between particle deposition and particle size/velocity (Eqs. 5.7–5.17), the total transport efficiency (η_t) versus particle size and filtration velocity for a clean filter, based on a particle size and a velocity range of 1–50 μm and 0.001–0.1 m/s, respectively, is plotted in Figure 5.7a, where $\eta_t > 1$ dictates that the particle will

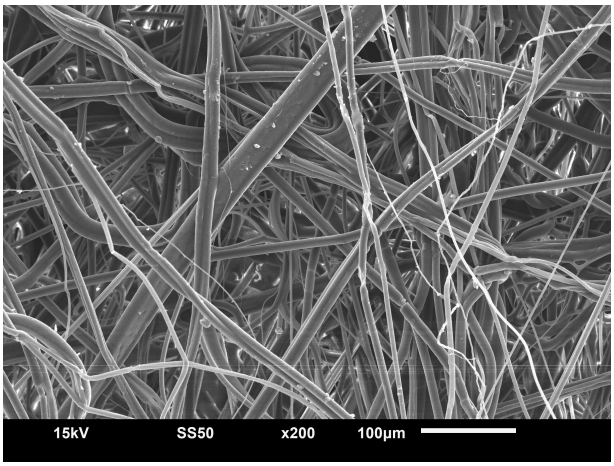

(a)

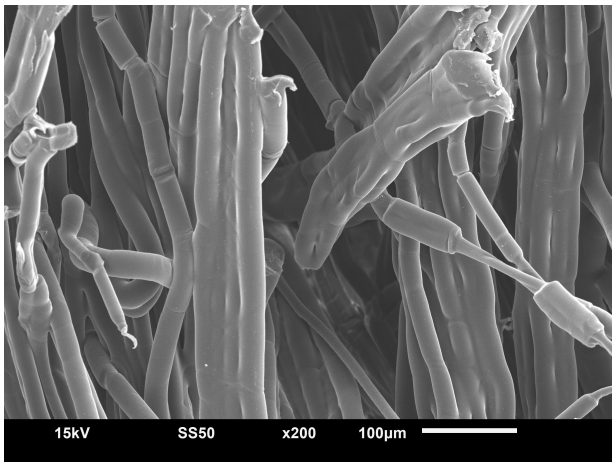

(b)

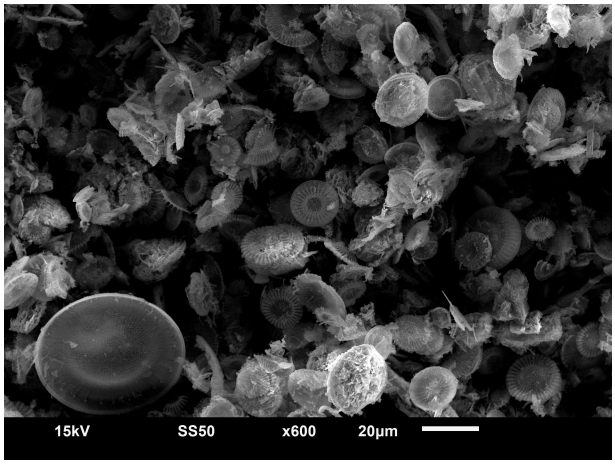

(c)

Fig. 5.5 SEM images of (a) the filter medium, (b) a slice of the filter placed vertically to measure the number of fibres in 1 mm, and (c) Standard Super-Cel® particles.

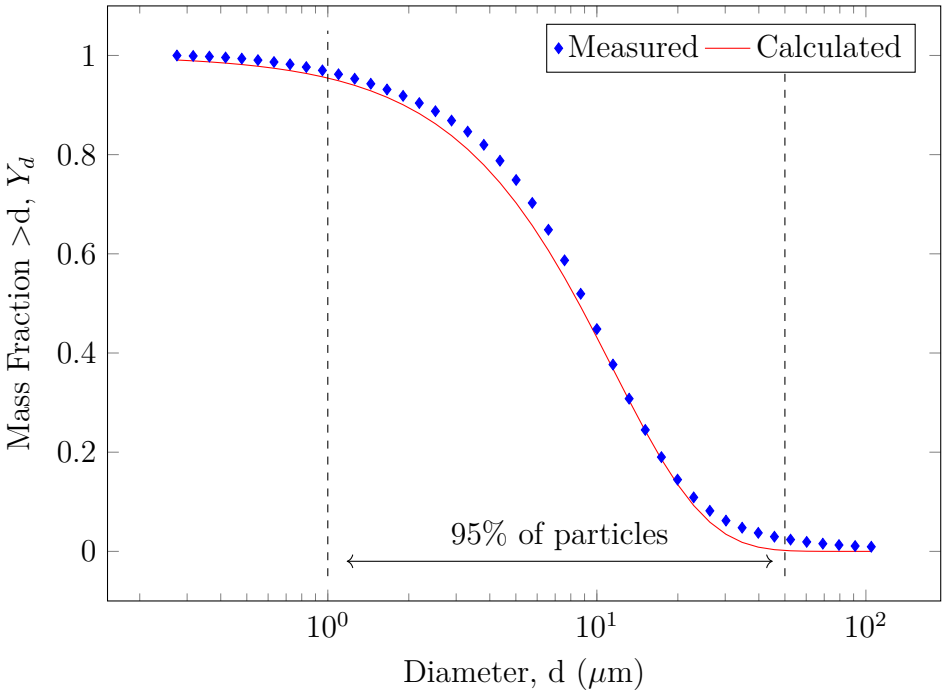

Fig. 5.6 The measured PSD for Standard Super-Cel® showing high correlation to that calculated by the Rosin-Rammler distribution function. The particle size range of 1–50 μm accounts for 95% of particles.

likely deposit on the first fibre that it encounters. For the mean fibre diameter of 25 μm, particle diameters above 32.6–49.7 μm had an η_t of >1 in the the velocity range of 0.001–0.0325 m/s, respectively. The velocity of a particle is inversely related to η_t; therefore, the likelihood of deposition increases as a particle loses momentum within the porous medium.

In order for a particle to be registered as deposited, the tangential drag force should not be larger than the friction force in the opposite direction, which is influenced by particle size, fibre size and pressure gradient as a result of local deposition. Figure 5.7b shows the results for the net tangential force (Eqs. 5.18–5.22) for a clean filter and the particle size and velocity range in the simulations. An F value below 0 implies a particle slips and will not be deposited. The net force has an inverse relationship with both particle size and velocity and through comparison of the results for the attachment and

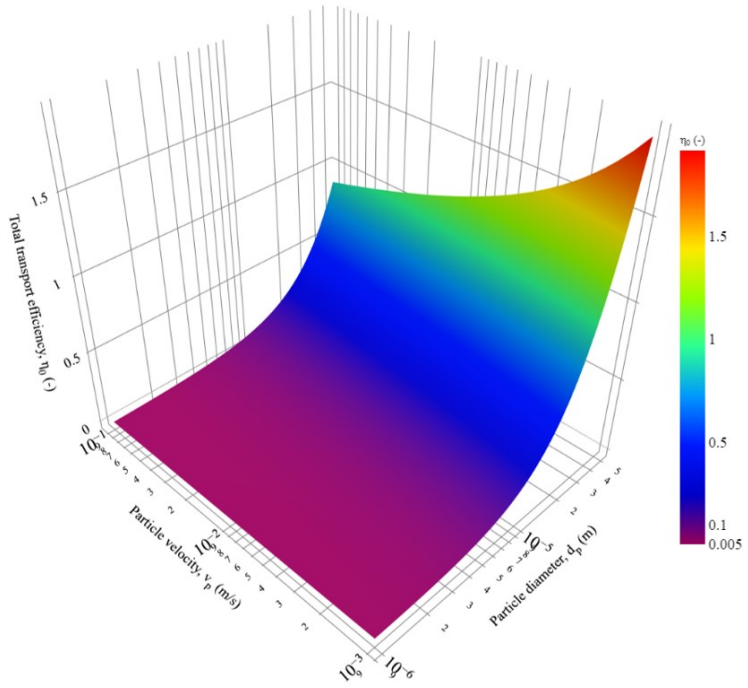

(a)

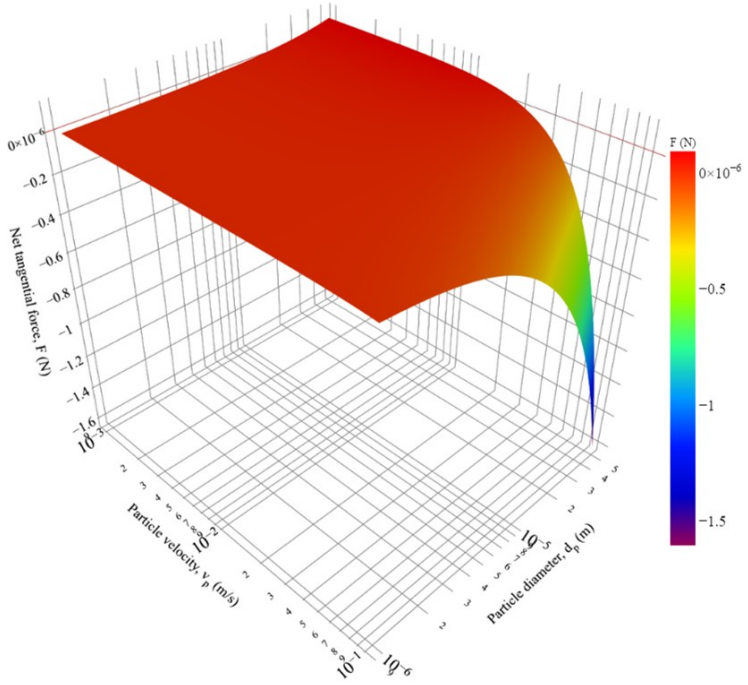

(b)

Fig. 5.7 (a) η_t versus particle size and velocity. (b) Net tangential force (F) versus particle size and velocity. ($d_f = 25\,\mu m$, $T = 288.15\,K$, $\epsilon_0 = 0.78$, $\rho_w = 998\,kg/m^3$, $\rho_p = 2300\,kg/m^3$, $k_f = 3.79 \times 10^{-6}$, $\delta = 3 \times 10^{-10}\,m$).

Table 5.3 Experimental results needed for the simulations.

Parameters	**Value**
Super-Cel particles	
Characteristic particle size, X_0 (μm)	11.48
Spread parameter, n	1.26
Particle sphericity	0.66
Porous media	
Filter cut-off size (μm)	90
Mean fibre diameter, d_f (μm)	25
Fibre diameter range, d_f (μm)	14.57–34.3
Filter porosity, ϵ	0.78
Filter initial permeability, α_0 (m^2)	11.5×10^{-12}
Eq. 5.24 constant, D ($1/m^5$)	1.49×10^{17}

detachment models, it can be concluded that as the velocity of a small particle decreases, it is more likely for the particle to attach without slipping, while a particle of larger size leads to increased probability of both deposition and slippage. Therefore, particle size alone cannot be a sole determinant of particle deposition, with a requirement for the consideration of local velocity.

5.5.3 Cross section velocity gradient and particle deposition

Modelling confirmed the velocity of the fluid changed within the cartridge filter both horizontally and vertically due to the cylindrical geometry (e.g. Figure 5.8a). The velocity gradient could be also impacted upon by particle deposition (e.g. Figure 5.8b), leading to dispersed deposition of particles between the inner and outer surfaces (Figure 5.8c). Figures 5.8c shows the contour of deposited particles' average diameter at 12.5 cm from the top (middle of the filter) at the end of the simulation (after processing 2.4 g Super-Cel), demonstrating the penetration of particles as a result of particle size. Particles above 90 μm were removed close to the outer surface of the filter given the cut-off size included in the simulations. As $V_p \propto d_p^3$, deposition of large particles in small numbers

resulted in a much higher mass (Figure 5.8d) and consequently reduction in porosity (Figure 5.8f) than fine particles in larger numbers (Figure 5.8e).

To validate the model, SEM images of filters following processing of 2.4 g Super-Cel

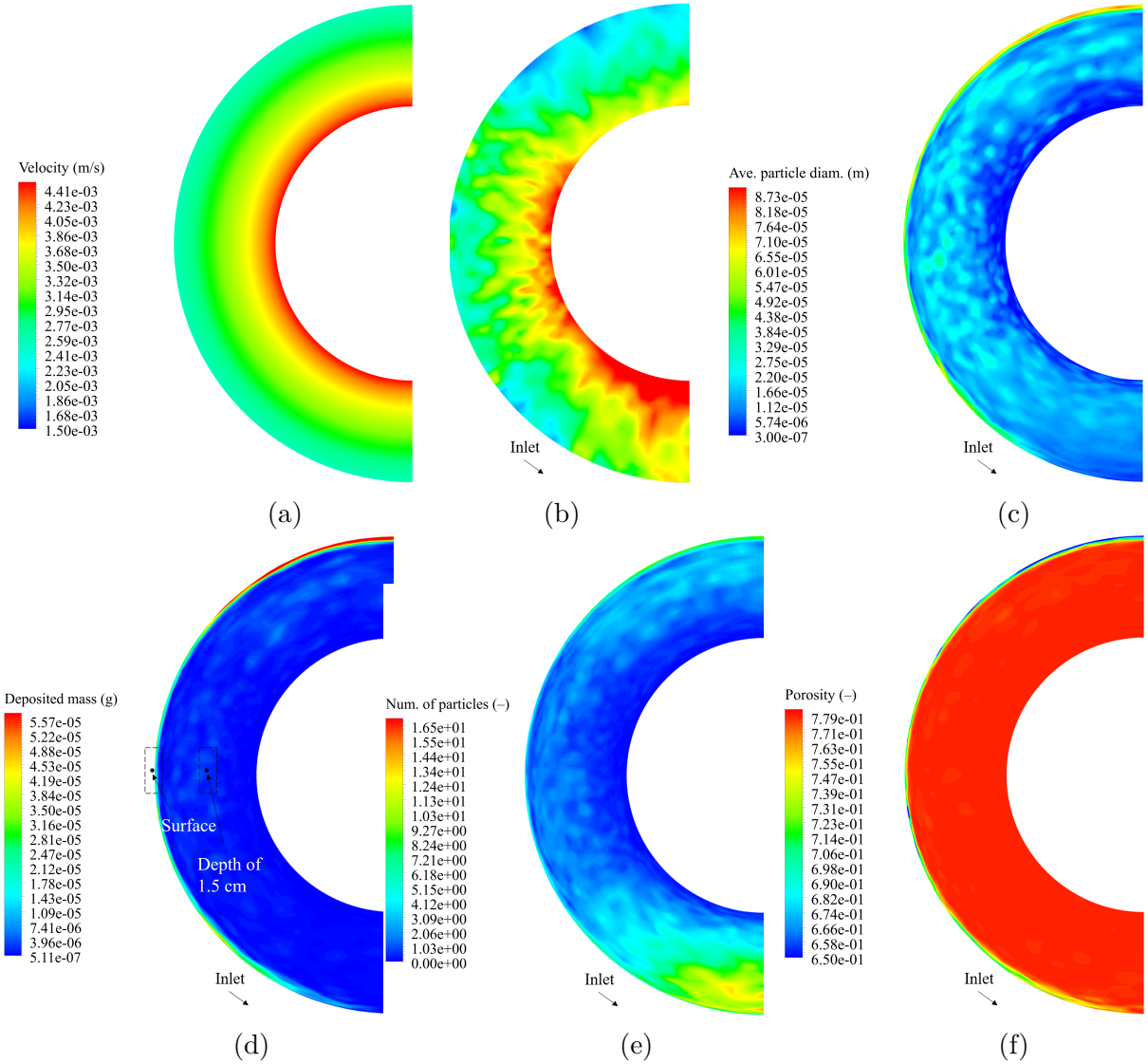

Fig. 5.8 Velocity contours on a plane (a cross sectional slice) at the middle (12.5 cm from the top) of the filter (a) at the start (clean) and (b) end of the simulation (2.4 g Super-Cel processed). Contours of (c) average diameter, (d) mass, and (e) number of deposited particles as well as (f) local porosity at the middle of the filter (12.5 cm from the top) after processing 2.4 g Super-Cel.

were examined. Figure 5.9 shows images of cross sectional slices of the filter taken at the midway point of 12.5 cm, with a higher number of particles observed at the surface

(Figure 5.9a) than at a depth of 1.5 cm into the filter (Figure 5.9b)—at the magnification of the images—confirming that a higher particle mass was likely to deposit on the outer region than within the filter.

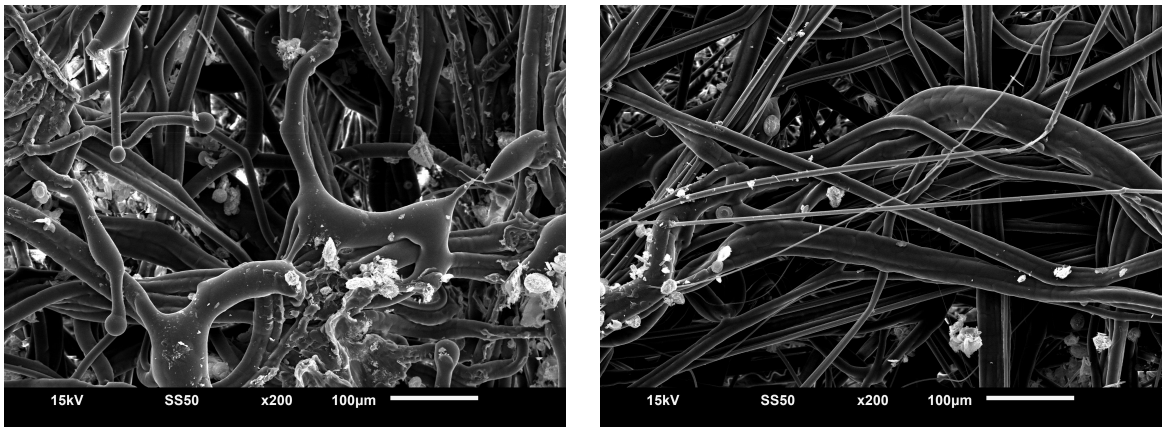

(a) (b)

Fig. 5.9 SEM images of two slices of the filter taken from the middle (12.5 cm from the top) of the filter after processing 2.4 g Super-Cel. A slice taken from (a) the surface and (b) the depth of 1.5 cm (approximate locations shown in Figure 5.8d).

5.5.4 Surface deposition and streamlines

Figure 5.10 shows the deposition of particles onto the surface of the filter attained through simulation in comparison to images of the filters taken from validation experiments, based on the mass of solids processed (i.e. total mass in the domain minus the mass floating in the housing). Particle deposition was observed to start in the lower and middle regions of the filter, and as the hydraulic resistance in these regions increased, the flow path in the housing was altered, as shown in Figure 5.11. The highlighted zones (dashed rectangles) point to the recirculation zone (number 1) and the density of streamlines at the upper region of the housing (number 2). As parcels deposit, the recirculation zone moved upward and, consequently, the flow field progressed towards the upper region of the filter, resulting in increased rates of particle deposition. Although water circulated in the housing, the streamlines in the filter were perpendicular to the Z

direction (Figure 5.11), however, once water passed through the porous zone, it moved upward towards the outlet with increased velocity given the lower resistance in the pipe network.

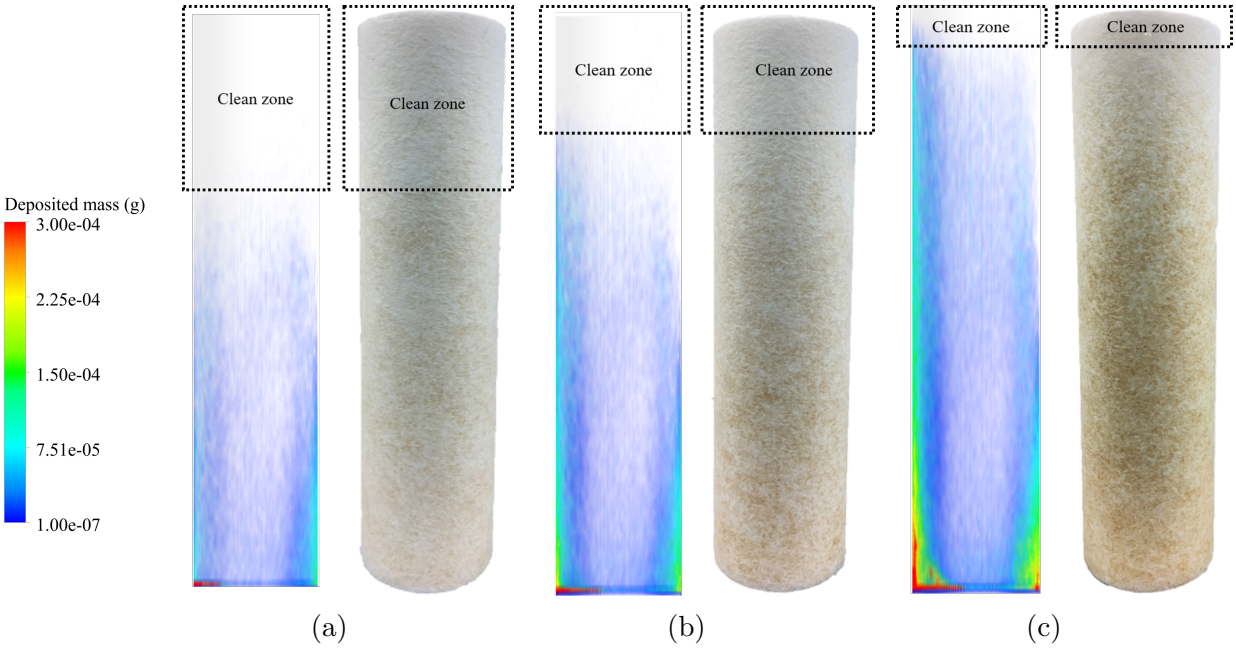

Fig. 5.10 Deposition of particles on the filter (real and simulation side by side). After (a) 0.6 g, (b) 1.2 g and (c) 2.4 g was processed. (Due to the transparency of the contour in the simulation results, deposition in the depth is also visible but cannot be observed in the images of the experimental filters.)

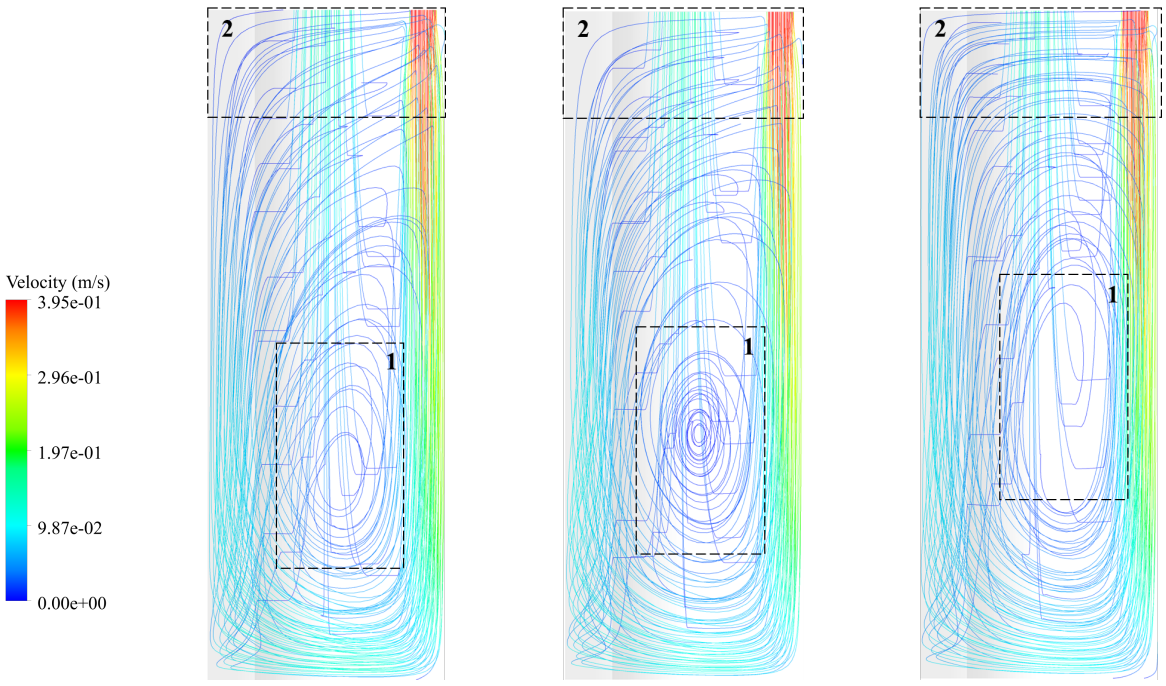

(a) (b) (c)

Fig. 5.11 The fluid streamlines alter due to the deposition of particles and change in the local permeability. After (a) 0.6 g, (b) 1.2 g and (c) 2.4 g was processed.

5.5.5 Pressure drop and particle removal efficiency

Figure 5.12 shows the pressure drop (ΔP) obtained against the processed mass for both the simulations with different mesh sizes and validation experiments. Excellent agreement can be observed between the results, with Root Mean Square Percentage Error (RMSPE) value being 2.46%, 1.49% and 1.95% for 1.2m, 3.6m and 4.8m mesh cells. Regarding particle removal results, the removal in the experiments were variable, but turbidity removal reached >90% after a short period. In the simulation, a total removal efficiency of 91.5%, of which 85% was due to filtration and 6.5% due to settling, was recorded during the simulation, showing excellent agreement with the laboratory experiments.

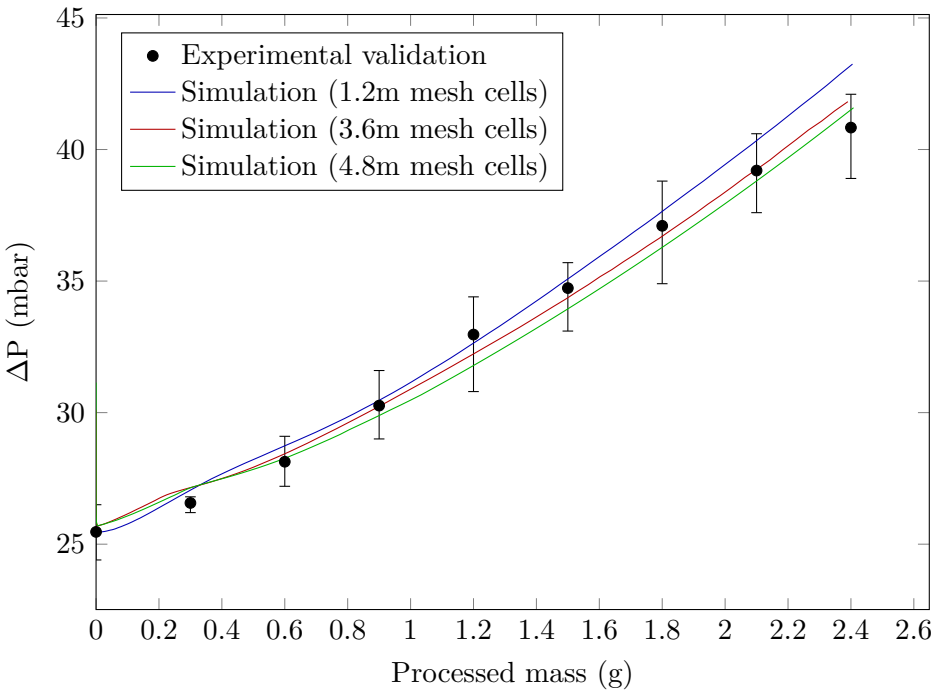

Fig. 5.12 ΔP against the processed mass for both the experiment (mean and standard error) and the simulation.

5.6 Conclusion

This work explored the process both at micro- and macro-level to provide a complete understanding the underpinning filtration mechanisms. The process was simulated by considering the fluid dynamics and particle motion equations as well as models for particle deposition, detachment and rebound, and for the first time providing a comprehensive modelling methodology for cartridge filtration units.

This study showed that the larger particles were entrapped at the outer part of the filter, significantly reducing permeability. Hence, manufacturing multilayer filters with declining porosity from the outer to inner part can result in improved filter runs. Novel housing designs which promote particle settlement, e.g. a hydrocyclone, can remove large particles responsible for the loss in permeability at the outer surface; therefore, improving efficiency and filter lifetime. In addition, based on the PSD of particles in a

specific water, customized filters can be designed by performing a CFD simulation and adjusting the filter thickness and porosity, developing new opportunities to improve filter efficiency and ultimately increase the usable lifetime of the filters—providing safe water at lower cost to users.

The simulation and experimental validation demonstrated excellent agreement with respect to particle removal, pattern of particle deposition (i.e., particles first depositing on the lower and middle region of the filter and as the local pressure drop increased particles depositing in the upper region) and pressure drop (RMSPE= 1.49%–2.46%). The method and approach developed in this study can be used as a powerful tool to test different filter designs and filter materials with minimal parameter adjustment, saving laboratory time and expense.

The visualisation of the deposited particles within the filter according to their size demonstrated the influence of size distribution on the penetration of particles within the filter media. This helped in conceptualising a filtration process based on using fine particles to precoat filters to remove fine suspended particles in water, discussed in the next chapter (Chapter 6).

Chapter 6

Improving Cartridge Filtration Removal Efficiency by Precoating

6.1 Introduction

In Chapter 4, it was demonstrated that the pleated filters achieved a turbidity level of <5 NTU, recommended by the WHO, when a cake layer of the test dust particles was formed. To achieve the turbidity target from the start, it was envisioned that precoating the filter with an inert material can be the solution. It was found out that there is already a process based on this principle, called precoat filtration, widely used for solid-liquid separation in different industries. This chapter presents the adaptation and development of this process specifically for HWT systems.

In the water treatment industry, cake filtration is widely used with a precoated incompressible cake formed on the septum of filtration units. Precoat has three primary functions: (1) to remove particles from raw water, (2) to protect the septum from fouling, and (3) to facilitate cake (precoat plus trapped particles) removal at the end of a cycle [69].

In the context of HWT for developing world applications, processes must be low-cost,

based on minimal maintenance and not require specific operator expertise in water chemistry, as such commonly employed granular filtration and coagulation present significant challenges [94]. Precoat filtration offers significant promise; however, limited studies have been conducted focusing on lab-scale units [182–186] with little investigation of appropriate precoat materials (filter aids) with specific focus on low-cost cartridge systems.

Diatomaceous earth (DE), a common filter aid, is composed of fossilized skeletons of microscopic single-cell water plants [69]. Due to the high porosity and permeable structure, chemical resistance and high specific surface area, DE precoat filtration is used in industries including pharmaceuticals, wine and beer manufacture and water treatment [69, 93, 94]. Whilst guidelines for the amount of deposited DE and resultant precoat thickness are available for standard continuous flow systems, 3–5 mm (deposition of 0.5–1.0 kg/m^2) [69], 1–5 mm (0.1–0.5% w/w suspension) [78], 3.2–6.3 mm (>10% w/w suspension) [94], translation to the intermittent format of HWT is unknown akin to this issue is the stability of DE based precoats in HWT where intermittent use can result in sudden changes of pressure with potential for filter cake to separate from the supporting media [78].

The size distribution of suspended particles in surface water frequently contains difficult to remove negatively charged sub-micron sized contaminants (inorganic compounds and pathogens); for these particles, coating of DE with cationic polyelectrolytes (PE) results in an electropositive precoat media, ensuring particle removal [69, 94, 187, 188] (a schematic of this concept is provided in Fig. 6.1). Moreover, coating sand/DE with metal (hydr)oxides has been reported to improve microbial removal [182, 183, 185, 189, 190].

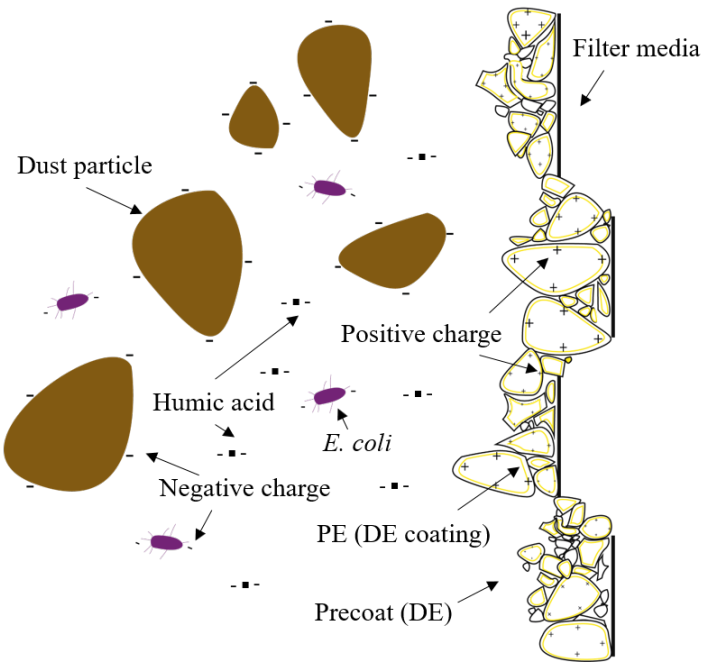

Fig. 6.1 A schematic of the electropositive precoat layer for the removal of negatively charged particles in water.

6.2 Aim and objectives

6.2.1 Aim

This chapter aims to investigate a low-cost and simple method to precoat commercial pleated cartridge filters with a multifunctional precoat layer for intermittent use of the HWT system to ensure production of turbidity-free effluent with additional capability to effectively reduce the concentration of both organic matter and pathogenic microorganisms as well as protecting the surface of the filter, facilitating cleaning and re-use. This will ensure effective performance of the consequent disinfection process.

6.2.2 Objectives

i. To design a precoating process and precoat materials specifically for application in HWT systems using commercial pleated cartridge filters.

ii. To characterise the filter aid particles (e.g., size and surface charge) and the cakes formed by them (e.g., permeability) to be able to compare the results with data in literature.

iii. To investigate the stability of different precoat materials in intermittent use.

iv. To develop precoats to reduce natural organic matter (colour) and pathogen load as well as protect the filter media, in addition to effective and rapid removal of turbidity below 5 NTU.

v. To assess the viability of cleaning and reusing of the filters, improving the sustainability of the system.

6.3 Materials and Methods

6.3.1 HWTS system and filter precoating procedure

The cartridge filtration based HWT system used in this study, previously been described in detail, comprised a filter housing, filter cartridge, pump (Model 2095-204-412, Shurflo), pressure gauges, pipes, valves, etc., and was modified to include a tank for storage and delivery of filter aid-water slurry (see process flow diagram in Fig. 6.2).

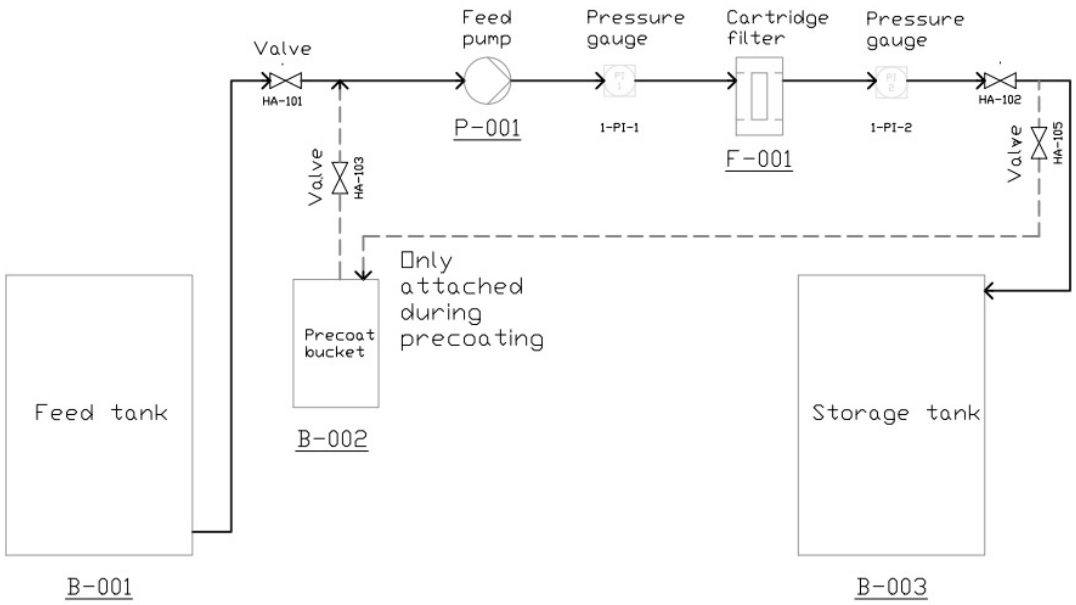

Fig. 6.2 The process flow diagram (PFD) of the system used, showing the treatment system as well as the pipes and fittings needed.

1 micron, polyester pleated filter elements (The Water Filter Men, UK), which provide a high surface area due to being folded into zigzag shape (Fig. 6.3a), were used as received from the manufacturer (Fig. 6.3b); the filters had a surface area of 0.3864 m^2 (measured manually). To precoat the filters, DE was added to 3 L of tap water and stirred on a magnetic stirrer. The pleated filter was placed into the cartridge housing and mounted, the pump was turned on and the slurry recirculated until DE particles were captured by the precoat layer, and the filtrate turbidity reached <1 NTU. Different amounts of DE (50, 40, 25 and 10 g) were tested in terms of precoat stability and coverage, with 25 g chosen as the amount for comparison of the filter aids.

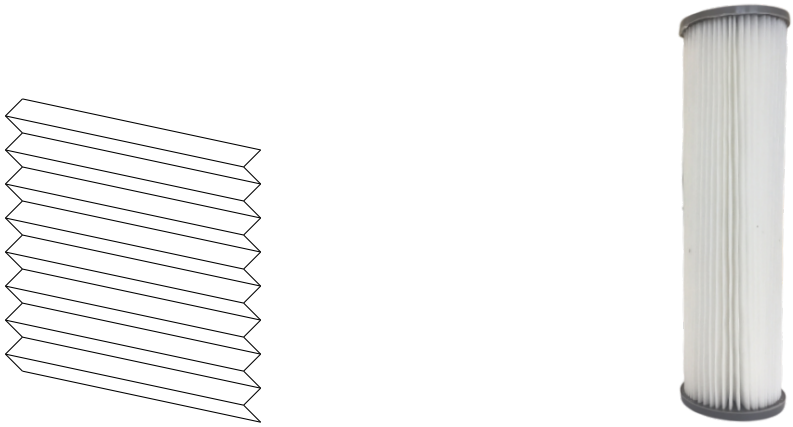

(a) (b)

Fig. 6.3 Pleated filters: (a) a schematic of a pleated filter (b) a commercial, cylindrical cartridge pleated filter element.

6.3.2 Filter aid surface modification

To make DE electropositive using a PE, 0.005 g PDADMAC/g DE (chosen based on zeta potential measurements discussed in Section 6.4.5) was added in liquid form to the DE slurry during stirring. Moreover, iron oxide covered DE was prepared by first adding 0.04 g ferric chloride/g DE to DE in powder form (amount selected based on the precoat stability considerations discussed in Section 6.4.4), followed by recirculating the slurry and gradually adding ammonium hydroxide (25% NH_3, Sigma-Aldrich) after the formation of the precoat layer to convert soluble ferric chloride to insoluble iron (hydr)oxide, meanwhile, the UV transmittance at 254 nm was followed until >95% transmission was observed to confirm the high levels of conversion.

6.3.3 Evaluation of precoat stability

In order to evaluate how well the precoat layer will hold onto the vertical pleated filter during intermittent use and withstand hard impacts in the field, the pump was turned off once the precoating procedure was over and the housing was manually struck hard by

hand. If the impact had no effect (visually) on the precoat layer, it was concluded that the precoat will be stable in practice.

6.3.4 Filter aids

Food grade, fine DE (FoodPURA®, UK) was used as the filter aid for precoating. Calcining was performed by heating the DE in a laboratory chamber furnace (AWF 12/12, Lenton) at 1000℃ for 1 h. Large agglomerates were manually broken down using a mortar and pestle.

The finest commercial grade DE available in the UK specifically for water treatment, Celite® Standard Super-Cel (Alfa Aesar), was purchased to aid in comparison to locally supplied DE.

Ferric chloride (FC) anhydrous (BDH Chemicals Ltd.) and poly(diallyldimethylammonium chloride), PDADMAC, (Mw 200,000–350,000, 20 wt. % in water, Sigma-Aldrich), a clear, light yellow and water soluble liquid with no reported health, safety and environmental hazard [191], were used to coat the DE.

6.3.5 Particle and cake characterisation

The bulk density of the powders was obtained by measuring the volume of 10 g in a graduated cylinder, tapped and sonicated before reading the volume, and specific gravity (SG) was measured using a pycnometer—the specific gravities of the modified filter aids were also measured by keeping the same weight ratios as the precoats (e.g., adding PDADMAC with the weight ratio of 0.005 g PDADMAC/g DE).

To characterise the precoats (cakes) formed, the methodology provided by Inglethorpe [192] was adopted. Filter aid/turbidity agent (5 g) was mixed with 10–20 mL of water (in a beaker) and transferred to a lab-scale filtration apparatus (steps shown in Fig. 6.4), consisting of a vacuum pump (WOB-L® 2511, WELCH), a vacuum gauge, a funnel with

filter support, a disk filter (CAT No. 1017047, Whatman), tubing, etc. to form a cake under vacuum suction of 27–32 cmHg (1 cmHg= 1333.224 Pa).

The vacuum pump was turned on to remove the water in the slurry and after that the surface of the cake was dry, 4 mL of water was added and the time taken until the cake became dry again was measured in order to obtain the flow rate; then, the depth of the cake in the funnel was measured using a depth gauge (a caliper).

The beaker with the remaining slurry was put in an oven to dry, and the weight of the dry solids was calculated and subtracted from the total weight of solids (5 g) initially added to water, obtaining the net dry weight of the cake (slurry transferred to the filtration unit).

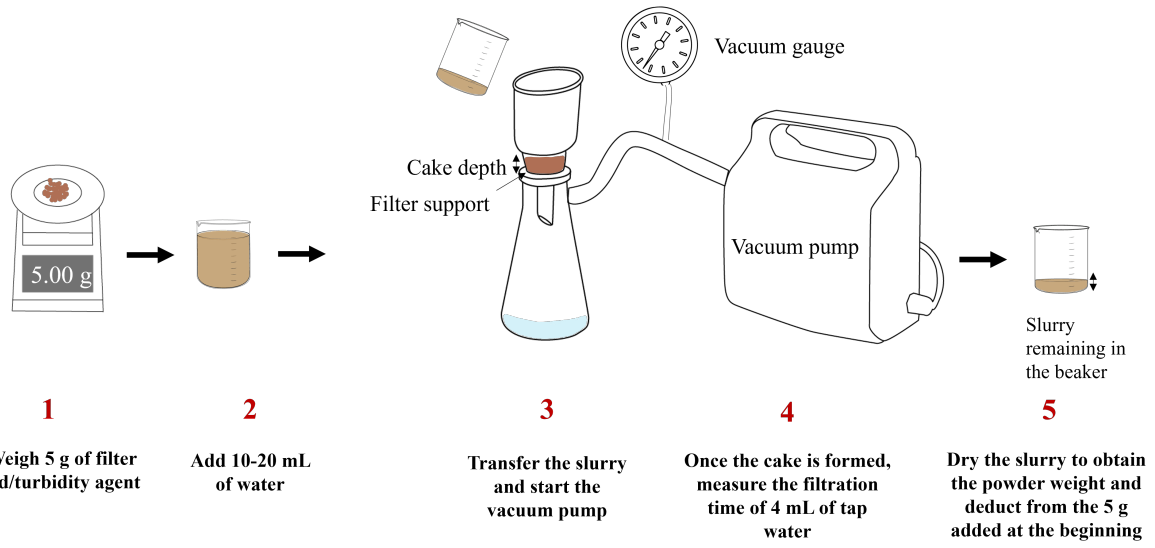

Fig. 6.4 Steps followed to obtain the filtration flow rate, filter cake depth and dry weight of the cake.

The wet-cake density was calculated according to Eq. 6.1:

$$WD = \frac{m_c}{A_c \cdot L_c} \tag{6.1}$$

where m_c, A_c and L_p are the dry weight, surface area and depth of the cake, respectively. Permeability (k) was calculated by Darcy's law:

$$k = \frac{Q \cdot \mu \cdot L_c}{A_c \cdot \Delta P} \tag{6.2}$$

where Q is the water flow rate, μ the water viscosity and ΔP the pressure drop.
Porosity was calculated based on the dry weight, specific gravity and the total volume (wet cake volume) of the cakes:

$$\varepsilon_c = 1 - \frac{m_c}{A_c \cdot L_c \cdot SG_c} \tag{6.3}$$

where SG_c and ε are the specific gravity and porosity of the cake.

6.3.6 Instrumentation

Particle size distribution (PSD) was measured by a particle size analyser (Mastersizer 2000, Malvern Panalytical) and zeta potential (ZP) via electrophoretic light scattering (Zetasizer Nano ZS, Malvern Panalytical) using folded capillary cells (DTS 1060, Malvern Panalytical).
A portable turbidity meter (HI-93703, Hanna Instruments) was used to measure turbidity of water samples. UV absorbance at 254 nm was measured using a spectrometer (6305, Jenway).
A pH meter (pH510, Eutech Instruments) was used to determine pH of the tap water periodically. A portable, strip-based chlorine measurement photometer (eXact® Chlorine Plus Photometer, Industrial Test Systems) was used to measure free chlorine.
A scanning electron microscope (JSM-6010, JEOL) was used to take images of the filter aid particles, the turbidity agent and the fibres of the filters, before and after

experimentation; samples were gold coated using a sputter coater (K500X, Emitech) prior to SEM imaging.

6.3.7 General experimental procedure

Tap water (Belfast, UK) with a pH of 6.9–7.4 and turbidity of 0.05–0.3 NTU was used as the raw water. Fine test dust (ISO 121031, A2, Powder Technology Inc.), a red brown insoluble mineral composed mainly of silica, was used to represent particles in natural waters and humic acid sodium salt (Sigma-Aldrich) was used as a surrogate for dissolved organic matter in water.

Several test waters were prepared with different concentrations of the test dust (TD) and/or humic acid (HA) to evaluate the removal efficiency with the precoats under different conditions. The concentrations used for the 'Challenge Test Water' described within the 'WHO International Scheme to Evaluate Household Water Treatment Technologies' [193], 40±10 turbidity and 15 mg/L HA, were adopted as the challenge test water—the turbidity level was achieved by adding 60 mg/L of TD.

In order to assess the individual removal rates for organics and particles, test waters with only a) 60 ml/L TD and b) 15 mg/L HA were prepared. Another test water with TD and HA concentrations a quarter of the challenge test water concentrations, 15 mg/L TD and 3.75 mg/L HA, was also tested. A summary of all the test waters and precoat systems investigated is provided in Table 6.1. The trials were continuous (constant flow system configuration) and the concentration of TD and HA was maintained in the feed tank through constant dosing of stock suspensions using a peristaltic pump (101U, Watson Marlow).

Table 6.1 The test waters used, the precoats trialled with each test water and the names used for the trials throughout this text.

Test water	**Precoats trialled**	**Trial name**
60 mg/L TD	No precoat	No precoat (60TD)
	DE	DE (60TD)
	Calcined DE	Calcined DE (60TD)
	DE+PDADMAC	DE+PDADMAC (60TD)
	DE+Fe_2O_3	DE+Fe_2O_3 (60TD)
15 mg/L HA	No precoat	No precoat (15HA)
	DE	DE (15HA)
	Calcined DE	Calcined DE (15HA)
	DE+PDADMAC	DE+PDADMAC (15HA)
	DE+Fe_2O_3	DE+Fe_2O_3 (15HA)
60 mg/L TD + 15 mg/L HA	No precoat	No precoat (60TD+15HA)
	DE	DE (60TD+15HA)
	Calcined DE	Calcined DE (60TD+15HA)
	DE+PDADMAC	DE+PDADMAC (60TD+15HA)
	DE+Fe_2O_3	DE+Fe_2O_3 (60TD+15HA)
15 mg/L TD + 3.75 mg/L HA	No precoat	No precoat (15TD+3.75HA)
	DE	DE (15TD+3.75HA)
	Calcined DE	Calcined DE (15TD+3.75HA)
	DE+PDADMAC	DE+PDADMAC (15TD+3.75HA)
	DE+Fe_2O_3	DE+Fe_2O_3 (15TD+3.75HA)
60 mg/L TD + 15 mg/L HA + 10^7 *E. coli* colonies	DE+PDADMAC	DE+PDADMAC (60TD+15HA+*E. coli*)
15 mg/L TD + 3.75 mg/L HA + 10^7 *E. coli* colonies	DE+PDADMAC	DE+PDADMAC (15TD+3.75HA+*E. coli*)

When filters had been precoated, test water was then processed from the feed tank, through the filter and to the storage tank. During the course of the experiments, the water flow rate was variable with the gauge pressure, declining from 5.2 L/min at 0.02 bar to 4.4 L/min at 1 bar, resulting in a filtration flux of 0.81–0.68 m/h.

Samples (50 mL) were taken from the inlet and the outlet of the system (sampling valves shown in the PFD) to measure turbidity and UV_{254} absorbance following processing of 50 or 100 L depending on the nature of the experiment—the first sample was taken after 5 L. Samples were shaken prior to triplicate analysis of turbidity, with the average recorded.

Pressure drop (ΔP) was measured by two analogue pressure gauges (Ferro, UK) installed before and after the filter housing, and the volume of water treated was measured by an analogue water meter (Ferro, UK). The trials were continued until the 1 bar pressure drop limit was reached or the removal and pressure drop trends were predictable.

6.3.8 Preparation and enumeration of *E. coli*

To prepare the *E. coli* (NCTC 10538) stock, a single colony of *E. coli* (extracted with a sterilized loop from a stock agar plate) was spiked in autoclaved tryptic soy broth (Oxoid, UK), which was then placed in a shaking incubator (SI 50, Stuart Scientific) for 24 h for incubation at 37℃.

To enumerate *E. coli* colonies, 0.1 mL samples were serially diluted and poured on plates with an overlay of Chromocult® agar (Millipore) and incubated at 37℃ for 24 h (INC Genlab incubator).

6.3.9 Experimental procedure for trials with *E. coli*

For experiments with *E. coli*, trials were performed in 50 L batches. Non-pathogenic *E. coli*-K12 was used as a model of faecal contamination and micron sized particles (*E. coli*

average cross section diameter ≈ 1 µm [194]). Tap water in the feed tank (60 L) was previously dechlorinated with 30 mg/L of sodium thiosulfate (Minerals Water Ltd., UK). Then, 5 mL of the *E. coli* stock was added to the feed water reservoir containing TD and HA (Table 6.1). To compare the *E. coli* removal of all the precoats, short (50 L) trials with the '60 mg/L TD + 15 mg/L HA + 10^7 *E. coli* colonies' test water were performed, and two longer trials (multiple 50 L batch runs) were performed, limited by the pump's maximum operating pressure, only with the DE+PDADMAC precoat (Table 6.1). Water samples (50 mL) were periodically removed for enumeration (in triplicate), as described in Section 6.3.8.

6.3.10 Cleaning and reuse of pleated cartridge filter

A simple method of basic manual cleaning was investigated with the primary objective to remove the cake and ensure *E. coli* inactivation and as such permit safe reuse of the filter.

The filter was shaken in its housing containing tap water (1.7 L) and 5 mL of sodium hypochlorite with 6–14% active chlorine (Millipore) for a few minutes; then, the housing was emptied and filled with clean tap water, the filter was manually shaken.

To assess the physical effect of the cleaning procedures on filter structure, slices were physically removed from the pleated filters for SEM analysis and compared to samples removed from a clean filter, the latter being previously wetted with ultra-pure water.

The same cleaning procedure was repeated after a replicate trial, but this time, the filter was placed back in the housing, clean dechlorinated water was passed through the filter and a sample was taken from the outlet sampling valve after 5 L to enumerate *E. coli* in the filtrate.

6.4 Results and discussion

6.4.1 Particle characterisation

Representative bulk and SEM images of DE and TD powders are shown in Fig. 6.5. Natural DE (Fig. 6.5a) was a white powder and following calcination, transformed into a pink powder (Fig. 6.5b). Calcination resulted in sintering and agglomeration which was measured using the particle analyser—the D90 (representing the maximum size of 90% of the particles) and the span (D_{90}–D_{10}/D_{50}), which represents the width of distribution, for natural DE were 8.70 µm and 3, respectively, whereas for calcined DE were 16.66 µm and 4.33 (Table 6.2, Fig. 6.6), respectively.

Calcination also increased the specific gravity of DE from 1.97 to 2.11 (Table 6.2) as impurities were removed. The higher specific gravity, coarser PSD and similar span of the calcined DE in comparison to the unprocessed DE resulted in a smaller bulk density of 281 kg/m^3 than 360 kg/m^3—generally, span has a direct relationship with bulk density as smaller particles can fill the inter-particle voids.

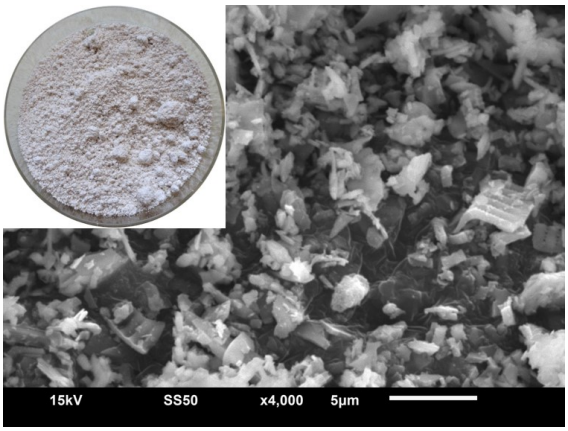

(a) DE

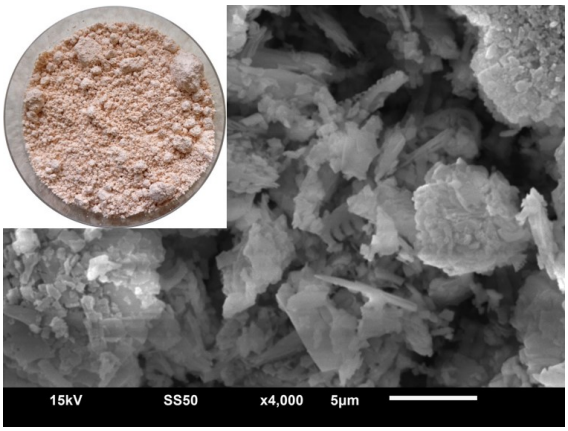

(b) Calcined DE

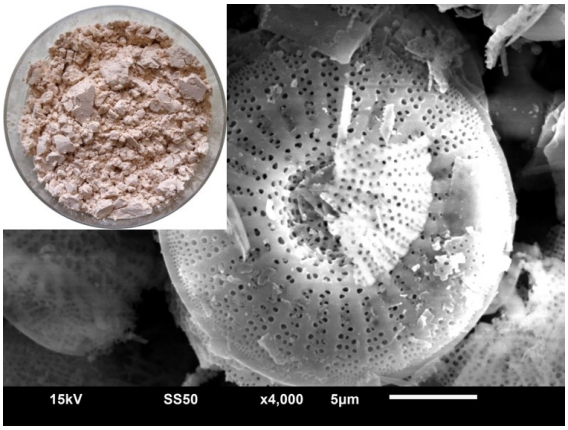

(c) Super-Cel

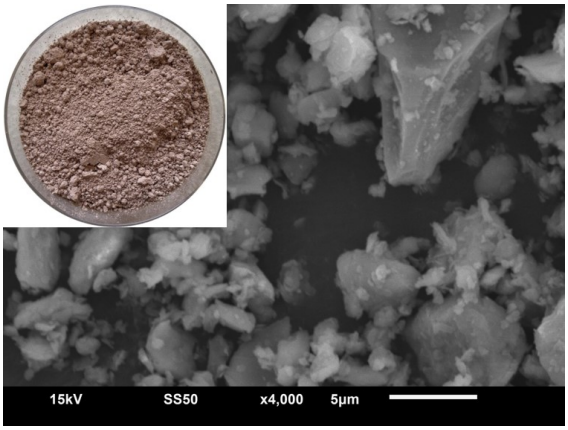

(d) Test dust

Fig. 6.5 SEM images of particles of different grades of DE and TD together with images of their bulk powders.

Table 6.2 D_{10}, D_{50}, D_{90} (the subscript represents the percentage of particles that have a smaller size than $_x$) and the span (width of size distribution) of the filter aids and the turbidity agent used in this study.

Filter aid/ turbidity agent	**D_{10} (µm)**	**D_{50} (µm)**	**D_{90} (µm)**	**Span (–)**	**Bulk density (kg/m³)**	**Specific gravity**
DE	0.63	2.69	8.70	3	360	1.97
Calcined DE	0.724	3.68	16.66	4.33	281	2.11
Standard Super-Cel	2.25	9.18	24.52	2.42	196	2.15
A2 Test dust	0.79	4.90	36.20	7.22	800	2.52

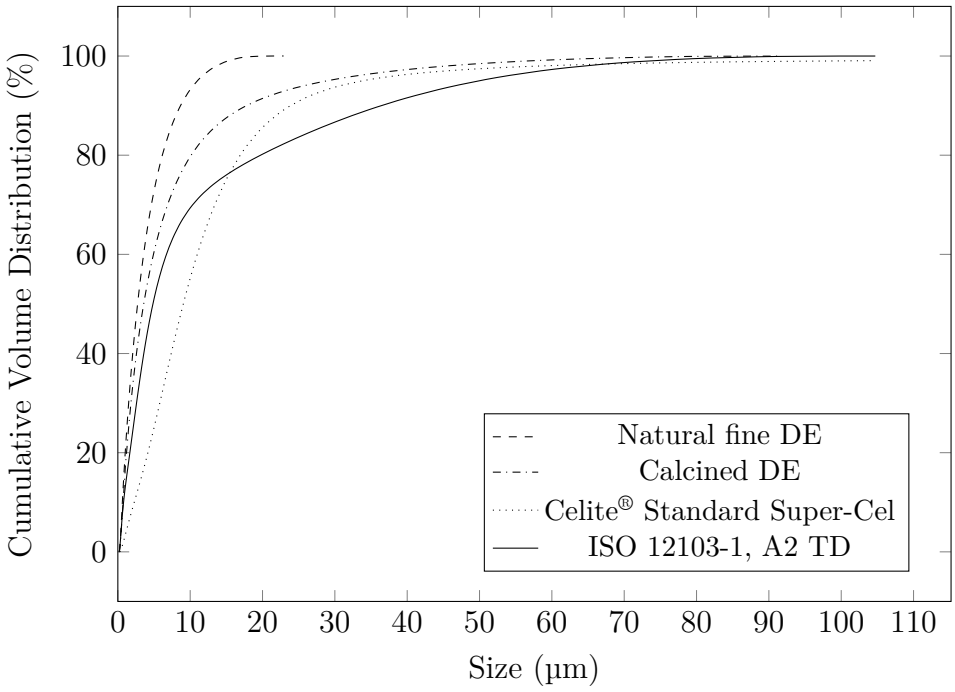

Fig. 6.6 Cumulative volume PSD of the DE grades and TD.

A commonly used DE filter aid, Celite® Standard Super-Cel, was also imaged (Fig. 6.5c) as a commercial specimen to compare with the locally supplied DE materials used within this study. Super-Cel particles were visibly larger than the other two DE grades with an

associated coarser PSD and smaller span (Table 6.2, Fig. 6.6), resulting in the smallest bulk density among the particles characterised despite its greater specific gravity.

Images of TD (Fig. 6.5d), the turbidity agent used in this work, shows the shape and polydispersity of particles with an associated coarser PSD than both of the locally supplied DE grades (Table 6.2, Fig. 6.6); however, as it has a greater specific gravity and span, it has a greater bulk density.

6.4.2 Precoat characteristics

Table 6.3 provides the characteristics of the cake layers formed by the filter aids and the turbidity agent under vacuum. Calculated via Darcy's Law (Table 6.3), the locally supplied DE had a much lower permeability (2.9 mD) than Standard Super-Cel (237.1 mD) or the grades reported in other works [80, 93, 98, 195–197], due to a higher fraction of very fine particles, causing a much lower permeability even at low volume fractions [198]. Calcination resulted in a higher porosity (0.62 vs. 0.54) and permeability (18.0 mD).

DE was coated with either PDADMAC or Fe_2O_3 to prepare a modified precoat material. The specific gravity of DE+PDADMAC and DE+Fe_2O_3 was 1.83 and 2.12, respectively, with those values used to calculate the porosity of prepared filter cakes (Table 6.3). Both coated filter aids formed cakes with higher permeability as the coating affected the wet density. However, despite the different wet densities of DE+PDADMAC (801 kg/m^3) and DE+Fe_2O_3 (698 kg/m^3) cakes, their permeability was almost the same (7.6 and 7.7 mD, respectively) due to the different cake structures.

The turbidity agent (TD) showed the lowest porosity (0.35) and permeability (2.6 mD) and the highest wet density (1626 kg/m^3) among all the cakes characterized. TD has a higher specific gravity and finer PSD resulting in a higher wet density and lower porosity. Nevertheless, the permeability of TD and DE were similar (2.6 mD and 2.9 mD,

respectively), demonstrating porosity alone cannot determine the precoat permeability, as such permeability should be measured experimentally.

Table 6.3 Characteristics of the cake layers formed by the filter aids/turbidity agent.

Cake	**Porosity** (–)	**Wet density** (kg/m^3)	**Permeability** (mD)
DE	0.54	900	2.9
Calcined DE	0.62	793	18.0
DE+PDADMAC	0.56	801	7.6
DE+Fe_2O_3	0.72	698	7.7
Standard Super-Cel	0.77	501	237.1
A2 Test dust	0.35	1626	2.6

6.4.3 Precoat stability

The amount of filter aid that would fully cover the surface of the pleated filter while not too thick to fall was investigated. While 10 g of DE (a loading rate of 0.026 kg/m^2) did not cover the whole surface of the filter, it was observed that 40 g DE, still a much lower loading rate (0.1 kg/m^2) than the guidelines (0.5–1.0 kg/m^2 [69]), resulted in an unstable precoat that some patches would fall as soon as the pump was turned off. With 25 g DE (0.065 kg/m^2) the surface of the filter was fully covered, but the layer was not too thick to fall; therefore, it was the selected amount for all precoating trials.

Higher amounts of DE resulted in more layers of particles that were not supported by the filter media; hence, increasing the probability that patches of precoat separate from the surface of the filter. There are several other underlying factors affecting the precoat stability such as particle size distribution and particle shape which influence the solids packing structure (quantified by wet density) [199], and specific gravity, which determines

particle buoyancy.

The effect of PSD on solids packing was noticeable as the Standard Super-Cel that had the coarsest PSD, largest span and smallest wet density among the DE grades tested (Table 6.2, Fig. 6.6, Table 6.3), formed an unstable precoat layer, which could only be used in continuous systems and not in HWT systems that are operated intermittently as it needs the constant pressure to 'hold' it to the septum.

The use of modified filter aids resulted in formation of a stable and uniform precoat in the case of DE+PDADMAC, but a low stability cake in the iron based system. PDADMAC acted as a glue and kept the precoat strongly attached to the filter, withstanding hard impacts (hand striking the housing) which resulted in the collapse of all other precoat system.

6.4.4 Turbidity removal

To evaluate the turbidity removal efficiency of each precoat, continuos trials were performed with 60 mg/L of TD (40±10 NTU) test water. While in the 'No precoat (60TD)' trial, the turbidity removal never satisfied the 5 NTU target or an equivalent removal percentage of above 88–90% (Fig. 6.7), the filters precoated with DE or calcined DE did achieve the 5 NTU target, indeed surpassing it with <1 NTU routinely observed. They also very quickly reached the point where they gave the desired removal, this was maintained for the full duration of the 1100L trial.

Calcined DE resulted in almost the same average turbidity removal efficiency (96.00%) as with plain DE (97.93%), and due to the higher permeability (18.0 vs. 2.9 mD), ΔP caused by the trapped particles was always lower (Fig. 6.8).

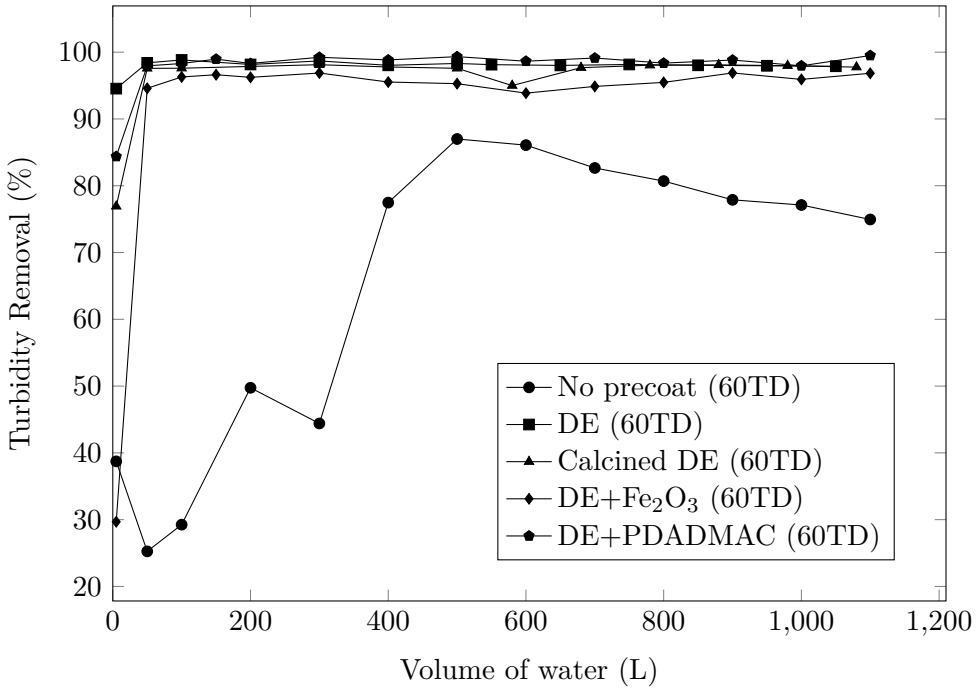

Fig. 6.7 Turbidity removal of the precoats with the '60 mg/L TD' test water (initial turbidity: 40±10 NTU, starting point: 5 L).

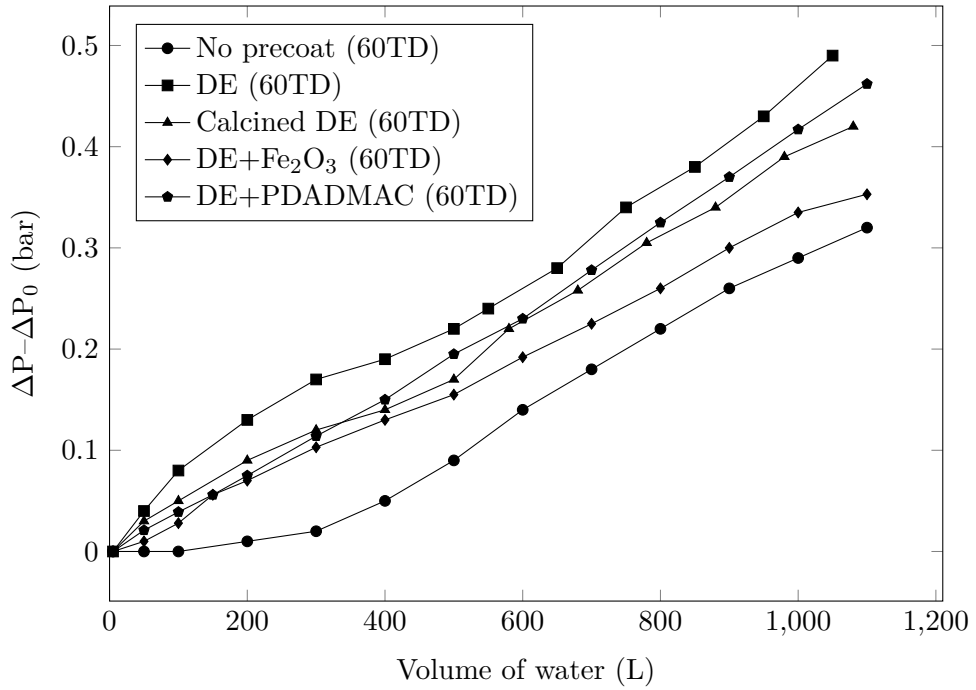

Fig. 6.8 Pressure drop caused by the trapped TD particles during the trials with the '60 mg/L TD' test water (initial turbidity: 40±10 NTU, starting point: 5 L).

The DE+PDADMAC precoat also achieved a similar turbidity removal (average of 97.69%) as the plain DE precoat while the ΔP caused by the trapped particles was lower due to a higher initial permeability (Table 6.3). The DE+Fe_2O_3 precoat showed a lower turbidity removal than the other precoats (still <5 NTU) due to the poor precoat stability.

The turbidity removal results with the '60 mg/L TD' test water was equal to removal of TD particles, whereas in other trials in which HA was present, the measurement was affected by the concentration of HA concentration as well (discussed in Section 6.4.6)

In experiments comparing turbidity removal with commercial filter aids (Harbolite®, Aquatec perlite and Arbocel®) and sand filters for treatment of swimming pool water with inlet turbidity values of 0.26–0.36 NTU (significantly lower than 40 NTU initial turbidity reported in this work), Christensen et al. [79] reported higher removal efficiency of precoat filters for small dirt particles (<10 µm) based on the measured number of particles in the inlet and outlet. Even though the PSD of filter aids used were different, the cake permeabilities and removal efficiencies were similar. However, no pressure drop data was provided.

6.4.5 HA removal

Removal of organic matter (HA) was also investigated as the precoat layers provided a high surface area for adsorption. Whereas the pristine filter had a negligible removal of 7.60% (Fig. 6.9), in the 'DE (15HA)' and 'Calcined DE (15HA)' trials, 34.13% and 26.71% average removal, respectively, were achieved. In trials with the '15 mg/L HA' test water, the UV_{254} removal equated to HA removal (Fig. 6.9) as no interference was caused by TD particles.

The ΔP results (Fig. 6.10) showed that the removal of HA can quickly reduce the permeability as after 200 L, no change in ΔP was observed without a precoat, while

with DE or calcined DE precoats, ΔP was 0.74 bar. By comparing the ΔP results for the trials performed with the '15 mg/L HA' test water (Fig. 6.10) and the '60 mg/L TD' (Fig. 6.8), it can be demonstrated that smaller constituents in water can completely block the pores leaving no space for the water to pass through, significantly affecting the rate of change in ΔP, as after treatment of 200 L with the DE precoat, 15 mg/L of HA (1.1 g retained within the filter based on the percentage removals) caused a ΔP of 0.74 and 60 mg/L of TD (11.8 g retained), a ΔP of 0.17. This conclusion agree with the study by Rebhun et al. [108] where ΔP was higher due to HA removal than kaolinite particles.

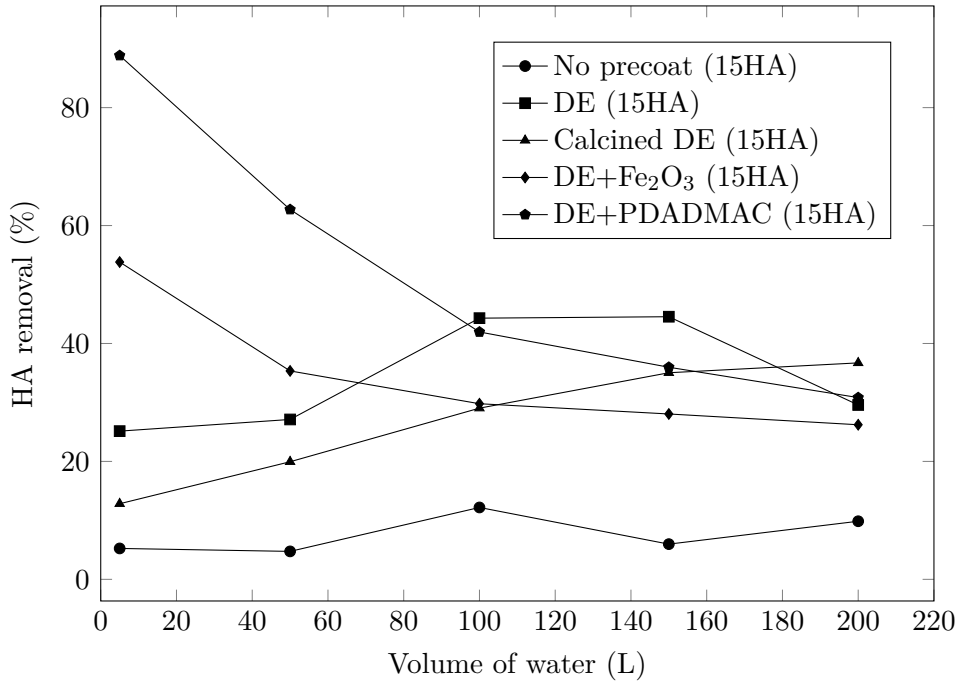

Fig. 6.9 HA removal of the precoats with the '15 mg/L HA' test water (initial absorbance: 0.4±0.1, starting point: 5 L).

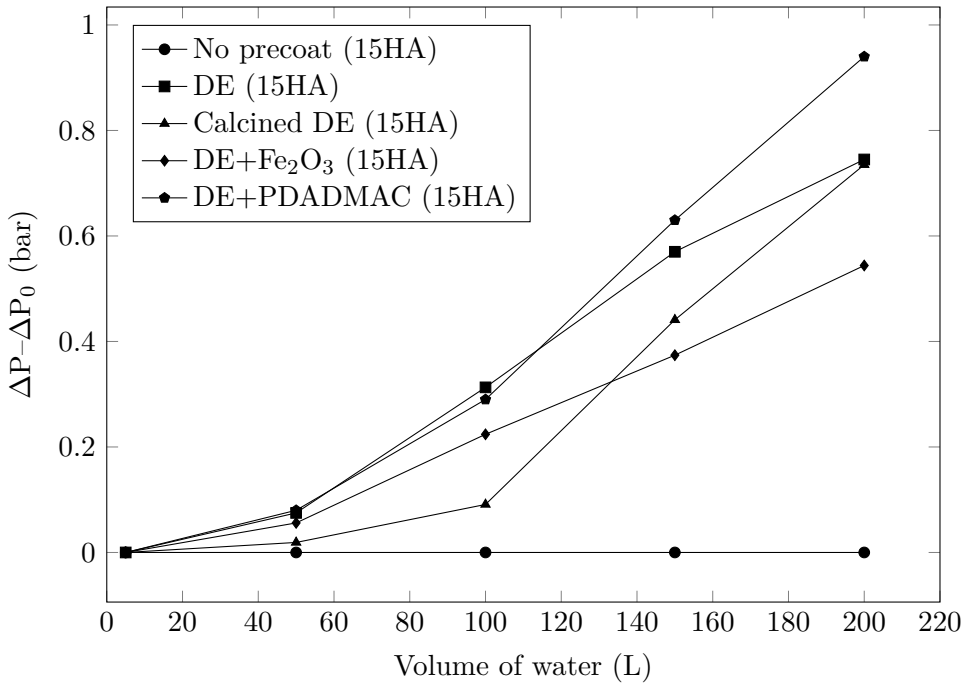

Fig. 6.10 Pressure drop caused by the trapped HA for trials with the '15 mg/L HA' test water (absorbance: 0.4±0.1, starting point: 5 L).

The particle size and zeta potential (ZP) of HA were measured to be 254.66±25.6 nm and -15.07±0.42 mV, respectively, in neutral pH range (6.9–7.4). As such, physical removal via filtration using the DE precoated system was limited with the negative surface charge of both DE (ZP: -20.40±0.44 mV in pH of 6.9–7.4) and HA creating poor conditions for adsorption on the precoat.

The zeta potential (ZP) of DE could be modified from -20 mV with increasing weight loadings of PDADMAC (Fig. 6.11). A plateau in zeta potential was reached at 0.005 g PDADMAC/g DE corresponding to +26 mV, and as such this weight ratio was used for subsequent experiments. A positive zeta potential would result in a higher rate of attachment of negatively charged particles/dissolved organic matter to the DE precoat. DE+PDADMAC provided the highest average HA removal among the precoats, which was higher (88.8%) at the first sample point (Fig. 6.9)—equivalent to filtration of 5 L of test solution. A decrease in HA removal percentage was observed during the trials, with

all precoat systems attaining only approximately 35% removal following processing of 200 L.

For the iron oxide system, ZP of DE increased as a function of ferric chloride loading, however upon conversion to iron oxide the ZP dropped, e.g. at 0.04 g FC/g DE loading, a ZP of -18.4 mV was observed. In the absence of electrostatic attraction, removal of HA can be attributed to the higher adsorptive capacity of iron oxide than DE [200], resulting in an HA removal of 53.81% at the first sample point, which was depleted quicker than the DE+PDADMAC precoat (Fig. 6.9). However, due to lower removal and higher permeability, the rate of ΔP was more gradual with DE+FE_2O_3 (Fig. 6.10). The rate of ΔP was faster with DE+PDADMAC precoat than the plain DE due to the higher removal of HA.

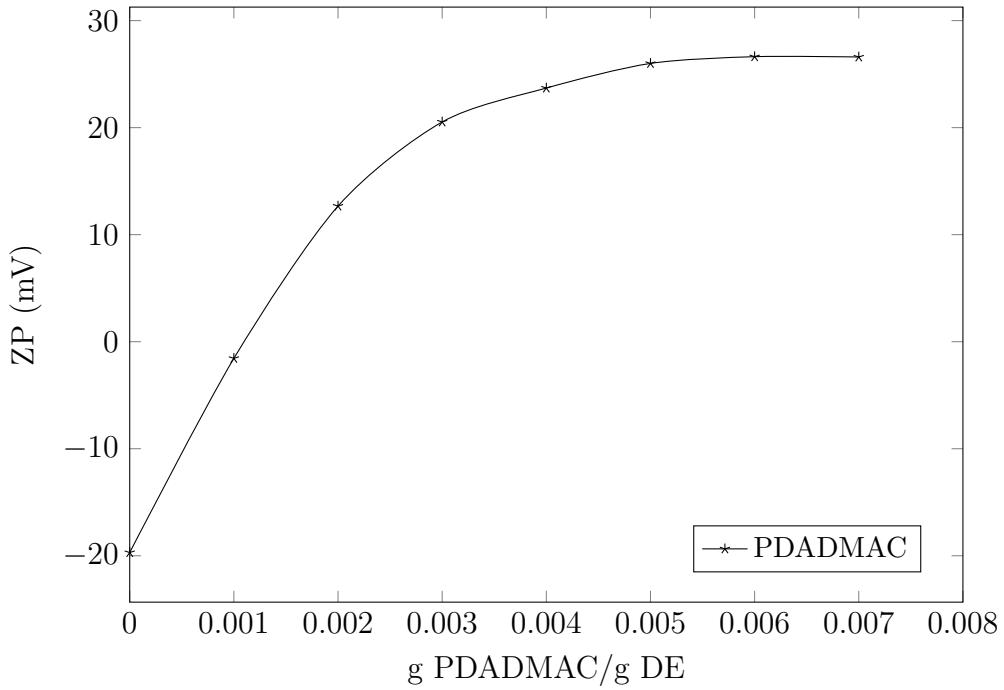

Fig. 6.11 ZP of DE coated with different amounts of PDADMAC at neutral pH (6.9–7.4).

6.4.6 Simultaneous turbidity and UV_{254} removal

Table 6.4 shows the average turbidity and UV_{254} removal as well as the volume of water processed until that 1 bar limit was reached for the trials with both TD and HA in water, which is more representative of surface waters.

In Section 6.4.4, it was shown that the precoat layers effectively removed TD; however, in the trials with the '60 mg/L + 15 mg/L HA' test water, due to the presence of HA, which also affects turbidity (15 mg/L of HA caused a turbidity of 6.07 NTU), the turbidity removal (Fig. 6.12) was lower than the trials with the '60 mg/L TD' (Fig. 6.7) as HA was present in the treated water (according to UV_{254} removal percentages in Table 6.4) and the filtrate turbidity did not satisfy the <5 NTU target. This shows that using HA as a model compound for organic matter can be misleading regarding particle removal efficiency of filters.

As expected, ΔP gradients for each precoat layer was steeper when both TD and HA were present (Fig. 6.13) than with either '60 mg/L TD' (Fig. 6.8) or '15 mg/L HA' (Fig. 6.10) test waters. For example, with the calcined DE precoat, ΔP after 100 L was 0.09, 0.73 and 0.83 bar when tested with 60 mg/L TD, 15 mg/L HA and 60 mg/L TD + 15 mg/L HA, respectively.

Table 6.4 Average turbidity and UV_{254} removal as well as duration of trials before reaching 1 bar for trials with the '60 mg/L + 15 mg/L HA' and '15 mg/L TD + 3.75 mg/L HA' test waters.

Trial name	**Avg. turbidity removal (%)**	**Avg. UV_{254} removal (%)**	**Volume treated (L)**
No precoat (60TD+15HA)	26.03	14.01	–[†]
DE (60TD+15HA)	92.35	43.07	138
Calcined DE (60TD+15HA)	88.76	39.14	205
DE+PDADMAC (60TD+15HA)	84.75	67.73	149
DE+Fe_2O_3 (60TD+15HA)	67.94	55.78	99
No precoat (15TD+3.75HA)	14.09	7.44	–[*]
DE (15TD+3.75HA)	69.40	38.96	471
Calcined DE (15TD+3.75HA)	89.11	41.12	365
DE+PDADMAC (15TD+3.75HA)	71.29	66.72	288
DE+Fe_2O_3 (15TD+3.75HA)	64.21	51.51	264

[†] During 200 L no increase in pressure drop was observed.

[*] During 500 L no increase in pressure drop was observed.

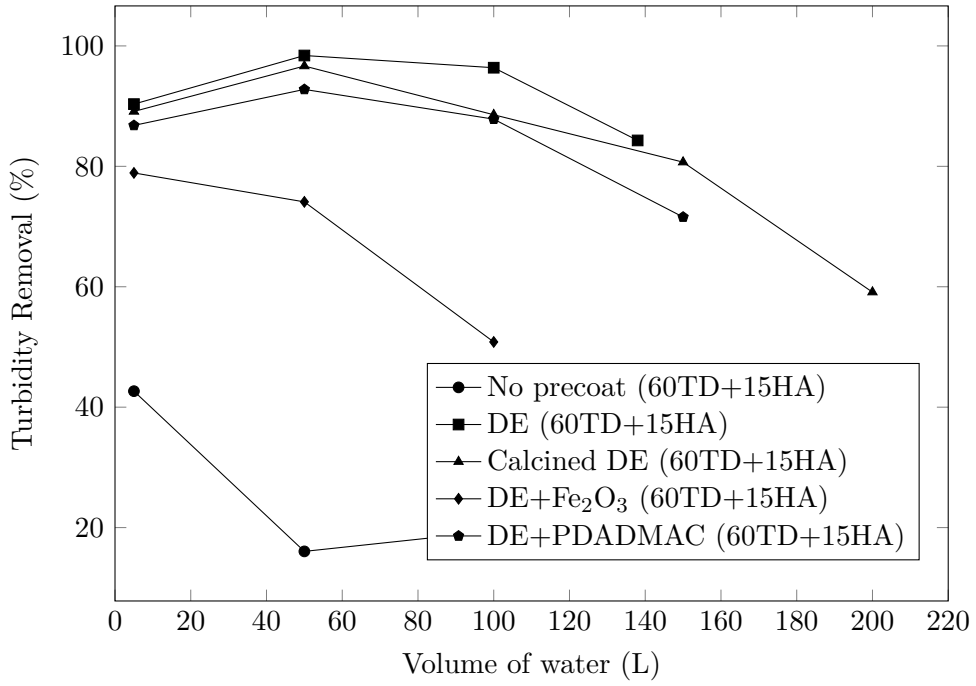

Fig. 6.12 Turbidity removal of the precoats when trialled with the '60 mg/L TD + 15 mg/L HA' test water (starting point: 5 L).

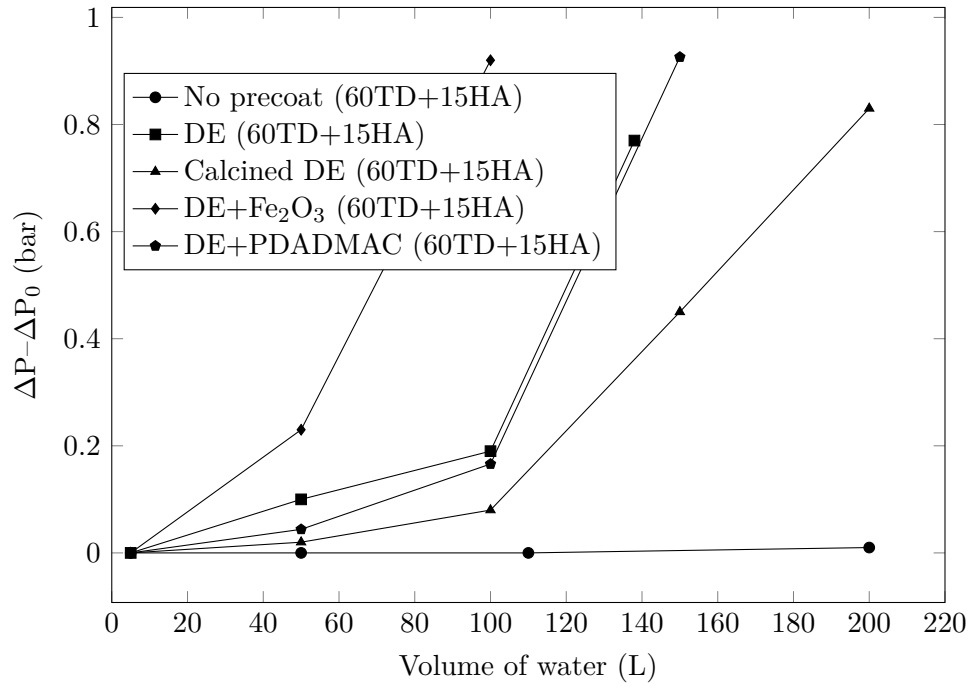

Fig. 6.13 Pressure drop caused by the trapped TD and HA for trials with the '60 mg/L + 15 mg/L HA' test water (starting point: 5 L).

However, the 'Challenge Test Water' used by the WHO to test HWT systems [193] represents the worst case scenario, so it was more realistic to use a test water that represents medium-quality surface waters. When a lower concentration of 15 mg/L TD (turbidity of 10±3 NTU)—the turbidity level recommended for precoat filtration [94]—and 3.75 mg/L HA ('15 mg/L TD + 3.75 mg/L HA' test water) were used, the filtrate turbidity of the precoats tested always met the <5 NTU target. Due to the lower initial turbidity, it was already expected that the precoats achieve a lower removal in percentage terms (Table 6.4, Fig. 6.14) compared with their respective trials with the '60 mg/L + 15 mg/L HA' test water (Table 6.4, Fig. 6.12).

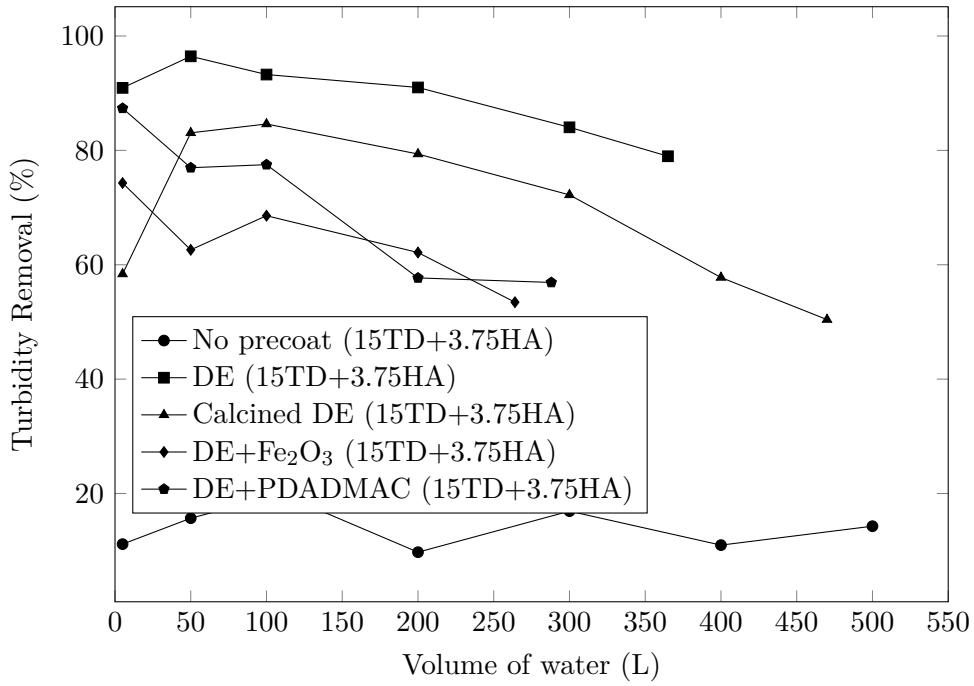

Fig. 6.14 Turbidity removal of the precoats when trialled with the '15 mg/L TD + 3.75 mg/L HA' test water (starting point: 5 L).

The average UV_{254} percentage removal with the precoats were similar for both the test waters (Table 6.4), while the adsorption capacity was depleted at a slower rate at the lower concentration of HA (Fig. 6.15, Fig. 6.16).

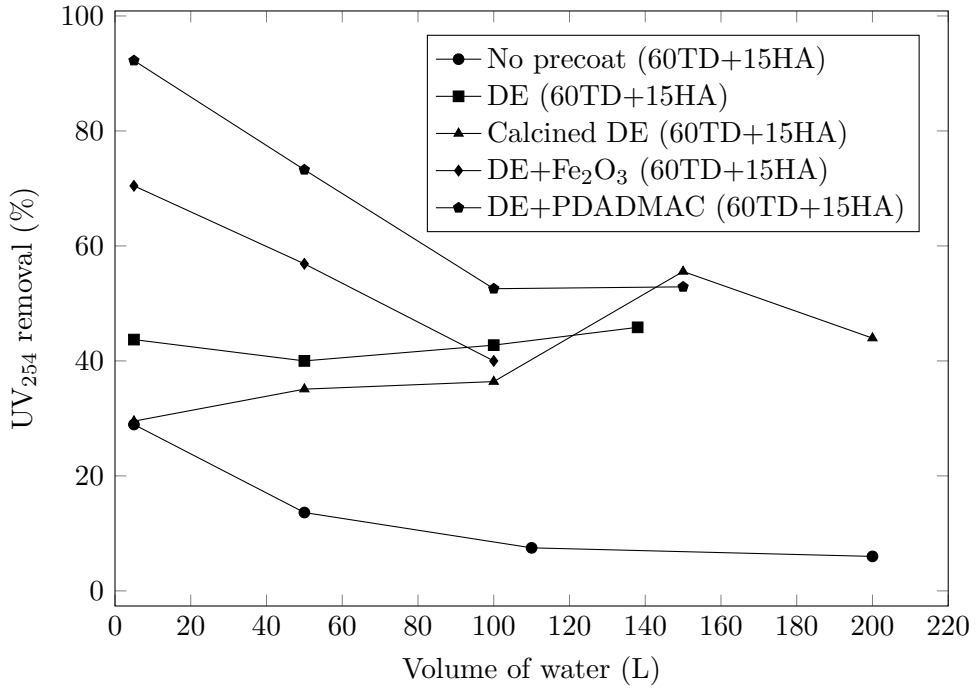

Fig. 6.15 UV_{254} removal of the precoats when trialled with the '60 mg/L TD + 15 mg/L HA' test water (starting point: 5 L).

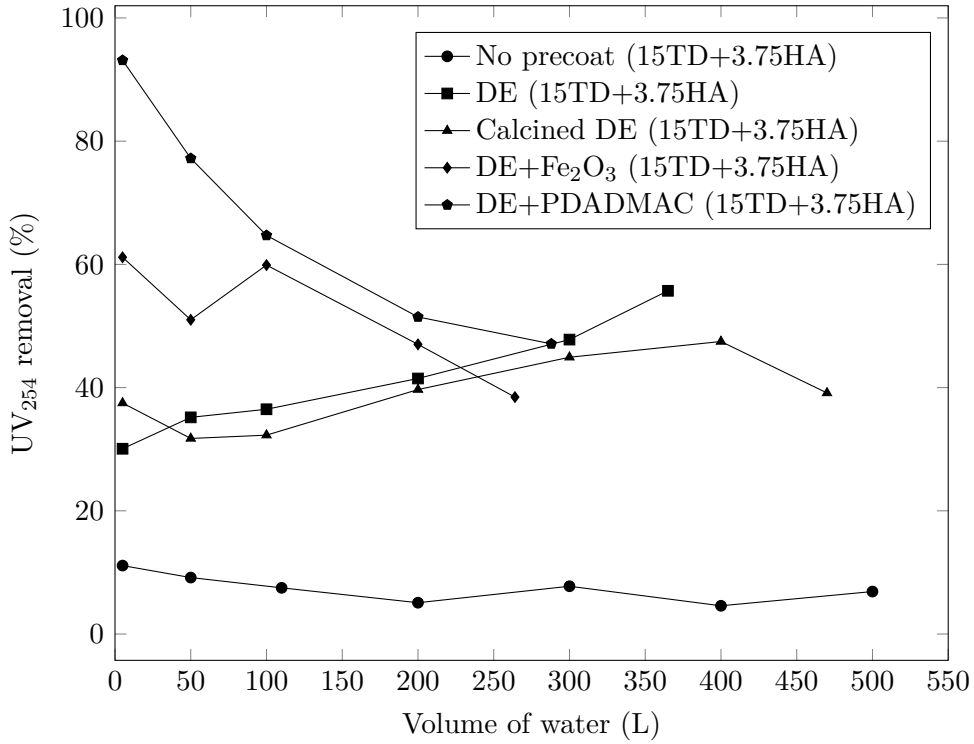

Fig. 6.16 UV_{254} removal of the precoats when trialled with the '15 mg/L TD + 3.75 mg/L HA' test water (starting point: 5 L).

The volume of water treated in the trials with the '15 mg/L TD + 3.75 mg/L HA' test water were higher than the '60 mg/L + 15 mg/L HA' (Table 6.4) and increase in ΔP more gradual (Fig. 6.13, Fig. 6.17) due to the lower amounts of TD and HA blocking the filter.

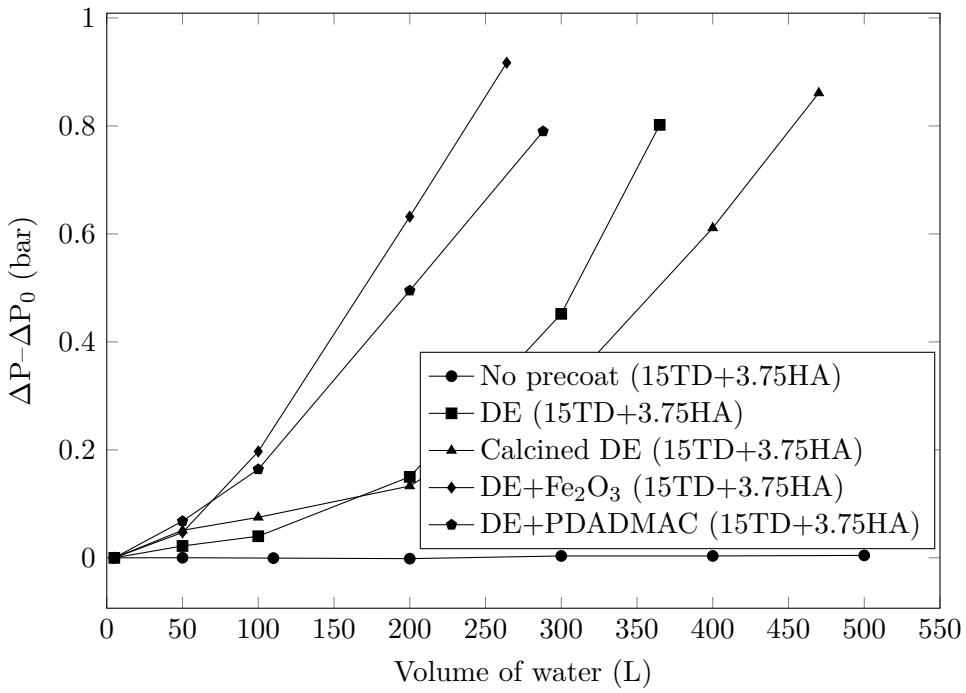

Fig. 6.17 Pressure drop caused by the trapped TD and HA for trials with the '15 mg/L TD + 3.75 mg/L HA' test water (starting point: 5 L).

In the lab-scale study by Burns et al. [187], modified DE (a commercial grade of DE mixed in a dilute solution of a commercial PE) with ZP of +36 mV and D_{10} of 5.5 µm was precoated on a horizontal septum with a diameter of 3.81 cm and hole size of 100-mesh (149 µm) at a loading rate of 3.51 kg/m^2.

The precoat removed 100% of sub-micron clay particles up to 2.4 mg clay applied/g DE. In trials with 30 mg/L of of instant coffee as a source of colour, 85% removal was achieved at the start, declining to 25%–10%, whereas plain DE had a removal of 7% declining to 0%. The DE used in our study had a D_{10} of 0.63 µm (Table 6.2), providing a higher surface area for adsorption despite a much lower loading rate (0.065 kg/m^2) that even when the enhanced adsorptive capacity, as a result of surface modification with PDADMAC or iron oxide, was depleted, a removal of ≈30% was still achieved.

6.4.7 Removal of *E. coli*

Table 6.5 presents the average *E. coli* percentage and log removal for each of the precoats during the short 50 L trials with the '60 mg/L TD + 15 mg/L HA + 10^7 *E. coli* colonies' test water. The *E. coli* removal by a pristine filter was low (9.77%), while DE+PDADMAC precoat provided the highest *E. coli* removal, 97.91%. However, good removal efficiencies with other precoats were also attained.

Table 6.5 The average performance of different precoats during the 50 L trials with the '60 mg/L TD + 15 mg/L HA + 10^7 *E. coli* colonies' test water.

Precoat	***E. coli* removal (%)**
No precoat	9.77 [0.045-log]
DE	96.44 [1.449-log]
Calcined DE	91.3 [1.060-log]
DE+PDADMAC	97.91 [1.680-log]
DE+Fe_2O_3	92.93 [1.151-log]

Even though all the precoats performed similarly in the short trials, the DE+PDADMAC precoat that had the highest stability and removal was selected for larger volumes of water with *E. coli* (Table 6.1). In Fig. 6.18, the markers and error bars show the average and variation of log removal obtained after processing 5 and 50 L in each batch run. The average log removal started at 1.81 and 1.91 in DE+PDADMAC (60TD+15HA+*E. coli*) and DE+PDADMAC (15TD+3.75HA+*E. coli*) trials, dropping to 1.47 and 1.53, respectively, when the pressure drop reached 1 bar and the trials were stopped.

While it is not expected that filters remove bacteria, the log removals achieved with precoated filters demonstrate the removal efficiency for pathogens/particles larger than the size of *E. coli*. We can speculate that protozoa such as *Cryptosporidium parvum* that

are much larger in size (3–6 µm) than *E. coli* and persistence against chlorine disinfection [201], can be removed at above the log removal values reported here.

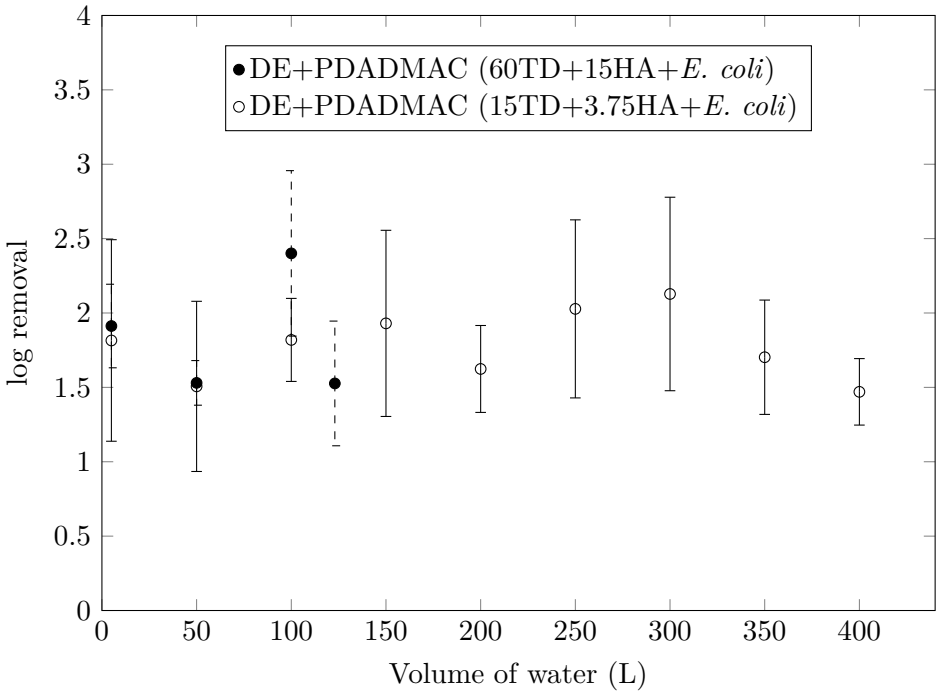

Fig. 6.18 *E. coli* removal during 'DE+PDADMAC (60TD+15HA+*E. coli*)' and 'DE+PDADMAC (15TD+3.75HA+*E. coli*)' trials (pressure drop limit: 1 bar, starting point: 5 L).

In a study by Boittelle et al. [80] using 2 kg/m^2 of a commercial grade of DE with a higher permeability of 4500 mD, a much lower bacteria removal of 48% was reported. Amburgey et al. [195] investigated the removal of 1 µm polystyrene microspheres (the same size range of *E. coli*) in swimming pool water by a precoat filter (permeability of 1215.9 mD), operated in continuous mode at a flux of 6.1 m/h, and reported a log removal of 0.86, much lower than the *E. coli* removal reported for the fine DE used in our work. This again shows that the commonly used commercial grades of DE would have more limited removal efficiency of particles as small as bacteria even at much higher loading rates.

6.4.8 Cleaning and reuse of the filters

Due to cost considerations in low-income settings, it would be desirable to clean and reuse the pleated filters with minimal cost and effort. Although backwashing is a common practice for membrane systems, there are no cartridge filters with this option and the additional capital costs (e.g., a backwash pump) are prohibitive. Therefore, manual cleaning is more practical for HWT systems.

Cleaning the used filters was done with less effort than the un-precoated filter as flakes of the precoat and the cake formed on the surface fell as soon as the filter was being taken out of the housing. However, the DE+PDADMAC or DE+Fe_2O_3 precoats were harder to remove as the PDADMAC acted like a glue (a trade off between stability and cleaning) and Fe_2O_3 had covered the filter surface as well.

SEM images of slices of precoated (with DE) and un-precoated filters after the trials with the '60 mg/L TD + 15 mg/L HA' test water showing the remaining dirt on fibres after cleaning are presented in Fig. 6.19, which demonstrate the improved cleaning as a result of the precoat protecting the fibres. Entrapped particles lower the permeability of the filter leading to a higher initial pressure drop after each cleaning cycle and a shorter lifespan.

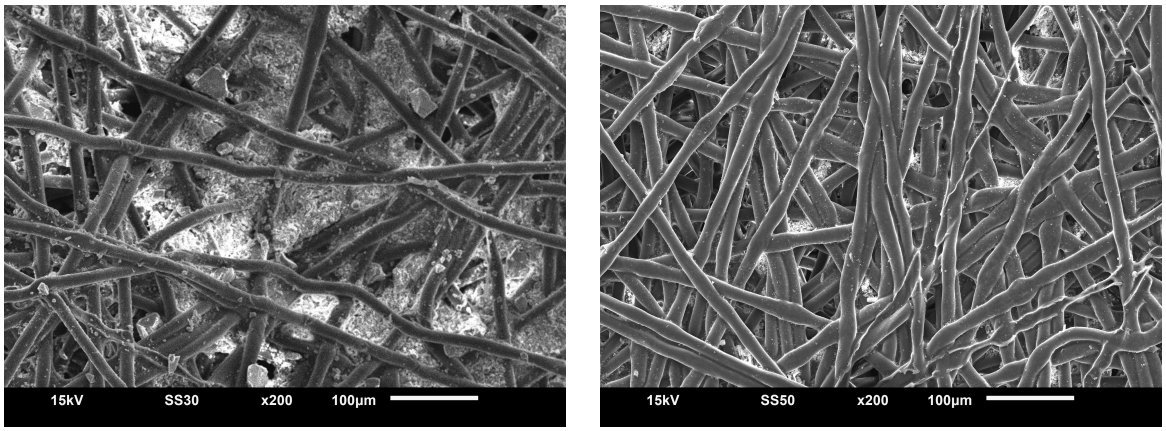

(a) (b)

Fig. 6.19 SEM images of (a) un-precoated and (b) precoated (with DE) filters after cleaning ('60 mg/L TD + 15 mg/L HA' test water), showing the improved cleaning because of precoating.

Galjaard et al. [202] applied precoating in membrane filtration, mainly to protect the membranes from fouling caused by suspended and colloidal particles as well as removing organic matter. It was observed that despite the higher fouling rate of the precoated membrane during the first filtration cycles, permeability of the membranes was better restored after a backwash, and backwashing took less time.

When the filter was disinfected after the 'DE+PDADMAC (60TD+15HA+*E. coli*)' trial and clean dechlorinated water was passed through the filter, no colony was detected in the sample of filtrate taken after processing 5 L. SEM images of the slices physically removed from the pleated filter afterwards compared to a clean filter showed no differences (Fig. 6.20); therefore, no damage to the fibres was incurred.

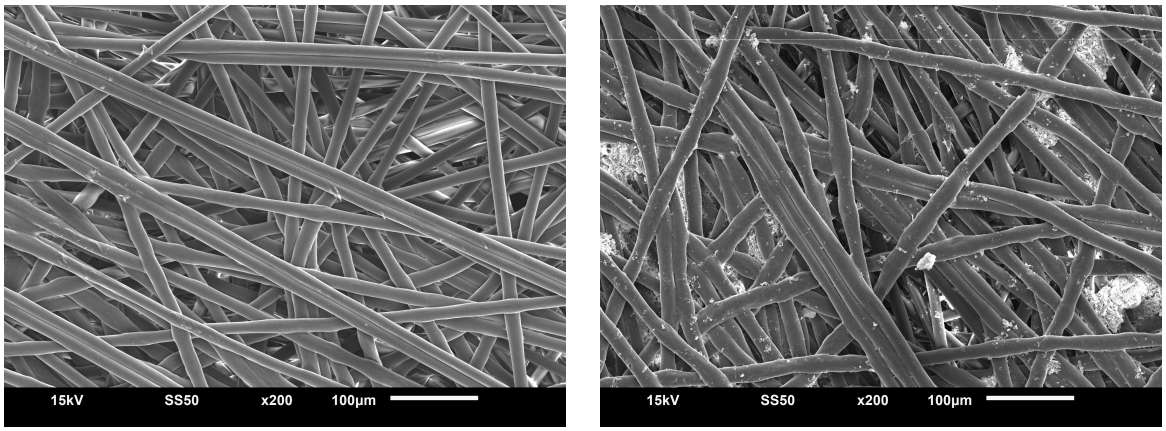

(a) (b)

Fig. 6.20 SEM images of (a) a clean filter and (b) the filter used in the 'DE+PDADMAC (60TD+15HA+*E. coli*)' trial after disinfection with 5 mL sodium hypochlorite (6–14% active chlorine).

A problem associated with precoat filtration is the disposal of the spent filter cake, which causes environmental issues at industrial volumes. However, only small amounts are needed for HWT systems and the only health risk associated is the presence of cysts, which decay by time [69].

6.5 Conclusion

Due to the intermittent nature of HWT systems, the industrial guidelines for precoating were not applicable, necessitating the development of new processes and precoat materials for HTW applications. Using a very fine grade of DE with D_{50} of 2.69 µm and permeability of 2.9 mD made it possible to use a very small loading rate of 0.065 kg/m^2 to cover the vertical septum (i.e., pleated filter), which did not detach easily. The stability of the precoat was enhanced by modifying its surface with a cationic polyelectrolyte (PDADMAC) which acted as a glue, keeping the precoat firmly attached to the surface of the filter. Therefore, the procedure presented demonstrated the relative easiness and practicality of this approach for HWT systems.

In the absence of organic matter (i.e. humic acid), a natural DE precoat removed >95% of the influent turbidity (40±10 NTU) during the whole duration of the trial (>1000 L). The permeability of DE could be improved by calcining and its surface charge modified by electropositive coating (using PDADMAC) to remove organic matter or be coated with iron oxide for higher adsorptive capacity.

The concentrations used based on the WHO scheme for testing HWT systems only represented the worst case scenario and in order to simulate the turbidity level in medium-quality surface waters, a test water with 15 mg/L TD (turbidity of 10±3 NTU) and 3.75 mg/L HA was prepared as well. When the water had a medium to low turbidity (10±3 NTU) as recommended for the precoat filtration process [94], the <5 NTU target was achieved in the presence of organic matter (3.75 mg/L HA).

The PSD and zeta potential of the DE and the turbidity agent were measured, making comparison with the results in literature possible. Characterisation of the cake layers helped explain the difference in pressure drops with different precoat materials.

The improvement in filter cleaning due to precoating was demonstrated by SEM imaging, and for safe reuse of filters, a simple procedure that inactivated *E. coli* without damaging the fibres of the filters was proposed. Although it was desired to test the proposed precoat filtration process in the field, the global pandemic made it impossible.

The results in this chapter showed the effectiveness of surface charge modification for HA removal. However, the rate of pressure drop was high, making the precoat filtration less suitable for cases where removal of organic matter is necessary. The next chapter (Chapter 7) will explore a hybrid process that could be implemented specifically for such situations.

Chapter 7

Contact filtration for household water treatment systems

7.1 Introduction

Although reducing the pore size of filters result in removal of finer particles, as demonstrated in the previous chapter (Chapter 6), surface charge of both the filter media and particles determine the removal efficiency of organic matter. In industry, the coagulation process usually precedes filtration, and whilst very effective for the removal of both particles and organic matter, coagulation, flocculation and sedimentation system units (Fig. 7.1) account for a significant part of the capital cost of water treatment plants [71, 105]. In addition to cost, the systems can be complex to operation if levels of pollutants in raw water vary, and as such these processes are not well studied or applied to HWT systems.

Direct filtration, defined as a filtration process not followed by sedimentation (Fig. 7.1), is an economical alternative to the conventional filtration process for raw water with low levels of turbidity (max. 15 NTU) and natural organic matter (NOM) [106, 107].

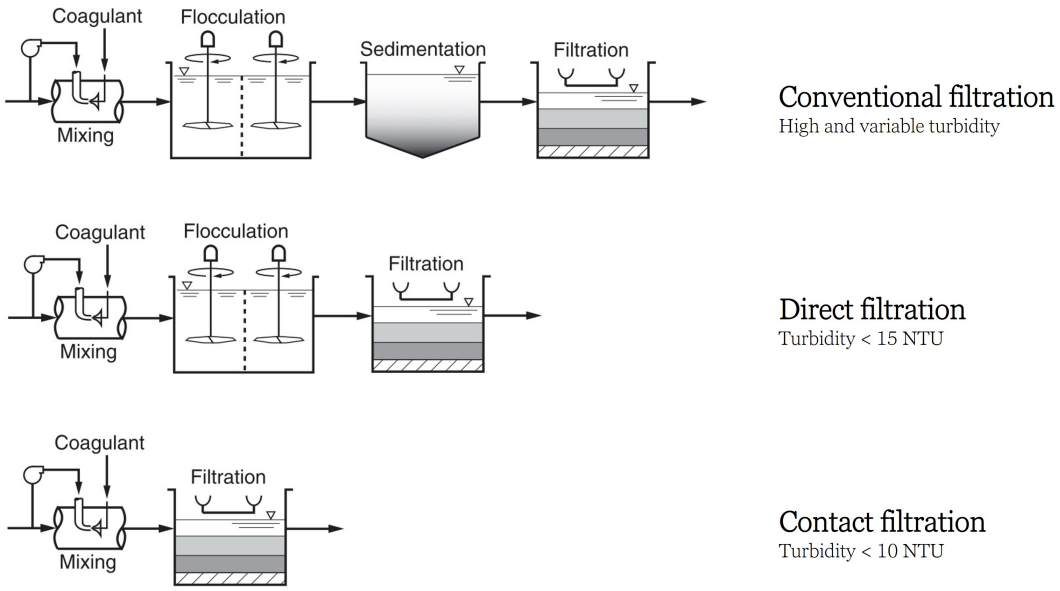

Fig. 7.1 Application of unit processes for the removal of turbidity [6].

A subset of direct filtration is called contact filtration or direct in-line filtration, in which the coagulant is dosed immediately prior to filtration (Fig. 7.1), with subsequent flocculation and deposition occurring in contact with the filter media, eliminating the capital cost needed for coagulation/flocculation basins [203, 204]. Also, this results in lower coagulant consumption as small filterable flocs are required rather than large 'settleable' flocs [203]. In contact filtration, the action of the coagulant must be rapid, therefore the coagulant dose and injection point can directly affect the final effluent quality [107]. However, when the effective dose is coupled with a large surface area of the filtration medium, such as that provided by the filter in a HWT system, effective removal of turbidity can be achieved [105].

Natural organic matter (NOM) imparts colour to water, causes odour and taste, provides substrate for bacteria, increases corrosion and most importantly is a precursor to the formation of cancerogenic disinfection by-products (DBPs) such as trihalomethanes (THMs) and halo-acetic acids (HAAs) when water is disinfected with chlorine [85, 205]. When filtration is followed by UV treatment in an HWT system, NOM can absorb UV

energy and thereby prevent effective control of pathogens. Practices to measure the concentration of NOM include total organic carbon (TOC) analysis, alternatively, UV absorbance at 254 nm is often used as surrogate measurement which doubles as a more accurate indicator of the potential for chlorination by-products than TOC [152, 153]. Therefore, in addition to turbidity, the US EPA requires conventional treatment plants to remove 15–50% of TOC depending on the alkalinity and initial TOC concentration of the source water (see Table 7.1) [15].

Table 7.1 The required percentage removal of TOC by enhanced coagulation, determined by the US EPA [15].

Source water TOC (mg/L)	**Source water alkalinity (mg/L as $CaCO_3$)**		
	<60	60–120	>120
2.0–4.0	35%	25%	15%
4.0–8.0	45%	35%	25%
>8.0	50%	40%	30%

In natural waters, inorganic and organic particulates typically have a negative charge, measured indirectly via zeta potential, thus preventing aggregation for long periods of time. During the coagulation process, the addition of metal salts or polyelectrolytes can neutralize the negative surface charge of most particles in natural waters at neutral pH (6–8) [6, 69, 85], and when followed by flocculation and sedimentation, effectively reduces turbidity. However, dissolved organic matter (DOM) has a greater negative charge than that of inorganic particles and as such requires a higher coagulant dose than coagulation for effective particle removal. A coagulation process optimised for removing dissolved constituents, which are likely to form disinfection by-products, is termed ‘enhanced coagulation’ [6, 206].

In the conventional filtration process, measuring zeta potential can facilitate determining the coagulant dose to neutralise particles (reaching the isoelectric point) by plotting

zeta potential versus coagulant dose [69, 85]. However, this practice is not applicable to contact filtration due to the short mixing times and the fact that removal occurs due to contact with filter media rather than flocculation and sedimentation [207].

Mechanisms involved in NOM removal by hydrolysing coagulants are charge neutralization, adsorption, complexation and enmeshment. Optimum removal of NOM occurs at slightly acidic pH values (4.5–6), while mineral turbidity is effectively removed at the neutral pH range. At a higher pH than the minimum solubility of inorganic coagulants, NOM removal occurs primarily by enmeshment and bridging [100].

In the water industry, alum (aluminum sulfate), sold in a hydrated form as $Al_2(SO_4)_3\ xH_2O$, is the first coagulant of choice, due to its availability and low cost [6, 100, 102]. However, residual aluminium is problematic in the distribution system, due to post-precipitation and pipe scaling [208]. The optimal pH (minimum solubility pH) for alum is in the range of 6.0–6.7 for warm (20 ℃) and 6.3–7.1 for cold waters (5 ℃), producing a treated water with a dissolved aluminium concentration of less than 0.05 mg/L [208].

Addition of alum decreases alkalinity and pH of water as it undergoes acid hydrolysis [209], consequently, pH adjustment is not usually necessary for most low-alkaline waters, since alum would sufficiently reduce pH to permit effective coagulation. In cases where pH adjustment is necessary for coagulation with alum, or change in alkalinity is undesired, a cationic polymer could be used instead as the sole coagulant [210].

Polyelectrolytes (PEs) have several advantages compared to inorganic coagulants including lower dose requirement, they do not impact the pH and alkalinity, and operate over wide pH range [69, 102, 103]. Cationic polyelectrolytes adsorb strongly to the surfaces of negatively charged particles, with unattached segments attaching to other particles. However, PEs such as PDADMAC (polydiallyldimethyl ammonium chloride) have not shown the same performance as inorganic coagulants in removing NOM in conventional

treatment plants [102], but are used in smaller niche applications.

In direct filtration, PEs provide longer filter runs, but at the expense of lower quality filtrate [210]. When the flocculation period is short, low to medium molecular weight (10,000–100,000) cationic polyelectrolytes have been shown to be the most effective, as during direct filtration headloss is directly related to the molecular weight of a polymer [104].

In summary, the contact filtration process could be a suitable process for HWT systems where turbidity is below 10 NTU, and NOM are a concern. Previous studies on contact filtration use sand or dual media filters typically used in water treatment plants with no research directed towards cartridge filter assemblies. Given the approach used in HWT must be low cost, with minimal user input and ideally operating independently of complex analysis/control, coagulant dose optimisation requires careful consideration.

7.2 Aim and objectives

7.2.1 Aim

This chapter aims to develop a contact filtration process for HWT systems ensuring high levels of particle and NOM removal, while considering the limitations faced in low-cost settings such as a lack of user water chemistry knowledge and limitations in the use of automated dosing equipment and control systems.

7.2.2 Objectives

i. To investigate whether coagulants can be dosed by hydraulic means instead of using a dosing pump, thereby minimizing cost and complexity for HWT systems.

ii. To evaluate the efficiency of turbidity and organic matter removal, coupled to pressure drop, during contact filtration in a HWT system. Treated water should leave the system with the recommended turbidity of 5 NTU.

iii. To compare filtration performance based on variables such as water pH, filter micron rating, choice of coagulant and coagulant dose.

iv. To evaluate coagulant dosing strategies to optimize contact filtration with fibrous cartridge filters and ensure that user does not need to adjust the coagulant dose frequently.

v. To gain further understanding of the mechanism of coagulation, through study of zeta potential.

vi. To evaluate the impact of coagulation on pH and alkalinity following addition of coagulants.

7.3 Materials and Methods

7.3.1 Experimental set-up and procedure

The process flow diagram (PFD) of the household water treatment system used in this work is shown in Fig. 7.2. Tap water (Belfast, UK) with the characteristics given in Table 7.2 was fed into the feed tank (B-001) by a hose. The concentrations of the test dust (TD), humic acid (HA) and sodium hydroxide (used to mimic turbidity, NOM and to regulate alkaline pH, respectively) in the water were controlled by dosing from a concentrated stock of TD and HA (B-004) using a peristaltic pump (P-001) (101U, Watson Marlow). An aquarium pump (Intercept, PF Mini) was utilized to internally recirculate the suspension within the feed tank preventing settlement of large particles inside the tank.

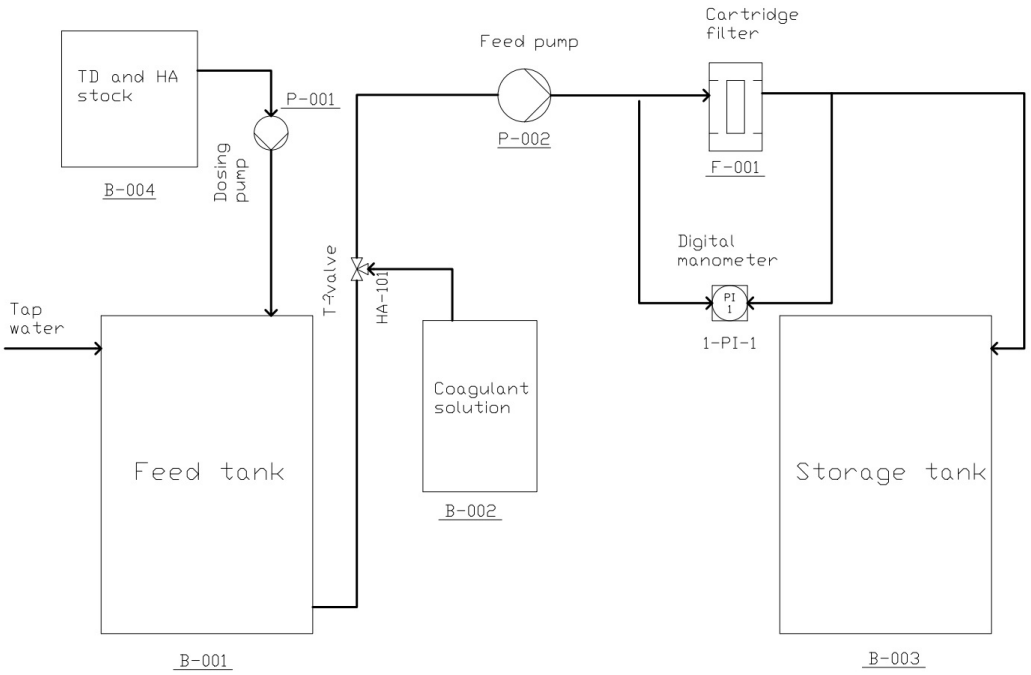

Fig. 7.2 The process flow diagram (PFD) of the HWT contact filtration system.

Table 7.2 The characteristics of the tap water used for contact filtration experiments.

Turbidity (NTU)	**pH (–)**	**Temperature (°C)**	**Alkalinity (mg/L as $CaCO_3$)**	**TOC (mg/L)**
0.05–0.3	6.9–7.4	12–19	60–69	4.15

A coagulant stock solution was prepared by adding alum powder and/or PDADMAC liquid solution to tap water in a container (B-002); after stirring, the solution was injected directly to the feed stream by connecting a T-valve (HA-101) to the feed inlet pipe, creating a manifold. There was no need for an additional dosing pump given the T-valve was located on the suction side of the feed pump (P-001), a small diaphragm pump (Model 2095-204-412, Shurflo) with a variable flow rate of 5.74–4.82 L/min within the pressure drop range of 29–834 mbar. The resulting coagulant flow rate was 0.054–0.094 L/min (1.06%–1.67% of the total flow), achieved by reducing the diameter at the coagulant intake to ≈1 mm using a plastic insert. The ratio of coagulant flow to raw water varied

by 5–20% with pressure drop.

Coagulant mixing with suspended and colloidal particles of the raw water occurred within a few seconds as the suspension travelled through the pipes, fittings and filter housing (F-001) before contact was made with the fibres of the filters. During experiments, the pressure drop across the filter was recorded from a digital manometer (1-PI-1) (Digitron, 2028P7) with turbidity, absorbance at UV_{254}, pH and zeta potential measured manually by taking samples (50 mL) from the feed tank (B-001) and the outlet after 50 L of water was processed, and subsequently every 100 L (i.e., samples were removed for analysis upon treatment of 50, 100, 200, 300 L and so on). The turbidity measurements were performed in triplicate and the average was calculated. In addition, alkalinity measurements were performed for each concentration of alum used (4, 8, 16 and 32 mg/L) and for a single concentration of PDADMAC (0.45 mg/L) to investigate the effect of coagulant dose on the pH of treated water.

7.3.2 Test water and experimental variables

A water containing 15±4 mg/L TD (turbidity of 10±3 NTU) and 4.5±0.75 mg/L HA (UV_{254} absorbance of 0.122±0.021), resulting in a zeta potential of -13±2 mV, was prepared as the baseline test water with concentration of pollutants only modified in specific circumstances. Table 7.3 shows the groups of trials performed (in duplicate) to explore the variables affecting the process, including: (i) concentration of alum (0, 2, 4, 8, 16 and 32 mg/L) with a 0.5 micron spun filter; (ii) adjustment of the quality of the feed water (half and double the concentration of the constituents in the baseline feed water), using 8 mg/L of alum and 0.5 micron spun filters; (iii) filter micron rating (0.5, 5 and 50 micron) of the spun filter with three concentrations of alum (0, 4 and 16 mg/L); (iv) effect of pH, across two ranges 6.9–7.4 (neutral pH) and 7.9–8.4 (alkaline pH), with three alum concentrations (0, 8 and 16 mg/L), and 5 micron spun filters;

(v) effect of PDADMAC concentration (0.225, 0.45 and 0.9 mg/L) and alum (8 and 16 mg/L) with 5 micron filters at alkaline pH; (vi) effect of PDADMAC concentration (0.225 and 0.45 mg/L) with or without 4 mg/L of alum (alum:PDADMAC ratios of 9 and 18, respectively) and 50 micron filters.

Table 7.3 Trials grouped by the variables under study.

Trial group	Filter micron rating	Feed Water, with Baseline conc.×	Water pH	Coagulant(s)	Coagulant conc. (mg/L)
i	0.5	1	Neutral	Alum	0, 2, 4, 8, 16, 32
ii	0.5	0.5, 1, 2[†]	Neutral	Alum	0, 8
iii	0.5, 5, 50	1	Neutral	Alum	0, 4, 16
iv	5	1	Neutral, Alkaline	Alum	0, 8, 16
v	5	1	Alkaline	PDADMAC or Alum	0.225, 0.45, 0.9 (PD) or 8, 16 (Alum)
vi	50	1	Neutral	PDADMAC and Alum	0.225, 0.45 (PD) and 4 (Alum)

[†] Multiple of 2 means twice the concentrations in the baseline feed water (15±4 mg/L TD and 4.5±0.75 mg/L HA).

7.3.3 Materials

Fine test dust (ISO 12103-1, A2, Powder Technology Inc.), a red brown insoluble mineral composed mainly of silica, was used as the turbidity agent, and humic acid sodium salt (Sigma-Aldrich) used to mimic natural organic matter.

Aluminium sulphate (17% Al_2O_3, Pure Chem, UK), the industry standard inorganic coagulant was used within this study. PDADMAC (Mw 200,000–350,000, 20 wt. % in water, Sigma-Aldrich) a 100% cationic polymer of low-to-medium molecular weight [103] was chosen as the polyelectrolyte given it is a widely used coagulant in water treatment with no reported health, safety and environmental hazards [191].

A 10 inch standard spun filter element (Filter Logic, UK) and a 10 inch cartridge filter housing (Finerfilters, UK) constituted the filtration unit. Filter elements with nominal micron ratings of 0.5, 5 and 50 were trialed.

7.3.4 Instrumentation

A portable turbidity meter (HI-93703, Hanna Instruments) was used to measure the turbidity of water samples. Zeta potential (ZP) was measured via electrophoretic light scattering by using a particle analyser (Zetasizer Nano ZS, Malvern Panalytical).
The concentration of organic matter was measured via UV absorbance at 254 nm using a spectrometer (6305, Jenway) as a surrogate for HA concentration and TOC. Alkalinity of water was measured using a freshwater alkalinity colorimeter (HI-775, Hanna Instruments) and associated reagents (HI-775-26, Hanna Instruments). A pH meter (pH510, Eutech Instruments) was used to determine the pH of the raw and finished water.

7.4 Results and discussion

The removal of both particles and HA was followed during high volume trials (500 L) in the lab based HWT filtration system. The quality of treated water was assessed to meet regulations and guidelines (particle removal measured via turbidity, TOC removal assessed based on absorbance at 254 nm and pH) along with the pressure drop across the filtration system and data relating to the underpinning mechanistic approach (the zeta potential) were monitored to establish parameters achieving effective contact filtration for HWT applications.
Trials were considered successful if the turbidity of treated water was reduced to the WHO limit of 5 NTU [48] (i.e. a removal of 62% from the inlet turbidity of 10±3 NTU) and required TOC removal met with the standards described in Table 7.1, i.e. >25% removal of TOC/UV_{254}. For example, where the water alkalinity was 60–69 mg/L $CaCO_3$ and TOC due to the addition of HA (7.5–30 mg/L) calculated to be 0.65–2.62 mg/L (see the calibration curve in Fig. 7.3), a TOC/UV_{254} removal efficiency of >25% was required.

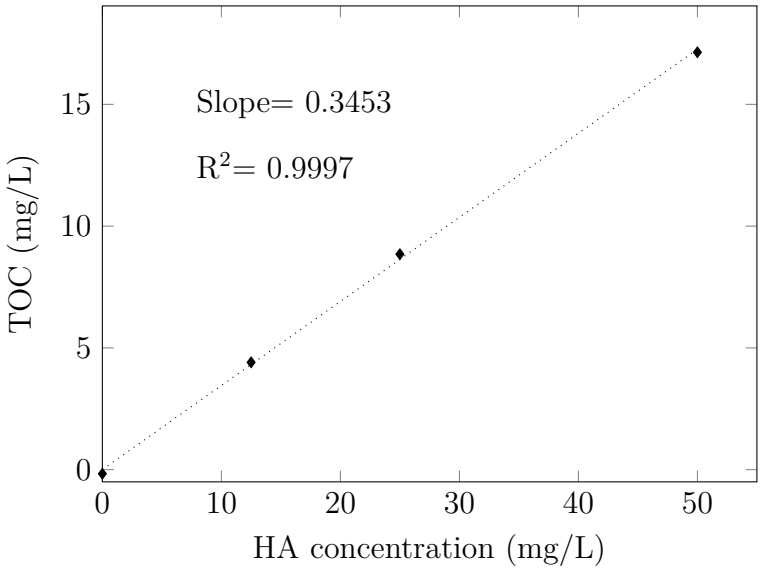

Fig. 7.3 The calibration curve for TOC (mg/L) versus HA concentration (mg/L).

7.4.1 Performance with different alum concentrations

In the absence of a coagulant, low levels of turbidity removal were observed in trials using a 0.5 micron filter (Fig. 7.4), with treated water not satisfying the 5 NTU limit recommended by the WHO [48]. The addition of alum significantly increased turbidity removal with as low as 4 mg/L resulting in 79.97% average removal (Table 7.4), achieving the 5 NTU limit. Increased alum concentrations permitted additional turbidity removal, however, percentage removal plateaued with alum concentrations above 8 mg/L (90.64%, 91.13% and 90.16% removal with 8, 16 and 32 mg/L of alum, respectively).

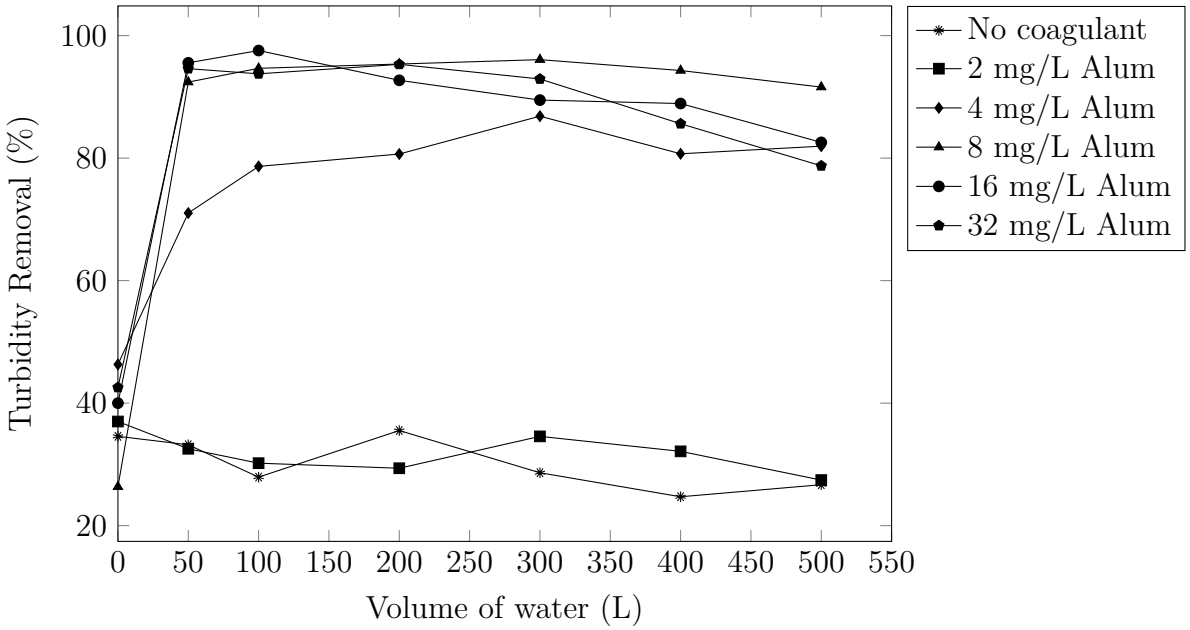

Fig. 7.4 Turbidity removal with 0.5 micron spun filters and various concentrations of alum injected in-line. (Inlet water: 15 mg/L TD, 3.75 mg/L HA, pH=6.9–7.4)

Table 7.4 Trial group i – the average turbidity and UV_{254} removal as well as the change in zeta potential and pH measured at 50L up to 500L and pressure drop after treating 500 L. (0.5 micron filters, inlet water: 15 mg/L TD, 3.75 mg/L HA, pH=6.9–7.4)

Alum conc. (mg/L)	**Turbidity removal (%)**	**UV_{254} removal (%)**	**$\Delta P - \Delta P_0$ (mbar)**	**Zeta potential change (%)**	**pH change (%)**	**Alkalinity change (%)**
0	29.45	8.59	-22.55	NA	NA	NA
2	29.76	10.78	-20.75	5.78	-0.27	NA
4	79.97	57.83	-2	23.58	0.15	-1.6
8	90.64	80.04	78	39.30	-1.90	-2.56
16	91.13	85.07	160	57.34	-2.48	-7.73
32	90.16	88.49	427.5	69.57	-5.08	-15.08

Removal of HA (i.e. reduction in absorbance at UV_{254}) required a higher concentration of alum, referred to as 'enhanced coagulation'. Alum concentrations of 4 and 8 mg/L resulted in 57.83% and 80.04% UV_{254} removal, respectively (Table 7.4 and Fig. 7.5);

however, higher alum concentrations (16 and 32 mg/L) resulted in diminishing returns (85.07% and 88.49% removal, respectively). Increased alum concentrations resulted in increased zeta potential, but again a diminishing return was observed at high alum concentrations (Table 7.4).

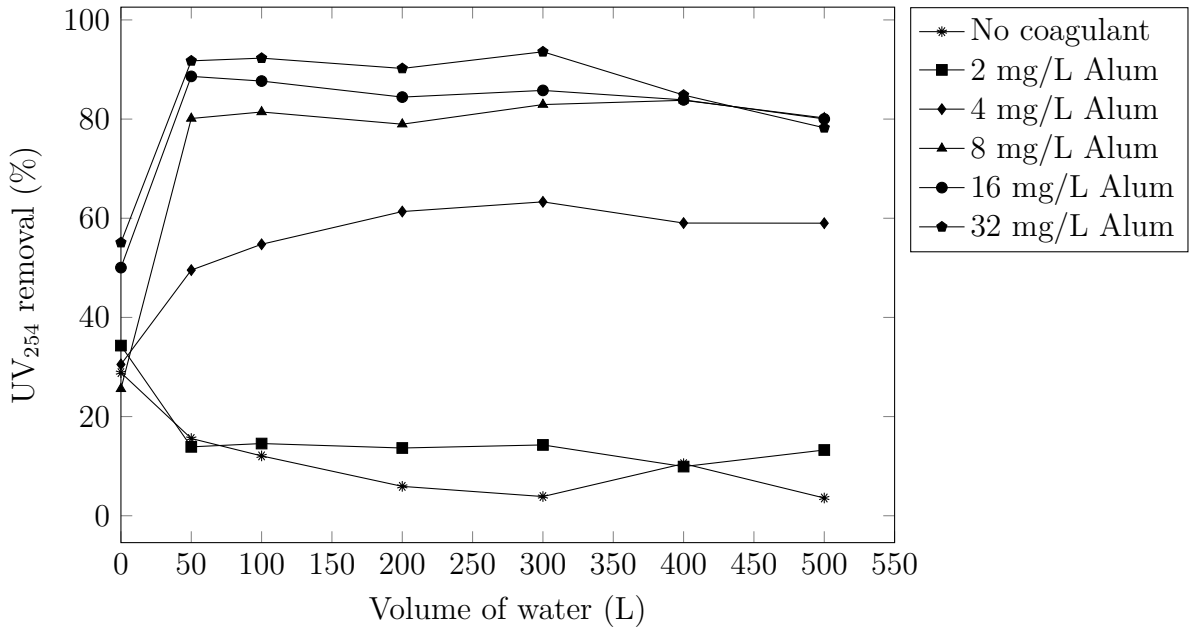

Fig. 7.5 UV_{254} removal with 0.5 micron spun filters and various concentrations of alum injected in-line. (Inlet water: 15 mg/L TD, 3.75 mg/L HA, pH=6.9–7.4)

The increased removal of particles and HA with higher alum concentrations resulted in increase pressure drop across the filter (Table 7.4 and Fig. 7.6). In the trial with 8 mg/L of alum, the ΔP caused by accumulation of particles during the 500 L trial was 78 mbar and double for 16 mg/L, 160 mbar. In conclusion, the optimum alum dosage for the baseline feed water in this study was 8 mg/L; nevertheless, the dose range for effective removal of turbidity and UV_{254} was wide, 4–16 mg/L.

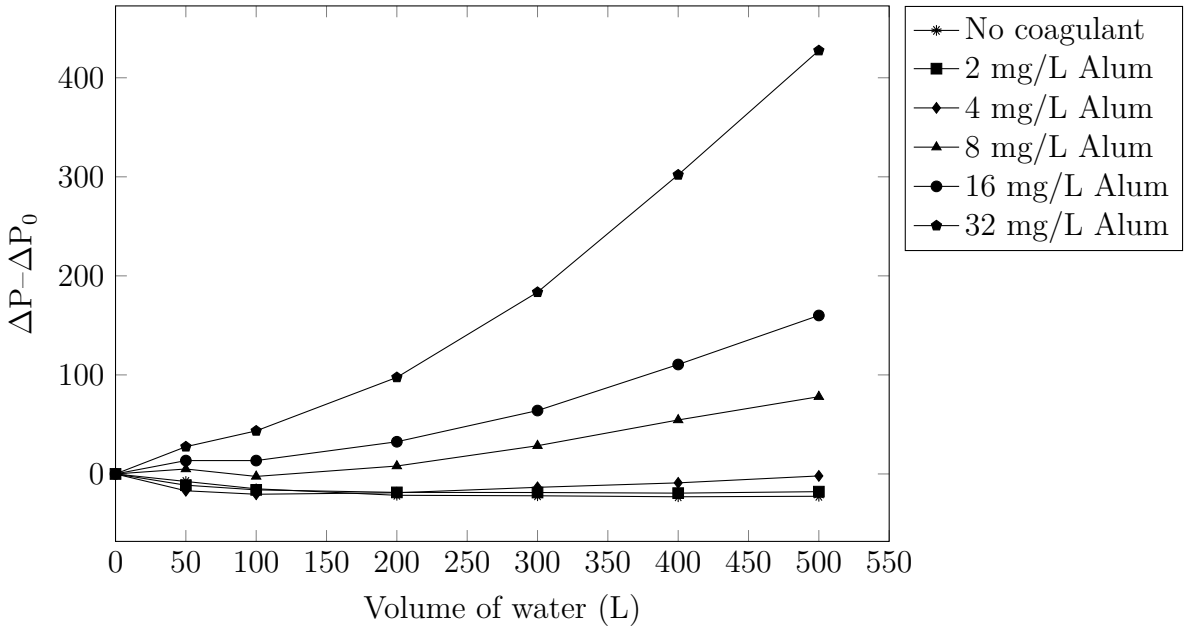

Fig. 7.6 $\Delta P - \Delta P_0$ with 0.5 micron spun filters and various concentrations of alum injected in-line. (Inlet water: 15 mg/L TD, 3.75 mg/L HA, pH=6.9–7.4)

Cleasby et al. [210] also reported similar observations regarding overdosing for contact filtration of natural waters: below the optimum alum dosage (found based on trial runs) filtrate quality improved by increasing the dose, but had diminishing return while the rate of headloss increased. Therefore, the choice of alum dosage was a compromise between improved filtrate quality and processing time. When the dosage was excessive, the filtrate quality was not increased, but the rate of headloss was more rapid.

In addition to filter performance factors (removal efficiency and pressure drop), the change in pH should be considered to ensure treated water remains within the recommended range for drinking water (i.e., 6.5–8.5 [48]). Table 7.4 shows the average change in alkalinity and pH with additional concentration of alum. As expected, increasing the alum concentration resulted in lower alkalinity and pH, with 32 mg/L alum resulting in a pH less than 6.5; this would be only problematic for distribution systems and not in HWT systems where water is consumed directly from the system.

Krupińska [209] reported that when 1–3 mg Al/L of aluminium sulphate (VI) was added

to a raw water collected at a water treatment plant with pH in the range of 7.60–7.84 and alkalinity of 3.55–3.80 mmol/L (177.5–190 mg/L as $CaCo_3$), the pH decreased to the range of 7.26–7.47 (1.71%–7.39% change) and alkalinity to the range of 3.30–3.70 mmol/L (2.63%–7.04% change), respectively. Considering that the alum used in our study contained 17% Al_2O_3 or 8.99% Al^{3+}, in a similar range of 0.72–2.88 mg Al/L (8–32 mg/L alum), the changes observed were similar to this study—change in pH was 1.90%–5.08% and in alkalinity, 2.56%–15.08%.

7.4.2 Performance with higher and lower feed water quality

As the quality of natural waters are variable over time, it was essential to perform trials with higher and lower feed water quality than the baseline to evaluate the performance with the optimum alum dose (8 mg/L) determined in the previous section.

The turbidity removal achieved with 0.5 micron filters and 8 mg/L of alum using test waters with lower and higher concentrations of TD and HA are shown in Fig. 7.7, with the averages of duplicate runs shown in Table 7.5. High levels of turbidity removal were observed, with all runs attaining the 5 NTU guideline. The average turbidity removal was almost the same irrespective of change in TD and HA in the test water, 94.83%, 90.64% and 92.72% removal observed for half the pollutant concentration (7.5 mg/L TD + 1.87 mg/L HA), the baseline test water (15 mg/L TD + 1.87 mg/L HA) and double the pollutant concentration (30 mg/L TD + 7.5 mg/L HA), respectively.

UV_{254} removal results (Fig. 7.8 and Table 7.5) showed an inverse relationship between the HA concentration in the test water with percentage UV_{254} removals of 85.30%, 80.04% and 73.72% for half strength test water (7.5 mg/L TD + 1.87 mg/L HA), baseline test water (15 mg/L TD + 1.87 mg/L HA) and double strength test water (30 mg/L TD + 7.5 mg/L HA), respectively. Nonetheless, the >25% UV_{254} removal was satisfied with all the test waters.

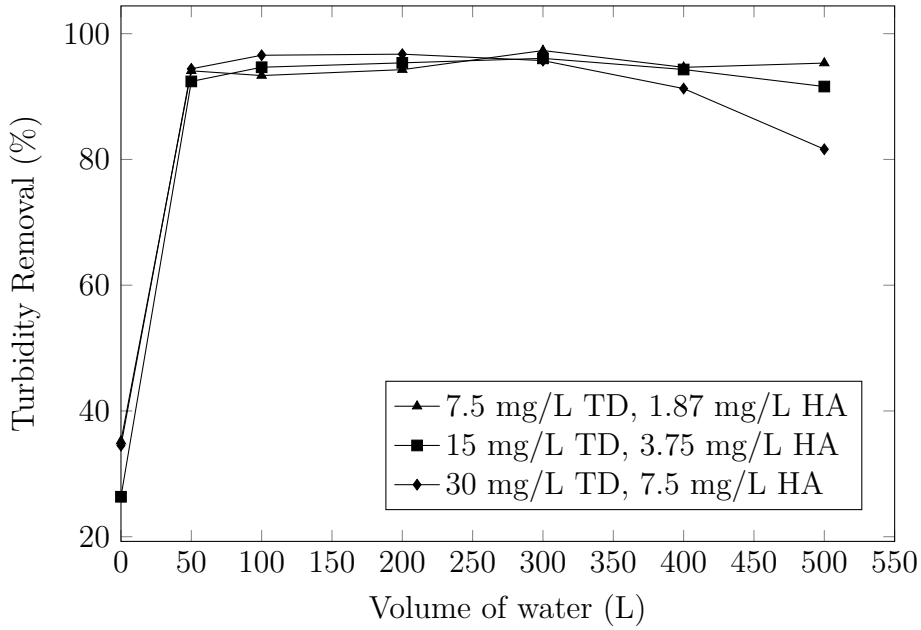

Fig. 7.7 Turbidity removal with 0.5 micron spun filters and 8 mg/L alum tested with different concentrations of TD and HA. (pH=6.9–7.4)

Table 7.5 Trial group ii – the average turbidity and UV_{254} removal measured at 50L up to 500L and pressure drop after treating 500 L. (0.5 micron filters, alum concentration= 8 mg/L, pH=6.9–7.4)

TD conc. (mg/L)	**HA conc. (mg/L)**	**Turbidity removal (%)**	**UV_{254} removal (%)**	**$\Delta P - \Delta P_0$ (mbar)**
7.5	1.87	94.83	85.30	71.5
15	3.75	90.64	80.04	78
30	7.5	92.72	73.72	121

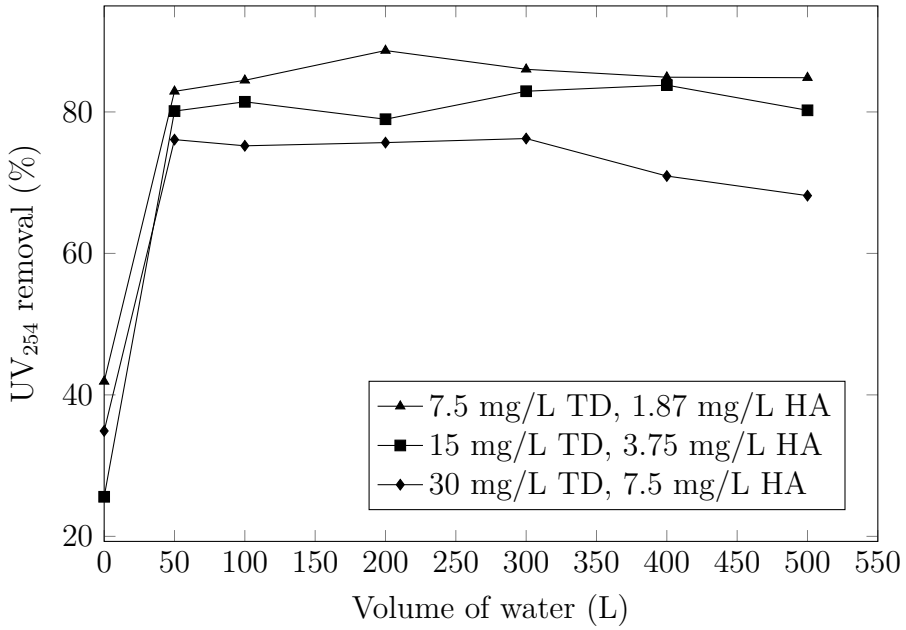

Fig. 7.8 UV_{254} removal with 0.5 micron spun filters and 8 mg/L alum tested with different concentrations of TD and HA. (pH=6.9–7.4)

The results demonstrated that even when the source water turbidity and organic matter concentration increased, the dose of alum determined previously could deliver acceptable turbidity and organic removals, with the caveat being the higher ΔP (Fig. 7.9 and Table 7.5) as a result of higher amounts of deposited particles from more polluted waters, shortening filter lifetime.

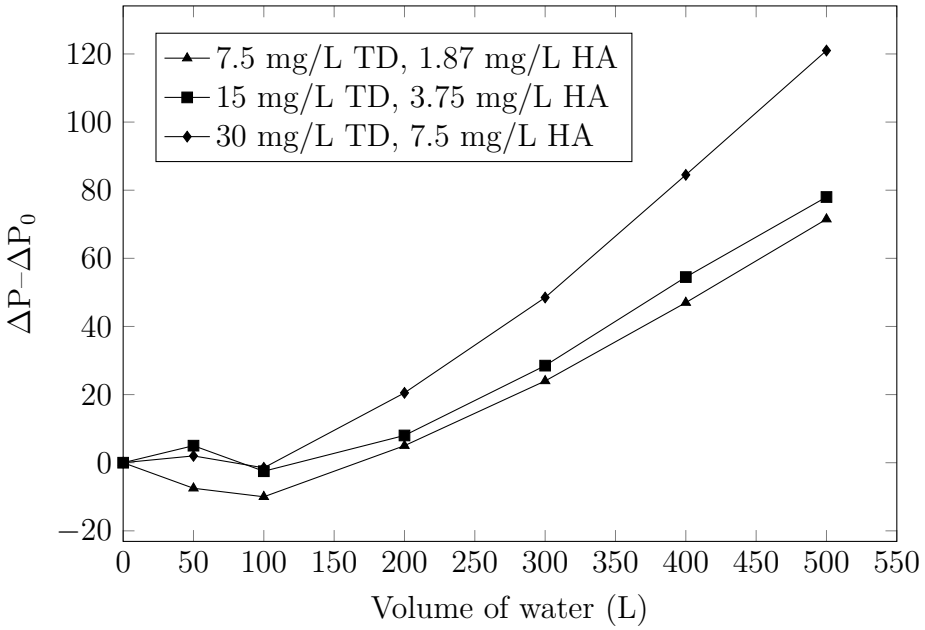

Fig. 7.9 $\Delta P – \Delta P_0$ with 0.5 micron spun filters and 8 mg/L alum tested with different concentrations of TD and HA. (pH=6.9–7.4)

Although the lower concentrations of TD and HA (7.5 mg/L TD + 1.87 mg/L HA) resulted in similar TD and UV_{254} removals, very low turbidities (<1 NTU) can be problematic for contact filtration, due to the lack of particle collisions [100], as the survey of a treatment facility by Monscvitz et al. [207] demonstrated. However, in the context of HWT, a source water with turbidity below 5 NTU does not require filtration and removal of organic matter alone can be achieved with other processes. If filtration was determined to be necessary, coagulant aids such as clay and diatomite can be added to enhance the coagulation process [6].

The observation that the turbidity removal did not vary with different concentrations of TD and HA, but UV_{254} removal did, can be confirmed with the results of the study by Saxena et al. [100] who used jar testing to investigate the coagulation performance of an aluminium based coagulant (polyaluminium chloride) at alkaline pH to remove different concentrations of HA as the organic matter (0–20 mg/L TOC) and kaolin clay as the turbidity agent (0–20 NTU). It was observed that the percentage removal was directly

related to HA concentration as it affected the collision frequency. The same conclusion was reported by Clark et al. [204] that in contact filtration (using a sand filter), the optimal dosage was not strongly correlated with turbidity, but rather influenced by NOM concentration. This observation can be further explained given that in the presence of NOM, the enmeshment mechanism is not affected by the type of particles and same dosage is required, instead the dose depends on the type and concentration of NOM as well as pH [6].

However, it appears that in contact filtration, the required alum dose does not follow the stoichiometric relationship between the humic acid concentration and alum ($Al_2(SO_4)_3 \cdot 18H_2O$) dose reported by Narkis and Rebhun [205], which is almost linear for HA concentrations up to 10 mg/L, and much higher than the doses used in this study—7, 13.6 and 24 mg/L of alum for 1.87, 3.75 and 7.5 mg/L HA as opposed to 8 mg/L reported here. However, the lower alum dose requirement in this work can be partially attributed to the presence of TD particles as Saxena et al. [100] has reported increasing turbidity above 5 NTU increased both particle collisions and TOC removal.

7.4.3 Performance of filters with different micron ratings

To investigate the trade-off between removal efficiency and pressure drop, spun filters of different micron rating were trialled. By comparing the turbidity removal obtained by 0.5, 5 and 50 micron spun filters (Fig. 7.10 and Table 7.6), it can be seen that without any coagulant, 5 and 50 micron filters had similar average removals, 14.38% and 13.51%, whereas 0.5 micron filter removed 29.45%, due to the fine PSD of TD discussed in Chapter 4. Dosing 4 mg/L of alum improved the removal for all filters, with the micron rating being inversely related to the removal efficiency as 0.5, 5 and 50 micron filters provided 79.97%, 63.92% and 47.81% removal, respectively. The filters with smaller micron ratings have more compact layers of fibres [173], increasing the probability of

particles coming into contact with a fibre, therefore retaining a greater number of particles with more significant levels of reduction of turbidity in treated water.

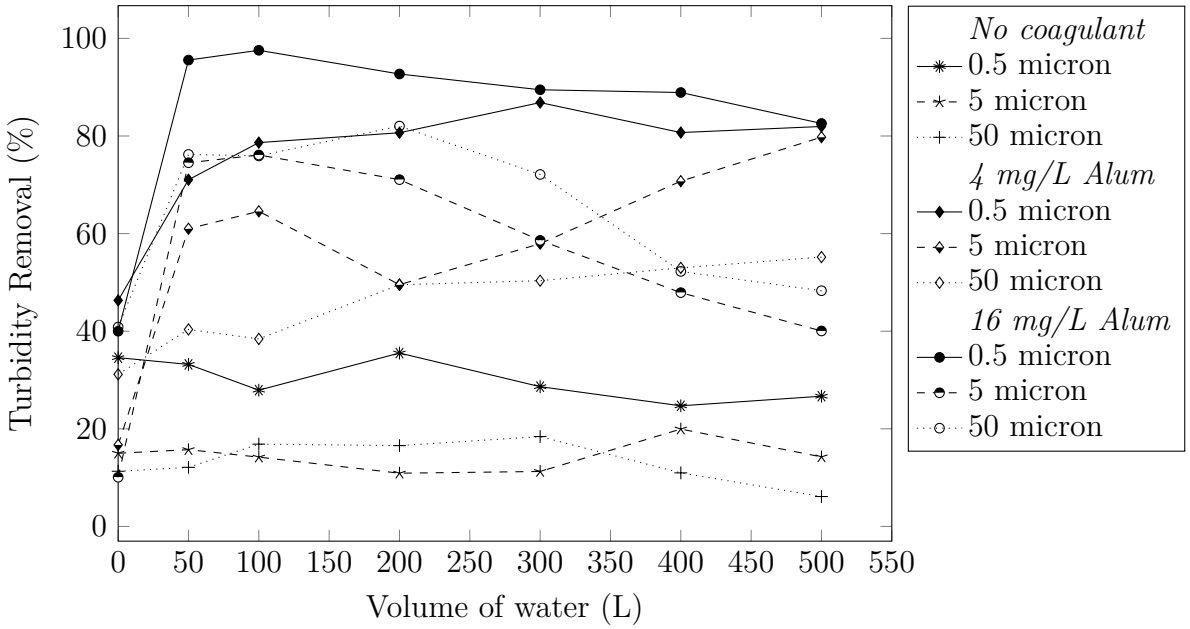

Fig. 7.10 Turbidity removal with different micron ratings of spun filters and various concentrations of alum injected in-line. (Inlet water: 15 mg/L TD, 3.75 mg/L HA, pH=6.9–7.3)

Table 7.6 Trial group iii – the average turbidity and UV_{254} removal as well as the change in zeta potential and pH measured at 50L up to 500L and pressure drop after treating 500 L. (Inlet water: 15 mg/L TD, 3.75 mg/L HA, pH=6.9–7.3)

Filter micron rating	**Alum conc. (mg/L)**	**Turbidity removal (%)**	**UV_{254} removal (%)**	**$\Delta P - \Delta P_0$ (mbar)**	**Zeta potential change (%)**	**pH change (%)**
	0	29.45	8.59	-22.55	NA	NA
0.5	4	79.97	57.83	-2	23.58	0.15
	16	91.13	85.07	160	57.34	-2.48
	0	14.38	6.71	-16	NA	NA
5	4	63.92	33.20	-2	11.77	-0.64
	16	61.38	53.17	102	63.63	-4.98
	0	13.51	6.35	-8.5	NA	NA
50	4	47.81	31.28	3	17.79	-0.04
	16	67.81	52.1	55.5	41.61	-2.90

When 4 mg/L of alum was used, the turbidity removal improved over time during the 500 L trials as the filters were continuing to be loaded with alum (Fig. 7.10). Increasing the alum concentration to 16 mg/L resulted in a smaller improvement in the average removal for 0.5 micron (91.13%) and 5 micron (61.38%) filters than 50 micron (67.81%). With 16 mg/L of alum, filters were loaded with alum in less than 50 L (Fig. 7.10), but turbidity decreased after filtering 100 L with 0.5 and 5 micron filters and 150 L with 50 micron filters. This trend suggests that the micron rating resulting in good removal efficiencies with the lowest alum dose would be preferred, striking a balance between good filtrate quality whilst maximizing the volume of water produced before requirement to replace the filter.

The results for UV_{254} removal with different micron ratings are provided in Table 7.6 and Fig. 7.11; without any coagulant, there was only a small difference in the average removal with 0.5, 5 and 50 micron filters, 8.59%, 6.71% and 6.35%, respectively, whereas dosing 4

mg/L of alum resulted in 57.83%, 33.2% and 31.28% removal, respectively, satisfying the >25% UV_{254} removal target; increasing the alum concentration to 16 mg/L increased the removal to 85.07%, 53.17% and 52.1%, respectively—this demonstrate that enmeshment of HA in alum results in fine particles that were removed more effectively in 0.5 micron filters.

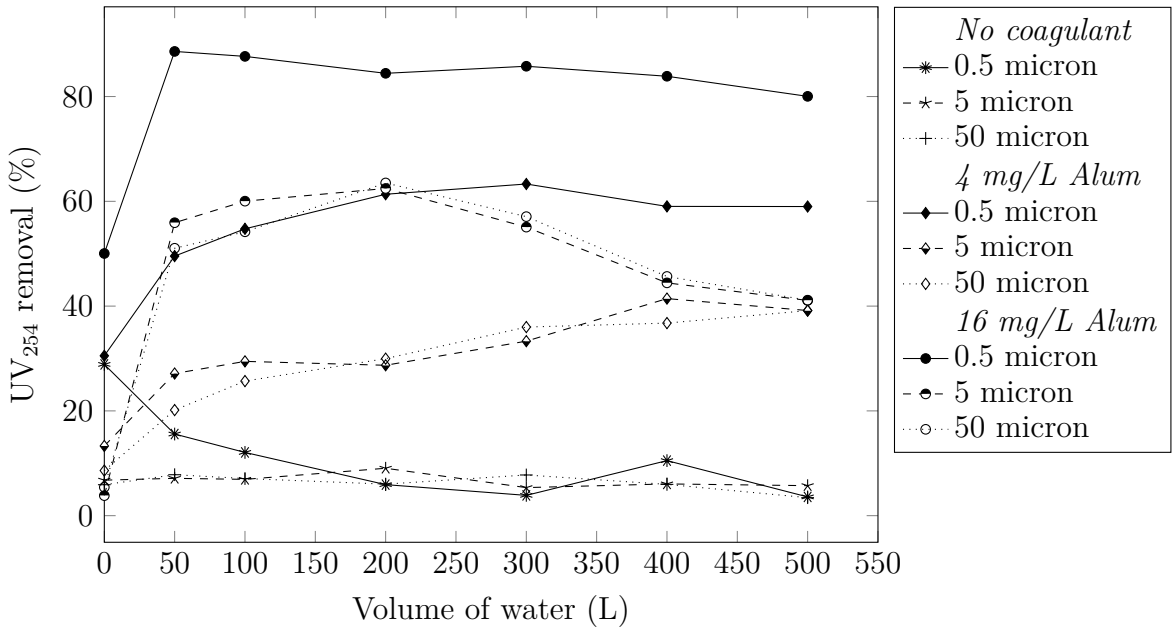

Fig. 7.11 UV_{254} removal with different micron ratings of spun filters and various concentrations of alum injected in-line. (Inlet water: 15 mg/L TD, 3.75 mg/L HA, pH=6.9–7.3)

Without a coagulant, the change in the pressure drop after 500 L of treatment ($\Delta P–\Delta P_0$) was a negative value for all the ratings as the accumulation of particles in the filters was insignificant while the air entrapped in the filters was vented lowering the internal resistance to the flow. The change for 50 micron was the smallest as the fibre layers were less dense and the flow regime was established in a shorter time. The alum dose had a direct relationship with ΔP as more alum particles were trapped in the filter, the greater the pressure differential.

The difference in pressure drop observed with different micron rating filters was more pronounced with 16 mg/L of alum, 0.5, 5 and 50 micron had $\Delta P–\Delta P_0$ of 160, 102 and

55.5 bar, respectively. However, with 4 mg/L alum, 0.5 micron filter showed a higher turbidity and UV_{254} at a lower pressure drop than with 50 micron filter and 16 mg/L of alum. Therefore, as mentioned earlier, the coarsest micron rating coupled with the lowest alum dose achieving the desired removals represents the preferred system.

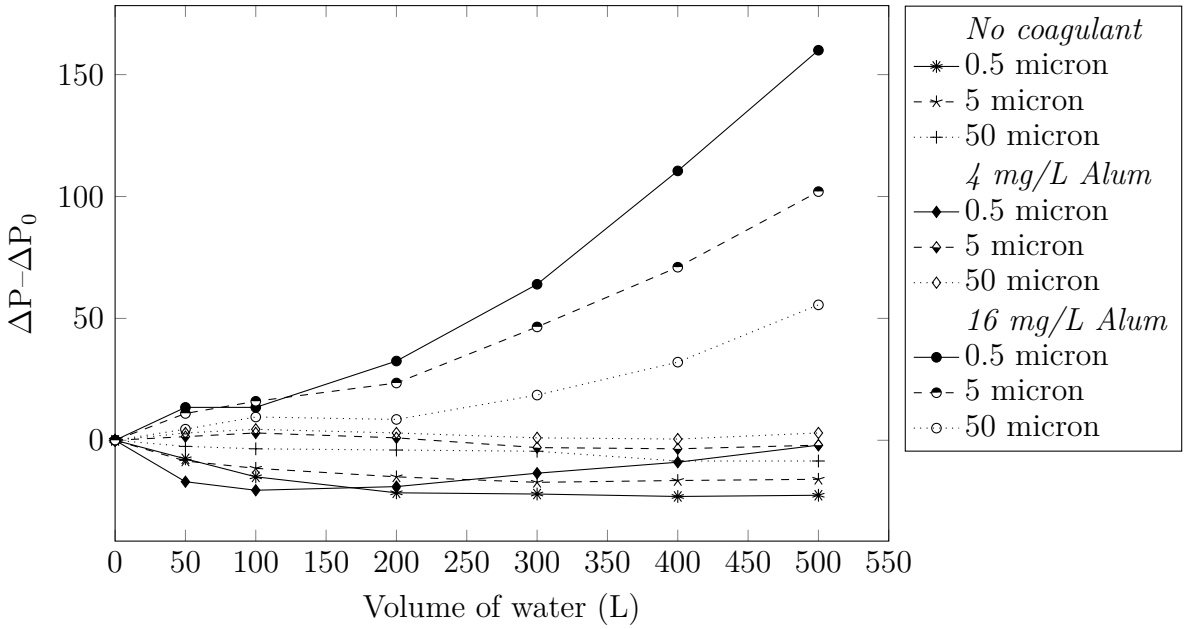

Fig. 7.12 $\Delta P–\Delta P_0$ with different micron ratings of spun filters and various concentrations of alum injected in-line. (Inlet water: 15 mg/L TD, 3.75 mg/L HA, pH=6.9–7.3)

7.4.4 Performance at neutral and alkaline pH ranges

pH adjustment is not feasible in HWT systems due to additional monitoring/control equipment needed; therefore, the performance of contact filtration at alkaline pH, reported to negatively impact coagulation, was evaluated and compared with performance at neutral pH.

The turbidity removal results achieved using 5 micron filters and alum doses of 8 and 16 mg/L—the higher end of the alum concentration range (4–16 mg/L) was chosen to compare the effect on water pH—at neutral (6.9–7.4) and alkaline (7.9–8.4) pH ranges are shown in Fig. 7.13 and the averages in Table 7.7. The average removal without

coagulation was 14.38% (neutral pH) and 18.47% (alkaline pH), while with 8 mg/L of alum removal efficiency increased to 78.68% and 86.13% at neutral and alkaline pH, respectively. However, at a higher alum concentration of 16 mg/L, turbidity removal was reduced at both neutral (61.38%) and alkaline (71.95%) pH conditions, demonstrating that 16 mg/L was above the optimum dose. The higher removal of turbidity at alkaline pH can be related to the solubility of alum at these two pH ranges [6], which can be confirmed with the smaller change in zeta potential (Table 7.7), resulting in slightly different coagulation mechanisms (enmeshment at higher pH values).

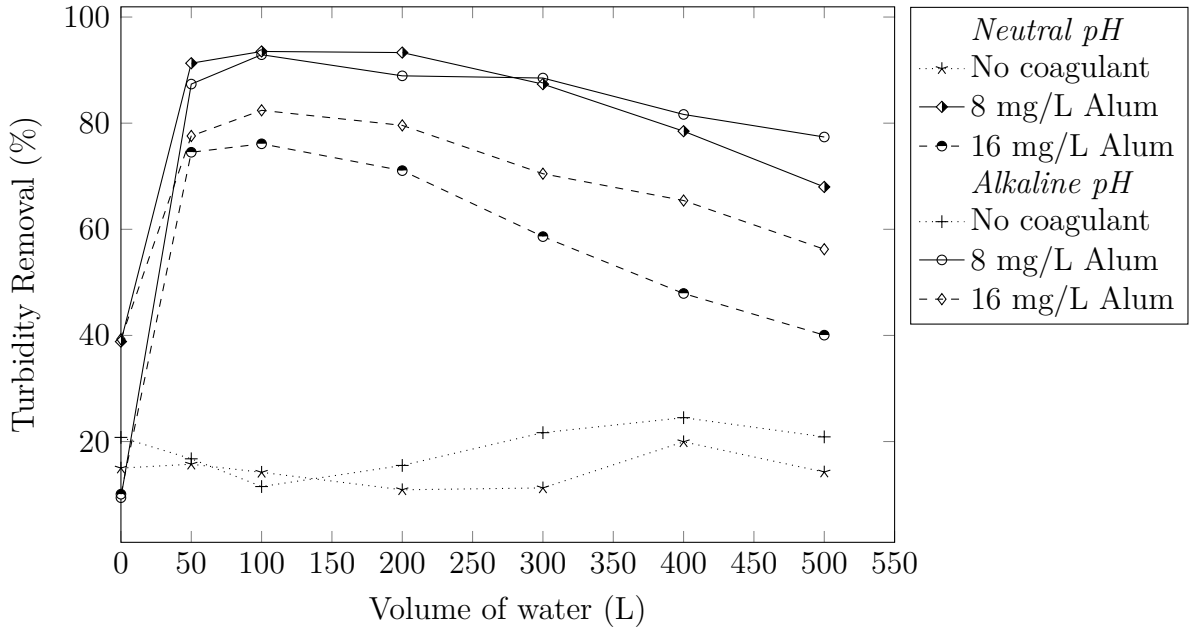

Fig. 7.13 Turbidity removal with 5 micron spun filters and various concentrations of alum in neutral and alkaline pH. (Inlet water: 15 mg/L TD, 3.75 mg/L HA, pH (neutral)= 6.9–7.4, pH (alkaline)= 7.9–8.4)

Table 7.7 Trial group iv – the average turbidity and UV_{254} removal as well as the change in zeta potential and pH measured at 50L up to 500L and pressure drop after treating 500 L. (5 micron filters, inlet water: 15 mg/L TD, 3.75 mg/L HA, pH (neutral)= 6.9–7.4, pH (alkaline)= 7.9–8.4)

Water pH	**Alum conc. (mg/L)**	**Turbidity removal (%)**	**UV_{254} removal (%)**	**$\Delta P - \Delta P_0$ (mbar)**	**Zeta potential change (%)**	**pH change (%)**
	0	14.38	6.71	-16	NA	NA
Neutral	8	78.68	72.14	140.5	41.46	-3.01
	16	61.38	53.17	102	63.63	-4.98
	0	18.47	5.50	-19.5	NA	-2.28
Alkaline	8	86.13	59.94	58	28.54	-7.71
	16	71.95	53.17	155.25	33.59	-13.03

However, UV_{254} removal (Fig. 7.14 and Table 7.7) with 8 mg/L of alum in neutral pH (72.14%) was higher in comparison to alkaline pH (59.94%) as HA removal is more sensitive to pH than turbidity removal [100], with UV_{254} removal being inversely related to pH above 6 [211]. The difference in UV_{254} removal with 16 mg/L of alum at neutral (53.17%) and alkaline (53.17%) pH ranges was smaller, due to close pH values achieved after the addition of a higher concentration of alum, causing a change of -13.03% at alkaline pH, higher than -4.98% at neutral pH.

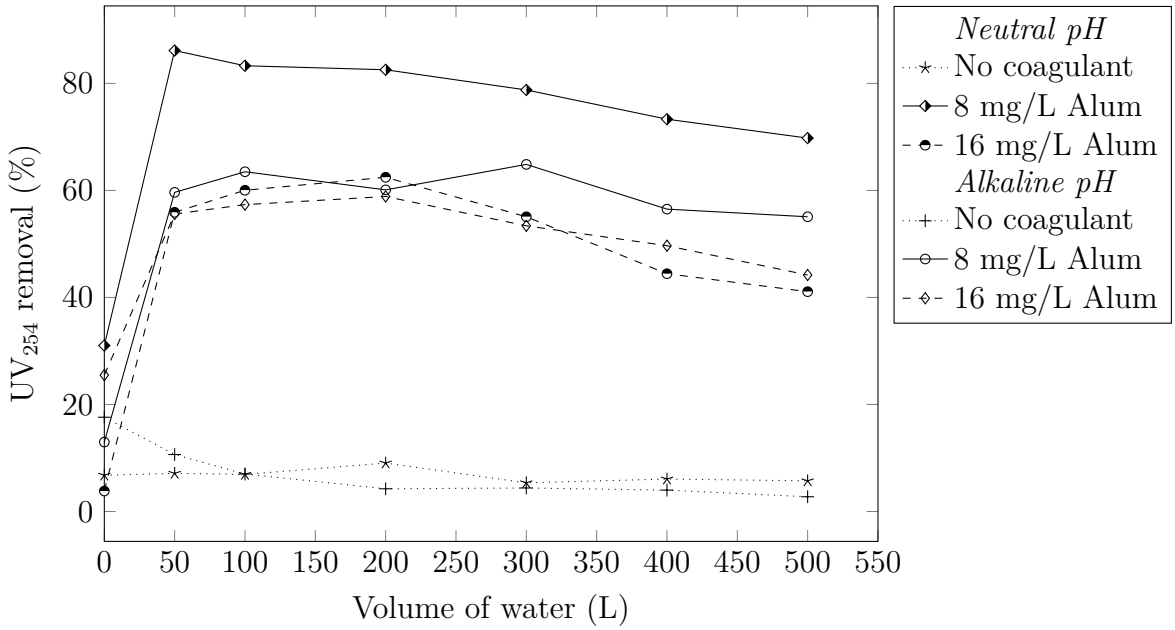

Fig. 7.14 UV_{254} removal with 5 micron spun filters and various concentrations of alum in neutral and alkaline pH. (Inlet water: 15 mg/L TD, 3.75 mg/L HA, pH (neutral)= 6.9–7.4, pH (alkaline)= 7.9–8.4)

These results confirm that in contact filtration using cartridge filters, pH adjustment is not required (in the pH range of 6.9–8.5) as the particles and organic matter are removed through direct contact with the fibres. On the contrary, Narkis and Rebhun [205] demonstrated that based on the stoichiometric relationship between humic acid and alum, at high pH values (pH=8) the dose requirement was higher and the optimal dose range wider, whereas at low pH (pH=6) the reverse was observed.

Due to the higher HA achieved with 8 mg/L of alum rather than 16 mg/L of alum in neutral pH, the ΔP increased faster (Fig. 7.15) reaching 140.5 mbar versus 102 mbar. However, in alkaline pH conditions where HA removal was similar with both 8 and 16 mg/L alum, a higher ΔP was reached with 16 mg/L (155.25 mbar) than 8 mg/L (58 mbar) due to the additional alum deposited within the filter.

In conclusion, water pH in the range of 6.9–8.4 did not affect the alum dose required and

the chosen alum dose for the baseline test water, 8 mg/L, achieved the desired turbidity and HA removal targets.

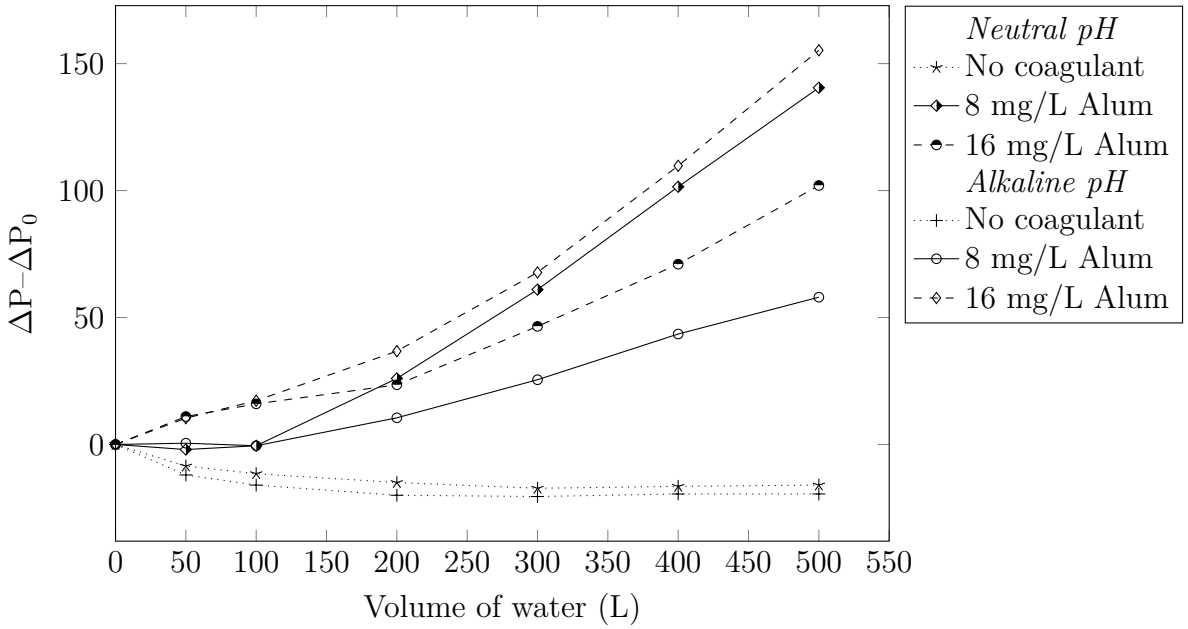

Fig. 7.15 $\Delta P–\Delta P_0$ with 5 micron spun filters and various concentrations of alum in neutral and alkaline pH. (Inlet water: 15 mg/L TD, 3.75 mg/L HA, pH (neutral)= 6.9–7.4, pH (alkaline)= 7.9–8.4)

7.4.5 Performance comparison for PDADMAC and alum

Unlike alum, PDADMAC, a soluble coagulant, does not add particle load to the stream, as such it was expected to have a smaller impact on pressure drop across the filter; however, the removal efficiency was unknown. Different doses of PDADMAC (0.225, 0.45 and 0.9 mg/L) were trialled and the filter performance was compared against trials using 8 and 16 mg/L of alum (Fig. 7.16 and Table 7.8). PDADMAC doses of 0.45 and 0.9 mg/L resulted in similar average turbidity removals than that of 8 mg/L of alum, 86.50%, 89.84% and 86.13%, respectively, surpassing the 5 NTU turbidity target level. The turbidity removal with 16 mg/L of alum showed a decline after 100 L as the pressure drop increased (Fig. 7.17). As can be observed in Fig. 7.16, alum was faster acting;

however, once PDADMAC was sufficiently loaded in the filter media, a slightly higher turbidity removal was obtained.

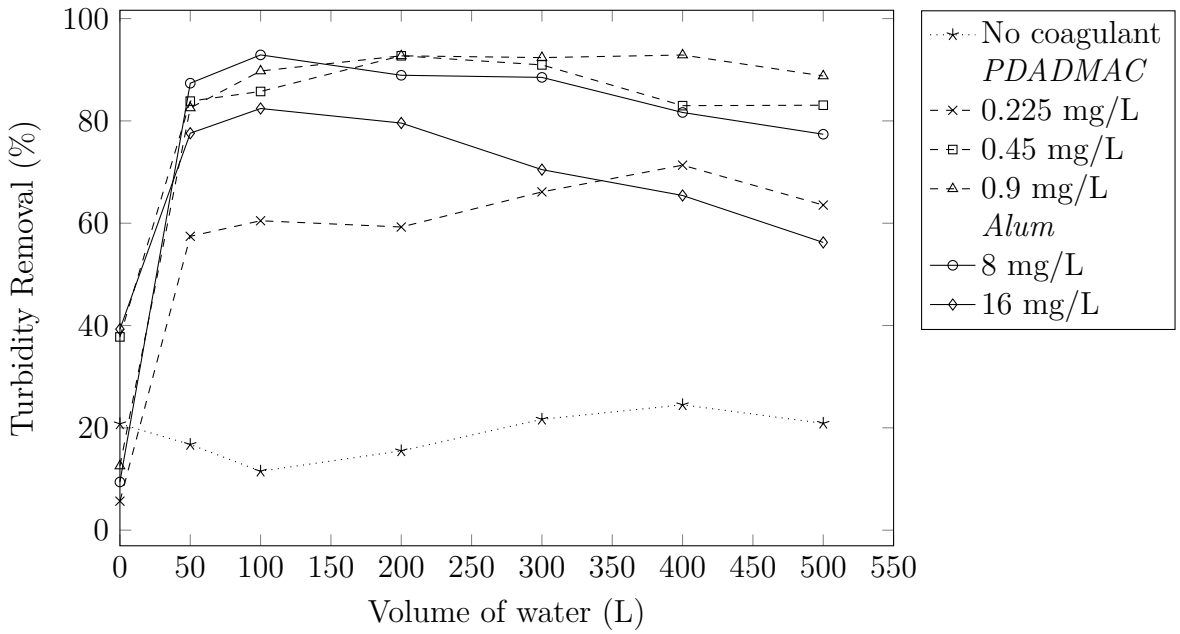

Fig. 7.16 Turbidity removal with 5 micron spun filters and various concentrations of alum or PDADMAC injected in-line. (Inlet water: 15 mg/L TD, 3.75 mg/L HA, pH=7.9–8.4)

Table 7.8 Trial group v – the average turbidity and UV_{254} removal as well as the change in zeta potential and pH measured at 50L up to 500L and pressure drop after treating 500 L. (5 micron filters, inlet water: 15 mg/L TD, 3.75 mg/L HA, pH = 7.9–8.4)

Coagulant	**Coagulant conc. (mg/L)**	**Turbidity removal (%)**	**UV_{254} removal (%)**	**$\Delta P - \Delta P_0$ (mbar)**	**Zeta potential change (%)**	**pH change (%)**
–	0	18.47	5.50	-19.5	NA	-2.28
Alum	8	86.13	59.94	58	28.54	-7.71
	16	71.95	53.17	155.25	33.59	-13.03
PDADMAC	0.225	63.03	33.16	-9	1.24	-0.23
	0.45	86.5	56.61	6	45.68	-1.22
	0.9	89.84	59.78	45.5	80.80	1.52

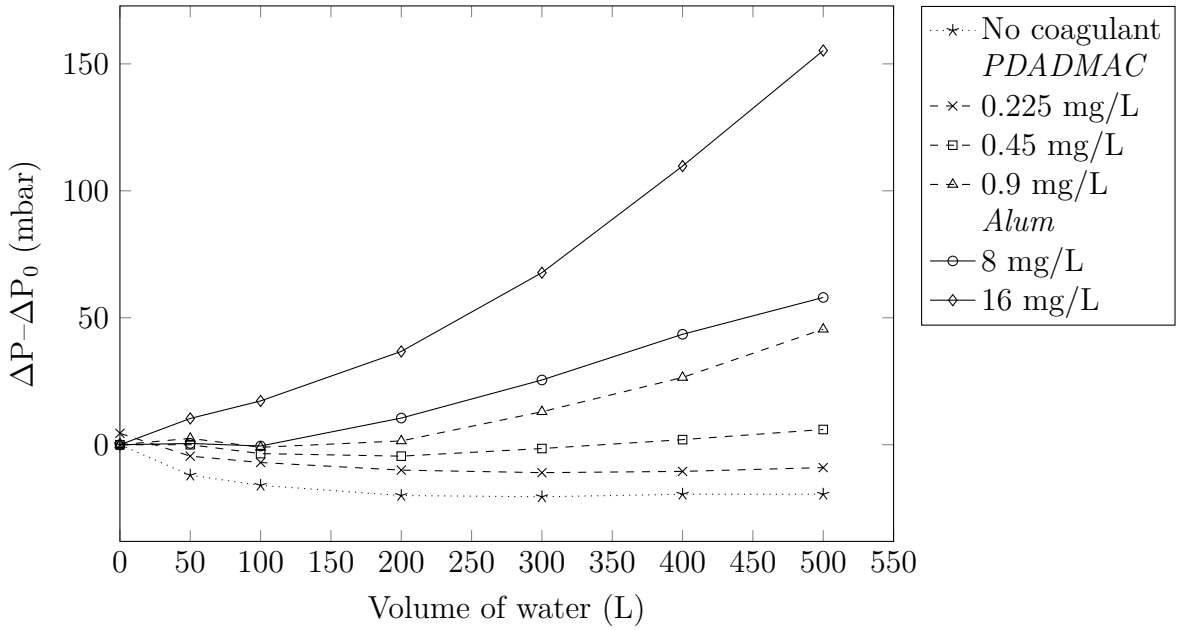

Fig. 7.17 $\Delta P–\Delta P_0$ with 5 micron spun filters and various concentrations of alum or PDADMAC injected in-line. (Inlet water: 15 mg/L TD, 3.75 mg/L HA, pH=7.9–8.4)

The average UV_{254} removal with 0.45 and 0.9 mg/L of PDADMAC and 8 mg/L of alum were all similar (Table 7.8 and Fig. 7.18), 56.61%, 59.78% and 59.94%, respectively. The increase in ΔP after 500 L was higher for 8 and 16 mg/L of alum, 58 and 155.25 mbar, than 0.45 and 0.9 mg/L PDADMAC, 6 and 45.5 mbar, respectively. Considering the high TD and HA removal and low pressure drop achieved with 0.45 mg/L of PDADMAC, it would be a better coagulant choice for contact filtration within HWT systems.

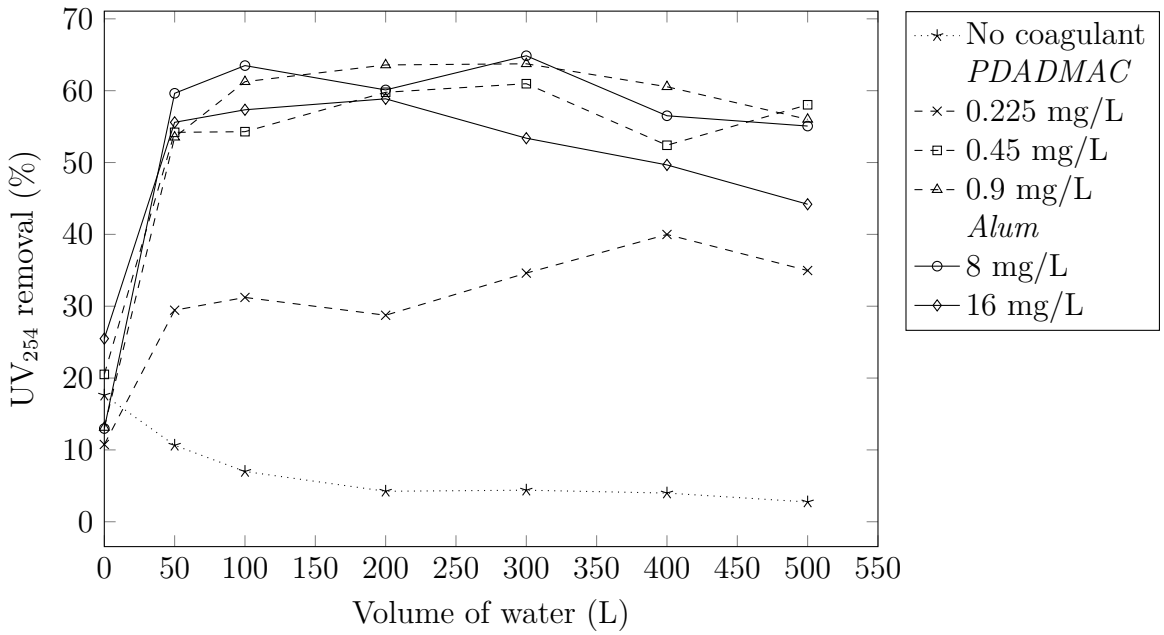

Fig. 7.18 UV_{254} removal with 5 micron spun filters and various concentrations of alum or PDADMAC injected in-line. (Inlet water: 15 mg/L TD, 3.75 mg/L HA, pH=7.9–8.4)

Table 7.8 provides the average change in zeta potential and pH for the trialled concentrations of alum and PDADMAC in an alkaline pH (7.9–8.4). PDADMAC does not cause any pH changes in theory and the reported change is negligible, while alum showed to change the pH by -7.71% and -13.03% with doses of 8 and 16 mg/L. Similarly, PDADMAC concentration of 0.45 mg/L showed a negligible change in alkalinity, +2.88%. The change in zeta potential was more pronounced with 0.45 and 0.9 mg/L of PDADMAC, causing a change of 45.68% and 80.80%, much higher than with 8 and 16 mg/L of alum, 28.54% and 33.59%, respectively, which demonstrated the different coagulation mechanisms—charge neutralization with PDADMAC and enmeshment with alum. Consequently, the lower removals of turbidity (63.03%) and UV_{254} (33.16%) with 0.225 mg/L of PDADMAC can be explained by the smaller change in the average zeta potential (1.24%).

The study by Yeh and Ghosh [104] showed that the optimum dosage for 75 mg/L of bentonite clay (turbidity of 20 NTU) determined in jar tests with polyethylenimine (Mw

40,000) had a zero electrophoretic mobility. However, in the work presented here, zeta potential values of >-10 mV were sufficient for >50% UV_{254} removal when PDADMAC was used, most likely due to the polymers being already adsorbed on the fibres of the filters.

Other researchers have provided comparisons between alum and PDADMAC for removal of either particles (turbidity) or organic matter. Adin and Rebhun [105] reported the turbidity removal for 20 mg/L of kaolinite in contact filtration using sand filters with PDADMAC or alum as the coagulant. When alum was used, the removal improved at a higher rate because of the quicker coating of the bed grains with alum; however, the volume of water that could be processed before the filter needed cleaning was smaller, demonstrating the advantage of PEs under stringent hydraulic conditions.

In a later study, Rebhun et al. [108] evaluated the removal of humic acid (10 mg/L) in contact filtration using sand filters, reporting that cationic PEs such as PDADMAC (mol. wt 5×10^4) to be ineffective for HA removal at concentrations of up to 0.12 mg/L (half of the lowest concentration used in this chapter). The jar tests showed that a dose of 25 mg/L of alum (10% solution of $Al_2(SO_4)_3 \cdot 18H_2O$) was sufficient for complete precipitation of humic acid. Although a PDADMAC concentration of above 0.12 mg/L was deemed impractical by the authors due to the cost, the volumes treated by HWT systems and the fact that cartridge filters are disposable on the contrary to sand filters, helps to justify the higher concentrations/cost of PDADMAC due to longer lifetime of the filter as it is the main component of operating cost.

Cleasby et al. [210] performed contact filtration experiments with natural waters, reporting that in the absence of algal blooms, addition of 5–10 mg/L $Al_2(SO_4)_3 \cdot 18H_2O$ or 0.09–1.49 mg/L cationic polymer was optimal to treat raw waters with average turbidities of 8 NTU and peak turbidities of 16 NTU, providing finished water with average turbidities below 1 NTU and reasonable treated volume. However, alum was less sensitive to

raw water quality as the change in water turbidity from 2 to 20 NTU did not affect the filtrate quality when filters were operated at an alum dosage of 5–10 mg/L. Furthermore, they reported that the filter performance (i.e. turbidity removal and head loss) of direct filtration was not affected by water temperature as low as 2 ℃.

7.4.6 Performance with combinations of alum and PDADMAC

It was necessary to consider cases where availability/cost of PDADMAC or low water alkalinity might be a concern and investigate the filtration performance with a combination of alum and PDADMAC. The turbidity removal with 50 micron filters and 4 mg/L of alum with or without PDADMAC at alum:PDADMAC ratios of 9 (0.45 mg/L PDADMAC) and 18 (0.225 mg/L PDADMAC) as well as results solely with 0.225 and 0.45 mg/L PDADMAC are provided in Table 7.9 and Fig. 7.19.

Whereas 4 mg/L of alum and 0.225 mg/L of PDADMAC individually achieved an average turbidity removal of 47.81% and 58.18%, respectively, a combination system performed at a higher level. A combinations of 4 mg/L alum and 0.225 mg/L PDADMAC (ratio of 18) resulted in removal of 77.26% turbidity, with the system at the lower PDADMAC concentration of 0.45 mg/L PDADMAC (ratio of 9) also attained excellent levels of removal, 73.32%. It can be concluded that the cumulative effect of both coagulants should not result in overdosing.

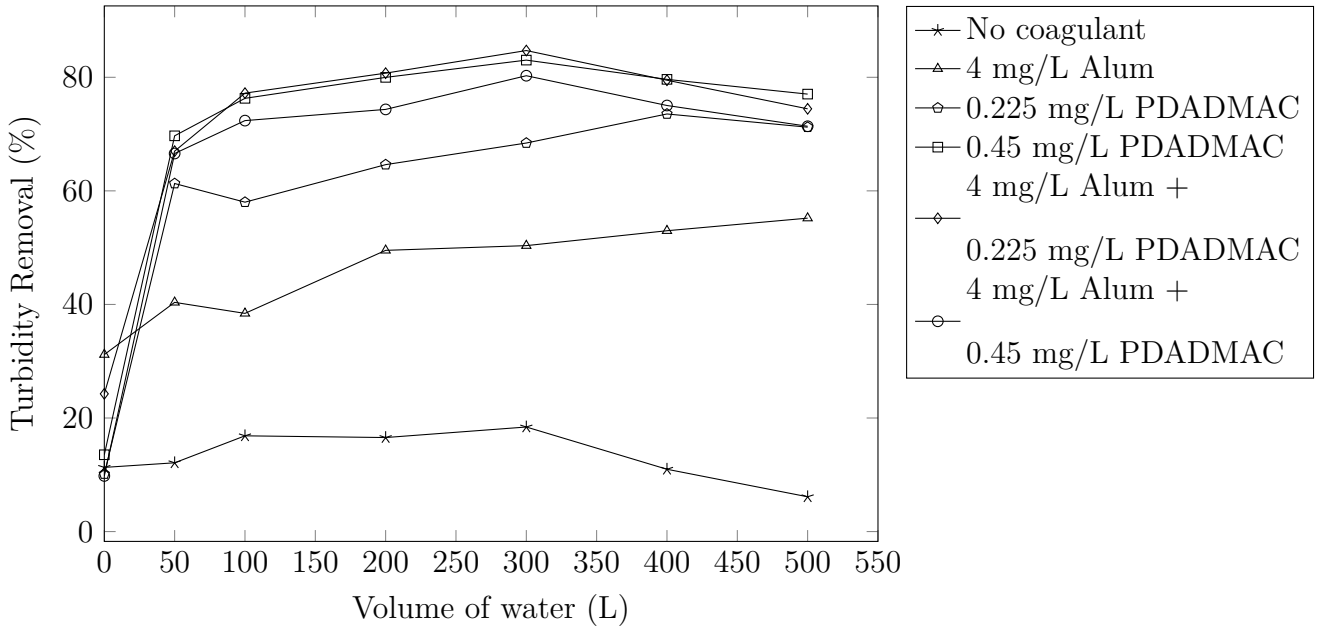

Fig. 7.19 Turbidity removal with 50 micron spun filters and 4 mg/L of alum with or without PDADMAC injected in-line. (Inlet water: 15 mg/L TD, 3.75 mg/L HA, pH=7.9–8.4)

Table 7.9 Trial group vi – the average turbidity and UV_{254} removal as well as the change in zeta potential and pH measured at 50L up to 500L and pressure drop after treating 500 L. (50 micron filters, inlet water: 15 mg/L TD, 3.75 mg/L HA, pH=6.9–7.3)

Coagulant(s)	**Coagulant conc. (mg/L)**	**Turbidity removal (%)**	**UV_{254} removal (%)**	**$\Delta P - \Delta P_0$ (mbar)**	**Zeta potential change (%)**
–	0	13.51	6.35	-8.5	NA
Alum	4	47.81	31.28	3	17.79
PDADMAC	0.225	58.18	29.59	-8	7.05
PDADMAC	0.45	77.61	40.65	8.5	21.52
Alum/PDADMAC	4/0.225	77.26	52.26	14	24.35
Alum/PDADMAC	4/0.45	73.32	41.75	47.50	34.13

A similar trend can be observed for UV_{254} removal results (Table 7.9 and Fig. 7.20); using 0.225 mg/L PDADMAC + 4 mg/L alum (ratio of 18) improved removal of HA was observed over alum or PDADMAC alone, 31.28% removal with 4 mg/L alum; 29.59% with

0.225 mg/L PDADMAC, and 52.26% removal with the tandem system. However, trials with 0.45 mg/L of PDADMAC with or without alum showed almost equal removals—41.75% with 4 mg/L alum + 0.45 mg/L PDADMAC (ratio of 9) and 40.65% with 0.45 mg/L PDADMAC. Even though 4 mg/L of alum satisfied the >25% UV_{254} removal, turbidity removal was below 62% (above 5 NTU limit), whereas addition of 0.225 mg/L PDADMAC satisfied both turbidity and UV_{254} removal limits.

The change in zeta potential (Table 7.9) with the combination of 0.225 mg/L PDADMAC + 4 mg/L alum (24.35%) was very similar to 0.45 mg/L PDADMAC (21.52%) that was already determined to be an effective dose. Therefore, the approach to minimising the cost could be choosing the PDADMAC dose that is affordable and adding alum so that the same level of zeta potential is achieved.

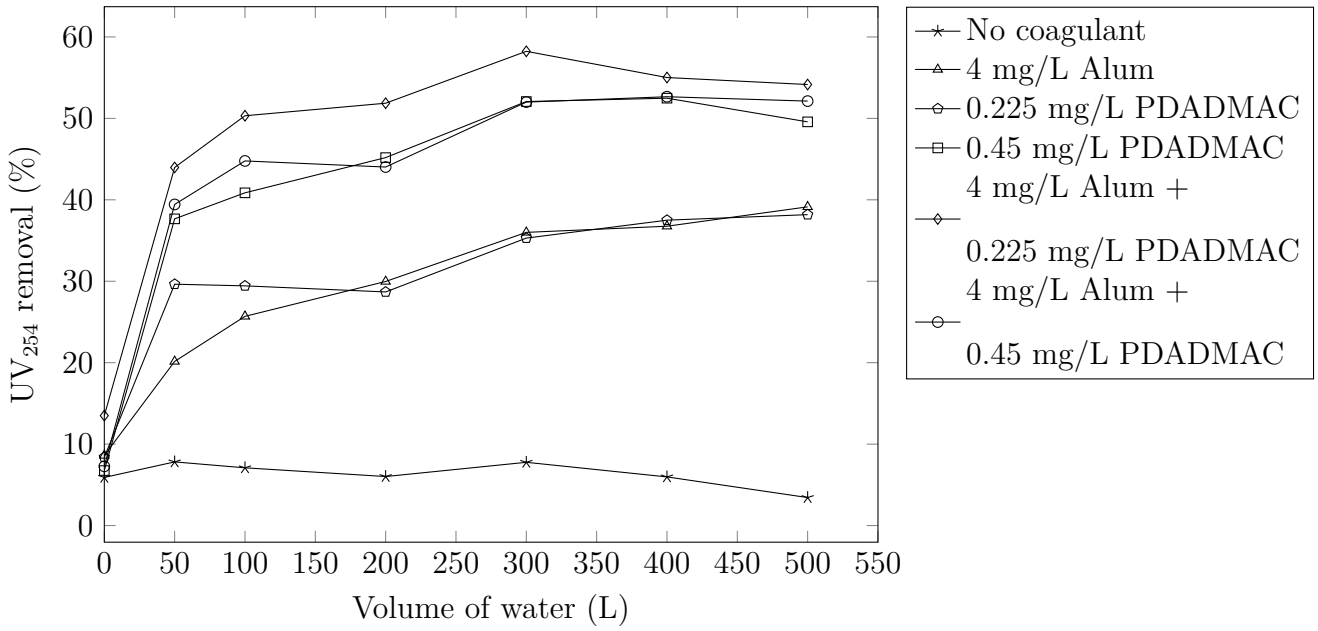

Fig. 7.20 UV_{254} removal with 50 micron spun filters and 4 mg/L of alum with or without PDADMAC injected in-line. (Inlet water: 15 mg/L TD, 3.75 mg/L HA, pH=6.9–7.3)

The pressure drop results (Table 7.9 and Fig. 7.21) show the adverse effect of overdosing as 4 mg/L alum + 0.45 mg/L PDADMAC caused a $\Delta P – \Delta P_0$ of 47.50 mbar, higher than the trials with 4 mg/L alum + 0.225 mg/L PDADMAC, 14 mbar, despite the lower

turbidity and UV_{254} removal. In comparison to 0.45 mg/L PDADMAC, the combination of a lower concentration of PDADMAC of 0.225 mg/L and 4 mg/L resulted in slight higher (14 vs 8.5 mbar) pressure drop, which was due to the higher removal of HA. Therefore, a combination of alum and PDADMAC can achieve the target removal efficiency while consuming a lower amounts of PDADMAC or alum.

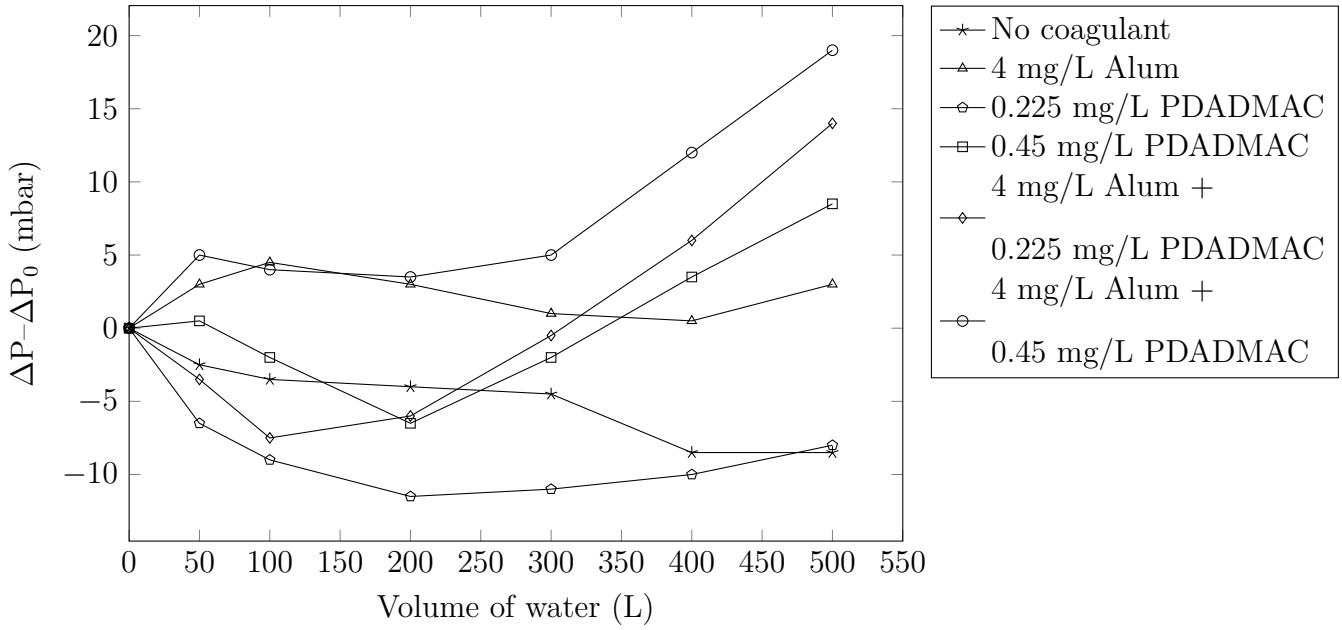

Fig. 7.21 $\Delta P–\Delta P_0$ with 50 micron spun filters and 4 mg/L of alum with or without PDADMAC injected in-line. (Inlet water: 15 mg/L TD, 3.75 mg/L HA, pH=6.9–7.3)

Edzwald and Tobiason [206] recommended a combination of alum and a cationic polymer for water with low alkalinity as pH control can be avoided while achieving higher DOC (dissolved organic carbon) removal. Even though the cationic polymers used were more expensive than alum, they found that the overall chemical cost was lower when an alum:polymer ratio of 22 was implemented.

A study by Saltnes et al. [212] followed up on this work, demonstrating use of inorganic:organic coagulant blends in a coarse sand filter bed, applying a combination of alum and polyacrylamide at a ratio of 60:1. They concluded that the combined system

can prolong the filtration runs of humic contaminated waters. Our results has showed that for very short mixing times using filters with smaller micron ratings and lower coagulant concentration would be a more effective approach as the trial with 0.5 micron filters and 4 mg/L of alum resulted in higher turbidity and UV_{254} removal and lower pressure drop than the trial with 50 micron filters and 4 mg/L alum + 0.225 mg/L PDADMAC. Therefore, in contact filtration with fibrous cartridge filters, the main benefit of combining alum and PDADMAC can be reducing the cost of PDADMAC or change in pH/alkalinity.

7.5 Conclusion

This chapter has shown that adding in-line coagulant dosing prior to cartridge filtration can enhance the removal of turbidity and organic matter at both neutral (6.9–7.4) and alkaline (7.9–8.4) pH ranges. The system is applicable for use when the raw water quality varies (greater or lower concentrations of particles and HA) without the need for dose optimisation. Additionally, it was demonstrated that simply connecting a T-valve on the suction side of the feed pump, prevents the need for an additional dosing pump thereby permitting dosing of coagulant within a HWT system.

The fibrous cartridge filters can be regarded as a more suitable choice for the contact filtration process than standard granular filters (i.e. sand or dual media filters), as the filter media is more compact, with fibres having an average diameter of 25 µm [173] much smaller than the typical sand grain sizes of 0.5–1 mm, providing a higher surface area in an equal volume, and consequently, increasing the probability of a coagulant interaction with the filtration medium.

Traditionally there is an optimum coagulant dose for specific water characteristics, with doses adjusted to the water conditions, however with the contact filtration process, a wider range of coagulant doses are adsorbed on the media therefore the process can

enhance pollutant removal without significant increase in filter pressure. This is in keeping with the constraints of the HWT system where the user will not need to adjust the dose frequently even with variations in the turbidity level or concentration of organic matter in the raw water. Moreover, it was demonstrated that an alkaline pH (up to 8.5) did not affect the performance in contact filtration, and as reported by other researchers, temperatures as low as 2 ℃ do not affect the performance [210].

However, as with all filtration processes, a higher load of contaminants will lead to shorter filter runs and the need to replace the filters. Another limitation is the applicability of the approach at low turbidity waters (<1 NTU) due to the lack of particle collisions. Therefore, if the contact filtration is to be used in HWT systems, it is only suitable process when the average turbidity of the raw water is between 1 NTU and 10 NTU.

The results showed that using PDADMAC rather than alum could achieve similar turbidity and HA removals while causing a lower pressure drop, however, the choice of coagulant in developing countries will depend on availability.

Using a combination of alum and PDADMAC might be necessary in cases where the cost of PDADMAC is a concern or water alkalinity is low and addition of alum can change the pH unacceptably. Our results showed that an alum:PDADMAC ratio of 18 improved the turbidity and UV_{254} removal in comparison to use of the individual coagulants, reducing the amount of PDADMAC needed by half without affecting the pH.

Chapter 8

Conclusions and future work

8.1 Conclusions

This PhD aimed to address the primary limitations and challenges relating to the sustainable use of cartridge filters in a household water treatment system, with outputs feeding into the SAFEWATER project in which trials of a HWT system consisting of filtration and UV disinfection are planned for communities in rural Mexico and Colombia. In Chapter 4, the lab trials demonstrated that test water produced to the standards proposed by the World Health Organisation HWT scheme, could be effectively treated, with removal of turbidity routinely achieving the <5 NTU threshold. Turbidity removal and pressure drop (ΔP) trends of a range of commercial filters were assessed in a study designed to simulate long term performance of a HWT system (>1000 L). When A2 test dust was used as the turbidity agent, a cake layer of dust particles built up on the outer surface of the pleated filters, improving the turbidity removal, whereas the efficiency of turbidity removal with spun and wound filters did not improve over time as accumulation of particles within the filters caused a higher pressure drop, and consequently particle detachment and poor effluent quality. With a test water containing an initial turbidity of 40$\pm$10 NTU, high quality filtrate could be quickly produced with two pleated filter

elements of 5 and 1 micron, were used in series. The <5 NTU turbidity target was reached after processing 0.35 m^3 of water, and the high rate of turbidity removal maintained without significant pressure during processing of 1000 L of test water. In addition, a straightforward method was developed enabling pleated filters to be cleaned manually and be reused for at least three cycles, whereas the spun and wound filters had to be discarded after single use.

To address the short lag time in provision of low turbidity water at the start of a new/washed pleated filter, precoating the pleated filters with an inert filter aid (diatomaceous earth) was investigated in Chapter 5. Due to the intermittent nature of HWT systems, the industrial guidelines for precoating were not applicable, but this work presented a precoating procedure and material specification suitable for this purpose. The procedure and the process flow diagram proposed demonstrated the relative ease and practicality of this approach for HWT systems, without the need for a run-in time to prepare the filter surface. The upgraded system can now run with a single filter, significantly reducing both capital and running costs for the HWT system.

In the absence of organic matter (i.e. humic acid), a single pleated filter precoated with natural DE removed >95% of the influent turbidity (40±10 NTU) during the whole duration of the trial (>1000 L). A fundamental study of the inherent materials properties of the DE permitting understanding of the relevant physical and chemical properties enabling custom precoats to be designed and trialed. The permeability of DE could be improved by calcining and its surface charge modified by inclusion of an electropositive coating (PDADMAC) to remove organic matter, or DE may be coated with iron oxide for additional adsorptive capacity. Moreover, the PDADMAC coating increased the stability of the precoat, preventing the precoat fracturing and mechanically deforming due to impact. When the test water had a medium to low turbidity (10±3 NTU) as recommended for the precoat filtration process [94], the <5 NTU filtrate quality target

was achieved in the presence of organic matter (3.75 mg/L of humic acid). Moreover, filter cleaning was improved due to the inclusion of precoating, demonstrated by SEM imaging, and safe reuse of filters could be achieved by a simple disinfection procedure that inactivated *E. coli* without damaging the fibres of the filters.

In Chapter 6, the contact filtration process was investigated with respect to implementation in HWT systems. Incorporating in-line coagulation in cartridge filtration was achieved simply adding a T-valve on the suction side of the existing water feed pump (no addition pump or control system was required). Although there is an optimum coagulant dose to aid with treatment of specific water characteristics (particulate and organic content), the contact filtration process offers potential to treat a wider range of influent water conditions (a broader range of particle and organic pollution) as coagulants are adsorbed on the filter media and not solely reliant on batch processing. Therefore, with the new method/materials proposed, the user will not need to adjust the coagulant dose frequently even if there is variations in the turbidity level or concentration of organic matter in the influent—-and they can be assured that treated water remain within the associated water quality guidelines (particles, organic matter and pH). Based on this research and literature, contact filtration was found to be a suitable process when the average turbidity of the raw water is between 1 and 10 NTU—a higher turbidity will lead to a shorter filter run and a lower turbidity in unsatisfactory removal due to the lack of particle collisions. Moreover, it was demonstrated that an alkaline pH (up to 8.5) did not affect the performance in contact filtration, and as reported by others temperatures as low as 2 ℃ does not affect the system performance [210].

The choice of coagulant in developing countries will depend on availability, with alum being widely used worldwide. However, the results in this work showed that using PDADMAC could achieve the same turbidity and UV_{254} while causing a lower pressure drop across the system. Combining alum and PDADMAC at half of their effective

concentrations with an alum:PDADMAC ratio of 18 showed a synergic effect, providing an enhanced performance. Combining alum and PDADMAC may be necessary in cases where the cost of PDADMAC is prohibitive or water alkalinity is very low and the addition of alum can change the pH significantly.

In Chapter 7, the cartridge filtration process was simulated by considering the fluid dynamics and particle motion equations as well as models for particle deposition, detachment and rebound, providing the first modelling methodology for cartridge filtration units. The simulation and experimental validation results for particle deposition on the filter media were shown to be in high agreement. This work explored the process both at micro- and macro-level to provide a greater understanding of the process of particle removal. The CFD study showed that the larger particles were entrapped at the outer part of the filter, significantly reducing permeability. Hence, manufacturing multilayer filters with declining porosity from the outer to inner part can result in improved filter runs. Moreover, novel housing designs which promote particle settlement, e.g. a hydrocyclone, can remove large particles responsible for the loss in permeability at the outer surface. Lastly, based on the PSD of particles in a specific water, customized filters can be designed by performing a CFD simulation and adjusting the filter thickness and porosity.

8.2 Future work

As reported in Chapter 4, the common micron ratings of the cartridge filters on the market cannot effectively remove fine particles, and as such under certain circumstances achieving the <5 NTU effluent target can be challenging. Development of reusable cartridge micro- or ultra-filtration membranes, with pore sizes below 0.1 µm, would ensure removal of very fine particles and could play an important role in additional removal of bacteria. However, the membranes should be designed to ensure there is

not a high pressure drop and they must be suitable for use with the widely available pumps currently employed in HWT systems. Moreover, manual cleaning as opposed to automatic backwash should be possible as the latter will make the system too complicated for deployment in the field.

In Chapter 5, precoat filtration using cartridge pleated filters was presented as a solution ensuring production of turbidity-free filtrate without the need for filter conditioning—low turbidity water from the start of the treatment to the end. The precoating procedure could be further simplified by designing a novel filter housing with an additional storage compartment for the filter aids at the bottom where the water inlet could be. This configuration would result in precoating of the filter as feed water enters from the bottom, thereby preventing the need for manual introduction of the precoat, and saving the end user time and effort.

Within the experimental set-up in Chapter 6, the coagulants had a very short mixing time of few seconds, and therefore, floc growth could not be achieved. An additional mixing unit could be designed based on an investigation on the mixing duration needed for the optimal filtration performance. The mixing unit can either be as simple as a small container/a pipe extension or based on CFD studies a complex system could be developed to maximise particle collisions and ensure high levels of removal of both organic material and particles across an even wider range of challenge waters.

The CFD modelling provided in Chapter 7 was the first attempt at considering the different physics involved in cartridge filtration, with the underpinning phenomena addressed at macro-scale level while fundamental models were incorporated for particle removal; however, these models had several empirical variables which were based on the filters that were different structurally. A better method would be linking micro-scale simulations by taking 3D images of a small slice of the filter via X-ray imaging and

determining the removal efficiency of each fibre versus particle size. Whilst complex, this would aid in tailored models and could advance filter structure design.

References

[1] WHO. Safely managed drinking water, 2017.

[2] UNICEF/WHO. Progress on household drinking water, sanitation and hygiene 2000–2020: Five years into the SDGs, 2021.

[3] WHO. Results of round I of the WHO international scheme to evaluate household water treatment technologies, 2016.

[4] WHO. Preventing diarrhoea through better water, sanitation and hygiene: exposures and impacts in low- and middle-income countries, 2014.

[5] February 21) Turbidity (2022. Retrieved from https://waterontheweb.org/under/waterquality/turbidity.html.

[6] John C. Crittenden, R. Rhodes Trussell, David W. Hand, Kerry J. Howe, and George Tchobanoglous. *MWH's Water Treatment*. 2012. doi: 10.1002/9781118131473.

[7] WHO. Results of round II of the WHO international scheme to evaluate household water treatment technologies, 2019.

[8] Daniele Lantagne, Robert Quick, and Eric D. Mintz. Household Water Treatment and Safe Storage Options in Developing Countries: A Review of Current Implementation Practices, 2011.

[9] Mark D. Sobsey, Christine E. Stauber, Lisa M. Casanova, Joseph M. Brown, and Mark A. Elliott. Point of use household drinking water filtration: A practical, effective solution for providing sustained access to safe drinking water in the developing world. *Environ. Sci. Technol.*, 42(12):4261–4267, 2008. doi: 10.1021/es702746n.

[10] Stefanie M. L. Stubbé, Alida Pelgrim-Adams, Gabor L. Szántó, and Doris van Halem. Household water treatment and safe storage – effectiveness and economics. *Drink. Water Eng. Sci.*, 9(1):9–18, apr 2016. doi: 10.5194/dwes-9-9-2016.

[11] J. K. Mwabi, F. E. Adeyemo, T. O. Mahlangu, B. B. Mamba, B. M. Brouckaert, C. D. Swartz, G. Offringa, L. Mpenyana-Monyatsi, and M. N.B. Momba. Household water treatment systems: A solution to the production of safe drinking water by the low-income communities of Southern Africa. *Phys. Chem. Earth*, 36(14-15): 1120–1128, 2011. doi: 10.1016/j.pce.2011.07.078.

[12] Tommy K.K. Ngai, Roshan R. Shrestha, Bipin Dangol, Makhan Maharjan, and Susan E. Murcott. Design for sustainable development - Household drinking water filter for arsenic and pathogen treatment in Nepal. *J. Environ. Sci. Heal. - Part A Toxic/Hazardous Subst. Environ. Eng.*, 42(12):1879–1888, 2007. doi: 10.1080/10934520701567148.

[13] Andrea Pérez-Vidal, Jaime Diaz-Gómez, Jose Castellanos-Rozo, and Olga Lucía Usaquen-Perilla. Long-term evaluation of the performance of four point-of-use water filters. *Water Res.*, 98:176–182, 2016. doi: 10.1016/j.watres.2016.04.016.

[14] WHO. WHO International Scheme to Evaluate Household Water Treatment Technologies Harmonized Testing Protocol: Technology Non-Specific, 2018.

[15] US EPA. Enhanced Coagulation and Enhanced Precipitate Softening Guidance Manual, 1999.

[16] UN General Assembly. Transforming our World: the 2030 Agenda for Sustainable Development, 2015.

[17] GBD 2015 SDG Collaborators. Measuring the health-related Sustainable Development Goals in 188 countries: a baseline analysis from the Global Burden of Disease Study 2015. *Lancet*, 388(10053):1813–1850, oct 2016. doi: 10.1016/S0140-6736(16)31467-2.

[18] Guy Alaerts. Financing for Water—Water for Financing: A Global Review of Policy and Practice. *Sustainability*, 11(3):821, feb 2019. doi: 10.3390/su11030821.

[19] Tomáš Hák, Svatava Janoušková, and Bedřich Moldan. Sustainable Development Goals: A need for relevant indicators. *Ecol. Indic.*, 60:565–573, jan 2016. doi: 10.1016/j.ecolind.2015.08.003.

[20] Joseph Alcamo. Water quality and its interlinkages with the Sustainable Development Goals. *Curr. Opin. Environ. Sustain.*, 36:126–140, feb 2019. doi: 10.1016/j.cosust.2018.11.005.

[21] Mohamed Ait-Kadi. Water for Development and Development for Water: Realizing the Sustainable Development Goals (SDGs) Vision. *Aquat. Procedia*, 6:106–110, aug 2016. doi: 10.1016/j.aqpro.2016.06.013.

[22] Jeffrey D. Sachs. From millennium development goals to sustainable development goals. *Lancet*, 379(9832):2206–2211, 2012. doi: 10.1016/S0140-6736(12)60685-0.

[23] Johanna Weststrate, Geske Dijkstra, Jasper Eshuis, Alberto Gianoli, and Maria Rusca. The Sustainable Development Goal on Water and Sanitation: Learning from the Millennium Development Goals. *Soc. Indic. Res.*, 143(2):795–810, 2019. doi: 10.1007/s11205-018-1965-5.

[24] WHO/UNICEF. Progress on drinking water, sanitation and hygiene: 2017 update and SDG baselines, 2017.

[25] UN-Water. Summary Progress Update 2021 : SDG 6 — water and sanitation for all, 2021.

[26] Anik Bhaduri, Janos Bogardi, Afreen Siddiqi, Holm Voigt, Charles Vörösmarty, Claudia Pahl-Wostl, Stuart E. Bunn, Paul Shrivastava, Richard Lawford, Stephen Foster, Hartwig Kremer, Fabrice G. Renaud, Antje Bruns, and Vanesa R. Osuna. Achieving Sustainable Development Goals from a Water Perspective. *Front. Environ. Sci.*, 4(OCT), oct 2016. doi: 10.3389/fenvs.2016.00064.

[27] WHO. WHO water, sanitation and hygiene strategy 2018-2025, 2018.

[28] WHO. Quantitative Microbial Risk Assessment: Application for Water Safety Management. *WHO Press*, page 187, 2016.

[29] WHO/UNICEF. Drinking Water, Sanitation and Hygiene in Schools: Global baseline report, 2018.

[30] WHO/UNICEF. WASH in health care facilities: Global Baseline Report 2019, 2019.

[31] Amrita Ahuja, Michael Kremer, and Alix Peterson Zwane. Providing safe water: Evidence from randomized evaluations. *Annu. Rev. Resour. Econ.*, 2:237–256, 2010. doi: 10.1146/annurev.resource.012809.103919.

[32] WHO/UNICEF. Drinking Water, Sanitation and Hygiene in Schools - Global baseline report 2018, 2018.

[33] WHO. WHO International Scheme to Evaluate Household Water Treatment Technologies - Harmonized Testing Protocol: Technology Non-Specific, 2014.

[34] John Briscoe. The Changing Face of Water Infrastructure Financing in Developing Countries. *Int. J. Water Resour. Dev.*, 15(3):301–308, sep 1999. doi: 10.1080/07900629948826.

[35] Guy Hutton, Laurence Haller, and Jamie Bartram. Global cost-benefit analysis of water supply and sanitation interventions. *J. Water Health*, 5(4):481–501, 2007. doi: 10.2166/wh.2007.009.

[36] Thomas Clasen. Household Water Treatment and Safe Storage to Prevent Diarrheal Disease in Developing Countries. *Curr. Environ. Heal. Reports*, 2(1):69–74, mar 2015. doi: 10.1007/s40572-014-0033-9.

[37] Paul A. Berg. The World's Need for Household Water Treatment. *Am. Water Work. Assoc.*, 107(10):36–44, oct 2015. doi: 10.5942/jawwa.2015.107.0144.

[38] Wolf-Peter Schmidt and Sandy Cairncross. Household Water Treatment in Poor Populations: Is There Enough Evidence for Scaling up Now? *Environ. Sci. Technol.*, 43(4):986–992, feb 2009. doi: 10.1021/es802232w.

[39] Aaron Bivins, Nikki Beetsch, Batsirai Majuru, Maggie Montgomery, Trent Sumner, and Joe Brown. Selecting Household Water Treatment Options on the Basis of World Health Organization Performance Testing Protocols. *Environ. Sci. Technol.*, 53(9):5043–5051, may 2019. doi: 10.1021/acs.est.8b05682.

[40] Guy Howard and Jamie Bartram. Domestic Water Quantity , Service Level and Health, 2003.

[41] Paul R. Hunter. Household water treatment in developing countries: Comparing different intervention types using meta-regression. *Environ. Sci. Technol.*, 43(23): 8991–8997, 2009. doi: 10.1021/es9028217.

[42] Adie D B Igboro and S B Daouda. Determination of the Filter Potential of Luffa Sponge (luffa aegyptiaca) in Water Quality Analysis. *Am. Int. J. Contemp. Res.*, 3 (3):117–123, 2013.

[43] Jianhu Shen, Yi Min Xie, Xiaodong Huang, Shiwei Zhou, and Dong Ruan. Mechanical properties of luffa sponge. *J. Mech. Behav. Biomed. Mater.*, 15:141–152, 2012. doi: 10.1016/j.jmbbm.2012.07.004.

[44] Ching Kwek Pooi and How Yong Ng. Review of low-cost point-of-use water treatment systems for developing communities. *npj Clean Water*, 1(1), 2018. doi: 10.1038/s41545-018-0011-0.

[45] Larry Forney. Advances in disinfection techniques for water reuse. In *Handb. Water Energy Manag. Food Process.*, pages 700–719. Elsevier, 2008. doi: 10.1533/9781845694678.5.700.

[46] WHO. Water quality and health - review of turbidity: information for regulators and water suppliers, 2017.

[47] R. B. Grayson, B. L. Finlayson, C. J. Gippel, and B. T. Hart. The potential of field turbidity measurements for the computation of total phosphorus and suspended solids loads. *J. Environ. Manage.*, 47(3):257–267, 1996. doi: 10.1006/jema.1996.0051.

[48] WHO. *Guidelines for Drinking-water Quality*. World Health Organization, 2017.

[49] Hadas Mamane, Joel J. Ducoste, and Karl G. Linden. Effect of particles on ultraviolet light penetration in natural and engineered systems. *Appl. Opt.*, 45(8): 1844–1856, 2006. doi: 10.1364/ao.45.001844.

[50] Hussein Mohamed, Joe Brown, Robert M. Njee, Thomas Clasen, Hamisi M. Malebo, and Steven Mbuligwe. Point-of-use chlorination of turbid water: results from a field study in Tanzania. *J. Water Health*, 13(2):544–552, 2015. doi: 10.2166/wh.2014.001.

[51] Michael R. Templeton, Robert C. Andrews, and Ron Hofmann. Removal of particle-associated bacteriophages by dual-media filtration at different filter cycle stages and impacts on subsequent UV disinfection. *Water Res.*, 41(11):2393–2406, 2007. doi: 10.1016/j.watres.2007.02.047.

[52] Jason Christensen and Karl G Linden. How particles affect UV light in the UV disinfection of unfiltered drinking water. *Am. Water Work. Assoc.*, 95(4):179–189, 2003.

[53] US EPA. Guidance Manual for Compliance with the Surface Water Treatment Rules: Turbidity Provisions, 2020.

[54] B S Iso. Road vehicles — Test dust for filter evaluation — Part 2 : Aluminium oxide test dust. 1997.

[55] LeChevallier Mark W. and Au Kwok-Keung. *Water Treatment and Pathogen Control*. 2004.

[56] US EPA. Small Drinking Water Systems Handbook. A Guide to " Packaged " Filtration and Disinfection Technologies with Remote Monitoring and Control Tools. Technical report, EPA, 2003.

[57] Chi Tien. *Principles of Filtration*. Elsevier B.V., 2012.

[58] Jerry E. Ongerth and Primrose E. Hutton. Testing of Diatomaceous Earth Filtration for Removal of Cryptosporidium Oocysts. *J. Am. Water Works Assoc.*, 93(12): 54–63, dec 2001. doi: 10.1002/j.1551-8833.2001.tb09355.x.

[59] Satinderpal Kaur, Renuga Gopal, Wun Jern Ng, Seeram Ramakrishna, and Takeshi Matsuura. Next-Generation Fibrous Media for Water Treatment. *MRS Bull.*, 33 (January):21–26, 2008.

[60] Health Canada. Guidelines for Canadian Drinking Water Quality: Guideline Technical Document – Turbidity. Technical report, 2012.

[61] Trevor Sparks and George Chase. *Filters and Filtration Handbook*. Elsevier Ltd., 2016.

[62] George Skouteris, Devendra Saroj, Paraschos Melidis, Faisal I. Hai, and Sabèha Ouki. The effect of activated carbon addition on membrane bioreactor processes for wastewater treatment and reclamation - A critical review. *Bioresour. Technol.*, 185:399–410, 2015. doi: 10.1016/j.biortech.2015.03.010.

[63] Ewa Sikorska, Jakub M. Gac, and Leon Gradoń. Performance of a depth fibrous filter at particulate loading conditions. Description of temporary and local phenomena with structure development. *Chem. Eng. Res. Des.*, 132:743–750, 2018. doi: 10.1016/j.cherd.2018.02.020.

[64] Kazuho Nakamura, Jiro Nakamura, and Kanji Matsumoto. Filtration and backwashing behaviors of the deep bed filtration using long length poly-propylene fiber filter media. *J. Taiwan Inst. Chem. Eng.*, 94:31–36, 2019. doi: 10.1016/j.jtice.2018.01.011.

[65] Irwin M. Hutten. *Handbook of Nonwoven Filter Media*. Elsevier Ltd., 2016. doi: 10.1016/B978-185617441-1/50027-5.

[66] Marek B. Pawlowicz, James E. Evans, David R. Johnson, and Robert G. Brooks. A study of the efficacy of various home filtration substrates in the removal of microcystin-LR from drinking water. *J. Water Health*, 4(1):99–107, 2006.

[67] Giacomo Viccione, Stefania Evangelista, and Giovanni de Marinis. Experimental analysis of the hydraulic performance of wire-wound filter cartridges in domestic plants. *Water*, 10(3):1–15, 2018. doi: 10.3390/w10030309.

[68] Stefania Evangelista, Giacomo Viccione, and Orlando Siani. A new cost effective, long life and low resistance filter cartridge for water treatment. *J. Water Process Eng.*, 27(November 2018):1–14, 2019. doi: 10.1016/j.jwpe.2018.11.004.

[69] David W. Hendricks. *Fundamentals of Water Treatment Unit Processes: Physical, Chemical, and Biological*. 2011. doi: 10.1142/p063.

[70] Philip Brown and Christopher L Cox. *Fibrous filter media*. 2017.

[71] Charles R. O'Melia and Werner Stumm. Theory of Water Filtration. *Am. Water Work. Assoc.*, 59(11):1393–1412, 1967. doi: 10.1002/j.1551-8833.1967.tb03469.x.

[72] J. H. Raistrick. Fibrous materials for the filtration of liquids. *Composites*, 10(4): 206–208, 1979.

[73] Kuan Mu Yao, Mohammad T. Habibian, and Charles R. O'Melia. Water and Waste Water Filtration: Concepts and Applications. *Environ. Sci. Technol.*, 5(11): 1105–1112, 1971. doi: 10.1021/es60058a005.

[74] Iris Kaminski, Nicolae Vescan, and Avner Adin. Particle size distribution and wastewater filter performance. *Water Sci. Technol.*, 36(4):217–224, 1997. doi: 10.1016/S0273-1223(97)00428-9.

[75] Chi Tien and B. V. Ramarao. *Granular Filtration of Aerosols and Hydrosols*. Number July. 2007. doi: 10.1016/B978-1-85617-458-9.X5000-3.

[76] Chi Tien. *Introduction to Cake Filtration: Analyses, Experiments and Applications*. Elsevier Science, 2006. doi: 10.1017/CBO9781107415324.004.

[77] S Osterroth. *Mathematical models for the simulation of combined depth and cake filtration processes*. PhD thesis, University of Kaiserslautern, 2018.

[78] Toni Kuisma. *Development of a Filter Aid Proportioning, Mixing, and Feeding*. Master's thesis, Lappeenranta University of Technology, 2009.

[79] Morten Lykkegaard Christensen, Morten Møller Klausen, and Peter Vittrup Christensen. Test of precoat filtration technology for treatment of swimming pool water. *Water Sci. Technol.*, 77(3):748–758, 2018. doi: 10.2166/wst.2017.593.

[80] Caroline Boittelle, Christian Poupot, Vladan Milisic, and Martine Mietton-Peuchot. Advances in the Precoat Filtration Process. *Sep. Sci. Technol.*, 43:1701–1712, 2008. doi: 10.1080/01496390801974563.

[81] J. Zacharias, R. Schneid, and R. Scholz. Precoating filtration with compressible filtering aids featuring viscose fibres. *BrewingScience*, 70(7-8):110–117, 2017. doi: 10.23763/BrSc17-11Zacharias.

[82] Richard G. Holdich. *Fundamentals of Particle Technology*. 2002.

[83] Malvern Instruments Ltd. Zetasizer Nano Series User Manual, 2004.

[84] Malvern Instruments. What Is the Z Average?, 2021.

[85] Kanika Saxena, Urmila Brighu, and Aditya Choudhary. Parameters affecting enhanced coagulation: a review. *Environ. Technol. Rev.*, 7(1):156–176, jan 2018. doi: 10.1080/21622515.2018.1478456.

[86] A S. Elsenbast and D. C. Morris. Diatomaceous Silica Filter-Aid Clarification. *Ind. Eng. Chem.*, 34(4):412–418, 1942. doi: 10.1021/ie50388a006.

[87] Sascha Schiller and Hans-Joachim Schmid. Ultrafine Dust Filtration Using Precoat Materials Considering the Influence of Filter Media. *Chem. Eng. Technol.*, 37(6): 1009–1020, jun 2014. doi: 10.1002/ceat.201300856.

[88] A. B. Cummins. Clarifying Efficiency of Diatomaceous Filter Aids. *Ind. Eng. Chem.*, 34(4):403–411, 1942. doi: 10.1021/ie50388a005.

[89] Vipin Bhardwaj and Mel J. Mirliss. Diatomaceous Earth Filtration for Drinking Water. In *Water Encycl.* John Wiley & Sons, Inc., Hoboken, NJ, USA, jul 2005. doi: 10.1002/047147844X.mw1818.

[90] Yung-Tse Hung, Howard H. Lo, Lawrence K. Wang, Jerry R. Taricska, and Kathleen Hung Li. *Advanced Physicochemical Treatment Processes.* Humana Press, Totowa, NJ, 2006. doi: 10.1007/978-1-59745-029-4.

[91] Dan Guo, Hualin Wang, Pengbo Fu, Yuan Huang, Yi Liu, Wenjie Lv, and Fei Wang. Diatomite precoat filtration for wastewater treatment: Filtration performance and pollution mechanisms. *Chem. Eng. Res. Des.*, 137:403–411, sep 2018. doi: 10.1016/j.cherd.2018.06.036.

[92] Daniel J. Conley, Susan S. Kilham, and Edward Theriot. Differences in silica content between marine and freshwater diatoms. *Limnol. Oceanogr.*, 34(1):205–212, jan 1989. doi: 10.4319/lo.1989.34.1.0205.

[93] Nezahat Ediz, Ismail Bentli, and Ilknur Tatar. Improvement in filtration characteristics of diatomite by calcination. *Int. J. Miner. Process.*, 94:129–134, 2010. doi: 10.1016/j.minpro.2010.02.004.

[94] American Water Works Association. *M30 Precoat Filtration, Second Edition (Manual of Water Supply Practices).* 1995.

[95] Garrett Bergquist. Relationship, Selection, and Optimization of Filter Aid, Filter Media and Clarification Technologies for Contaminant Fines Removal from Process Slurries and Liquids. Technical report, BHS-Sonthofen Inc., 2018.

[96] Lihong DU, Xu CHEN, Wenping LI, and Qixin ZHU. A Study on Enhancement of Filtration Process with Filter Aids Diatomaceous Earth and Wood Pulp Cellulose. *Chinese J. Chem. Eng.*, 19(5):792–798, oct 2011. doi: 10.1016/S1004-9541(11)60058-X.

[97] Kelly P. Langé, William D. Bellamy, David W. Hendricks, and Gary S. Logsdon. Diatomaceous Earth Filtration of Giardia Cysts and Other Substances. *J. Am. Water Works Assoc.*, 78(1):76–84, jan 1986. doi: 10.1002/j.1551-8833.1986.tb05682.x.

[98] Thomas S. Brown, Joseph F. Malina Jr., and Barbara D. Moore. Virus Removal by Diatomaceous-Earth Filtration—Part 1. *Am. Water Work. Assoc.*, 66(2):98–102, 1974. doi: 10.1007/978-1-4614-8109-6_10.

[99] William H. Beauman, P. Regunathan, and Dennis I. Prepejchal. Bacteriostatic filter media, 1983.

[100] Kanika Saxena, Urmila Brighu, and Aditya Choudhary. Coagulation of humic acid and kaolin at alkaline pH: Complex mechanisms and effect of fluctuating organics and turbidity. *J. Water Process Eng.*, 31:100875, oct 2019. doi: 10.1016/j.jwpe.2019.100875.

[101] E.L. Sharp, P. Jarvis, S.A. Parsons, and B. Jefferson. Impact of fractional character on the coagulation of NOM. *Colloids Surfaces A Physicochem. Eng. Asp.*, 286(1-3): 104–111, sep 2006. doi: 10.1016/j.colsurfa.2006.03.009.

[102] Peter Gebbie. An Operator's Guide to Water Treatment Coagulants. In *31st Annu. Qld Water Ind. Work. Oper. Ski.*, 2006.

[103] Brian Bolto and John Gregory. Organic polyelectrolytes in water treatment. *Water Res.*, 41:2301–2324, 2007. doi: 10.1016/j.watres.2007.03.012.

[104] H. H. Yeh and M. M. Ghosh. Selecting polymers for direct filtration. *Am. Water Work. Assoc.*, 73(4):211–217, 1981.

[105] Avner Adin and Menahem Rebhun. High-Rate Contact Flocculation-Filtration With Cationic Polyelectrolytes. *J. Am. Water Works Assoc.*, 66(2):109–117, feb 1974. doi: 10.1002/j.1551-8833.1974.tb01983.x.

[106] Russell L Culp. Direct Filtration. *Am. Water Work. Assoc.*, 69(7):375–378, 1977.

[107] Ebubekir Yuksel, Murat Eyvaz, Tugrul S. Aktas, and Ahmet M. Saatci. A New Polyelectrolyte Dosing Method: Injection into Deep Bed Filter Media. *CLEAN - Soil, Air, Water*, 39(8):750–758, aug 2011. doi: 10.1002/clen.201000277.

[108] M. Rebhun, Z. Fuhrer, and A. Adin. Contact flocculation-filtration of humic substances. *Water Res.*, 18(8):963–970, 1984. doi: 10.1016/0043-1354(84)90246-X.

[109] Vitaly Gitis, Isaak Rubinstein, Maya Livshits, and Gennady Ziskind. Deep-bed filtration model with multistage deposition kinetics. *Chem. Eng. J.*, 163:78–85, 2010. doi: 10.1016/j.cej.2010.07.044.

[110] Yuri Osipov, Galina Safina, and Yuri Galaguz. Calculation of the filtration problem by finite differences methods. *MATEC Web Conf.*, 251, dec 2018. doi: 10.1051/matecconf/201825104021.

[111] Avner Adin and Menahem Rebhun. Model To Predict Concentration and Head-Loss Profiles in Filtration. *Am. Water Work. Assoc.*, 69(8):444–453, 1977. doi: https://www.jstor.org/stable/41292652.

[112] K. Wojciechowska. Modelling and Simulation of Filtration in the Development of Water Treatment Technologies. *Eng. Trans.*, 50(4):323–357, 2002.

[113] Tomihisa Iwasaki, Jr. J. J. Slade, and Wm. E. Stanley. Some Notes on Sand Filtration [with Discussion]. *Am. Water Work. Assoc.*, 29(10):1591–1602, 1937. doi: 10.1002/j.1551-8833.1937.tb14014.x.

[114] David C. Mays and James R. Hunt. Hydrodynamic aspects of particle clogging in porous media. *Environ. Sci. Technol.*, 39(2):577–584, 2005. doi: 10.1021/es049367k.

[115] C. R. O'Melia and W. Ali. *The role of retained particles in deep bed filtration*, volume 10. International Association on Water Pollution Research, 18th editi edition, 1978. doi: 10.1016/b978-0-08-022939-3.50019-2.

[116] B. F. Ruth, G. H. Montillon, and R. E. Montonna. Studies in Filtration - I. Critical Analysis of Filtration Theory. *Ind. Eng. Chem.*, 25(1):76–82, jan 1933. doi: 10.1021/ie50277a018.

[117] B. F. Ruth. Studies in Filtration... IV Nature of Fluid Flow through filter septa and Its Importance in the Filtration Equation. *Ind. Eng. Chem.*, 27(7):806–816, jul 1935. doi: 10.1021/ie50307a014.

[118] Matthew John Baker. *CFD simulation of flow through packed beds using the finite volume technique*. PhD thesis, 2011.

[119] Y.P. Rybakov and N.V. Semenova. Generalized Darcy's Law in Filtration Theory. *EPJ Web Conf.*, 173:1–4, 2018. doi: 10.1051/epjconf/201817302017.

[120] Jiyuan Tu, Guan-Heng Yeoh, and Chaoqun Liu. *Computational Fluid Dynamics: A Practical Approach*. 2018.

[121] John David Anderson. *Computational Fluid Dynamics: The Basics with Applications*. 1995. doi: 10.1136/bmj.332.7555.1456-a.

[122] T. J. Chung. *Computational Fluid Dynamics*. Cambridge University Press, feb 2010. doi: 10.1017/CBO9780511606205.

[123] Bas Anton Wols. *CFD in drinking water treatment*. PhD thesis, Delft University of Technology, 2010.

[124] R. W. Samstag, J. J. Ducoste, A. Griborio, I. Nopens, D. J. Batstone, J. D. Wicks, S. Saunders, E. A. Wicklein, G. Kenny, and J. Laurent. CFD for wastewater treatment: An overview. *Water Sci. Technol.*, 74(3):549–563, 2016. doi: 10.2166/wst.2016.249.

[125] Bruce R. Munson, Theodore H. Okiishi, Wade W. Huebsch, and Alric P. Rothmayer. Fundamentals of Fluid Mechanics. *John Wiley Sons, Inc.*, 2013.

[126] H K Versteeg and W Malalasekera. *An Introduction to Computational Fluid Dynamics: The Finite Volume Method*. 2007.

[127] Seyed Alireza Hosseini. *Modeling Particle Filtration and Caking In Fibrous Filter Media*. PhD thesis, Virginia Commonwealth University, 2011.

[128] A. Subrenat, J. Bellettre, and P. Le Cloirec. 3-D numerical simulations of flows in a cylindrical pleated filter packed with activated carbon cloth. *Chem. Eng. Sci.*, 58 (22):4965–4973, 2003. doi: 10.1016/j.ces.2003.07.012.

[129] Jelle Roegiers and Siegfried Denys. CFD-modelling of activated carbon fibers for indoor air purification. *Chem. Eng. J.*, 365:80–87, 2019. doi: 10.1016/j.cej.2019.02.007.

[130] Kan Liu, Yi Zhao, Liyang Jia, Rulong Hao, and Dong Fu. A novel CFD-based method for predicting pressure drop and dust cake distribution of ceramic filter during filtration process at macro-scale. *Powder Technol.*, 353:27–40, jul 2019. doi: 10.1016/j.powtec.2019.05.014.

[131] Zhuangbo Feng and Zhengwei Long. Modeling unsteady filtration performance of pleated filter. *Aerosol Sci. Technol.*, 50(6):626–637, 2016. doi: 10.1080/02786826.2016.1172058.

[132] Nausheen Basha. CFD study of filtration process in moulded filters within a vacuum pump. In *FILTECH 2016 Conf. Proc.*, 2016.

[133] P. Rosin and E. Rammler. Die Kornzusammensetzung des Mahlgutes im Lichte der Wahrscheinlichkeitslehre. *Kolloid-Zeitschrift*, 67(1):16–26, 1934. doi: 10.1007/BF01439773.

[134] ANSYS. ANSYS Fluent User's Guide, 2018.

[135] Nathalie Tufenkji and Menachem Elimelech. Correlation Equation for Predicting Single-Collector Efficiency in Physicochemical Filtration in Saturated Porous Media. *Environ. Sci. Technol.*, 38(2):529–536, 2004. doi: 10.1021/es034049r.

[136] ANSYS. ANSYS Fluent Theory Guide, 2018.

[137] A. D. Gosman and E. Ioannides. Aspects of Computer Simulation of Liquid-Fuelled Combustors. *J. Energy*, 7(6):482–490, 1983.

[138] O.l Levenspiel and A. Haider. Drag Coefficient and Terminal Velocity of Spherical and Nonspherical Particles. *Powder Technol.*, 58:63–70, 1989.

[139] T. Wakeman and W. Tabakoff. Measured particle rebound characteristics useful for erosion prediction. 1982.

[140] Abdellah Alem, Abdulghadir Elkawafi, Nasre-Dine Ahfir, and HuaQing Wang. Filtration of kaolinite particles in a saturated porous medium: hydrodynamic effects. *Hydrogeol. J.*, 21(3):573–586, may 2013. doi: 10.1007/s10040-012-0948-x.

[141] Nasre-Dine Ahfir, Ahmed Hammadi, Abdellah Alem, HuaQing Wang, Gilbert Le Bras, and Tariq Ouahbi. Porous media grain size distribution and hydrodynamic forces effects on transport and deposition of suspended particles. *J. Environ. Sci.*, 53:161–172, mar 2017. doi: 10.1016/j.jes.2016.01.032.

[142] Harold T. Glaser and James K. Edzwald. Coagulation and direct filtration of humic substances with polyethylenimine. *Environ. Sci. Technol.*, 13(3):299–305, mar 1979. doi: 10.1021/es60151a007.

[143] R. C. Medeiros, N.deM.N. Fava, B. L.S. Freitas, L. P. Sabogal-Paz, M. T. Hoffmann, J. Davis, P. Fernandez-Ibañez, and J. A. Byrne. Drinking water treatment by multistage filtration on a household scale: Efficiency and challenges. *Water Res.*, 178, 2020. doi: 10.1016/j.watres.2020.115816.

[144] Jerzy Weber, Yona Chen, Elżbieta Jamroz, and Teodoro Miano. Preface: humic substances in the environment. *J. Soils Sediments*, 18(8):2665–2667, aug 2018. doi: 10.1007/s11368-018-2052-x.

[145] AWWA. *Water Chlorination/Chloramination Practices and Principles - Manual of Water Supply Practices, M20.* American Water Works Association, 2006.

[146] Bhagya N Weerasinghe. *Kinetics of tap water dechlorination and aquatic health impacts of selected dechlorination chemicals.* Master's thesis, University of Toronto, 2008.

[147] Béla G. Lipták. *Instrumentation and Automation Engineers' Handbook: Volume II – Analysis and Analyzers.* CRC Press, fifth edition, 2017.

[148] HANNA instruments. HI 93703 Instruction Manual, 2005.

[149] Shimadzu Corporation. Shimadzu TOC-5000A Analyzer Instruction Manual, 1999.

[150] Richard M Emery, Eugene B Welch, and Russell F Christman. The Total Organic Carbon Analyzer and Its Application to Water Research. *Water Pollut. Control Fed.*, 43(9):1834–1844, 1971.

[151] D.W. Nelson and L.E. Sommers. Total Carbon, Organic Carbon, and Organic Matter. In *Methods Soil Anal. Part 2 Chem. Microbiol. Prop.*, pages 539–579. oct 1982. doi: 10.2134/agronmonogr9.2.2ed.c29.

[152] Issam N. Najm, Nancy L. Patania, Joseph G. Jacangelo, and Stuart W. Krasner. Evaluating surrogates for disinfection by-products. *J. Am. Water Works Assoc.*, 86 (6):98–106, jun 1994. doi: 10.1002/j.1551-8833.1994.tb06213.x.

[153] James K Edzwald, William C Becker, and Kevin L Wattier. Surrogate Parameters for Monitoring Organic Matter and THM Precursors. *J. Am. Water Works Assoc.*, 77(4):122–132, apr 1985. doi: 10.1002/j.1551-8833.1985.tb05521.x.

[154] Bibby Scientific Limited. Jenway Model 6305 Spectrophotometer Operating Manual, 2014.

[155] Zhining Shi, Christopher W. K. Chow, Rolando Fabris, Tianlong Zheng, Jixue Liu, and Bo Jin. Evaluation of the impact of suspended particles on the UV absorbance at 254 nm (UV254) measurements using a submersible UV-Vis spectrophotometer. *Environ. Sci. Pollut. Res.*, oct 2020. doi: 10.1007/s11356-020-11178-0.

[156] AWWA. *Instrumentation & Control: Manual of Water Supply Practices.* American Water Works Association, third edition, 2001.

[157] Ivars Jaunakais and Sanjay Mohan Anand. Photometric analysis, 2008.

[158] Ivars Jaunakais. Reagent delivery and photometric chlorine analysis, 2009.

[159] Malvern Instruments. Mastersizer 2000 User manuel. 2007.

[160] K.D. Vernon-Parry. Scanning electron microscopy: an introduction. *III-Vs Rev.*, 13(4):40–44, jul 2000. doi: 10.1016/S0961-1290(00)80006-X.

[161] Béla G. Lipták. *Instrumentation and Automation Engineers' Handbook: Volume I – Measurement and Safety.* CRC Press, fifth edition, 2016. doi: 10.4324/9781315370330.

[162] F. Arregui, E. Cabrera, and R. Cobacho. *Integrated Water Meter Management.* dec 2007. doi: 10.2166/9781780402253.

[163] AWWA. *Water Meters– Selection, Installation, Testing, and Maintenance.* American Water Works Association, 2012.

[164] D. van Halem, H. van der Laan, A. I.A. Soppe, and S. G.J. Heijman. High flow ceramic pot filters. *Water Res.*, 124:398–406, 2017. doi: 10.1016/j.watres.2017.07.045.

[165] H. H. Kleizen, A. B. de Putter, M. van der Beek, and S. J. Huynink. Particle concentration, size and turbidity. *Filtr. Sep.*, 32(9):897–901, 1995. doi: 10.1016/S0015-1882(97)84175-4.

[166] ISO 4572. Hydraulic fluid power — Filters — Multi-pass method for evaluating filtration performance, 1981.

[167] ISO 16889. Hydraulic fluid power — Filters — Multi-pass method for evaluating filtration performance of a filter element, 2008.

[168] Pall Corporation. Changes in the Presentation of Pall Filter Element Performance Ratings. Technical report, 2013.

[169] Shejiao Han, Caroline S. B. Fitzpatrick, and Andrew Wetherill. Mathematical Modelling of Particle Removal and Head Loss in Rapid Gravity Filtration. *Sep. Sci. Technol.*, 43(7):1798–1812, may 2008. doi: 10.1080/01496390801973631.

[170] Agnese Marcato, Gianluca Boccardo, and Daniele Marchisio. A computational workflow to study particle transport and filtration in porous media: Coupling CFD and deep learning. *Chem. Eng. J.*, 417(November 2020):128936, aug 2021. doi: 10.1016/j.cej.2021.128936.

[171] Liri Yoko Cruz Prieto Hojo, Ricardo Vicente de Paula Rezende, Sandro Rogério Lautenschlager, and Lyda Patricia Sabogal-Paz. Household slow sand filters operating in continuous and intermittent flows: Computational fluid dynamics simulation and validation by tracer experiments. *Chem. Eng. Sci.*, 247:117058, jan 2022. doi: 10.1016/j.ces.2021.117058.

[172] J. Saalbach and M. Hunze. Flow structures in MBR-tanks. *Water Sci. Technol.*, 57(5):699–705, 2008. doi: 10.2166/wst.2008.122.

[173] Arsalan Afkhami, Mattia Marotta, Dorian Dixon, Nigel G. Ternan, Luis Javier Montoya-Jaramillo, Margarita Hincapie, Laila Galeano, Pilar Fernandez-Ibanez, and Patrick S.M. Dunlop. Assessment of low-cost cartridge filters for implementation in household drinking water treatment systems. *J. Water Process Eng.*, 39(May 2020):101710, 2020. doi: 10.1016/j.jwpe.2020.101710.

[174] Caroline A. Schneider, Wayne S. Rasband, and Kevin W. Eliceiri. NIH Image to ImageJ: 25 years of Image Analysis. *Nat. Methods*, 9(7):671–675, 2012. doi: 10.1007/978-1-84882-087-6_9.

[175] Hakon Wadell. Sphericity and Roundness of Rock Particles. *J. Geol.*, 41(3):310–331, 1933.

[176] Kan Liu, Yi Zhao, and Liyang Jia. Simulation of dust deposition process in ceramic filter under different filtration modes by a novel CFD-based method. *Sep. Purif. Technol.*, 233(September 2019):116039, feb 2020. doi: 10.1016/j.seppur.2019.116039.

[177] Renbi Bai and Chi Tien. Particle Detachment in Deep Bed Filtration. *J. Colloid Interface Sci.*, 186(2):307–317, feb 1997. doi: 10.1006/jcis.1996.4663.

[178] Amy Li and Goodarz Ahmadi. Dispersion and Deposition of Spherical Particles from Point Sources in a Turbulent Channel Flow. *Aerosol Sci. Technol.*, 16:209–226, 1992.

[179] Amir A. Mofakham and Goodarz Ahmadi. On random walk models for simulation of particle-laden turbulent flows. *Int. J. Multiph. Flow*, 122:103157, 2020. doi: 10.1016/j.ijmultiphaseflow.2019.103157.

[180] M. Sommerfeld and N. Huber. Experimental analysis of modelling of particle-wall collisions. *Int. J. Multiph. Flow*, 25(6-7):1457–1489, 1999. doi: 10.1016/S0301-9322(99)00047-6.

[181] R. P. Chhabra, L. Agarwal, and N. K. Sinha. Drag on non-spherical particles: An evaluation of available methods. *Powder Technol.*, 101(3):288–295, 1999. doi: 10.1016/S0032-5910(98)00178-8.

[182] Jerzy Lukasik, Yueh Fung Cheng, Fuhua Lu, Mark Tamplin, and Samuel R. Farrah. Removal of microorganisms from water by columns containing sand coated with ferric and aluminum hydroxides. *Water Res.*, 33(3):769–777, 1999. doi: 10.1016/S0043-1354(98)00279-6.

[183] S. R. Farrah, D. R. Preston, G. A. Toranzos, M. Girard, G. A. Erdos, and V. Vasuhdivan. Use of modified diatomaceous earth for removal and recovery of viruses in water. *Appl. Environ. Microbiol.*, 57(9):2502–2506, 1991.

[184] Josef Vostrčil and Igor Tesařik. A study on the possibility of the water purification by means of the precoat filtration. *Water Res.*, 6(11):1367–1376, 1972. doi: 10.1016/0043-1354(72)90199-6.

[185] Jerzy Lukasik, S.R. Farrah, S. Truesdail, and D. O. Shah. Adsorption of microorganisms to sand and diatomaceous earth particles coated with metallic hydroxides. *KONA Powder Part. J.*, 14:87–91, 1996. doi: 10.14356/kona.1996014.

[186] M. Mansoor Ahammed and V. Meera. Iron hydroxide-coated sand filter for household drinking water from roof-harvested rainwater. *J. Water Supply Res. Technol. - AQUA*, 55(7-8):493–498, 2006. doi: 10.2166/aqua.2006.052.

[187] D. E. Burns, E. R. Baumann, and C. S. Oulman. Particulate Removal on Coated Filter Media. *Am. Water Work. Assoc.*, 62(2):121–126, 1970. doi: 10.1002/j.1551-8833.1970.tb03871.x.

[188] Charles S Oulman, Donald E Burns, and E Robert Baumann. Effect on Filtration of Polyelectrolyte Coatings of Diatomite Filter Media. *Am. Water Work. Assoc.*, 56(9):1233–1238, 1964.

[189] S. E. Truesdail, J. Lukasik, S. R. Farrah, D. O. Shah, and R. B. Dickinson. Analysis of Bacterial Deposition on Metal (Hydr)oxide-Coated Sand Filter Media. *J. Colloid Interface Sci.*, 203:369–378, 1998. doi: 10.1006/jcis.1998.5541.

[190] Jienan Chen, Steve Truesdail, Fuhua Lu, Guogen Zhan, Carter Belvin, Ben Koopman, Sam Farrah, and Dinesh Shah. Long-term evaluation of aluminum hydroxide-coated sand for removal of bacteria from wastewater. *Water Res.*, 32(7):2171–2179, 1998. doi: 10.1016/S0043-1354(97)00427-2.

[191] Sigma-Aldrich. Poly(diallyldimethylammonium chloride) solution SDS, 2019.

[192] S. D. J Inglethorpe. Industrial Minerals Laboratory Manual: Diatomite. Technical report, 1993.

[193] WHO. Procedure for Evaluation; WHO International Scheme to Evaluate Household Water Treatment (HWT) Technologies. (February), 2014.

[194] Yingying Wang, Frederik Hammes, Marcel Düggelin, and Thomas Egli. Influence of Size, Shape, and Flexibility on Bacterial Passage through Micropore Membrane Filters. *Environ. Sci. Technol.*, 42:6749–6754, 2008. doi: 10.1021/es800720n.

[195] James E. Amburgey, Kimberly J. Walsh, Roy R. Fielding, and Michael J. Arrowood. Removal of Cryptosporidium and polystyrene microspheres from swimming pool water with sand, cartridge, and precoat filters. *J. Water Health*, 10(1):31–42, 2012. doi: 10.2166/wh.2011.062.

[196] J. V. Hunter, G. R. Bell, and C. N. Henderson. Coliform Organism Removals by Diatomite Filtration. *Am. Water Work. Assoc.*, 58(9):1160–1169, 1966. doi: 10.1002/j.1551-8833.1966.tb01680.x.

[197] James H. Dillingham and E. Robert Baumann. Hydraulic and Particle Size Characteristics of Some Diatomite Filter Aids. *Am. Water Work. Assoc.*, 56(6): 793–808, 1964. doi: 10.1002/j.1551-8833.1964.tb01272.x.

[198] M. Mota, J. A. Teixeira, W. R. Bowen, and A. Yelshin. Interference of coarse and fine particles of different shape in mixed porous beds and filter cakes. *Miner. Eng.*, 16:135–144, 2003. doi: 10.1016/S0892-6875(02)00314-X.

[199] Eberhard Schmidt and Friedrich Löffler. The Analysis of Dust Cake Structures. *Part. Part. Syst. Charact.*, 8:105–109, 1991. doi: 10.1002/ppsc.19910080120.

[200] Zhe Wang, Yan Lin, Deyi Wu, and Hainan Kong. Hydrous iron oxide modified diatomite as an active filtration medium for phosphate capture. *Chemosphere*, 144: 1290–1298, feb 2016. doi: 10.1016/j.chemosphere.2015.10.015.

[201] Abidelfatah M. Nasser. Removal of Cryptosporidium by wastewater treatment processes: a review. *J. Water Health*, 14(1):1–13, feb 2016. doi: 10.2166/wh.2015.131.

[202] G. Galjaard, P. Buijs, E. Beerendonk, F. Schoonenberg, and J. C Schippers. Precoating (EPCE) UF membranes for direct treatment of surface water. *Desalination*, 139:305–316, 2001. doi: 10.1016/S0011-9164(01)00324-1.

[203] Reya Sadik Al-Khalili. *Contact flocculation filtration using natural coagulants for developing countries*. Phd thesis, University of Leicester, 1999.

[204] Sarah C. Clark, Desmond F. Lawler, and Robert S. Cushing. Contact Filtration: Particle Size and Ripening. *J. Am. Water Works Assoc.*, 84(12):61–71, dec 1992. doi: 10.1002/j.1551-8833.1992.tb05903.x.

[205] Nava Narkis and Menahem Rebhun. Stoichiometric Relationship Between Humic and Fulvic Acids and Flocculants. *J. Am. Water Works Assoc.*, 69(6):325–328, jun 1977. doi: 10.1002/j.1551-8833.1977.tb06752.x.

[206] James K. Edzwald and John E. Tobiason. Enhanced coagulation: US requirements and a broader view. *Water Sci. Technol.*, 40(9):63–70, 1999. doi: 10.1016/S0273-1223(99)00641-1.

[207] J.J. Monscvitz, D.J. Rexing, R.G. Williams, and J. Heckler. Some Practical Experience in Direct Filtration. *J. Am. Water Works Assoc.*, 70(10):584–588, oct 1978. doi: 10.1002/j.1551-8833.1978.tb04248.x.

[208] James K. Edzwald. Aluminum in Drinking Water: Occurrence, Effects, and Control. *J. AWWA*, 112(5):34–41, may 2020. doi: 10.1002/awwa.1499.

[209] Izabela Krupińska. Aluminium drinking water treatment residuals and their toxic impact on human health. *Molecules*, 25(3), 2020. doi: 10.3390/molecules25030641.

[210] John L. Cleasby, David J. Hilmoe, and Constantine J. Dimitracopoulos. Slow Sand and Direct In-line Filtration of a Surface Water. *J. Am. Water Works Assoc.*, 76 (12):44–55, dec 1984. doi: 10.1002/j.1551-8833.1984.tb05455.x.

[211] Qian Wang, Baoyu Gao, Yan Wang, Zhonglian Yang, Weiying Xu, and Qinyan Yue. Effect of pH on humic acid removal performance in coagulation–ultrafiltration process and the subsequent effects on chlorine decay. *Sep. Purif. Technol.*, 80(3): 549–555, aug 2011. doi: 10.1016/j.seppur.2011.06.010.

[212] T. Saltnes, B. Eikebrokk, and H. Ødegaard. Contact filtration of humic waters: performance of an expanded clay aggregate filter (Filtralite) compared to a dual anthracite/sand filter. *Water Supply*, 2(5-6):17–23, dec 2002. doi: 10.2166/ws.2002.0145.